Imperial College London

Exploring grain growth & hydride precipitation behaviour in Zircaloy-4

Ruth Birch

Department of Materials

Imperial College London

This thesis is submitted for the degree of

Doctor of Philosophy (Ph.D.)

September 2022

[Page intentionally left blank]

Abstract

Zirconium alloys are used extensively within the nuclear industry for structural components and fuel cladding, where their microstructure influences component performance. The final microstructure and properties are strongly influenced by the high temperature β phase microstructure, found during processing. To reconstruct this microstructure, a MATLAB based code was developed which includes analysis of the details of the orientation relationships between the parent β phase and child α variants. This enables deeper analysis of grain boundary types, and their influence on microstructural evolution (e.g. grain growth and hydride formation). In zirconium alloys, the final microstructure is controlled to optimise neutronic performance, and unexpected grain growth is detrimental to reactor performance. Previously, blocky-α grain growth has been observed in weld microstructures in short timescales with high temperature heat treatments (e.g. 1 hr @ 800 °C). In this work, *in situ* and *ex situ* heating experiments have been developed and used to study grain growth in these microstructures to enable the prediction of likely blocky-α grain growth from an initial weld microstructure, noting the influence of the prior-β grain boundaries. In-service, hydrogen ingress into Zr alloys can lead to the formation of brittle hydride phases which have a deleterious effect on the component performance. The misfit strain between hydrides and the matrix is thought to cause a localised stress field, which can influence hydride nucleation, growth, and reorientation. In this work, conventional EBSD and HR-EBSD were used to characterise hydride-matrix deformation fields near grain boundaries. These fields vary for hydrides that smoothly decorate the grain boundary and those that protrude into the matrix, providing insight into hydride-microstructure influenced component performance. In summary, this thesis provides microstructural characterisation of zirconium alloys to support the continued use of these alloys in demanding environments.

Statement of Originality

I declare that the research presented in this thesis is my own work and that contributions from the work of others have been appropriately referenced. Figures referenced from literature are reproduced under license from their respective copyright owners.

This thesis builds upon my Masters thesis, titled “Hydrides in Zircaloy-4: The effect of grain size on zirconium hydride precipitation”. A very small proportion of the literature review (Chapter 2) has been rewritten from this prior work.

Chapter 4 and some of the literature review are adapted from my paper entitled “Effective structural unit analysis in hexagonal close-packed alloys – reconstruction of parent β microstructures and crystal orientation post-processing analysis”[1].

Ruth Birch 11/09/22

Copyright Statement

The copyright of this thesis rests with the author. Unless otherwise indicated, its contents are licensed under a Creative Commons Attribution-Non Commercial 4.0 International Licence (CC BY-NC).

Under this licence, you may copy and redistribute the material in any medium or format. You may also create and distribute modified versions of the work. This is on the condition that: you credit the author and do not use it, or any derivative works, for a commercial purpose.

When reusing or sharing this work, ensure you make the licence terms clear to others by naming the licence and linking to the licence text. Where a work has been adapted, you should indicate that the work has been changed and describe those changes.

Please seek permission from the copyright holder for uses of this work that are not included in this licence or permitted under UK Copyright Law.

Acknowledgements

I would like to thank my supervisor Dr Ben Britton for the opportunity, training and support. In particular for continuing to supervise from Canada, figuring things out during the pandemic and always making the time to help with challenges.

I would also like to thank my supervisor Dr Katharina Marquardt for her support and guidance, and for her joining me for some experimental work.

I would like to thank all the experimental micromechanical characterisation research group members, past and present for helping to provide a friendly and supportive group in which to work. I have gained friends, knowledge and current/future collaborators.

I would like to thank Mike Rogers for support and encouragement, as well as supply of material.

I would like to thank Ben Wood for help and support in the lab, and Dr Mahmoud Ardakani for training and support in the EM suite (including a lot of support fixing the PECS machine).

Lastly I would like to thank my family and friends outside of academia for providing perspective and balance.

Contents

Abstract 3

Statement of Originality 4

Copyright Statement 4

Acknowledgements 5

Contents 6

List of Figures 12

List of Tables 16

Publications and conferences 17

Publications 17

Conferences 17

Glossary 18

1 Introduction 20

2 Literature Review 21

2.1 Introduction to zirconium alloys 21

2.1.1 Alloy compositions 21

2.1.2 Properties 22

2.1.3 Microstructure 22

2.2 Phase transformation (β to α) 25

2.2.1 Burgers orientation relationship (BOR) 25

2.2.2 β quench microstructure 26

2.3 Welding 31

2.3.1 Electron beam (EB) welding 31

2.3.2 Weld microstructures 31

2.3.3 Example microstructures 32

2.4 Challenges 33

2.4.1 Blocky-α 33

2.4.2 Hydrides....37
2.5 Parent grain reconstruction....47
2.5.1 Commercial software....49
2.6 Prior work....50
2.6.1 Experiment....50
2.6.2 Observations....50
2.6.3 Grain size....51
2.6.4 Comparison with literature....51
2.7 Review of analytical techniques....53
2.7.1 Ion beam polishing....53
2.7.2 Polarised light optical microscopy....54
2.7.3 Backscatter and forescatter electron imaging....54
2.7.4 Electron backscatter diffraction (EBSD)....56
2.8 Aims and objectives....59
3 Experimental Methods....60
3.1 Materials....60
3.2 Initial sample preparation....61
3.3 Heat treatments....62
3.4 Hydriding....63
3.4.1 Setup....63
3.4.2 Hydrogen content....64
3.4.3 Annealing time....66
3.4.4 Cooling rate.....67
3.5 Ion beam polishing....67
3.5.1 Broad ion beam (BIB) polishing....68
3.5.2 Focussed ion beam (FIB) polishing....70
3.6 *In situ* heating experiment....72
3.6.1 Equipment....72
3.6.2 Final setup....74

3.6.3 Heat treatment & data collection 74
3.7 *Ex situ* heating experiment 75
3.8 Analysis Techniques 76
3.8.1 Polarised light optical microscopy 76
3.8.2 Forescatter electron (FSE) imaging 76
3.8.3 Electron backscatter diffraction (EBSD) 77
3.8.4 High angular resolution electron backscatter diffraction (HR-EBSD) 77
3.9 Sample Log 79
4 Reconstruction Code 81
4.1 Overview 81
4.2 Symmetry and crystallography of the Burgers orientation relationship (BOR) 81
4.2.1 BCC to HCP 81
4.2.2 HCP to BCC 82
4.3 Reconstruction algorithm & microstructural post processing 83
4.3.1 Initial reconstruction 83
4.3.2 Post processing 86
4.4 Simulated dataset 88
4.5 Experimental materials & method 89
4.6 Results 89
4.6.1 Microstructure 90
4.6.2 Split grain 90
4.6.3 Reconstruction certainty 92
4.7 Post processing 93
4.8 Comparison with an alternative algorithm within MTEX 95
4.8.1 Type 1: Low angle β grain boundary 97
4.8.2 Type 2: <111> β twin 97
4.8.3 Type 3: Uncertainty of globular domains 97
4.8.4 Type 4: Misorientation 97
4.9 Discussion 98

4.10 Conclusion 99
5 *In Situ* Experiment Development 100
5.1 Aim 100
5.2 Introduction 100
5.3 Setup 101
5.4 Potential issues 101
5.5 Issue investigations 102
5.5.1 Temperature measurement 102
5.5.2 Heat damage issues 108
5.5.3 Forescatter imaging issues 112
5.5.4 Sample and stage considerations 114
5.6 High temperature trials 117
5.6.1 High temperature forescatter imaging 117
5.6.2 High temperature EBSD 120
5.7 Summary 122
5.7.1 Best practice 123
5.7.2 Experiment decisions 125
6 Macroscopic Observations of Blocky-α Grain Growth 126
6.1 Aim 126
6.2 Introduction 126
6.2.1 Initial weld microstructure 126
6.3 Results: Imaging observations 128
6.4 Results: EBSD analysis 128
6.4.1 Bulk material 132
6.4.2 Heat affected zone 132
6.4.3 Fusion zone 133
6.4.4 Parent microstructure vs. grain growth 134
6.5 Summary 137
7 Microscopic Observations of Blocky-α Grain Growth 139

7.1 Aim 139
7.2 Introduction 139
7.3 Part 1: Onset of grain growth 139
7.3.1 Initial growth location – weld region 141
7.3.2 Initial growth location – prior-β grain boundaries 142
7.3.3 Factors affecting the initial onset of growth 144
7.4 Part 2: grain growth 145
7.4.1 Pinning 146
7.4.2 α variants 147
7.4.3 Grain growth hypothesis 148
7.4.4 Extending observations to multiple regions within the *in situ* data sets 150
7.5 Summary 152
7.5.1 Onset of grain growth 152
7.5.2 Factors affecting grain growth 152
8 Hydride Stress Fields 153
8.1 Aim 153
8.1.1 Hydride orientation relationship (OR) 153
8.1.2 Sample surface preparation 153
8.2 Results 154
8.2.1 Smooth grain boundary hydride 155
8.2.2 Hydrides that protrude into the Zr matrix 163
8.3 Summary 174
9 Discussion 175
9.1 Reconstruction of the prior-β microstructure 175
9.1.1 Reconstruction 175
9.1.2 Post processing 175
9.1.3 Future development 175
9.2 Grain growth in weld microstructures 176
9.2.1 Grain growth location 176

9.2.2 Grain growth mechanism 176
9.2.3 Onset of grain growth 176
9.2.4 Factors affecting grain growth 177
9.2.5 Growth within new β domain 178
9.2.6 Completion of grain growth 178
9.2.7 Further experiments 179
9.3 Hydride-matrix deformation fields 179
9.3.1 Sample preparation 179
9.3.2 Grain boundary hydride 180
9.3.3 Future experiments 180
10 Summary 181
11 References 182
Appendix A: Plotting Details 197
EBSD maps 197
Reconstruction details 199
HR-EBSD settings 202
Appendix B: Figure permissions 203

List of Figures

Figure 1 - α phase microstructures in Zircaloy-4 23
Figure 2 - Phases in Zr alloys 25
Figure 3 - BOR schematic 26
Figure 4 - Basketweave vs. parallel plate microstructures 26
Figure 5 - SPPs in Zircaloy-4 28
Figure 6 - Carbon content and basketweave morphology 28
Figure 7 - Effect of oxygen concentration and cooling rate on plate (α lath) width 29
Figure 8 - Effect of cooling rate on α lath width 30
Figure 9 - Prior β grain size 30
Figure 10 - Weld microstructure overview 32
Figure 11 - EB weld microstructure example 33
Figure 12 - Strain and grain growth 34
Figure 13 - Blocky-α grain growth in electron beam welded Zircaloy-4 34
Figure 14 - Blocky-α growth in TIG welded Zircaloy-4 35
Figure 15 - Aging β quenched Zircaloy-4 35
Figure 16 - Blocky-α growth mechanism 36
Figure 17 - TTT diagram for recrystallisation in β quenched Zircaloy-4 37
Figure 18 - Zr-H phase diagram including ambient hydrogen partial pressures isobars 38
Figure 19 - Zirconium hydride phases 38
Figure 20 - Hydride redistribution as a result of temperature gradients 39
Figure 21 - Cooling rate and hydrides 40
Figure 22 - Schematic representation of hydride reorientation in zirconium alloy tubes 41
Figure 23 - Schematic of the delayed hydride cracking process 42
Figure 24 - Effect of stress field on hydride reorientation 42
Figure 25 - Dislocations around hydrides 43
Figure 26 - Local lattice strain around a hydride 44
Figure 27 - Lattice strain parallel to loading direction 45
Figure 28 - Modelling vs. experimental results for stress around a δ hydride 46
Figure 29 - Grain growth at 760 °C – prior work 50
Figure 30 - EB weld microstructure overview 52
Figure 31 - Extent of blocky-α grain growth. 52
Figure 32 - Polarised optical microscopy setup 54
Figure 33 - Backscatter vs. forescatter electron imaging 55
Figure 34 - Backscatter electron imaging example 55

Figure 35 - EBSD: Setup 56
Figure 36 - EBSD: Pattern formation 57
Figure 37 - EBSD: Background correction 58
Figure 38 - EBSD: Pattern indexing 58
Figure 39 - Fine grain as-received material 60
Figure 40 - Weld microstructure overview 61
Figure 41 - Specimen mounting for BIB polishing 62
Figure 42 - Blocky-α microstructure 63
Figure 43 - Schematic of the hydriding rig 64
Figure 44 - Planar BIB polishing 68
Figure 45 - Cross section BIB polishing 69
Figure 46 - Schematic showing how single modulation works 69
Figure 47 - Cross section polishing quality 70
Figure 48 - Sample holder and EBSD analysis conditions for pFIB cross sections 71
Figure 49 - Murano heating carriage 72
Figure 50 - Pre-tilted heating module 72
Figure 51 - High temperature (HT) phosphor 73
Figure 52 - Murano flange with external connections labelled 73
Figure 53 - External connections for the Murano stage 74
Figure 54 - In situ experiment setup 74
Figure 55 - Representative heating cycle and data collection points 75
Figure 56 - Polarised optical microscopy example 76
Figure 57 - Forescatter imaging examples 77
Figure 58 - β → α BOR shared planes and directions example 82
Figure 59 - α → β BOR shared planes and directions example 83
Figure 60 - Initial reconstruction code overview 84
Figure 61 - β grain orientation certainty flowchart 87
Figure 62 - Simulated dataset reconstruction example 89
Figure 63 - Experimental example – initial reconstruction results 90
Figure 64 - Split grain investigation – inflation power 91
Figure 65 - Split grain investigation – manual sorting 92
Figure 66 - Impact of the no. of unique α variants 93
Figure 67 - Experimental example – post processing results 94
Figure 68 - Comparison of ParentBOR reconstruction and MTEX 5.7.0 reconstruction 96
Figure 69 - In situ experiment setup 101
Figure 70 - Murano (in built) thermocouple position. 103

Figure 71 - Sample installation in Murano stage. 103
Figure 72 - Thermocouple positioning issue. 104
Figure 73 - Final thermocouple solution. 104
Figure 74 - Preheat cycles. 105
Figure 75 - Trial heating program for LG sample 107
Figure 76 - Program controlled heating cycle 108
Figure 77 - Forescatter diode (FSD) trial. 109
Figure 78 - Chamber view for the FSD temperature trial 109
Figure 79 - FSD temperature trial results. 110
Figure 80 - HT phosphor deterioration and EBSP quality 111
Figure 81 - Chamber light levels at elevated temperatures 112
Figure 82 - Bias control trials 114
Figure 83 - Oxidation at elevated temperatures 115
Figure 84 - Oxidation at 830 °C in a weld microstructure. 115
Figure 85 - Effect of oxidation on EBSD 116
Figure 86 - Maintenance of Murano stage - electrical contacts. 117
Figure 87 - High temperature FSD imaging 118
Figure 88 - Chamber view for FSD high temperature imaging trial. 120
Figure 89 - High temperature EBSD mapping at 500 and 720 °C 120
Figure 90 - EBSP examples at 500 and 720 °C 121
Figure 91 - EBSPs at 850 °C for a weld sample 122
Figure 92 - Weld region schematics 127
Figure 93 - Ex situ FSD overview 128
Figure 94 - Ex situ data segmented 129
Figure 95 - Ex situ EBSD results – α 130
Figure 96 - Ex situ EBSD results – reconstructed β 131
Figure 97 - HAZ grain size differences post-HT (map 3) 133
Figure 98 - Initial parent β boundaries overlaid on the post-HT grain map 134
Figure 99 - Parent β vs. post-HT orientation testing 135
Figure 100 - Neighbouring grain orientation testing 136
Figure 101 - In situ evolution of grain growth 140
Figure 102 - Blocky-α grain growth hypotheses 141
Figure 103 - Onset of grain growth across weld region 142
Figure 104 - In situ grain growth - small map examples (experiment 1) 143
Figure 105 - Microscopic grain growth mechanism 144
Figure 106 - Testing grain growth mechanism 144

Figure 107 - Pattern quality - influence of stored energy 145
Figure 108 - Points that pin growth 146
Figure 109 - 'cross' point α orientation examples 147
Figure 110 - α variant analysis for experiment 3 example 148
Figure 111 - Grain growth hypothesis example 149
Figure 112 - Comparison of model output and heat treatment results 149
Figure 113 - Blocky-α grain growth locations and directions 151
Figure 114 - pFIB hydride area overview 154
Figure 115 - Orientation analysis of the grain boundary hydride map 155
Figure 116 - Orientation relationships in the grain boundary hydride map 156
Figure 117 - HR-EBSD analysis of grain boundary hydride 157
Figure 118 - Orientation analysis of the triple junction grain boundary hydride map 159
Figure 119 - Orientation relationships in the triple junction grain boundary map 160
Figure 120 - δ/δ orientation relationships in the pFIB hydride map 161
Figure 121 - HR-EBSD analysis of triple junction hydride 162
Figure 122 - Orientation analysis of the pinch off hydride map 163
Figure 123 - Orientation relationships in the pinch off hydride map 164
Figure 124 - HR-EBSD analysis of the pinch off hydride map 166
Figure 125 - HR-EBSD analysis of the pinch off hydride map – Tip 1 168
Figure 126 - HR-EBSD analysis of the pinch off hydride map – Tip 2 169
Figure 127 - Orientation analysis of the spiky hydride map 170
Figure 128 - Orientation relationships in the spiky hydride map 171
Figure 129 - HR-EBSD analysis of the spiky hydride map 172
Figure 130 - HR-EBSD analysis of a section of the spiky hydride map 173
Figure 131 - Blocky-α grain growth initiation with time 177
Figure 132 - Multiple α grains into same β domain 178

List of Tables

Table 1 - Zr alloying elements....21
Table 2 - Zr alloy compositions....22
Table 3 - Zr alloy properties....22
Table 4 - SPPs in Zircaloys....24
Table 5 - β→α microstructures in Zircaloy-4....27
Table 6 - Dilatational misfit values for δ and γ hydrides....43
Table 7 - Grain size measurements....51
Table 8 - Symbol definitions for hydrogen content calculation....65
Table 9 - Lattice parameters for α-Zr and epsilon phase hydrides....66
Table 10 - Symbol definitions for annealing time calculation....66
Table 11 - Values of Arrhenius constants....67
Table 12 - Standard broad ion beam polishing recipes used....70
Table 13 - pFIB polishing recipe....71
Table 14 - Sample log....79
Table 15 - Misorientation between potential α variants....85
Table 16 - Details of simulated dataset....88
Table 17 - Potential issues....102
Table 18 - Temperature overshoot and stabilisation times for the range 500-850 °C....106
Table 19 - Setup details for FSD temperature trial....109
Table 20 - Temperatures reached during the FSD temperature trial....110
Table 21 - Heat treatment details for the high temperature phosphor....111
Table 22 - FSD imaging conditions for high temperature imaging trial....118
Table 23 - Potential issues: revisited....123
Table 24 - Summary of experimental decisions made as a result of preliminary trials....125
Table 25 - α lath dimensions....132
Table 26 - Angles between α grain directions in the triple junction map....159
Table 27 - EBSD settings....197
Table 28 - ParentBOR code settings and outputs....199
Table 29 - HR-EBSD plot settings....202

Publications and conferences

Publications

- **R. Birch** and T. B. Britton, "**Effective structural unit analysis in hexagonal close-packed alloys – reconstruction of parent β microstructures and crystal orientation post-processing analysis**," *J. Appl. Crystallography.*, vol. 55, no. 1, pp. 33–45, 2022. https://doi.org/10.1107/s1600576721011584
- **R. Birch***, N. Fang*, and T. Ben Britton, "**Optimizing broad ion beam polishing of zircaloy-4 for electron backscatter diffraction analysis**," 2022. Micron, p. 103268, 2022, https://doi.org/10.1016/j.micron.2022.103268
  (* = joint first author)

Conferences

June 2019	Annual international student conference in metallic materials (*Sheffield, UK*) **[Poster] R. Birch**, S. Wang, V. S. Tong, T. B. Britton, "The effect of cooling rate and grain size on hydride microstructure in Zircaloy-4"
April 2021	EBSD 2021 conference (*virtual*) [**Talk] R. Birch** and T. Ben Britton**,** "Parent grain reconstruction in zirconium alloys"
Sept 2021	MIDAS conference (*virtual*) **[Talk] R. Birch** and T. Ben Britton**,** "Understanding blocky-alpha grain growth in welded Zr-4 using in-situ methods and parent grain reconstruction"
April 2022	EBSD 2022 conference *(virtual*) **[Talk] R. Birch** and T. Ben Britton**,** "In situ EBSD-studies of blocky grain growth in welded Zircaloy-4"

Glossary

Acronym	Definition
BCC	Body centred cubic
BIB	Broad Ion Beam (polishing)
BOR	Burgers' orientation relationship
BSE	Backscatter electrons
CCD	Charged coupled device
DDP	Discrete dislocation plasticity
DHC	Delayed hydride cracking
DSC	Differential scanning calorimetry
E_B	Energy - backscattered electrons
E_{SE}	Energy - secondary electrons
EB	Electron beam (welding)
EBSD	Electron backscatter diffraction
EELS	Electron energy loss spectroscopy
FEG	Field emission gun
FIB	Focussed ion beam
FSD	Forescatter diodes
FSE	Forescatter electron (imaging)
FSE	Forescatter electrons
FWHM	Full width half maximum
gB	Grain boundary
GND	Geometrically necessary dislocation
HT	Heat treatment
HAZ	Heat affected zone
HCP	Hexagonal close packed
HPT	High pressure torsion
HR-EBSD	High (angular) resolution electron backscatter diffraction
HRXRD	High energy X-ray diffraction (HRXRD)
LB	Laser beam (welding)
LOCA	Loss of coolant accident
LUT	Look up table
MAD	Mean angular deviation
MAE	Mean angular error
MATLAB	MATrix LABoratory https://uk.mathworks.com/products/matlab.html
MCL	Markov clustering (algorithm)
MTEX	https://mtex-toolbox.github.io/
NBED	Nano-beam electron diffraction
ND	Normal direction

Acronym	Definition
OM	Optical microscopy
OPS/OP-S	Oxide polishing suspension (typically silica)
OR	Orientation relationship
PAG	Parent austenite grain
PECS	Precision etching and coating system
pFIB	Plasma focussed ion beam
PH	Peak height
PIG	Penning ion gun
PIPS	Precision ion polishing system
RD	Rolling direction
RT	Room temperature
SE	Secondary electron
SEI	Secondary electron imaging
SEM	Scanning electron microscope/microscopy
SIBM	Strain induced grain boundary migration
SPP	Secondary phase particle
STEM	Scanning transmission electron microscopy
TD	Transverse direction
TEM	Transmission electron microscopy
TIG	Tungsten inert gas
TSSd	Terminal solid solubility of dissolution
TSSp	Terminal solid solubility for precipitation
TTT	Time-temperature-transformation (diagram)
ZrH	Zirconium hydride

1 Introduction

The overall aim of this thesis is to provide greater understanding of some aspects of manufacturing and performance of Zircaloy-4 cladding materials.

In manufacturing, the microstructure of Zircaloy-4 is tightly controlled to optimise neutronic performance, and as such inadvertent grain growth and texture evolution can affect operation for the reactor. Welding results in localised regions of different microstructure and can be a point of failure. The focus of the work here is to characterise and understand blocky-α[1] grain growth in weld microstructures during post-weld heat treatments. In manufacturing, elevated temperatures could be used for post-weld stress relief, or in service they could be experienced during high temperature excursions (e.g. in a loss of coolant accident (LOCA) scenario).

Blocky-α grain growth is thought to be related to the high temperature (prior-β) microstructure [2]. In order to investigate this, a parent grain reconstruction code was developed to reconstruct the parent microstructure and identify different boundary types within the (room temperature) α microstructure. To understand more about the grain growth mechanism, and where the α grains form and grow during the heat treatments, an *in situ* heating experiment was developed. This enabled the study of the initial onset of grain growth, and was complemented by an *ex situ* heating experiment to look at longer term growth.

In performance, the presence of hydrides within Zr alloys has a deleterious effect on the materials properties and can lead to failure. In this thesis, the focus is on using new sample preparation and characterisation methods to explore hydride formation near interfaces such as α-α grain boundaries. The aim is to develop a better understanding of how hydrides decorate the grain boundaries and includes analysis of the orientation relationships (α-α, α-hydride and hydride-hydride) and stress fields.

This thesis is structured to provide context to the program of work with a review of prior literature (including aims and objectives), followed by details of the experimental methods used to characterise the materials. A chapter on development and testing of a new MATLAB based parent β reconstruction code follows. This code provides the ability to deliver new insight into the high temperature microstructure and resulting final microstructure. The thesis is then focussed on grain growth analysis, starting with development of a new high temperature (>600 °C) *in situ* heating experiment, followed by results from the *in situ* and *ex situ* heating experiments, divided into macroscopic and microscopic observations. The final results chapter discusses hydride formation, with advances in sample preparation enabling successful mapping of the microstructure and residual deformation fields near zirconium-hydride interfaces, analysed using EBSD and HR-EBSD. The thesis concludes with a short discussion and a summary chapter that draw together the results and brings them into context of the prior literature and my initial aims and objectives.

[1] Blocky-α grains are typically >300 μm with irregular and wavy boundaries [47], [48], as compared to the regular equiaxed grains (< 15 μm) found in the material.

2 Literature Review

2.1 Introduction to zirconium alloys

Zr alloys are used extensively in the nuclear industry for fuel cladding and other structural components. They are chosen due to their unique combination of properties that make them suitable for this purpose, for example, low thermal neutron absorption and radiation tolerance.

The use of Zr alloys in nuclear began in the 1940s with the decision by Admiral Rickover to use them as nuclear fuel cladding materials in naval nuclear reactors in the US [3]. This decision paved the way for development of both the production process and development of new alloys, as usage increased and problems needed to be overcome (for example, the corrosion rate of Zircaloy-1 increased with time [3]). Over the past 70-80 years, further development of alloys has occurred, with a lot of research (past and present) into performance and improvements. However, some issues such as long-term corrosion resistance, H ingress and hydride precipitate behaviour remain and are the topic of on-going research.

2.1.1 Alloy compositions

Typically nuclear-grade Zr alloys used in the fuel assembly are Zr-rich to minimise the neutron absorption cross section of the cladding. For the α-phase zirconium alloys, they are often alloyed with small additions of elements of tin, iron, chromium, nickel and/or niobium. The role of each of these elements is detailed at Table 1.

Table 1 - Zr alloying elements - the role of the five main alloying elements in Zr alloys[4]

Element	Reason for addition
Tin (Sn)	To reduce the corrosion enhancing effect of nitrogen
Nickel (Ni)	Increased corrosion resistance in high temp steam + water (Ni also increases hydriding)
Iron (Fe)	Increased corrosion resistance in high temp steam + water
Chromium (Cr)	Increased corrosion resistance in high temp steam + water (also increases hardness)
Niobium (Nb)	Increased strength – makes it suitable for higher burn up fuels

The relative amount of each additional element in the alloy depends on the end use of the alloy. For example, Zircaloy-4 has less Ni and Fe than Zircaloy-2 to reduce hydrogen pick up [5]. The addition of niobium for alloys such as Zr-2.5Nb (wt%) and ZIRLO is to increase the alloy strength, making it suitable for higher burn up fuels [4]. The chemical composition for the major components of five Zr alloys are found in Table 2.

Table 2 - Zr alloy compositions – chemical composition of the major components of common zirconium alloys, compiled from [6], [7].

Alloy	Composition* (wt %) of various zirconium alloys.				
	Tin	**Iron**	**Chromium**	**Nickel**	**Niobium**
Zircaloy-2	1.2-1.7	0.07-0.2	0.05-0.15	0.03-0.08	-
Zircaloy-3	0.2-0.3	0.2-0.3	0.10	0.05	-
Zircaloy-4	1.2-1.7	0.18-0.24	0.07-0.13	max 0.007	-
ZIRLO™	0.96	0.1	-	-	0.99
Zr-Nb	-	-	-	-	2.4-2.8

*balance Zirconium.

2.1.2 Properties

A summary of useful mechanical and thermal properties for common Zr alloys is found in Table 3, including the β phase transition temperature (see section 2.2). Note that these are typical properties which can be varied through processing, via microstructural engineering.

Table 3 - Zr alloy properties – Mechanical and thermal properties for Zirconium, Zircaloy-2, Zircaloy-4 and Zr-2.5Nb [8]–[12].

Property	Unit	Zirconium	Zircaloy-2	Zircaloy-4	Zr-2.5Nb
Density	g/cc	6.53	6.56	6.56	6.44
Ultimate tensile strength	MPa	330	≥ 413	514	≥ 448
Yield strength	MPa	230	≥ 241	381	≥ 310
Elastic modulus	GPa	94.5	99.3	99.3	97.9
Poisson's Ratio	-	0.34	0.37	0.37	0.33
Shear modulus	GPa	35.3	36.2	36.2	34.5
Thermal Conductivity	W/mK	16.7	21.5	21.5	17.1
β transition temperature	°C	870	865	865	854

2.1.3 Microstructure

Zirconium alloys used in nuclear power are typically α-phase alloys (excluding Zr-Nb binaries, which are near α-alloys and include a small volume fraction of β-phase). The α phase has a hexagonal close packed (HCP) microstructure. At high temperature Zr alloys have an allotropic phase transformation, to a β phase, which is body centred cubic (BCC) (see section 2.2). The α and β phases are related by Burgers' orientation relationship[13], BOR, (see Section 2.2.1).

For Zircaloy-4, there are additional secondary phase particles (SPPs) which are decorated throughout the microstructure. If there is a significant amount of hydrogen in the material (above the TSSp, the terminal solid solubility for precipitation), then solid phase hydrides can form either at temperature or when the material is cooled.

The thermomechanical processing route for a component made from a Zr alloy will control the microstructure and crystallographic texture of the final product.

2.1.3.1 Grain morphology

Typically two α-grain microstructures are observed, equiaxed and lenticular α (either in a basketweave or Widmanstätten structure), as shown in Figure 1.

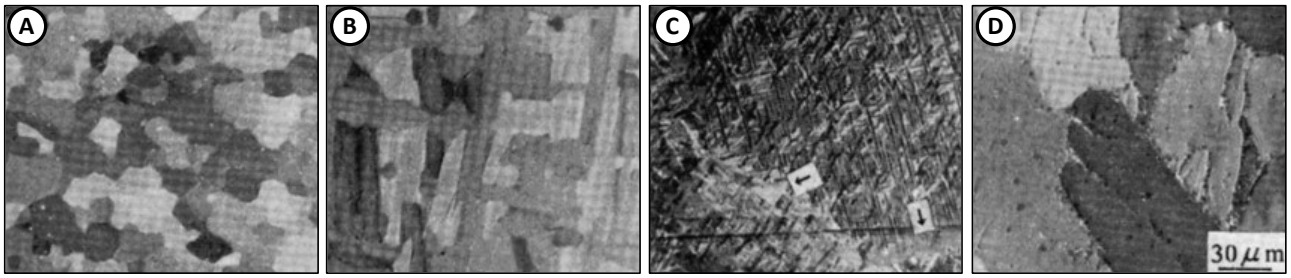


Figure 1 - α phase microstructures in Zircaloy-4. Optical micrographs showing (A) equiaxed α microstructure – as received Zircaloy-4 sheet; (B) α lath microstructure after water quench from β (cooling rate 1200 °C/s); (C) α lath microstructure after air cooling from β (cooling rate 3.66 °C/s); (D) α lath microstructure after slow furnace cooling from β (cooling rate 0.05 °C/s). Reproduced with permission of Taylor & Francis [14].

Typically, equiaxed α is preferred for nuclear fuel cladding applications, with fine (10-20 μm) grain size and split basal texture (basal poles +/- 30 ° from the z axis). This texture and grain structure provide suitable mechanical properties, and furthermore the texture and grain structure can be selected to optimise the neutronics, radiation tolerance, creep, and corrosion resistance. The microstructure and texture can be altered by changing the processing route (see [15] for an overview of the process).

Lenticular, or lath α is formed when the Zr alloy is heated to the β-phase and cooled. The exact size and shape of the laths depend on the cooling rate (and chemical composition) and may form in a parallel plate or basketweave formation (for more details see section 2.2.2). Equiaxed grains can be formed through rolling lenticular α in the α or α+β phase field and recrystallising [15].

Other grain sizes can be produced using different processing routes, for example, Wang et al.[16] used high-pressure torsion (HPT) to create nanocrystalline (<100 nm) Zircaloy-4 samples. Conversely, large, blocky-α grains (>300 μm) can form after heat treatment (see section 2.4.1).

2.1.3.2 Crystallographic texture

The α phase Zr structure has a c/a ratio of ~1.6 [17] forming a 'squat' unit cell and together with D-block bonding, this results in anisotropic properties that depend on the orientation of the unit cell. The crystallographic texture of the material is controlled by the thermomechanical processing route. In the HCP α phase, the <c> axis direction is important as this controls performance in the reactor (e.g. the neutronics, thermal expansion) and the <a> axis texture can be important for plastic deformation and failure mechanisms. For these reasons, the texture of the final Zr product is very carefully controlled for reactor components.

To describe the <c> axis texture often the Kearns' factor, f, is used [18], [19]. This is a way to measure the volume fraction of basal poles (<c> axis) in each of the principal directions (e.g. in a tube f_r, f_θ, f_z). A strong basal texture would approach 1 in the given direction, whilst a random texture would give a value of 1/3 in

each of the principal directions [19]. Example Kearns' factors for Zircaloy-4 sheet are: f_{ND} 0.56; f_{RD} 0.05 and f_{TD} 0.39 [20]. The Kearns' factor can be used to describe texture for multiscale reactor component performance codes (e.g. [21]).

2.1.3.3 Secondary phase particles (SPPs)

There are small secondary phase particles (SPPs) formed in Zr alloys from the alloying elements and/or impurities present. SPPs are usually less than 1 µm in diameter and dispersed throughout the material. Due to the small size and distribution of SPPs, characterisation has proven challenging. Techniques described in the literature to characterise the SPPs and their distribution have included optical microscopy, X-ray diffraction (conventional and synchrotron), electron energy loss spectroscopy (EELS) and TEM [22]–[26]. Sample preparation has included ion thinning and the use of extraction replicas [22], [23], [27].

The composition of the SPPs depends on the alloy, for example, in Zircaloy-4 the SPPs tend to be Fe or Cr rich, of the form $Zr(Fe,Cr)_2$ laves phases, whereas in Zircaloy-2, $Zr_2(Ni, Fe)$ tend to be found due to the higher Ni content [25]. Due to minor impurities, other SPP compositions found in Zircaloy-4 have included zirconium carbide (ZrC), zirconium phosphide (ZrP) and silicon [23]. A detailed list of commonly identified SPPs in Zircaloy-2 and Zircaloy-4 is found in Table 4.

Table 4 - SPPs in Zircaloys. SPP phases and structures identified in Zircaloy-2 and Zircaloy-4 in three different studies [22], [23], [27].

Zr alloy	SPP Phase	Structure	Lattice Parameters		Reference
			a (Å)	c (Å)	
Zircaloy-2	$ZrCr_2$	Hexagonal	5.079	8.279	[27]
	Zr_2Ni	Tetragonal	6.499	5.270	
	$ZrFe_2$	Cubic (Cu_2Mg type)	7.070	-	
	Zr_4Sn	Tetragonal	6.900	11.10	
Zircaloy-4	$ZrCr_2$	Hexagonal	5.079	8.279	[22]
	ZrC	Cubic – FCC	4.698	-	[23]
	ZrP	Cubic – FCC	5.242	-	
	Si	Cubic	5.430	-	

SPPs are important for nuclear fuel cladding as they strongly affect corrosion resistance [24]. Furthermore, hydrogen pick up is affected by the presence of SPPs and the ability of the SPPs to accommodate or transport H, particularly through the cladding oxide layer for nuclear fuel cladding.

From experiments, Annand et al.[26] studied the corrosion of $Zr(Fe,Cr)_2$ and Zr_2Fe SPPs in Zircaloy-4 using STEM imaging and DualEELS, focussing on shape and composition changes. They found that Zr_2Fe particles oxidise uniformly whereas $Zr(Fe,Cr)_2$ particles begin as faceted structures but oxidise to elongated shapes, with strong segregation of the elements into three regions. These are (1) a Cr rich region; (2) a Zr,Cr nanocrystalline region with very low Fe content and (3) metallic α-Fe veins with low O content. Annand also concluded that Zr_2Fe particles tend to lead to cracking in the vicinity due to the higher volume expansion

compared to the surrounding (ZrO_2) matrix, causing localised tensile strains. Conversely, $Zr(Fe,Cr)_2$ particles may leave small voids or cracks due to incomplete oxidation of the Fe rich region that remains after oxidation which results in a lower volume expansion than the matrix.

From simulations, Burr et al. [25] propose that the intermetallic $Zr(Cr,Fe)_2$ phases found in Zircaloy-4 will aid the migration of H through the oxide layer and aid H ingress into the material, even if the SPP itself is not readily available to accommodate H. The industrial development of Zircaloy-4, and the chemical composition as evolved from Zircaloy-2, resulted in a Zircaloy-4 having a maximum concentration of max 0.007 wt% Ni (see Table 2). This makes it interesting that Burr et al. find that the $Zr_2(Fe,Ni)$ phases accommodate H more readily than the α-Zr and at the Ni-rich SPPs H is trapped and stopped from migrating through the cladding oxide layer.

The presence of SPPs also affects the β→α transformation microstructure – see section 2.2.2.1 .

2.2 Phase transformation (β to α)

Zr alloys have an allotropic solid state phase transformation between 800-900 °C (depending on composition of the alloy) as shown in the Zr-H phase diagram in Figure 2. This phase transformation is between the high temperature β phase, which has a body centred cubic (BCC) crystal structure and the low temperature α phase, which has a hexagonal close packed (HCP) crystal structure.

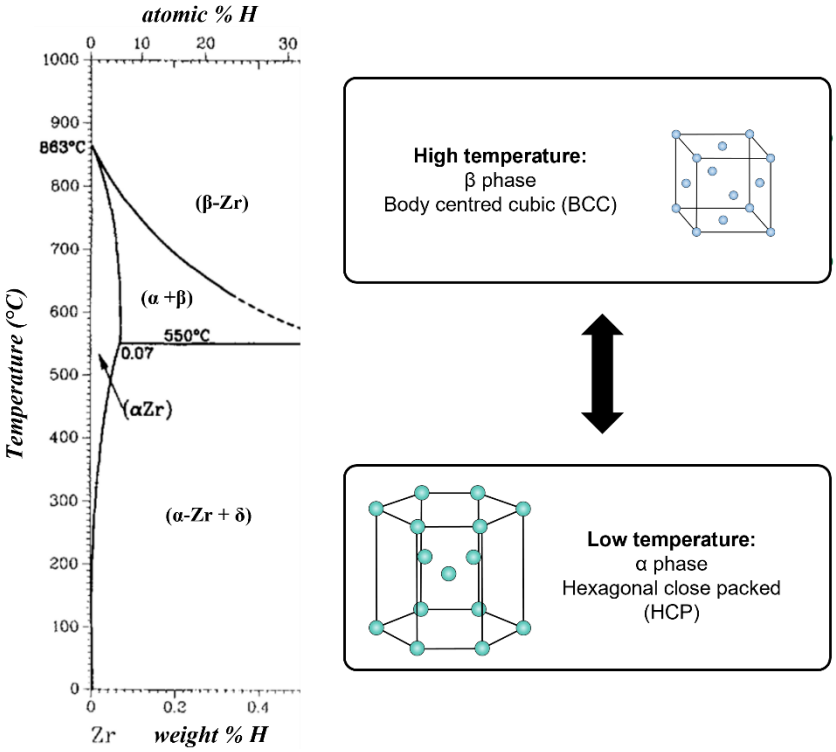


Figure 2 - Phases in Zr alloys. Excerpt from Zr-H phase diagram[28] *showing the high temperature β phase and low temperature α phase crystal structures. Phase diagram reproduced with permission of Springer Nature.*

2.2.1 Burgers orientation relationship (BOR)

Burgers reported on the body centred cubic to hexagonal close packed orientation relationship (OR) in zirconium [13] that had been previously reported by Vogel and Tonn [29] using X-ray rotation photograph

examination (which would now be called a variant of X-ray Laue diffraction) of very large zirconium crystals. In modern materials science, this OR is the so called "Burgers orientation relationship" (BOR). This transformation is important to understand the processing and performance of titanium, zirconium and hafnium alloys, which all have the allotropic phase transformations for high atomic fractions of the base metal in the alloy. BOR (as reported by Burgers [13]) is detailed at equation (1) and shown schematically in Figure 3.

$$(0001)_\alpha // \{110\}_\beta \text{ and } \langle 11\bar{2}0\rangle_\alpha // \langle 1\bar{1}1\rangle_\beta \quad (1)$$

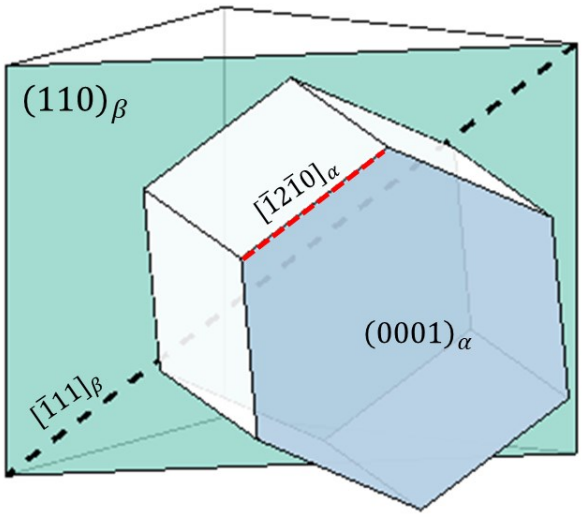


Figure 3 - BOR schematic showing an example where $(0001)_\alpha$ (blue hexagonal plane) and $(110)_\beta$ (green plane in the cube) are parallel and $[-12-10]_\alpha$ (red dashed line) is parallel with $[1-11]_\beta$ (black dashed line). Adapted from [30].

2.2.2 β quench microstructure

When Zr alloys are heated above the β transus (~865 °C in Zircaloy-4 [9]) and cooled, a number of β quenched microstructures can form. These range from a martensitic microstructure at high cooling rates (>2000 °C/s [31]) through to lenticular α at very slow cooling rates (<0.5 °C/s[32]). Between these two extremes, there are two main microstructures, basketweave and parallel plate, as shown in Figure 4.

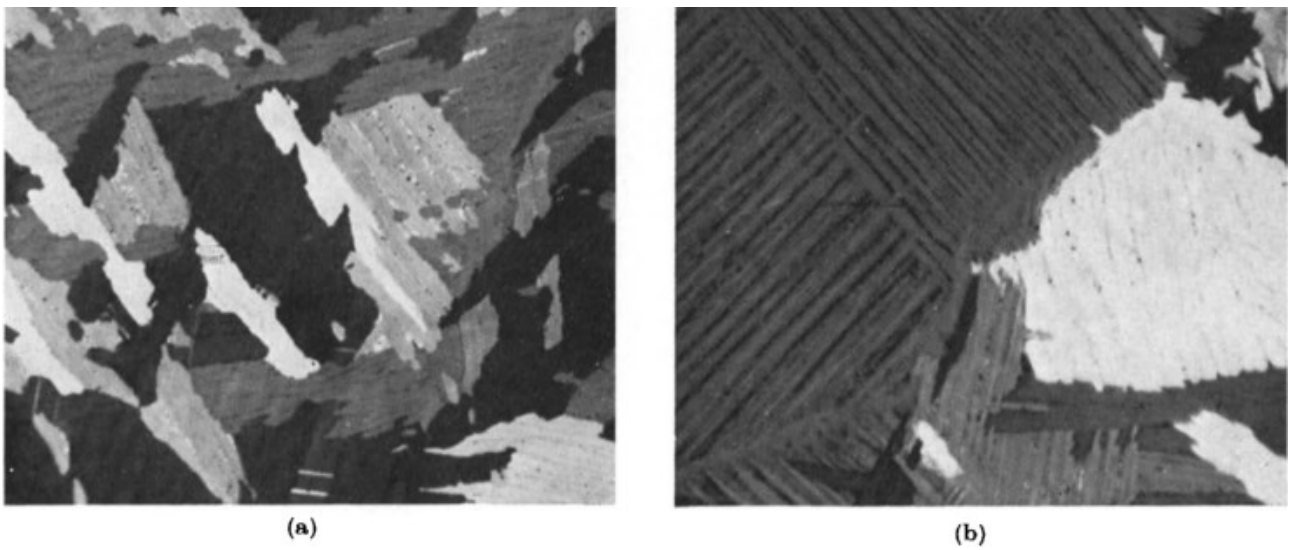


Figure 4 - Basketweave vs. parallel plate microstructures . Micrographs showing (a) basketweave and (b) parallel plate microstructures in Zircaloy-4 at 250x. Reproduced with permission of Elsevier [31].

A description of the microstructures and approximate cooling rates required (from Perez et al. [32]) are detailed in Table 5. Between the cooling rates stated, a mixture of the two microstructures forms [32]. This should be seen as a guide as the microstructure is also impacted by factors such as the presence of secondary phase particles and oxygen content.

Table 5 - β→α microstructures in Zircaloy-4. The 4 main transformation structures when cooling from β, as described by Woo et al.[33]*, with cooling rates defined by Perez et al.*[32]*. Based on table 2 in* [33]*.*

Structure	Description	Cooling rate (K/s)
Martensite α	Needle-like structure similar in appearance and mode of formation as ferrous martensites, formed by diffusionless transformation	≥ 1500
Basketweave α	Non-parallel structure of Widmanstätten α, resulting from random precipitation of α plates on a number of planes in one β grain	600-10
Parallel plate α	Widmanstätten α structure formed on one habit plane of prior-β	2-0.5
Lenticular α	Coarse plate-like structure with irregular and jagged boundaries, formed by slow cooling	≤0.5

2.2.2.1 Secondary phase particles (SPPs) and β-phase transformations

Several papers suggest that secondary phase particles act as nucleation points for the basketweave microstructure [[23], [31], [34]]. Fong et al. [23] identified the SPPs as zirconium carbide, zirconium phosphide and elemental silicon using X-ray powder diffraction and TEM. They found that phosphorous containing particles were most prevalent.

Holt [31], who was unable to conclusively identify the SPPs, evaluated two Zircaloy-4 samples with slightly different chemical compositions (see Figure 5 A). Holt showed that for the same heat treatment, the SPPs could either act as nucleation points (see material A in Figure 5 B) or non-nucleating particles (see material B in Figure 5 B), resulting in basketweave and parallel plate morphologies respectively.

Ökvist et al.[34] found that the presence of higher carbon content (up to 130 ppm) in Zircaloy resulted in basketweave microstructure, after previously establishing the presence of zirconium carbides in the basketweave structure formed after brazing (1060 °C for 1 min and air cool). They suggest that these carbides act as nucleation sites for α phase growth during nucleation due to their location at the centre of groups of α laths, as seen in Figure 6. Looking at the compositions used in Holt's work [31] (see Figure 5), this would correlate well given the higher C content of material A. Note that Ökvist et al.[34] noted no correlation between structure and oxygen content, which is in direct contradiction of other work (see below) – this is likely due to the cooling rate used for their experiments.

(A) Chemical composition

Element	A	B	Element	A	B
Sn	1.38 %	1.76 %	N	29 ppm	18 ppm
Cr	0.100%	0.109%	C	153 ppm	58 ppm
Fe	0.169%	0.118%	H	19 ppm	12 ppm
Ni	45 ppm	40 ppm	Si	75 ppm	180 ppm
O	1480 ppm	1420 ppm	W	20 ppm	< 5 ppm
P	below limit of analysis		Mg	< 5 ppm	< 5 ppm

(B)

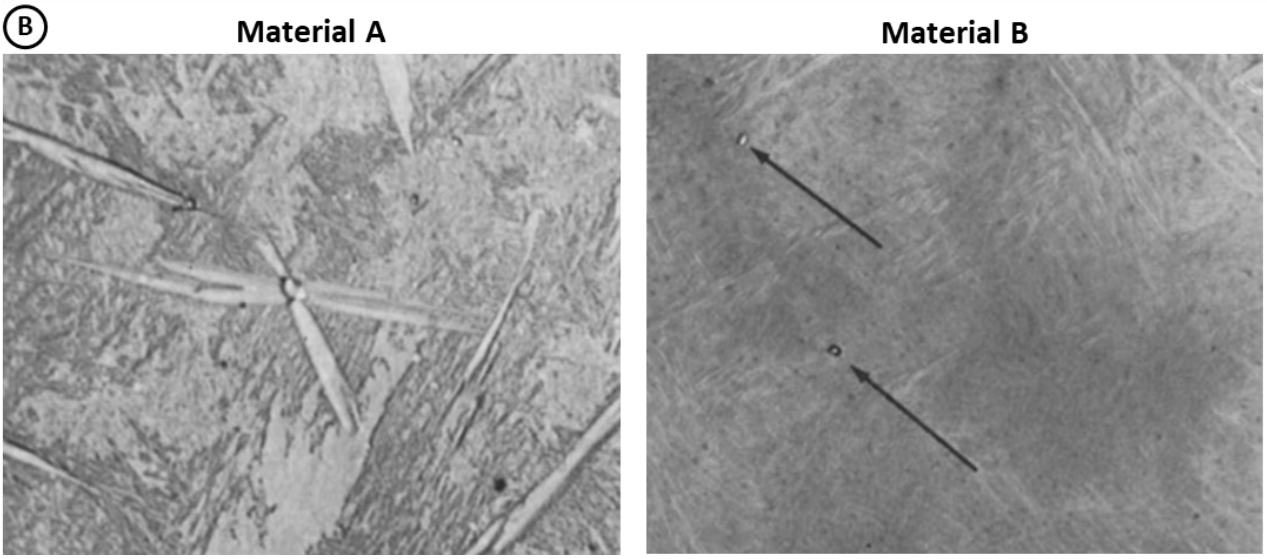


Figure 5 - SPPs in Zircaloy-4. (A) Chemical composition (by weight) of materials A and B. (B) Micrographs (x1000) showing material A, which has a basketweave morphology and shows the SPPs as nucleation points; material B, which shows a parallel plate morphology and the SPPs are non-nucleating. Heat treatment for both samples: 1050 °C for 30 mins, cooling at 11 °C/s for 10 s then water quenched. Reproduced with permission of Elsevier [31].

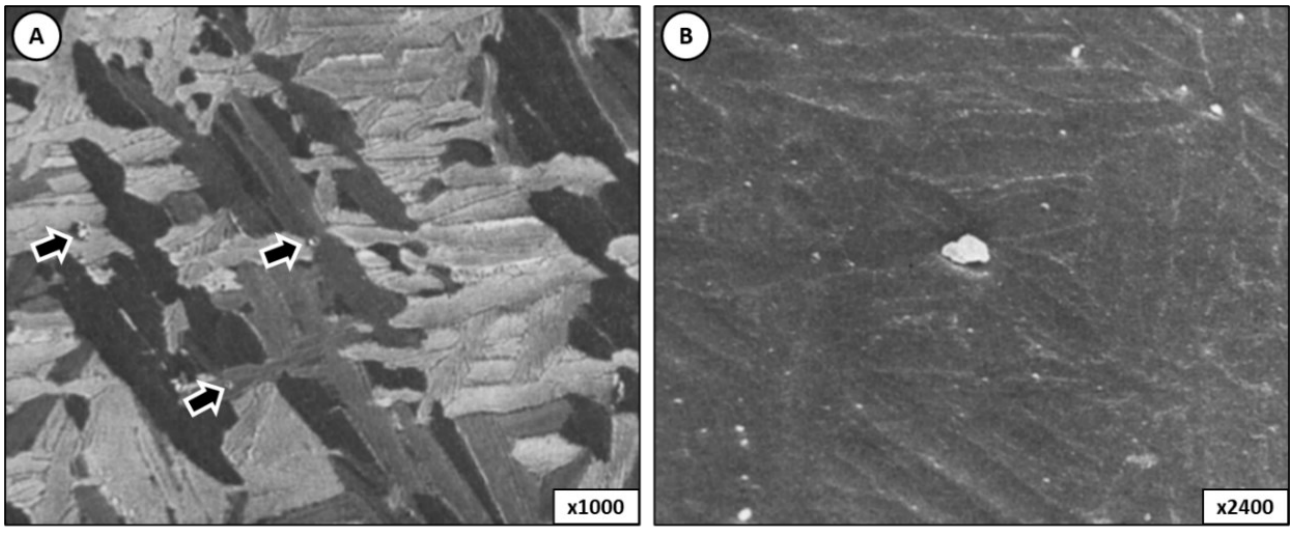


Figure 6 - Carbon content and basketweave morphology in Zircaloy. (A) β heat treated Zircaloy with basketweave microstructure – arrows indicate the position of small particles; (B) zoomed in view of a particle at the centre of a bundle of α laths, later identified as zirconium carbide. Reproduced with permission of Elsevier [34].

2.2.2.2 Oxygen content

Sawatzky et al.[35] found that α lath width increases with oxygen concentration, which they suggest is due to precipitation occurring at a higher temperature and diffusion rate. For 0.4-1.1 wt% O, when cooled from 1475 °C to 900 °C at between 0.4 and 160 °C, they observe a parallel plate morphology, but they do not state the cooling rate after 900 °C so it is hard to contextualise their results.

Woo et al.[33] carried out a detailed investigation of the effect of oxygen content and cooling rate on microstructure for Zircaloy-4 samples. Samples contained an oxygen content in the range 0.13-0.91 wt% and were tested at cooling rates of 90-2000 °C/s. They found that for a constant cooling rate (90 °C/s), increasing the oxygen concentration promotes parallel plate formation and reduces martensitic content. An example of their results is shown in Figure 7 combining α lath width, oxygen content and cooling rate. They go on to assert that the α lath width alone is sufficient to determine the cooling rate used – for details see [33].

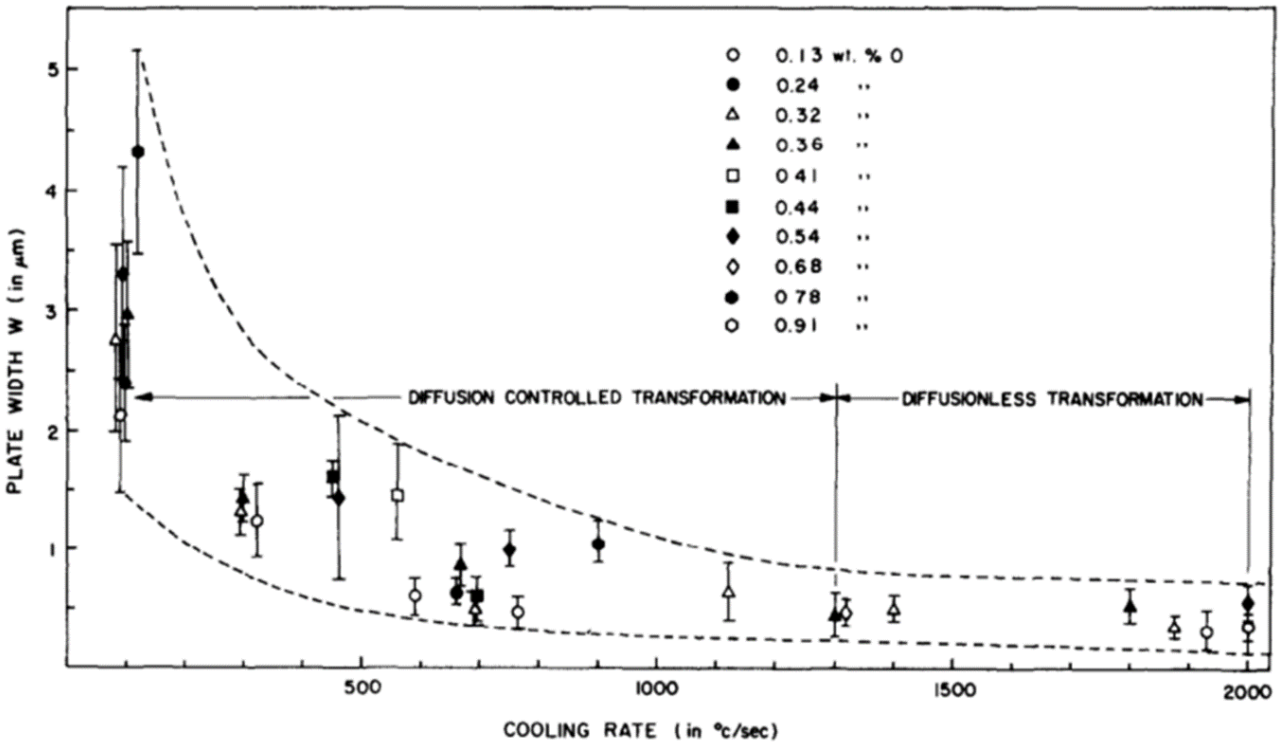


Figure 7 - Effect of oxygen concentration and cooling rate on plate (α lath) width. Reproduced with permission of Elsevier [33].

Cooling rate and α lamella width was later modelled by Massih et al.[36] at slower cooling rates in the range 0-90 Ks^{-1} ,as shown in Figure 8. The data used was a combination of their earlier work with Zircaloy-2 [37] and data from Woo et al.[33] for Zircaloy-4. This work indicates that a minimum lamella width of 1 µm can be achieved for very fast cooling rates in their work (>50 Ks^{-1}), and a lamella width of 2-5 µm can be achieved for cooling rates between 10 and 40 Ks^{-1}.

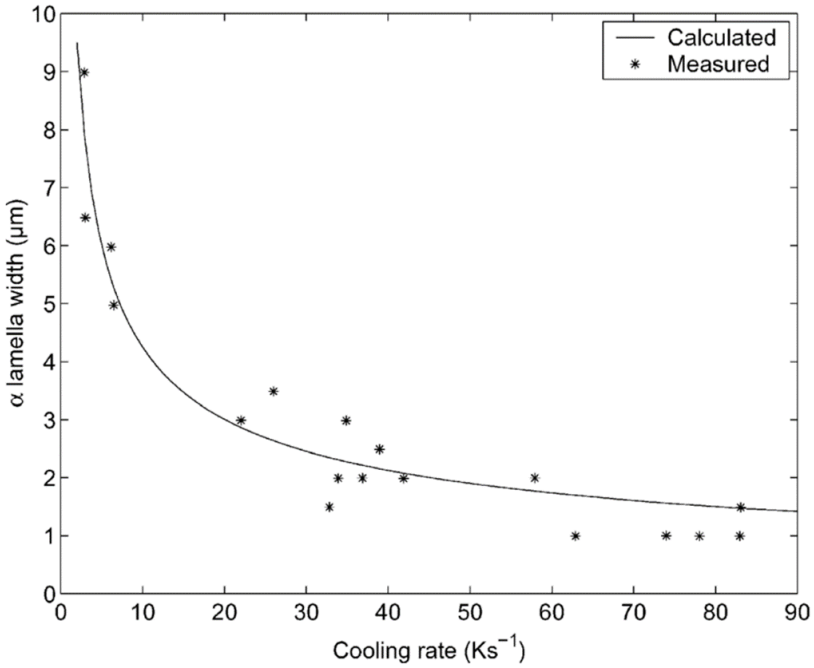


Figure 8 - Effect of cooling rate on α lath width for cooling rates 0-90 Ks^{-1}. Reproduced with permission of Elsevier [36].

2.2.2.3 β grain size

Prior β grain size is affected by peak temperature and duration at temperature as is illustrated in Figure 9. Jung et al. [38] found that the prior-β grain size approximately doubled from ~90 to ~180 μm when the peak temperature increases from 1000 to 1200 °C (see Figure 9 A). Their experiments used Zircaloy-4 cladding tube samples with a hold time of 30 s at max temperature and a cooling rate of 25 °C/s. Interestingly, they also noted a small change in α lath width (2 to 2.5 μm) when the peak temperature was increased in this range, as also shown in Figure 9 A.

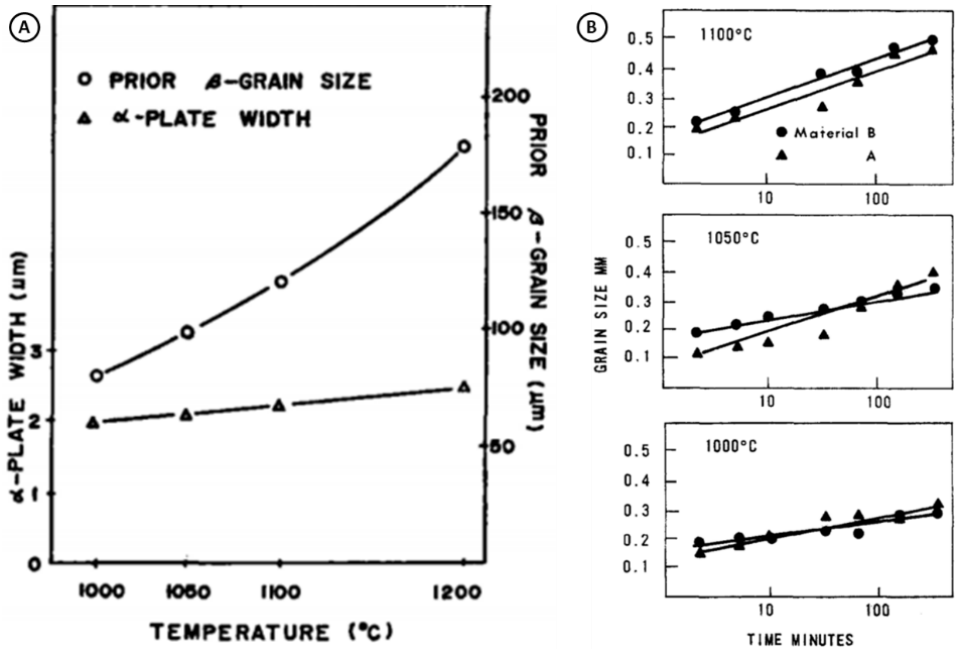


Figure 9 - Prior β grain size - relationship to maximum temperature and duration at temperature. (A) results for Zircaloy-4 fuel cladding samples at a peak temperature of 1000-1200 °C, with a 30s hold time and a cooling rate of 25 °C/s. Reproduced with permission Taylor & Francis [38]*; (B) results for Zircaloy-4 cladding using a maximum temperatures of 1000 °C, 1050°C and 1100 °C with different hold times and air cooled, for two Zircaloy-4 samples. Reproduced with permission of Elsevier* [31].

Holt [31], [39] also investigated the impact of maximum temperature on prior-β grain size, but with the added factor of hold time, as shown in Figure 9 B. The two Zircaloy-4 compositions used (material A & B) are detailed in Figure 5 A. The hold times were varied from 2-480 mins for peak temperatures of 1000-1100 °C followed by air cooling. The general trend is increasing prior-β grain size with both peak temperature and increased hold time. Minimal difference is seen in β grain size between the two material compositions A and B, except at 1100 °C where material B exhibits slightly larger grain sizes.

Comparing Holt [31], [39] and Jung et al.'s [38] results, the duration at peak temperature might be used to explain the lower prior-β grain sizes for the same peak temperatures, as Jung et al. used 30 s whereas Holt started at 2 mins. The Zircaloy-4 composition used in Jung's work is closer to material A which would fit reasonably well given that this generally exhibits smaller β grain sizes for short hold times in Holt's work.

It should be noted that in Holt's follow up comments paper [39], after revaluating the data and repeating the experiments with material from the same batches, Holt stands by the trends of increasing prior-β grain size with both peak temperature and increased hold time. However, Holt suggests that due to issues identifying prior-β grain boundaries, the β grain sizes in his original paper (and Figure 9 B) were overestimated. Holt also states that the β grain size of material B was generally larger than material A at the lower temperatures (1000 & 1050 °C).

2.3 Welding

Due to their use in the nuclear industry, Zr alloys are often joined using welding for applications such as fuel channels, fuel rod end plugs and spacer grids. Often the welds must be gas tight, with limited change in properties around the weld (due to the nature of property optimisation of the base metal). Very clean and precise welds are required, so fusion welding techniques are often chosen. The main fusion welding techniques used are tungsten inert gas (TIG) welding, electron beam (EB) welding and laser beam welding (LB) [40]. This section focuses mainly on EB welding as this was used to prepare some of the samples in this thesis.

2.3.1 Electron beam (EB) welding

EB welding is a high energy density fusion welding process that results in deep, small diameter welds [40], [41]. The process involves bombarding the surface with a focussed beam of high velocity electrons, leading to localised heating and sample melting [40], [42]. It is carried out in a vacuum to prevent dispersion of the electron beam, which also results in a clean weld without contamination from air. EB welding is suitable for high aspect ratio welds with a small heat affected zone (HAZ), and maintains up to 95 % of the strength of the base material [42], [43]. Welding of Zr-alloys is often highly automated, leading to precise and repeatable welds, however this results in high setup costs.

2.3.2 Weld microstructures

Generally, weld microstructures contain two regions, the fusion zone, where the melting temperature of the material has been exceeded, and the heat affected zone (HAZ) where the temperature has not caused

melting but has caused microstructural changes. This is shown schematically in Figure 10 where the effect on the grain size across the region is also indicated.

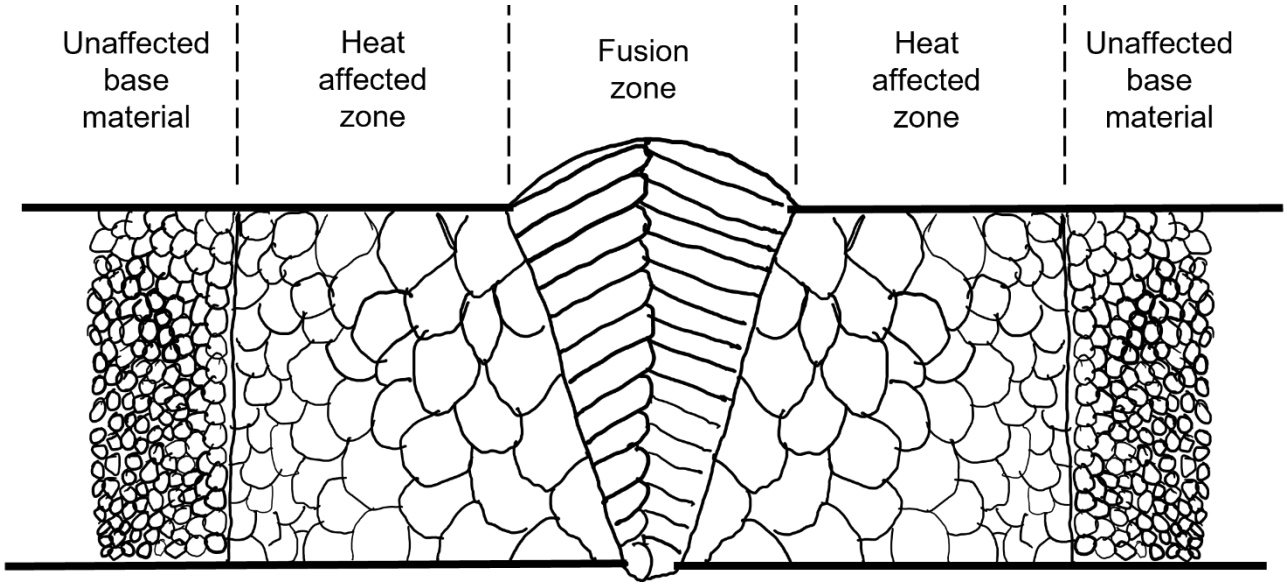


Figure 10 - Weld microstructure overview. Schematic showing typical weld microstructure with distance from centre of weld - Redrawn from [40].

The fusion zone cools quickly in EB welds, leading to either a Widmanstätten or parallel (α) lath microstructure depending on cooling rate and alloy content[32], [44]. These lath regions are often organised into columnar grains angled out from the weld centreline[41].

The HAZ may contain multiple grain sizes across the region as the heat decreases [44], particularly if there is a phase transition temperature to cross, as in the case of Zircaloy-4, where the outer edge of the HAZ may not reach temperatures above the β transus [44]. The size of the HAZ depends on the level of thermal diffusivity (which is a combination of factors including thermal conductivity, density, input heat, and welding speed) [45] and for some materials and conditions may not exist, instead transitioning straight from the fusion zone to the bulk material [46]. In general, a faster cooling rate leads to a smaller HAZ.

2.3.3 Example microstructures

Figure 11 shows an example of how the microstructure changes across an EB weld in Zircaloy-4. In this work, Parga et al.[43] show three distinct microstructures: (A) the weld (fusion) zone, which in their case contains Widmanstätten structures within columnar prior-β grains, and alloying-element-rich regions between the laths. (B) the HAZ, which has larger grains, which are generally coarse needles. (C) base metal, which contains fine equiaxed grains. For a further example, see section 2.6.4 which shows an EB weld closer to that used in this work.

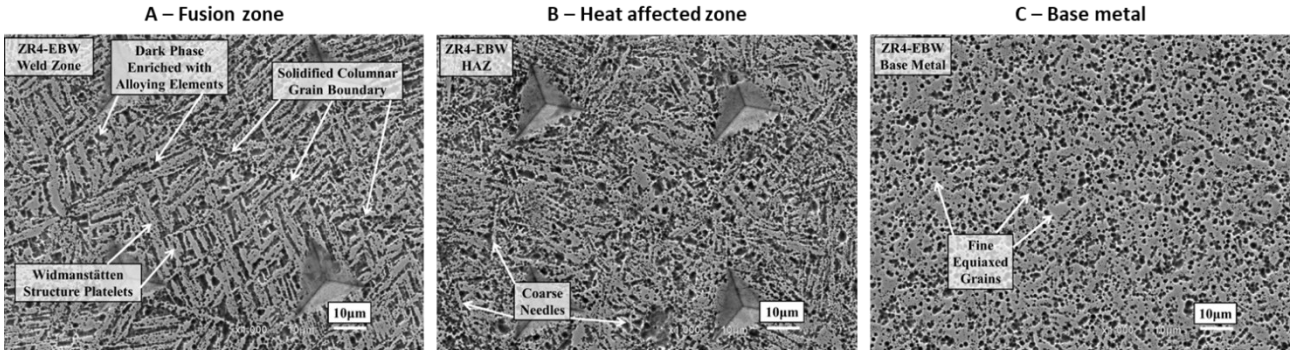


Figure 11 - EB weld microstructure example. Secondary electron micrographs showing (etched) Zircaloy-4 microstructures at different points across the weld. A: weld/fusion zone with Widmanstätten microstructure; B: HAZ with larger and morphologically different grains to the base metal (shown in C). Reproduced with permission of Elsevier [43].

2.4 Challenges

Despite their continued use over the past 75 years, there remain a few key challenges for Zr alloys, including blocky-α grain formation (abnormal grain growth) and hydride formation.

2.4.1 Blocky-α

The formation of large, so called 'blocky-α', grains (>300 μm with irregular and wavy boundaries [47], [48]) in Zr alloys are detrimental to performance of the components. In most cases, where Zr alloys are used in the nuclear industry, components have a fine, uniform grain size and controlled texture. The presence of large grains can detrimentally affect properties such as yield stress [49], thermal expansion [50] and strength [49]. Blocky-α grains area a particular safety issue for thin-walled components, where the size of the blocky-α grains can approach the wall thickness. For example, nuclear fuel cladding is approximately 600 μm thick and blocky-α grains of ≥500 μm have been seen in some experiments [48].

Blocky-α grain formation has been observed after heat treating strained material [47], [48], [51], weld microstructures [44], [52] and β-quenched Zircaloy-4 [53].

2.4.1.1 Strained material

Blocky-α grain growth has been systematically observed in strained Zircaloy-4 after heat treating at > 700 °C for 1-336 hrs [48], [51]. Washburn [51] showed that grain growth occurred in material strained from 2-10% when heat treated at 800 °C (see Figure 12 A where some of the data has been replotted by Tong [48]). The highest grain growth (approaching 500 μm) was seen at low strain (2%), but more time was required for this to occur, whereas at higher strains (8-10%) growth occurred rapidly but was limited (< 100 μm). Tong et al. [48] used a three point bend sample to produce a range of strains across the cross section and then heat treated this at 800 °C for 336 hrs to grow blocky-α. The resulting microstructure is shown in Figure 12 B, where in agreement with Washburn's results, the largest growth is seen in the low strain regions near the neutral axis, with small grains remaining in the high strain regions at the edges.

An outcome of Tong's work [48] was the creation of a heat treatment (800 °C for 2 weeks) to transform as received, fine grain α, Zircaloy-4, to a blocky-α microstructure. This allows samples with large grained

(blocky-α) microstructures to be systematically tested, for example with respect to hydride formation [54], [55] or crack growth [56].

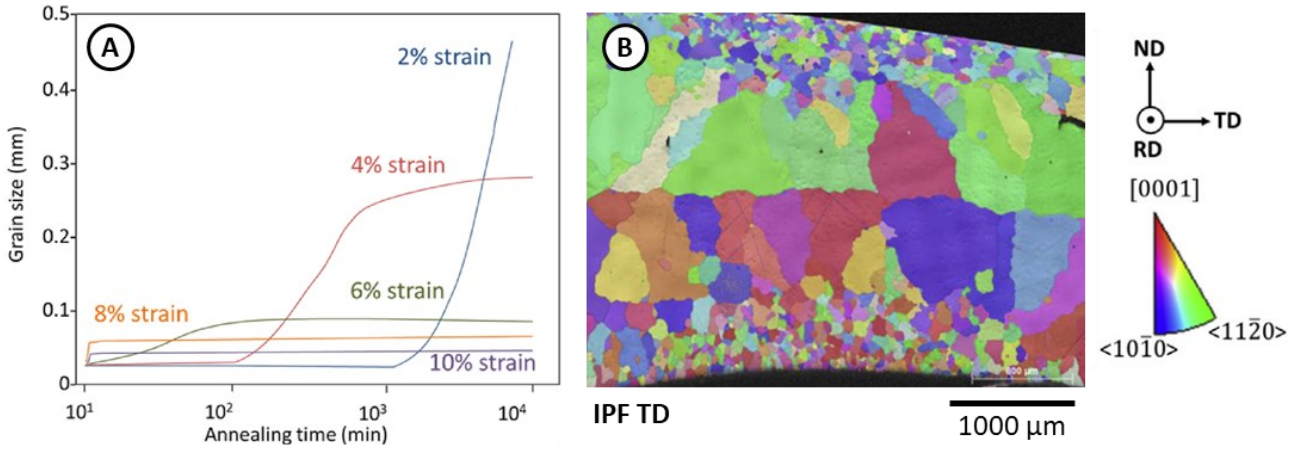


Figure 12 - Strain and grain growth. (A) Grain size vs. time for 2-10% strain at 800 °C showing the highest grain growth at lower strains but taking the longest time to transform [48], [51]*; (B) Blocky-α grain growth in a 3 point bend sample that was bent to 550 N and heat treated for 336 h at 800 °C - the largest grains are in the lower strain regions near the centre of the sample. Licensed under creative commons CC BY 4.0 – Figure 1(a) and extract from graphical abstract*[48]*.*

2.4.1.2 Blocky-α in welds

Welding Zr alloys heats the sample locally to above the β transition temperature, and cools rapidly leading to β quenched microstructures. Two examples of blocky-α grain growth after welding are detailed below.

Taylor et al. [44] investigated grain growth in the heat affected zone of electron beam welded Zircaloy-4. They found that blocky-α grain growth began in the HAZ after 0.5 hr at 760 °C and this region was fully transformed in 1 hr, as shown in Figure 13. More discussion of this work is found in section 2.6.4 .

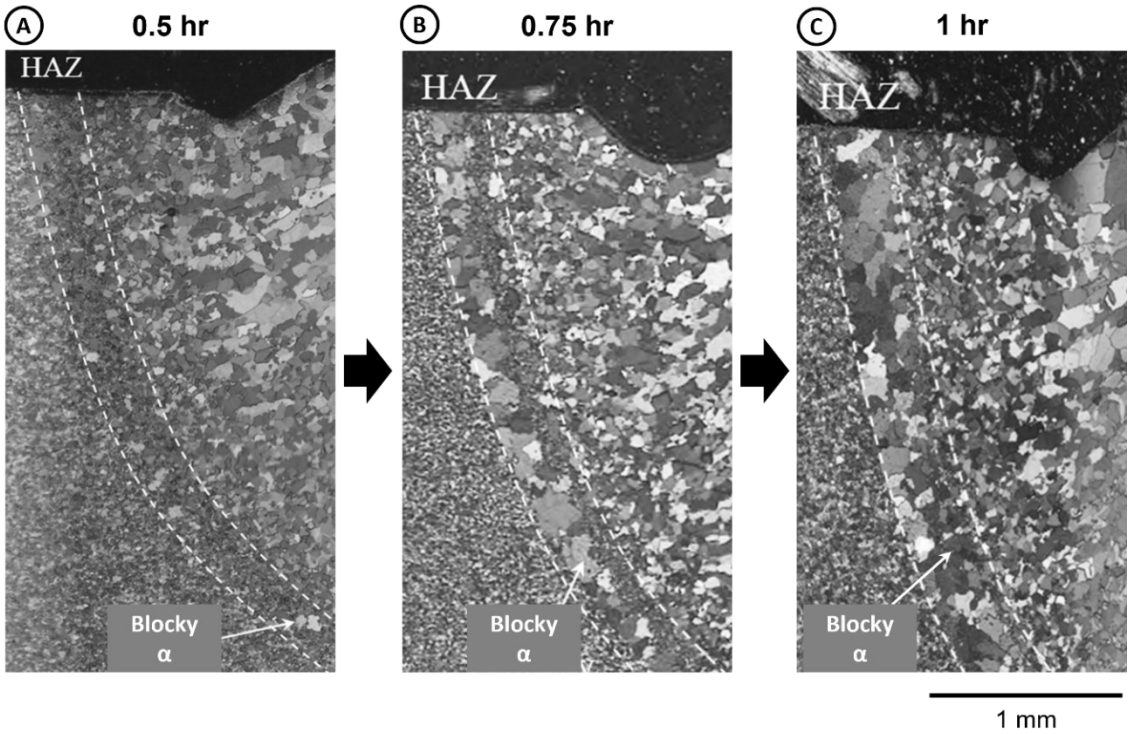


Figure 13 - Blocky-α grain growth in electron beam welded Zircaloy-4. Optical micrographs showing blocky-α grain growth within the heat affected zone (HAZ) after (A) 0.5 hr, (B) 0.75 hr and (C) 1 hr at 760 °C. Reproduced with permission of Springer Nature [44]*.*

Echols et al. [52] used a TIG welded Zircaloy-4 sample for their post weld heat treatment investigation. They only saw blocky-α grain growth in the HAZ in some (not all) cases after heat treating for >18 hrs at 800 °C. Grain growth was not observed in the fusion zone for these samples. An example microstructure is shown in Figure 14 A for a tensile sample heat treated at 800 °C for 48 hrs, with blocky-α only present in the HAZ. In their tensile experiments, they found that when blocky-α grain growth was present in the HAZ, this became the failure point as shown in Figure 14 B.

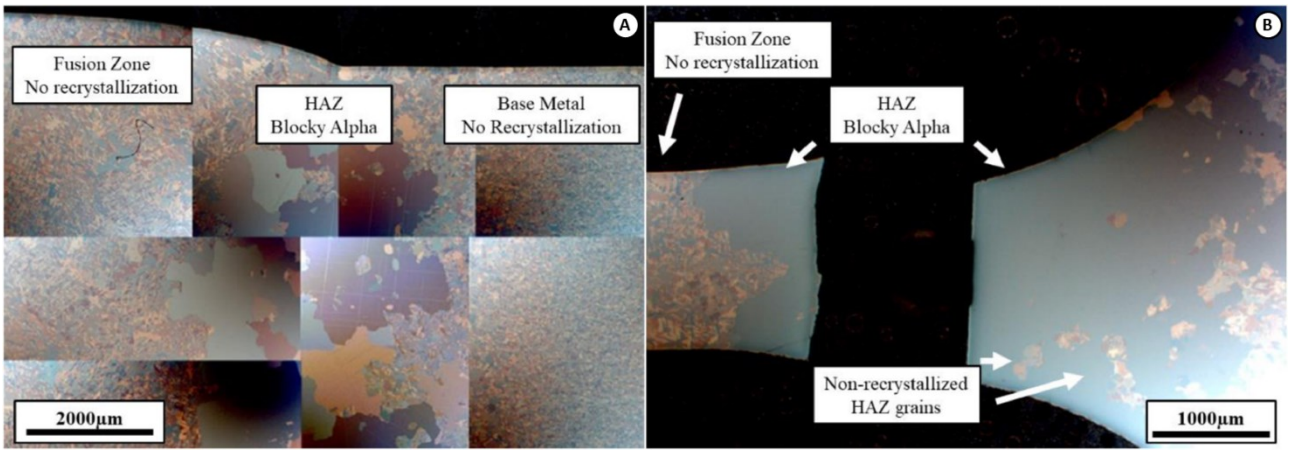


Figure 14 - Blocky-α growth in TIG welded Zircaloy-4. (A) composite polarised light micrograph showing the fusion zone, HAZ and base metal for a tensile sample after 48 hrs at 800 °C – only the HAZ contains blocky-α. (B) tensile testing failure in the blocky-α region (HAZ) of the sample. Reproduced with permission of Elsevier [52].

2.4.1.3 β quenched material

Loucif et al. [53] evaluated the impact of aging at temperatures between 100 and 750 °C on β quenched Zircaloy-4 microstructures using thermoelectric power measurements (as demonstrated in [57]). As seen in Figure 15 they observed grain growth (defined as recrystallisation in the paper) after heat treating at 650 °C for 2-72 hrs. Four different quench rates were investigated as part of this study, from water (fast) to argon (slow). The β quench rate was found to significantly impact onset of recrystallisation, from 600 mins for the water quenched samples to 2500 mins for the argon quench when heat treated at 625 °C.

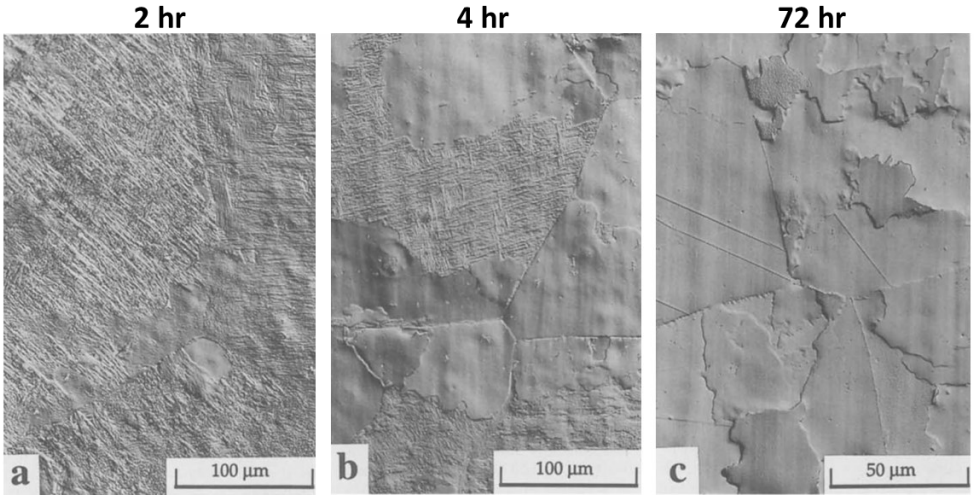


Figure 15 - Aging β quenched Zircaloy-4. Optical microscopy of β quenched (in water from 1030 °C) samples aged at 650 °C for (a) 2 hrs (b) 4 hrs and (c) 72 hrs. Large grains form along what appear to be prior-β grain boundaries and eventually fill the whole region. Reproduced with permission of Elsevier [53].

2.4.1.4 Growth mechanism

The mechanism proposed for the formation of blocky-α grains is nucleation, via strain induced grain boundary migration (SIBM), and growth (see Figure 16) [48]. SIBM is a nucleation method for recrystallisation that does not require the creation of new nuclei [58], [59]. Instead, the existing grain boundary bulges into an area of high stored energy, leaving behind it a region of lower strain with the same orientation of the original grain [48], [58]. Once nucleated, this grain grows to consume the adjacent grain (that it bulged into), and then further adjacent grains.

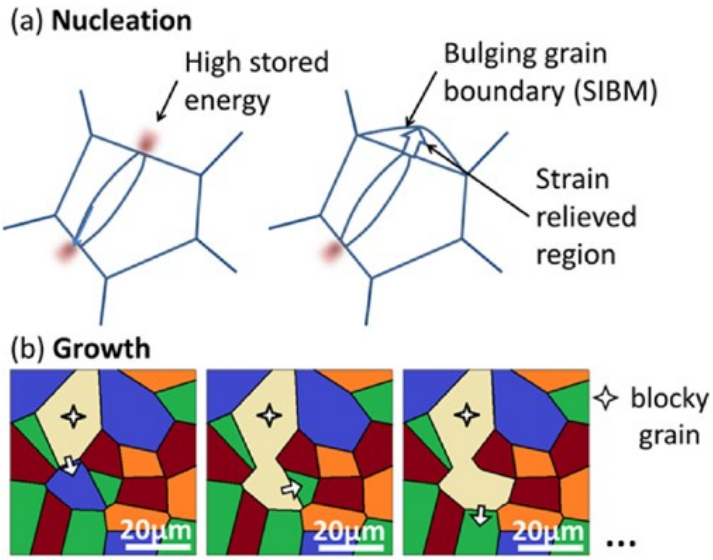


Figure 16 - Blocky-α growth mechanism. The process has two parts (a) nucleation – a grain boundary bulges via strain induced boundary migration (SIBM) into local regions of high strain energy (b) growth – the grain grows into adjacent grains by consuming each grain in turn. Licensed under creative commons CC BY 4.0 – Figure 8 [48].

2.4.1.5 TTT diagram

Attempts to capture and summarise the grain growth behaviour in β quenched/weld microstructures on a time-temperature-transformation (TTT) diagram have been made by Taylor et al. [44], Loucif et al.[53] and Echols et al.[52], the latter of which is shown in Figure 17. This would suggest that blocky-α grain growth is expected in timescales of ~1 hr at temperatures ≥700 °C, noting that the recrystallisation threshold temperature increases with slower quench times.

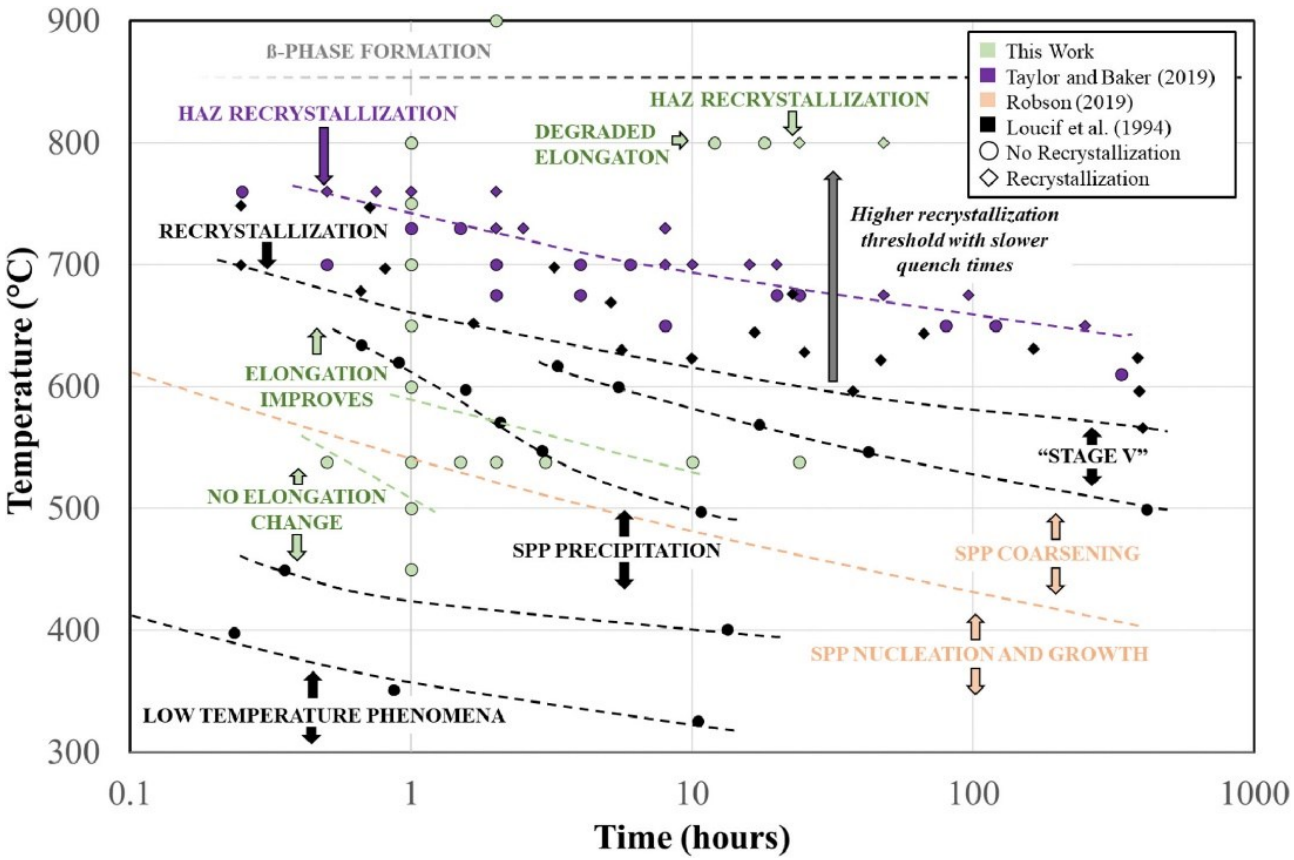


Figure 17 - TTT diagram for recrystallisation in β quenched Zircaloy-4. Combining data from Taylor & Baker[44] *for the HAZ of electron beam welds; Loucif et al.*[53] *for aging β-quenched Zircaloy-4; Echols et al.*[52] *for and Robson's simulation work on SPPs* [60]*. Reproduced with permission of Elsevier* [52].

2.4.2 Hydrides

The presence of hydrides within Zr alloys has a deleterious effect on the material properties. Hydrides are brittle (at all temperatures [61]), and cause a decrease in properties such as: fracture toughness, strength and ductility [62]. Hydrides and hydride metal interfaces can provide easy crack paths through the material. Furthermore, hydrides can reorient to align with their long axis perpendicular to the principal stress after a thermal cycle. This is important for delayed hydride cracking (DHC), where hydrides reorient under stress at crack tips leading to further cracking and failure, as discussed at section 2.4.2.5 .

2.4.2.1 Hydride formation

The zirconium-hydrogen phase diagram (Figure 18) shows that hydrogen has high solubility in zirconium at elevated temperatures (<50 at% at ~500 °C) but low solubility at room temperature (<1 at%) [62], [63]. This means that there is hydrogen ingress at in-service temperatures, and upon subsequent cooling this leads to the formation of hydride phases within the microstructure. For nuclear reactors, hydrides typically form due to the ingress and clustering of hydrogen in the fuel. Hydrogen is introduced from 3 sources: (1) the starting material; (2) hydrogen as a fission product; (3) hydrogen produced during corrosion of the cladding.

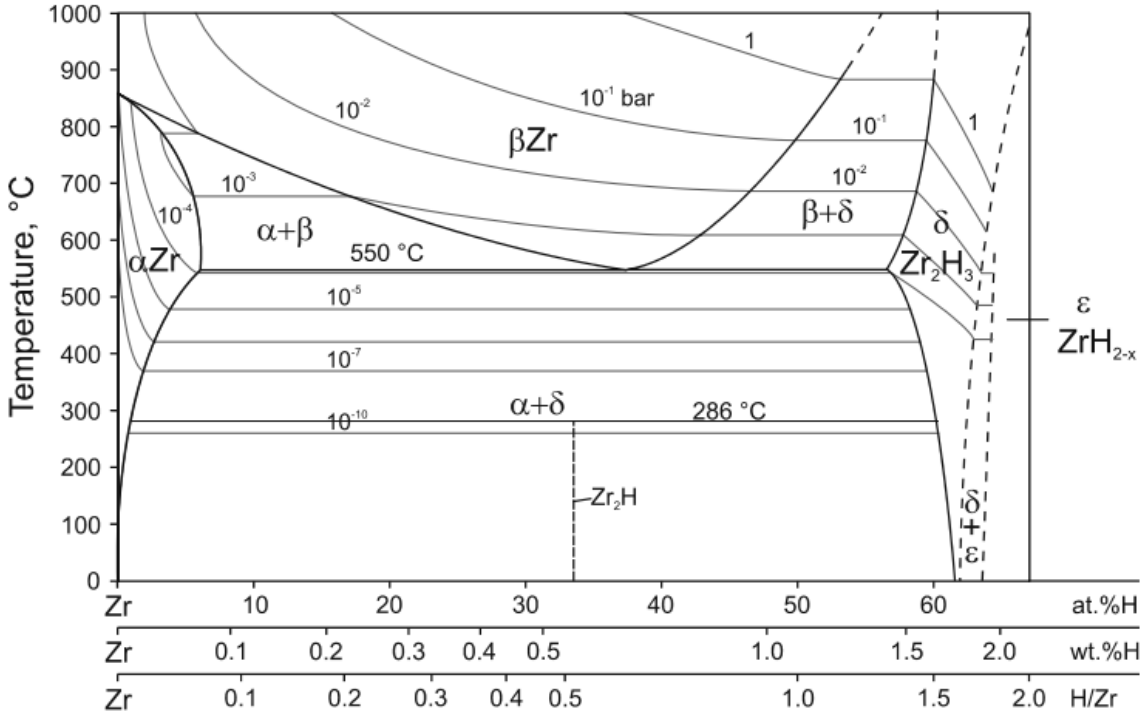


Figure 18 - Zr-H phase diagram including ambient hydrogen partial pressures isobars. Reproduced with permission of Springer Nature [64].

2.4.2.2 Hydride phases

There are four hydride phases observed: zeta (ζ), gamma (γ), delta (δ) and epsilon (ε), as detailed in Figure 19. These vary by stoichiometry and crystal structure have different effects on the mechanical properties, for example, there is a distinct drop in both young's modulus and yield strength with δ and ε phase hydrides but minimal effect for ζ and γ phases [65].

Hydride phase	Crystal structure	Lattice Parameters			Value of x in ZrH_x	
		a	c	c/a	Range	Most Common
Zeta (ζ)	Trigonal	3.300	10.290	3.12	0.25-0.50	0.50
Gamma (γ)	Tetragonal	4.586	4.948	1.08	~1.00	1.00
Delta (δ)	FCC	4.768	-	1.00	1.44-1.66	1.66
Epsilon (ϵ)	BCT	3.520	4.450	1.26	1.66-2.00	2.00

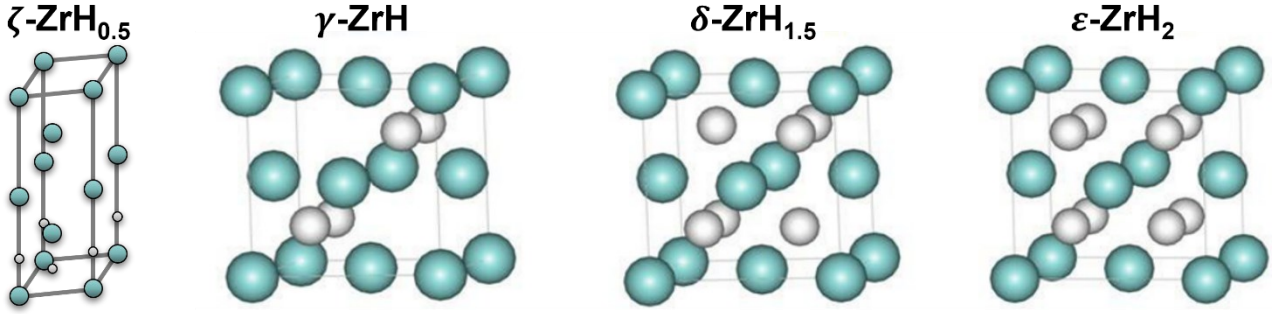


Figure 19 - Zirconium hydride phases. ABOVE: Table containing crystals structures, lattice parameters and stoichiometry for the four zirconium hydride phases [63], [66]–[69]*. BELOW: Relaxed crystal structure diagrams for each hydride phase – ζ hydride redrawn from* [70]*; γ, δ and ε hydrides reproduced from* [71]*. Larger green spheres represent Zr atoms, whilst the smaller grey spheres represent H atoms.*

As seen in Figure 18, δ and ε hydrides are stable, whereas γ and ζ hydrides are metastable phases and therefore not included. However, there has been some debate over whether the γ phase is stable or metastable [72], [73] so depending on the specifics of the experiment (e.g. cooling rate, microstructure) γ can be described as either stable or metastable.

2.4.2.3 Factors affection hydride precipitation

Factors affecting hydride precipitation include hydrogen content, temperature gradients, stress and cooling rate [63], [66]. Hydrides may form at the grain boundary or inside the grains, and often grow in chains of hydride known as 'stringers' (e.g. [54]) often containing twins [55]. The stringers, which macroscopically appear as long hydrides, are made up of smaller hydride packets that nucleate sympathetically due to the elastic strains associated [74], [75].

Temperature

Hydrogen is highly mobile [74] and will typically move down a temperature gradient, and so can accumulate in cold spots within the reactor. The effect of this is more pronounced with thermal cycling. The presence of these colder regions leads to areas with higher hydrogen content, resulting in phenomenon such as hydride blisters, hydride rims and concentrations of hydride axially within fuel pins as illustrated at Figure 20. The hydrides that form are typically δ phase or at very high concentrations (e.g. hydride rim outer edge or hydride blisters), ε phase. The consequence of these hydrides being formed is that they can reduce the mechanical performance of the fuel assembly, e.g. toughness reduces drastically [63].

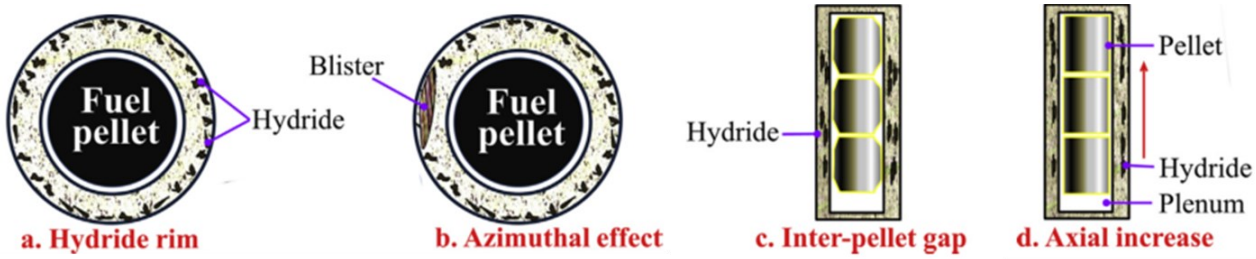


Figure 20 - Hydride redistribution as a result of temperature gradients. Reproduced with permission of Elsevier [63].

Cooling rate

The cooling rate affects the size of the hydride packets, hydride agglomeration, and nucleation site [54], [62], [76]. At high cooling rates (e.g. water quench), hydride packets are small and little agglomeration is seen [62]. Decreasing the cooling rate allows time for hydrides to agglomerate – this agglomeration tends to lead to the formation of long hydride stringers [20], where hydrides appear to nucleate on other hydrides, with a macroscopic orientation related to the texture. As the cooling rate is decreased, there is a switch from intragranular to intergranular hydrides. At the slowest cooling rates, grain boundaries become the preferred hydride nucleation sites [54], [76]. Figure 21 demonstrates the effect of reducing the cooling rate from water quench (fast) to furnace cool (v. slow), for two different grain sizes in Zircaloy-4 [54].

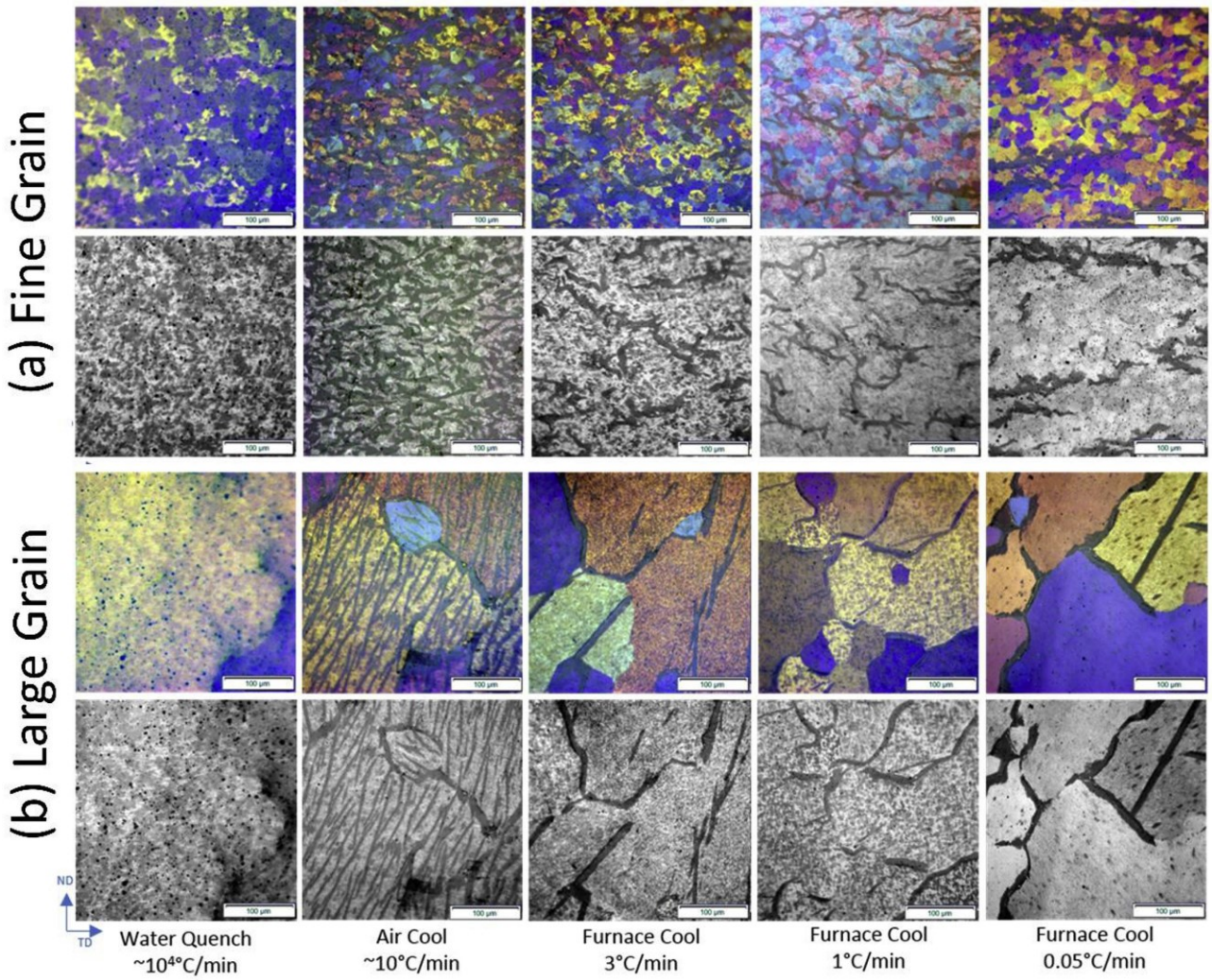


Figure 21 - Cooling rate and hydrides. Optical microscopy (polarised – rows 1 & 3 / normal – rows 2 & 4) showing the effect of varying the cooling rate from a fast cooling rate to a slow furnace cool (left to right) for Zircaloy-4 samples hydrogen charged to 120-220 ppm for two grain sizes. Reproduced with permission of Elsevier [54].

Stress

Hydrides tend to concentrate in regions of high stress, an effect that is amplified by thermal cycling or increasing the hydrogen content [63]. This can be problematic, as this is likely to be at a crack tip, as in the case of delayed hydride cracking (see section 2.4.2.5), or lead to hydride reorientation (see section 2.4.2.4).

2.4.2.4 Hydride reorientation

Hydride orientation, in the absence of stress, is controlled by the crystallographic texture [77]. However, when cooled under stress, hydrides tend to orient perpendicular to the applied stress [78]. Careful processing can minimise the impact of this, for example, for fuel cladding the final step [79] introduces compressive stresses such that hydrides should form circumferentially. Unfortunately, when heated, the solubility of hydrogen increases, and the hydrogen is dissolved back into solution. Upon cooling under stress hydrides then precipitate in a different orientation (reorient) with a detrimental effect on mechanical properties [62]. The worst case, for fuel cladding, is that the hydride reorients to radial hydrides, as shown

in Figure 22. This would allow an easy crack path through the cladding via the brittle hydrides.

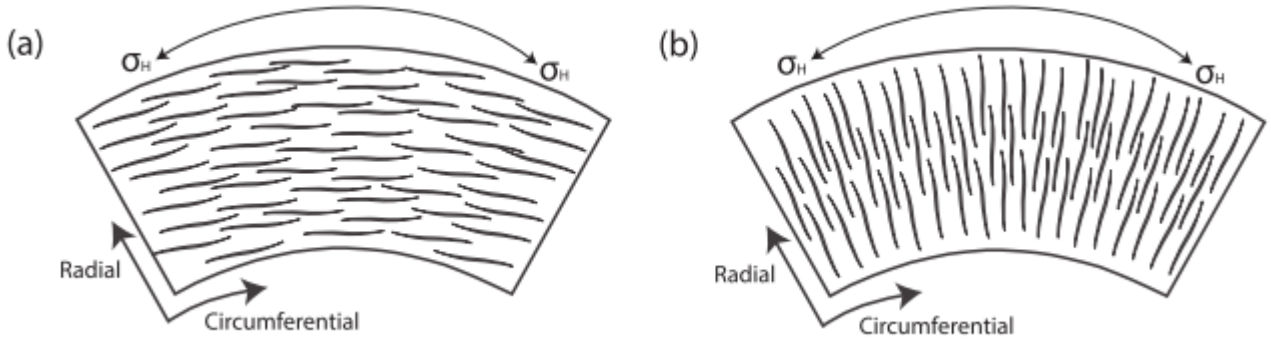


Figure 22 - Schematic representation of hydride reorientation in zirconium alloy tubes. Reproduced with permission of Elsevier [20].

2.4.2.5 Delayed hydride cracking (DHC)

The first experimental demonstration of DHC was in Zr-2.5Nb pressure tubes in 1974 [80] and most of the early literature applies to CANDU reactors [81]. DHC is a time dependent process that involves the stepwise reorientation of hydrides at a crack tip (due to stress) which leads to propagation of the crack [81]. For DHC to occur, the material must be under stress with an initial crack present.

The basic process [81], is shown schematically in Figure 22. During each thermal-mechanical cycle, there are three stages in DHC-related crack propagation:

(a) a crack is present under stress in hydrided material;
(b) hydrogen diffuses to the crack tip due to the high stress present then the hydrides reorient (through dissolution and reprecipitation under stress) perpendicular to the applied stress i.e. such that the long axis is parallel with the crack;
(c) the brittle hydride fractures under stress leading to extension of the crack. Propagation of the crack through the material occurs stepwise, although uncontrolled crack growth through the material will occur once a critical crack length is reached.

To predict DHC, it is useful to understand the interaction of hydrides and lattice strain (i.e. stress) and hydride reorientation.

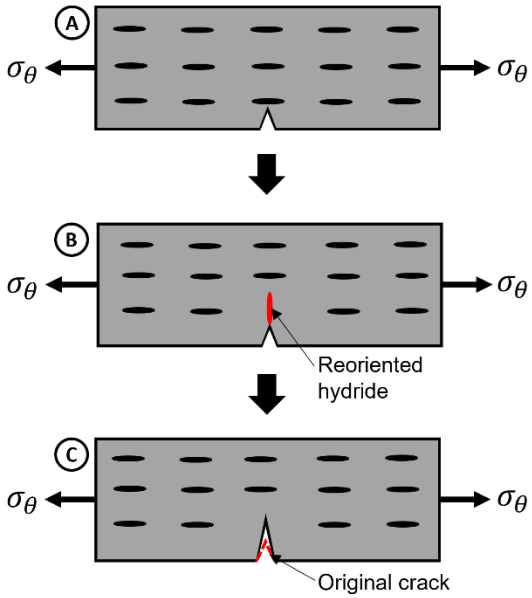


Figure 23 - Schematic of the delayed hydride cracking process . (A) a crack is present in hydrided material, and the initial hydrides are oriented perpendicular to the crack; (B) under stress, the hydrides reorient at the crack; (C) fracture of the hydride occurs, lengthening the crack. Redrawn from [81].

2.4.2.6 Local stress field

One driving force for hydride reorientation is that by reorienting, hydrides can relax the macroscopic stress state. This relaxation can occur as there is a superposition of local misfit strain from the hydrides and the macroscopic applied elastic strain. One example of this is related to the decoration of a notch under an applied load, and the degree of hydride reorientation is shown to be dependent on the local stress state by Bum et al. [82] as shown in Figure 24.

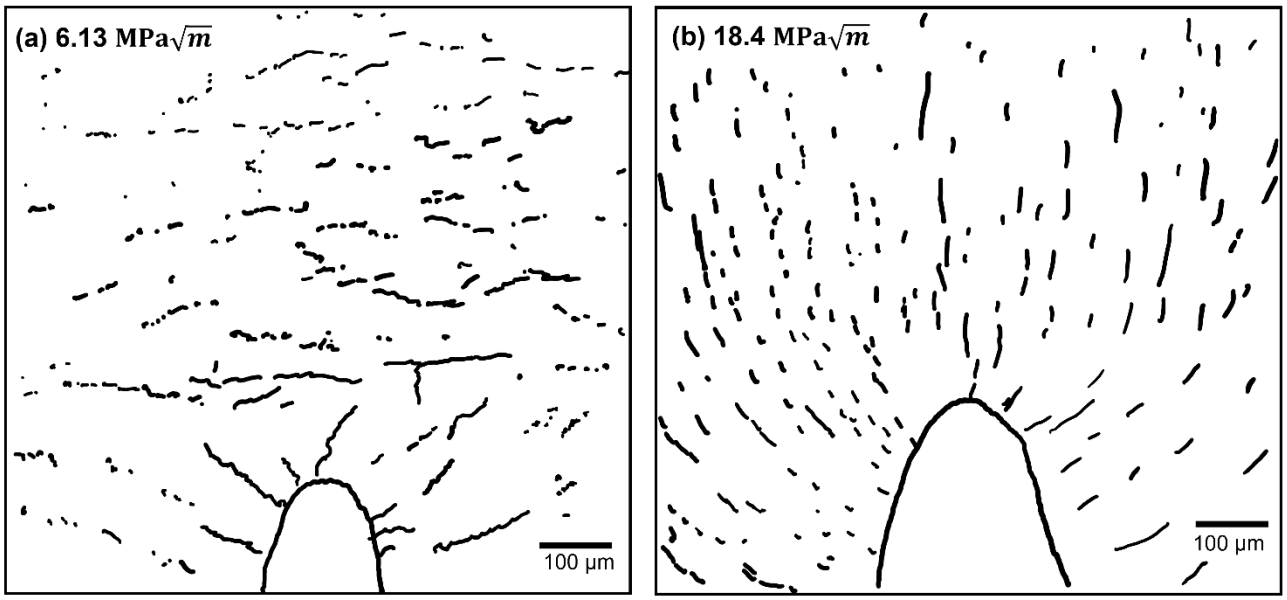


Figure 24 - Effect of stress field on hydride reorientation. Reorientation of hydrides in notched Zr-2.5Nb cladding tube material with stress intensity factor of (a) 6.13 $MPa\sqrt{m}$ (b) 18.4 $MPa\sqrt{m}$. Scalebar = 100 µm. Redrawn from figure 6 in [82].

If the hydrides are produced in the solid phase, there is a misfit strain induced which varies in direction and magnitude based upon the hydride phase. Carpenter [83] calculated the theoretical (stress-free) misfit

strain for δ and γ hydrides, for directions based on their orientation relationship with the Zr matrix (see Table 6).

Table 6 - Dilatational misfit values for δ and γ hydrides based on phase and direction in the Zr matrix. Compiled from [83].

Hydride phase	Orientation relationship	Direction (in Zr)	Misfit[2] (%)
Delta (δ)	Multiple ORs – common close packed direction between: $[1\bar{1}0]_\delta \parallel [11\bar{2}0]_\alpha$	$[0001]$	7.20
		$[11\bar{2}0]$	4.58
		$[1\bar{1}00]$	4.58
Gamma (γ)	$(111)_\gamma \parallel (0001)_\alpha$ and $[1\bar{1}0]_\gamma \parallel [11\bar{2}0]_\alpha$	$[0001]$	5.70
		$[11\bar{2}0]$	0.55
		$[1\bar{1}00]$	5.64

This results in local lattice strain, which is likely to be important in hydride reorientation. Carpenter [23] suggests that this local strain can result in the formation of dislocations near the hydride tips. Bailey [76] demonstrates the presence of dislocation lines around hydrides, as shown in Figure 25 B.

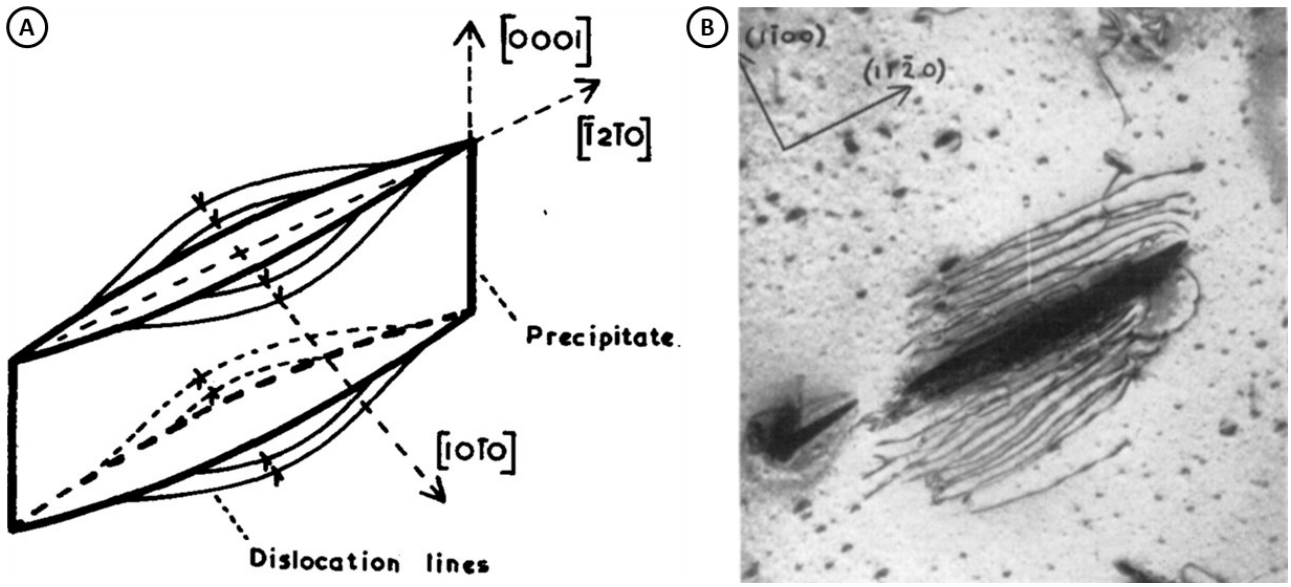


Figure 25 - Dislocations around hydrides .(A) schematic showing dislocation lines that form during growth of the hydride; (B) Micrograph showing dislocation structures around a hydride in rapidly cooled hydrided zirconium foil (magnification: 26,000x). Reproduced with permission of Elsevier [76].

In Bailey's work [76], dislocation loops around γ phase hydride needles are evaluated. These hydrides are aligned with the long axis along $[11\bar{2}0]_\alpha$ and growth occurs in the $[10\bar{1}0]_\alpha$ direction, as shown schematically in Figure 25A. If the strain is accommodated by dislocations, then prismatic dislocation loops would be punched out in the $[10\bar{1}0]_\alpha$ direction. Due to non-uniform growth of the hydride, some of these loops may not punch out as complete loops and instead may terminate at the tapered ends of the hydride precipitate. Figure 25 shows an example of dislocation loop segments around a hydride. This hypothesis is

[2] Misfit = volume change relative to the untransformed Zr.

also supported by the number of dislocation loops seen in Figure 25B, which matches well with the number required for the strain around the hydride precipitate, as calculated by Bailey [76].

Barrow et al. [84] evaluated the interfacial strain around hydrides in Zircaloy-2 using nano-beam electron diffraction (NBED) and electron energy loss spectroscopy (EELS), giving an experimental perspective of the theoretical work by Carpenter [83]. The (intragranular) hydrides were δ phase with a needle like structure, and OR: $(0001)_\alpha \parallel (111)_\delta$ and $[11\bar{2}0]_\alpha \parallel [1\bar{1}0]_\delta$. Interestingly, they found the hydride tips to be γ phase hydride, adding weight to the hypothesis that the 'metastable' γ phase is a precursor to the stable δ phase. Barrow observed peak strains in the α matrix up to 4x larger than in the hydride. Shear strains were observed in the $[1\bar{1}00]_\alpha$ direction (limited to the basal plane) whilst dilatational strains in the $[0001]_\alpha$ direction were consistent with Carpenter's misfit strain analysis [83]. The strains were highly localised, decreasing from a maximum of 5.5 % lattice strain at the interface (in $[0001]_\alpha$, measured normal to the long axis of the hydride) to 0.5 % at 50 nm [84], as seen in Figure 26.

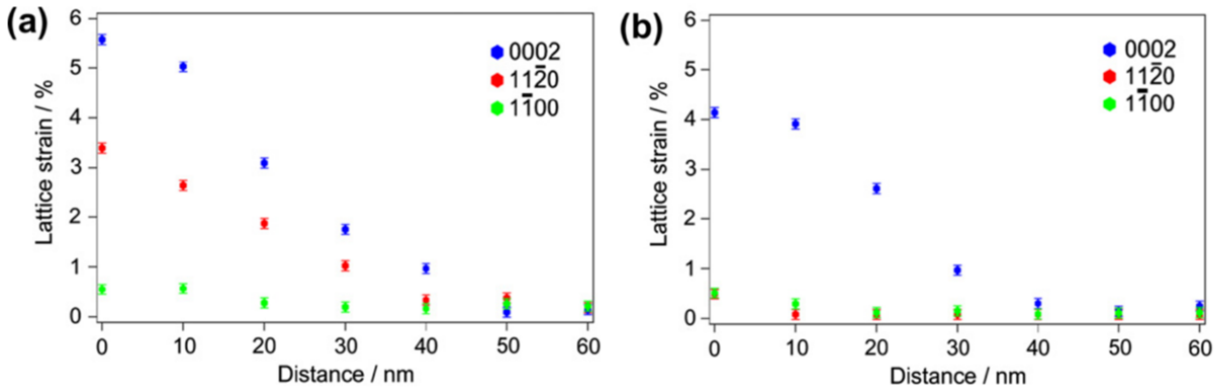


Figure 26 - Local lattice strain around a hydride in Zircaloy-2, observed using NBED. The lattice strain (%) caused by the anisotropic volumetric hydride/matrix misfit. Results shown for 3 Zr directions ($[0001]_\alpha$, $[11\bar{2}0]_\alpha$ and $[1\bar{1}00]_\alpha$) (a) normal to the hydride long axis ($[1\bar{1}00]_\alpha$) and (b) parallel to the hydride long axis ($[11\bar{2}0]_\alpha$), with the interface at 0 nm in each case. Reproduced with permission of Elsevier [84].

Kerr et al. [85] also looked at strain in hydrided Zircaloy-2, this time using *in situ* synchrotron X-ray diffraction combined with mechanical testing to enable analysis of the lattice strain evolution under an applied load (compressive and tensile). Their work focussed on the $\{111\}_{hydride}$ peak[3] and the $\{10\bar{1}0\}_\alpha$ peak, since this was the only resolvable pair due to the low hydrogen content (~90 wt%). They noted 3 distinct regimes: (1) elastic; (2) post-yield load transfer from the matrix to the hydride and (3) strain saturation (potentially due to hydride fracture). Similarly, Allen et al. [86] used high energy X-ray diffraction (HRXRD) to investigate strains around hydrides formed at a notch (stress concentration) in Zr-2.5Nb pressure tube material. Using larger hydrides than Kerr et al. [85] (formed through thermal cycling), they looked at the transfer of load between matrix and hydride and subsequent hydride failure by evaluating the lattice strain parallel to the loading direction (see Figure 27 A & B). They also evaluated the effect of pre-creep on hydride formation at the stress concentration, finding that a 24-hr pre-creep cycle reduced the

[3] The hydride phase is not specifically stated, but likely to be δ-phase due to the cooling rate (1 °C/min), which is the same as Barrow et al. [84]

peak strain at the notch tip in the matrix material but had no effect on the overload required for hydride fracture at the tip (see Figure 27 C & D). Strain profiles presented are based on the peak shifts after loading (using $\{111\}$ for the hydride) and show a similar drop, if at a larger distance (probably due to hydride size), to those presented in Barrow et al.'s results shown in Figure 26 [84]. They developed a finite element model for the stress state and the effect of hydrides on the strain profile at the notch tip. Their modelling of strain profiles demonstrate relatively good agreement with the experimental results.

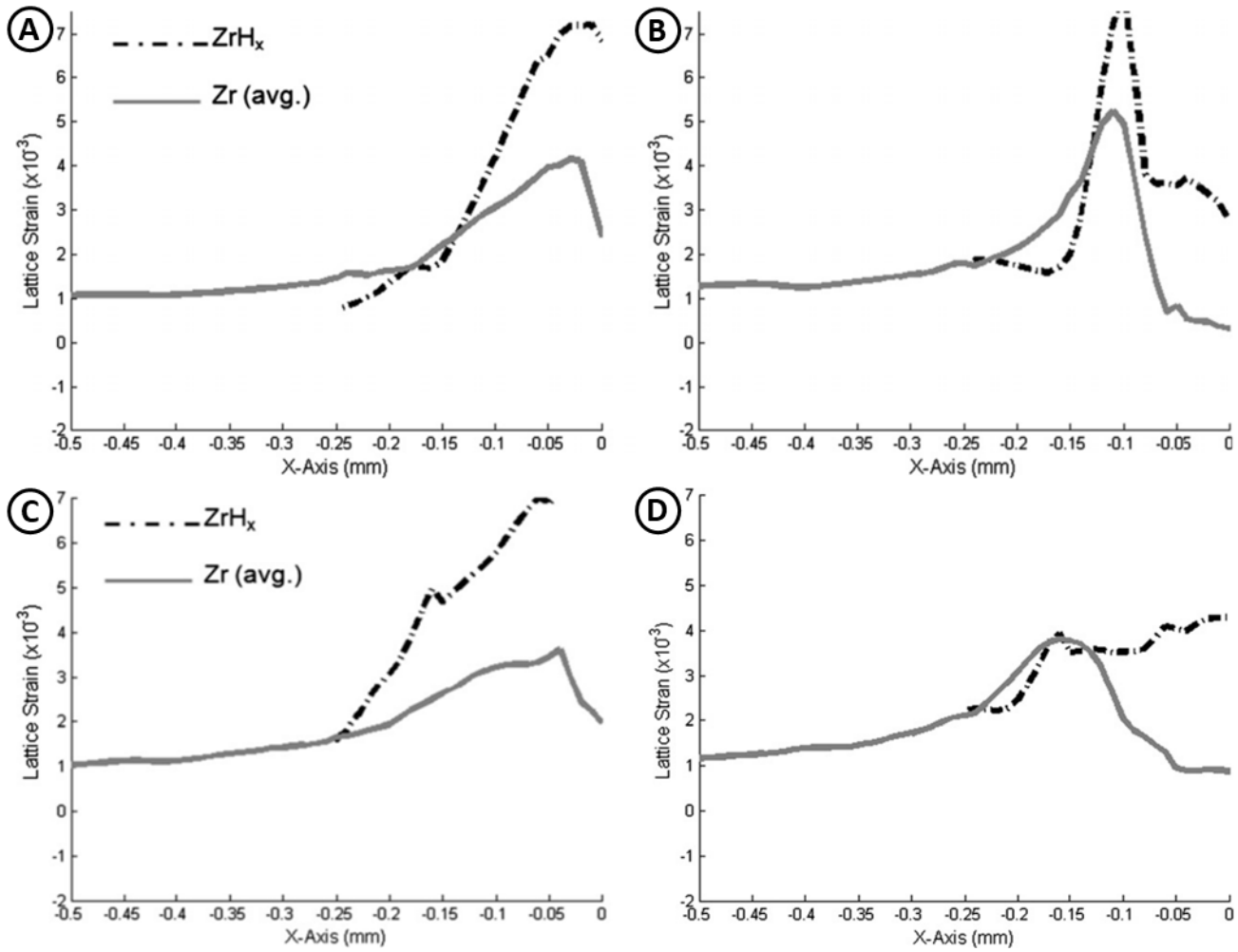


Figure 27 - Lattice strain parallel to loading direction . Comparison of hydride and matrix lattice strain in Zr-2.5Nb pressure tube material without pre-creep (top row) and with pre-creep (bottom row), for (A) & (C): 120% load [$K_I \sim 9.6\ MPa\sqrt{m}$] and (B) & (D): 130% load – $K_I \sim 10.4\ MPa\sqrt{m}$. Combined from figures 3 and 6 in [86] *. Reproduced with permission of Elsevier.*

Recently, Reali et al. [87] developed a discrete dislocation plasticity (DDP) model to look at the stress at the hydride/matrix interface and investigate plastic relaxation. Their work focuses on the anisotropic volumetric hydride/matrix misfit strain and builds on the theoretical work of Carpenter [83] and the experimental work of Barrow et al. [84] to try and reconcile the lower experimental values for misfit strain compared to higher theoretical values. Reali et al. [87] argue that this difference can be reconciled if dislocations (e.g. as shown by Bailey [76] in Figure 25) are adequately accounted for. Their model shows good agreement with Barrow et al.'s experimental results [84], as demonstrated in the example at Figure

28, despite being for different Zr alloys (Reali [87] modelled pure Zr and Zircaloy-4 whereas Barrow[84] used Zircaloy-2).

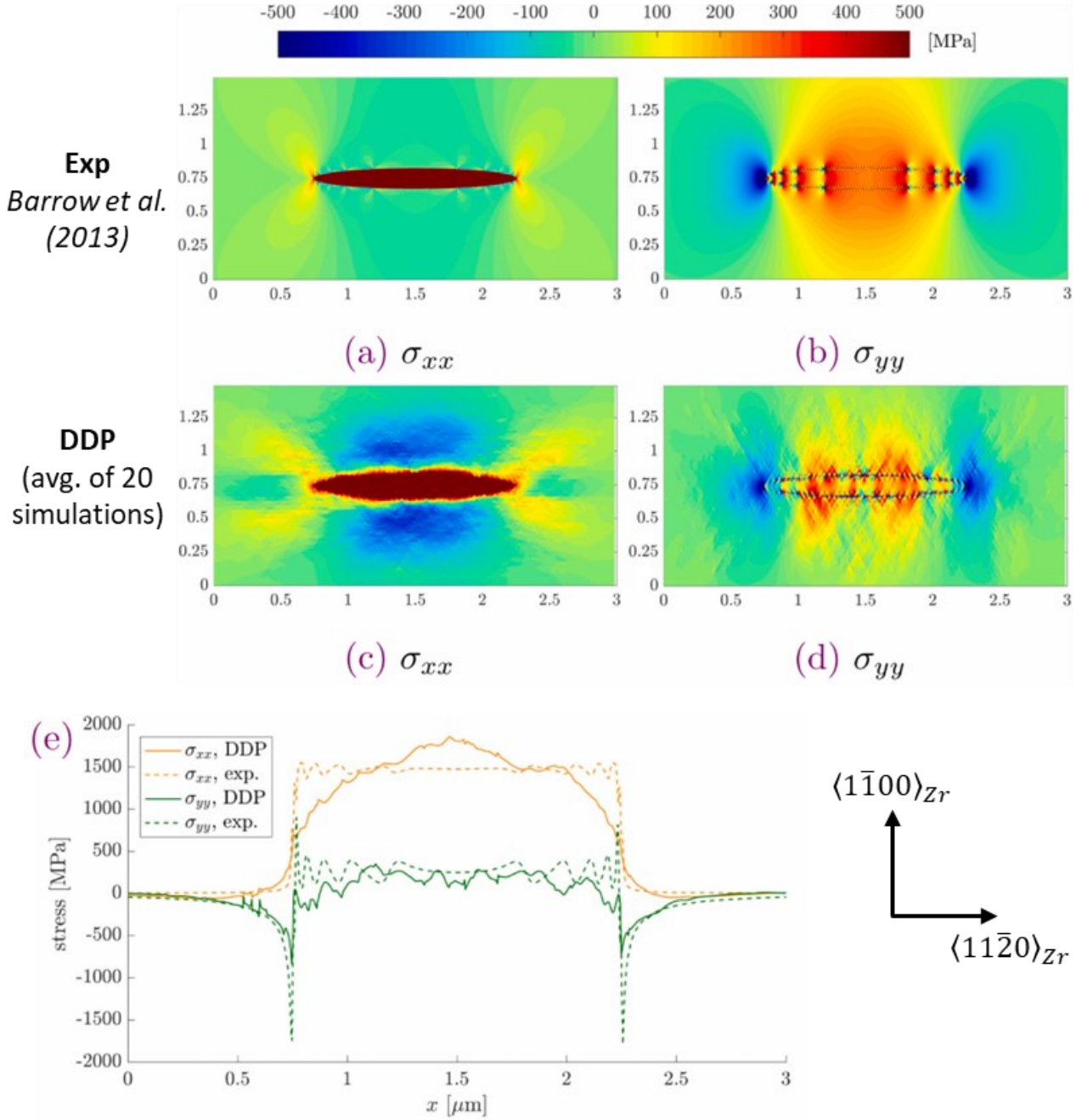


Figure 28 - Modelling vs. experimental results for stress around a δ hydride. Experimental [84] *vs. simulated* [87] *results for stresses generated by the misfit dislocations of a δ hydride in (a) & (c) σ_{xx} and (b) & (d) σ_{xx}. (e) compares the results for both approaches along <11-20> for both stresses. Axes for all plots are in µm. Licensed under creative commons CC BY 4.0 – Rearranged version of figure 7 from* [87].

From the literature we see that the misfit of the hydrides causes significant strain around the lenticular hydrides, and this strain is anisotropic, dependent on hydride phase and may be more complicated when a number of hydrides form together. This can result in build-up of lattice strain in the matrix which in turn affects hydride growth, propagation of hydrides into packets, hydride reorientation and cracking. From the literature so far, the magnitude and spatial variation of the misfit (elastic) strain has not been measured extending from larger hydride packet structures and near interfaces such as grain boundaries.

2.5 Parent grain reconstruction

The presence of related microstructural units on performance is well known and reported in the titanium literature, specifically in terms of cold dwell fatigue [88]. Regions of common orientation appear due to the BOR and anisotropy within the strain path which leads to regions of (near) common orientation. Reports of these features varies in the literature, broadly called “microtextured regions” (e.g. [89]), “macrozones” (e.g. [90]) or the “effective structural unit” [88]. Hafnium and zirconium are less well studied in the open literature, but there are limited reasons why similar processing-microstructure-mechanical property linkages will not exist. The only difference is that the loading conditions and safety considerations in their engineering applications will vary.

In practice, the microstructure of the high temperature phase is often difficult to observe directly. Instead, often the BOR can be observed due to orientation relationships between neighbour α-grains. If the two α-grains are from the same parent β-grain, then the α-α grain boundary will have a ‘special’ OR. This means the parent β-microstructure can be reconstructed from the α-grain structure, provided there is limited subsequent orientation change in the α domain.

To measure the local orientations between grains, electron backscatter diffraction (EBSD) can be used to create 2D (and 3D) microstructure maps where the orientation and phase of each grain is measured at high spatial resolution (for a brief review, see Wilkinson and Britton [91] and see section 2.7.4). EBSD mapping makes it possible to explore the BOR within these engineering alloys.

In a material that has a solid phase transformation, e.g. when cooling from a (parent) high temperature β phase to a (child) lower temperature α phase, the child phase orientation may be related to the parent grain orientation if an OR is present. For most ORs, the parent phase may have multiple different options for the transformation product orientation, the so-called variants, due to the symmetry relationships and transformation strain & rotation between the two crystal structures. This is complicated further by the symmetry of the parent crystal and the child crystal which can result in ambiguity in calculating the parent grain orientation from a single child grain. There is a similar challenge in predicting the orientation of the child orientation from an initial parent. However, if more than one child orientation is present (e.g. as the parent grain contained more than one nucleation site for the phase transformation), then it is possible to reduce the potential candidate parent phases.

The challenge of determining the parent grain orientation using EBSD is well explored in the literature, and many manual [92]–[95], semi-automated [96], [97], and fully automated [97]–[103] grain reconstruction codes have been developed. Groups of similar grains can be identified using the grain boundary misorientation, mean grain orientations or the pixel orientations in EBSD data. Refinements to this process include iterating the OR to take into account the experimental results or using more complex grain grouping methods, for example, using the Markov clustering algorithm [104].

Many reconstruction methods start with ideas shared by Humbert et al. [92]–[94]. These methods start by comparing the experimental grain boundary misorientations to the theoretical grain boundary misorientations (between potential α variants) from the OR [105], [106]. The aim is to identify the parent grain boundaries (i.e. those that do not match the theoretical misorientations between variants), usually as part of a grain grouping step.

A limitation of these methods is often that they do not deal well with experimental deviation from the OR, for example deviations caused by compatibility requirements that arise from thermal or mechanical processing. Cayron et al. [107] compared the tolerance for the misorientation of the room temperature phase vs the theoretical misorientations for the OR in titanium/zirconium alloys and steels, and found these to be ≈5 ° and ≈2-4 ° respectively. To overcome this issue, an iterative step for the OR has been introduced in some cases, such as work by Nyyssönen et al. [103], [108], [109] in steels**.**

The grain grouping step is where a lot of methods deviate, with some codes reconstructing without grouping grains first, and others grouping prior to reconstruction. For example, the triplet method [110] uses the groupoid method [107], [111] to identify triplets of grains with a low tolerance angle. These 'nucleus' triplet grains are then grown by adding neighbouring grains that meet a tolerance condition, with this nucleation and growth cycle repeated until no more nuclei can be found. This is a non-iterative and quick method, but it may not group all of the grains if they do not meet the tolerance condition to be grouped together if there are insufficient 'nucleus' triplets in the data set. Alternatively, there is the cluster method [101] which identifies clusters of the child phase which are highly likely to have originated from the same parent grain, then grows these clusters and back-transforms them to the parent phase using the summation of minimum misorientation angle (SMMA) method [95]. This is a computationally expensive, iterative method, with good accuracy.

Another potential issue is the artificial reunification of grains, particularly in cases where the grains are grouped prior to transformation. This can be addressed in some methods by adjusting tolerance values or coarsening parameters (e.g. for the MCL algorithm [103], [112]). Similarly, ambiguous grains (either at the grouping stage or to determine the parent orientation) are often an issue, either due to island grains within larger grains, or just small groups of child grains. These are dealt with in in a number of ways, from not being reconstructed [98], [107], to additional subroutines in the code (e.g. [97], [99]) or back-filling from neighbouring grains [110].

For large datasets, there is a tension between accuracy and computational time, so some methods employ statistical analysis to support parent grain reconstruction. These include work by Glavicic et al. [100], [113] which uses Monte-Carlo analysis and two misorientation minimisation steps and has the advantage of requiring no a priori knowledge of the parent grain boundary locations or variant selection. Also, work by Gomes [112] and Nyyssönen et al. [103], [108], [109] that employs the Markov clustering algorithm to create a network of discrete clusters of similar grains. This method is computationally efficient, has

excellent noise tolerance and only one coarsening parameter. Some groups have also worked to combine several of the above methods, for example, Bernier et al. [114], which brings together OR refinement[109], [115], [116]; local pixel-by-pixel analysis [115], [117]; and nuclei identification and spreading [97].

2.5.1 Commercial software

Some EBSD software providers now include parent grain reconstruction as part of their software. Whilst these codes are not interrogable, it is known which method they are based on.

EDAX's OIM Analysis™ v8.6 [118] uses a method from Ranger et al. [119], [120]. This is a graph based method which follows a series of three main steps: (1) classification; (2) growth; (3) cleaning/refinement [119]. Like many codes, this method starts by taking the orientations of identified child domains (grains) and calculating the potential parent orientations for each using the orientation relationship. The most probable parent orientation is chosen based on neighbouring grains and any retained β, and a confidence level is assigned to each domain (this forms the classification step and is based on work by Germain et al. [97]). In the following steps, the child domains are then grouped according to their assigned parent orientation and confidence level, iteratively, looking first at nearest neighbours (step 2) and then extending out to 2nd nearest neighbours for lower confidence domains (step 3). The output can then be cleaned and analysed using the OIM Analysis software [118], with the options to extensively clean the data, which would include removal any ambiguous or ungrouped parent grains.

Oxford instruments' AZtecCrystal software [121] incorporates a parent grain reconstruction tool [122] based on a method from Huang et al. [123]. This method includes a pixel based OR refinement step, followed by OR coalescence and a regional voting system. This method was originally developed for steels and the OR refinement step includes the approach from Miyamoto et al.[115] to determine the experimental (defined as 'real' in the paper) transformation matrix for the OR. In Huang et al.'s approach [123], a region where all the martensite laths originate from the same parent grain is manually selected to optimise the OR. The average deviation angle (from the calculated parent orientation[4]) is then minimised across the region (at a pixel level) iteratively using the Nelder-Mead method [124] until the average value is less than 0.1° to give the final transformation matrix (OR). It is not known how the region selection is incorporated into the software, but the size and placement of the region chosen may impact the final result if poorly chosen (i.e. including multiple parent grains). The OR coalescence step assigns the pixels into groups using a threshold value for the difference between the pixel and the potential variants for the group, working from the top lefthand corner of the map. Once the pixels have been grouped, regional voting is used to determine the final parent orientations across the map using the potential parent orientation variants for each group.

[4] Huang et al.[123] use the KS OR as a starting point for steels.

Both approaches build on prior work in the field and have been modified to accept other orientation relationships. For certain materials with ambiguous orientation relationships, e.g. steels or highly deformed materials, the orientation relationship refinement step available in the AZtecCrystal software [121] may be more useful. In both cases, easy clean-up of the data is possible (explicitly part of EDAX's version) at the end of the process to address likely artifacts created by the reconstruction algorithm. Care should be taken to document any data clean up applied as this may hide useful observations in the reconstructed map.

2.6 Prior work

The work in this thesis to study blocky-α growth in welds builds on work by Lusby in her MSc thesis [125] and uses weld samples sliced from the same original weld. Lusby's experiments were *ex situ* heat treatments looking at blocky-α grain growth in the EB weld samples and the impact of heat treatment duration on the grain growth.

2.6.1 Experiment

Thin (2.5 mm) slices of the EB welded material were encapsulated in quartz tubes, backfilled with argon to avoid oxidation in the furnace. They were inserted into a Lenton furnace, pre-heated to 760 °C and held for 1, 2 or 4 hours before air cooling. Analysis was carried out using large stitched polarised OM, with small supporting EBSD maps - results are shown in Figure 29.

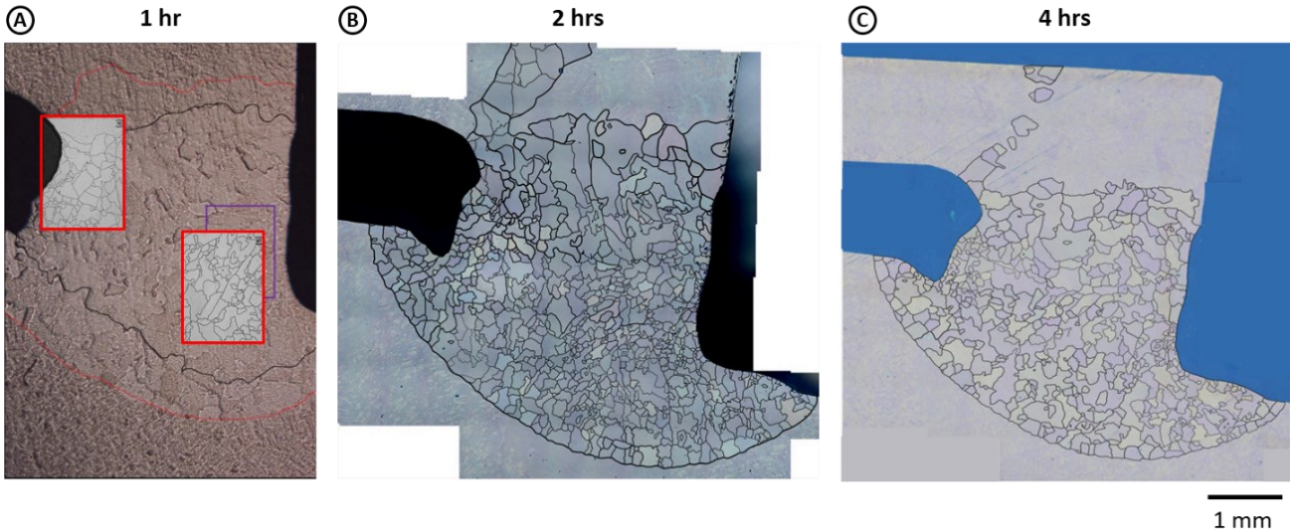


Figure 29 - Grain growth at 760 °C – prior work (ex situ trials from [125]). Polarised (stitched) optical micrographs showing (A) 1 hr heat treatment – inserts outline the blocky-α grains in those regions; black line indicated outer region fully transformed to blocky-α whilst the red line indicates partial growth. (B) 2 hr heat treatment – thick black lines indicate blocky-α grain boundaries (c) 4 hr heat treatment black lines indicate blocky-α grain boundaries. All adjusted to the same scale using the scalebars from Lusby's work.

2.6.2 Observations

The following observations on the growth and development of blocky-α based on Lusby's results in Figure 29 can be made:

- **1 hr HT**

  Full coverage of blocky-α grain growth is observed in the centre of the weld region, as indicated by the black boundary lines in Figure 29 (A), with partial growth in the regions between the black and red lines (red line = edge of weld region). A large view of the grains is not included in Lusby's work, but for the small regions (inserts), the microstructure appears to be a mix of grain sizes but relatively uniform in consistency between the two areas.

- **2 hr HT**

  The entire weld region is filled with blocky-α grains, with a distinct edge to this region. There are distinct changes in microstructure across the weld area, with a tendency for larger grains at the edges of the weld. A notable difference is also seen between the upper and lower halves of the weld, with larger blocky-α grains have formed on the side with the thinner piece (upper half in Figure 29).

- **4 hrs HT**

  The biggest change is an increase in uniformity of grain size across the weld region. A slight coarsening of the grains appears to have occurred. No further growth outside the weld region has occurred.

2.6.3 Grain size

In terms of grain size, using the linear intercept method, a large increase in grain size was noted from 1 hr to 2 hrs with a smaller coarsening effect from 2 to 4 hrs. Lusby also measured grain size using MTEX from the small area EBSD maps captured for the 2 and 4 hr maps. The latter method gave a very similar result for both microstructures but is unlikely to be an accurate representation due to the small areas. All grain size results reported in Lusby's work are included in Table 7 for completeness.

Table 7 - Grain size measurements – ex situ heat treatments, from [125].

Sample[5]	MTEX measurements			Linear intercept grain size (µm)
	Mean Grain Area (µm^2)	Mean Grain Aspect Ratio	Mean Grain Diameter (µm)	
1 hr HT	-	-	-	97
2 hr HT	1.34×10^4	1.87	160	145
4 hr HT	1.36×10^4	1.61	157	166

2.6.4 Comparison with literature

A similar EB weld was investigated by Taylor & Baker [44], with the aim of finding the minimum temperature at which blocky-α growth may occur in EB welds. In their case, bead-on-plate EB welding was carried out on rolled α plate, giving the geometry shown in Figure 30. They focussed on the heat affected

[5] Note: no grain size measurements were included for the initial weld region microstructure - this region is mainly very thin α laths with a high aspect ratio.

zone (HAZ) as the indicator for grain growth and concluded that grain growth was not expected below 600 °C in reasonable timescales (< 336 hrs) [44]. Due to the HAZ focus, it is challenging to directly compare with Lusby's results, however, there are some comparisons that can be made.

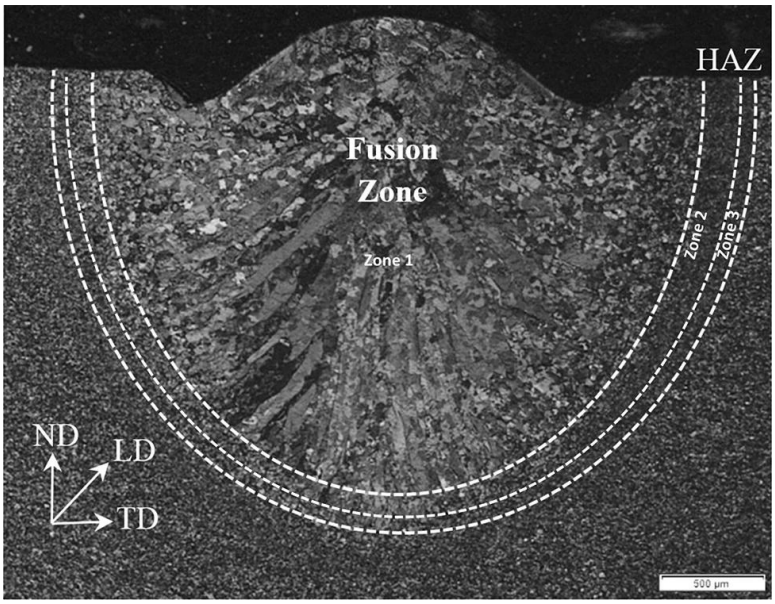


Figure 30 - EB weld microstructure overview. ND = normal direction, LD = longitudinal direction, and TD = transverse direction to the electron beam welding. Scalebar = 500 µm. Reproduced with permission of Springer Nature [44].

One difference from the conclusions might appear to be the results for the 1 hr HT (see Figure 29 (A) and Figure 31 (A)). In Taylor's work [44] this was the point at which the HAZ was fully transformed, whereas Lusby reports the outer region as partially transformed. Looking closely at Figure 31 (A), blocky-α can be seen in the weld centre with a gap between this and the blocky-α in the HAZ. This is broadly consistent with Lusby's result, although Lusby does not mention the presence of an outer ring of blocky-α.

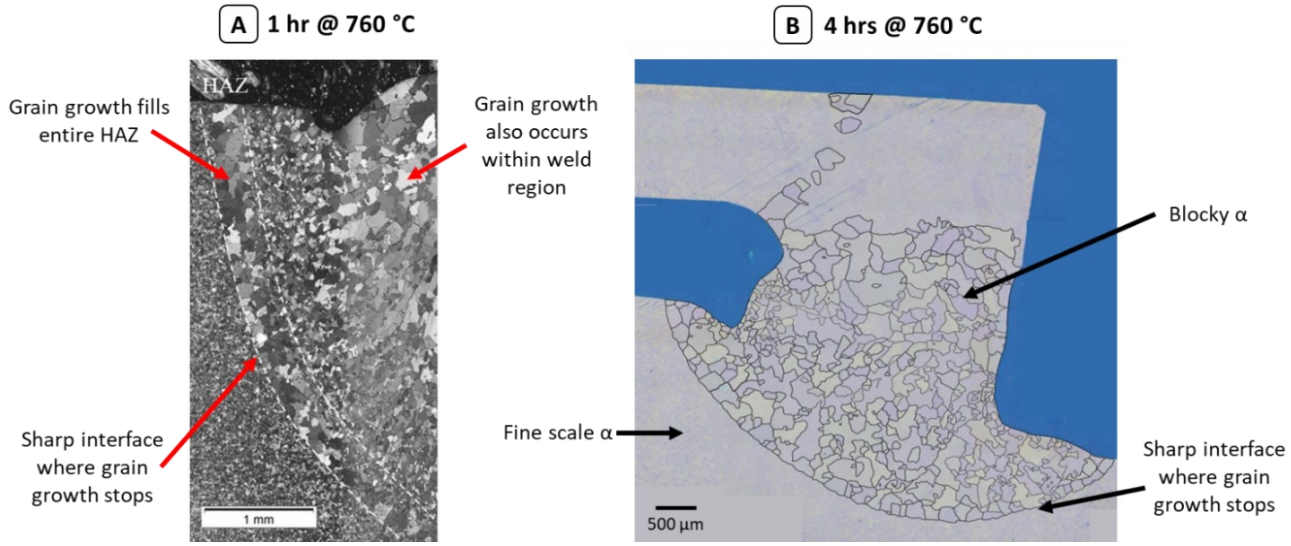


Figure 31 - *Extent of blocky-α grain growth. (A) 1 hr @ 760 °C from work by Taylor and Baker* [44] *(Reproduced with permission of Springer Nature); (B) 4 hrs @ 760 °C from work by Lusby* [125]*. In both cases, the limit of the grain growth is clearly defined by the edge of the heat affected zone.*

An important detail, consistent between the two experiments is the distinct change between the edge of the HAZ and the bulk material. Lusby's *ex situ* experiments [125] showed that even after a 4 hr heat treatment blocky-α grain growth is only contained within the weld region. Taylor et al. [44] also show the outer limit of grain growth is the HAZ. An example from each is shown at Figure 31, where there is a sharp interface between the edge of the weld region (i.e. outer edge of HAZ) where grain growth occurs and the bulk material.

Lusby's results [125] suggest grain growth may occur from the centre of the weld region and grow outwards, whilst Taylor et al.'s results [44]might suggest grain growth initially at the edge of the weld region.

2.7 Review of analytical techniques

This section contains a review of the literature for key sample preparation and analytical methods used for this thesis.

2.7.1 Ion beam polishing

Good quality sample preparation reduces the presence of surface defects, and mechanical an chemical methods both risk introducing a very thin surface layer of dislocations or chemical variation. This has motivated the development of ion beam polishing methods, which were first used to prepare TEM lamella [126] (e.g. with precision ion polishing systems, PIPS [127], [128]). In brief, these methods use a broad ion beam (typically Ar+) ions to gradually and gently sputter the surface of material, without creation of additional radiation or ion implantation defects. When used successfully, the surface can be prepared with less than 3 nm of surface damage (Xe focussed ion beam (FIB) [129]). More recently, the broad ion beam milling method has been used for SEM sample preparation and there are two main geometries used:

- **Glancing incidence (or planar)**. In this geometry, the ion beam hits the sample surface at a glancing angle to polish a large surface area. The aim is to remove the surface damaged layer, improve surface cleanliness, and optimise the sample for electron microscopy analysis. A large area of the surface is removed in parallel, and there a risk that shadowing or preferential sputtering/etching can result in increased topography, removal of different phases, and grain-to-grain variations in surface height and polishing quality (due to ion channelling effects).
- **Cross section.** In this geometry, the ion beam is used in normal incidence with a shield layer in order to create a new cross section of material. This reveals a new analysis surface which is a cross section of the (previously) prepared metallographic surface. The shield layer is used to control the location of the cross section and enables site specific analysis. The shield is typically made of a material which is reasonably resistant to ion beam sputtering than the sample and is of a sufficient thickness to maintain a sharp edge on the surface of the sample. The cross sectioning approach is useful for materials containing more than one phase, as the fresh surface is produced with limited shadowing effects.

Both of these geometries can be performed using either focussed or broad ion beam polishing methods.

2.7.2 Polarised light optical microscopy

Polarised light optical microscopy allows observation of grains in optically anisotropic materials. The optical anisotropy is caused by differences in the refractive index in perpendicular directions, and contrast can be seen in polycrystalline materials when this variation depends on the grain orientation (for HCP metals like titanium and zirconium this is related to the <c> axis alignment [130], [131]). This difference means that contrast (and colour) can be observed when the incident light is filtered to a single direction and then rotated to find the maximum contrast. Images are formed due to parallel (as opposed to scanning) beam illumination of large areas using an optical microscope.

Figure 32 shows a typical setup for polarised optical microscopy. Two linear polarising filters (polariser & analyser) are used, set at 90° to each other. The first polariser is used to filter the incident light to a single direction. This polarised light is incident on the sample and it is reflected back and passed through the analyser to the observing lens. As the analyser is set to 90° to the initial polariser, only shifted or depolarised light (wavefronts) will pass through the analyser. Contrast can be varied by rotating the polariser, to enable selection of a combination of polariser and analyser angle to reveal maximum grain-to-grain contrast. Post processing can enhance the contrast and colour balance of the image.

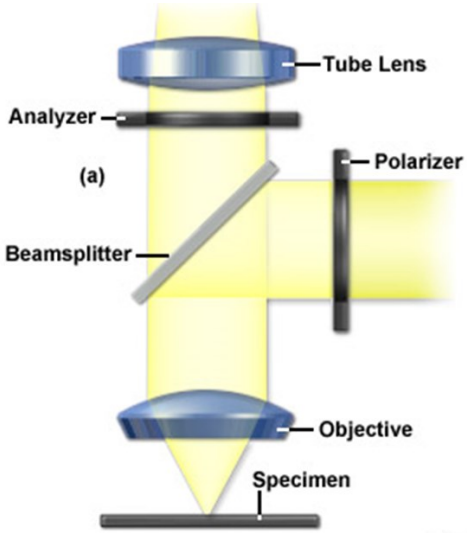


Figure 32 - Polarised optical microscopy setup (reproduced from [132]). Basic setup for polarised reflected light optical microscopy using a polariser and analyser (second polariser) that are oriented at 90° to each other. Optical anisotropy (different grain orientations) in the sample causes the wavefront to shift and allows observation of grains in the sample.

2.7.3 Backscatter and forescatter electron imaging

Backscatter and forescatter electron (BSE and FSE) imaging both use low energy loss electrons. Reimer [133] states that "by convention electrons with exit energies $E_B > 50$ eV are called backscatter electrons and those with $E_{SE} < 50$ eV secondary electrons (SE)". These imaging modes reveal contrast associated with surface topography, phase, and crystal orientation. If the contrast associated with topography and phase is suppressed, then the crystal orientation contrast can be used to reveal microstructure quickly.

The distinction between the two imaging types is the angle between the incoming beam and the trajectory of the detected electron. BSE travel back towards the incident beam [133], whilst FSE go forwards. This is shown in Figure 33 in both a flat (Figure 33 (A)) and tilted (Figure 33 (B)) configuration. Typically, the backscatter electron signal is captured using semiconductor diodes to maximise signal to noise. These diodes can be located across different regions within the SEM, and often they are co-located within a EBSD detector system. For the Bruker ARGUS system [134] they are located at the top (for BSE) and bottom (for FSE) edges of the EBSD camera, as shown in Figure 33 (C). These imaging modes are discussed below.

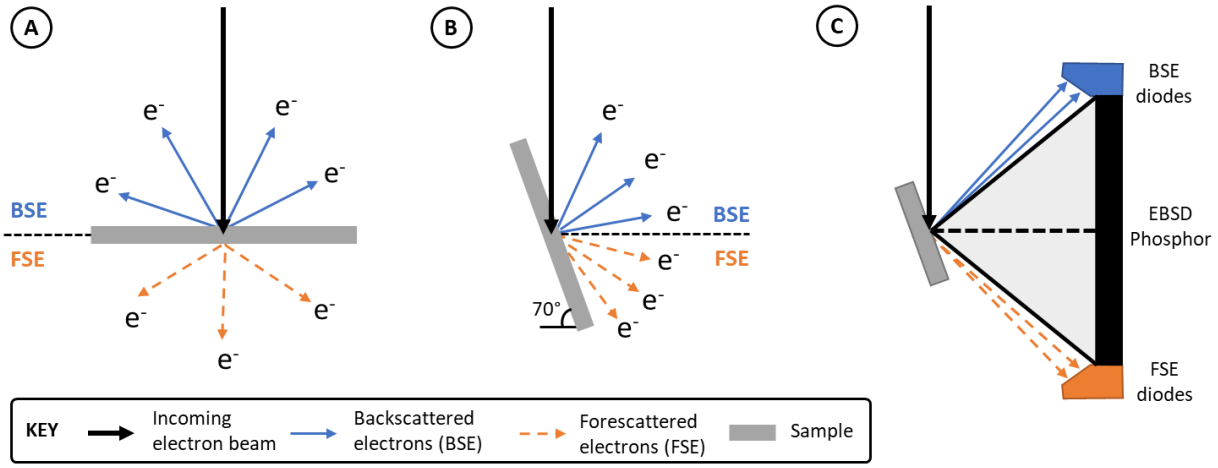


Figure 33 - Backscatter vs. forescatter electron imaging. The angle at which the electrons are diffracted determines whether they are classified as backscattered or forescattered. (A) flat setup (B) tilted setup, as used for EBSD (C) tilted setup including the location of the detection diodes on the Bruker EBSD camera.

Backscatter electron (BSE) imaging is usually carried out with the sample flat and beam at normal incidence to the sample. In this case, the BSE detector is usually mounted on or below the pole piece. BSE imaging gives strong phase contrast and when carried out in an un-tilted geometry, has minimal spatial distortions that might be expected in the tilted geometry due to mounting. However, BSE imaging can also be carried out in a tilted geometry using detectors mounted on the EBSD detector.

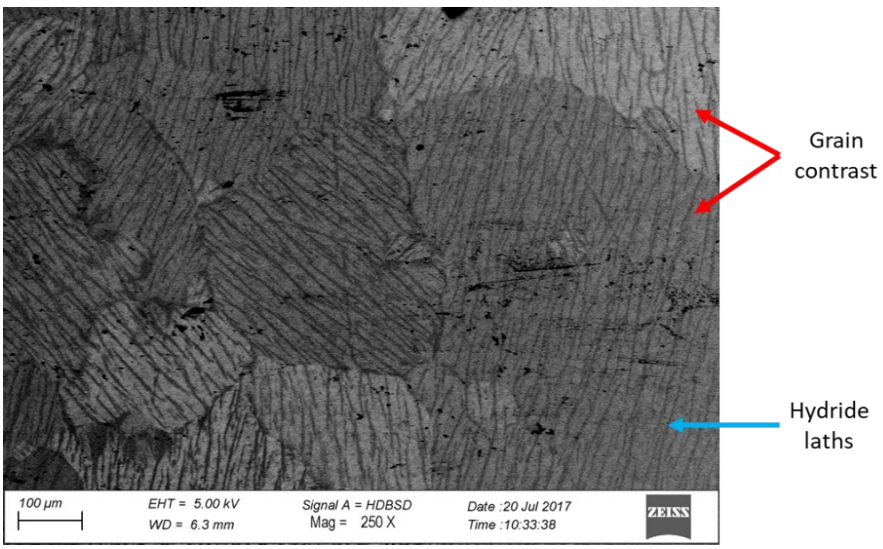


Figure 34 - Backscatter electron imaging example. Hydrided large grain Zircaloy-4 BSE image showing lath hydrides within the α Zr grains (Hydride cooling rate = air cool). [Author's data]

BSE imaging is of particular use when hydrides are present, as there is strong contrast between the hydrides and the Zr matrix, as shown in Figure 34. This contrast is related to the changes in backscatter coefficient, which is related to the Z-number of the material and the effective density within the interaction volume. Higher Z-number and more dense materials have a higher backscatter coefficient and will appear brighter in a BSE micrograph.

FSE imaging has similar characteristics to BSE (low energy loss) and can show topographic, phase & crystallographic contrast [135].

2.7.4 Electron backscatter diffraction (EBSD)

Electron backscatter diffraction (EBSD) is a method of capturing crystallographic data (i.e. orientation, phase, and strain) from the surface (~20 nm depth) of a crystalline sample. EBSD is used extensively in this project to collect orientation data for the samples.

2.7.4.1 Pattern formation

EBSD patterns are formed from scattering and diffraction of electrons incident on a sample. The patterns contain bands of raised intensity, the Kikuchi bands, which correspond to crystal planes. In conventional EBSD, the sample is typically tilted to 70 ° within the chamber as shown in Figure 35 (A). Due to the scattering of the electrons in this geometry, the interaction volume is asymmetric and a schematic volume is shown in Figure 35 (B).

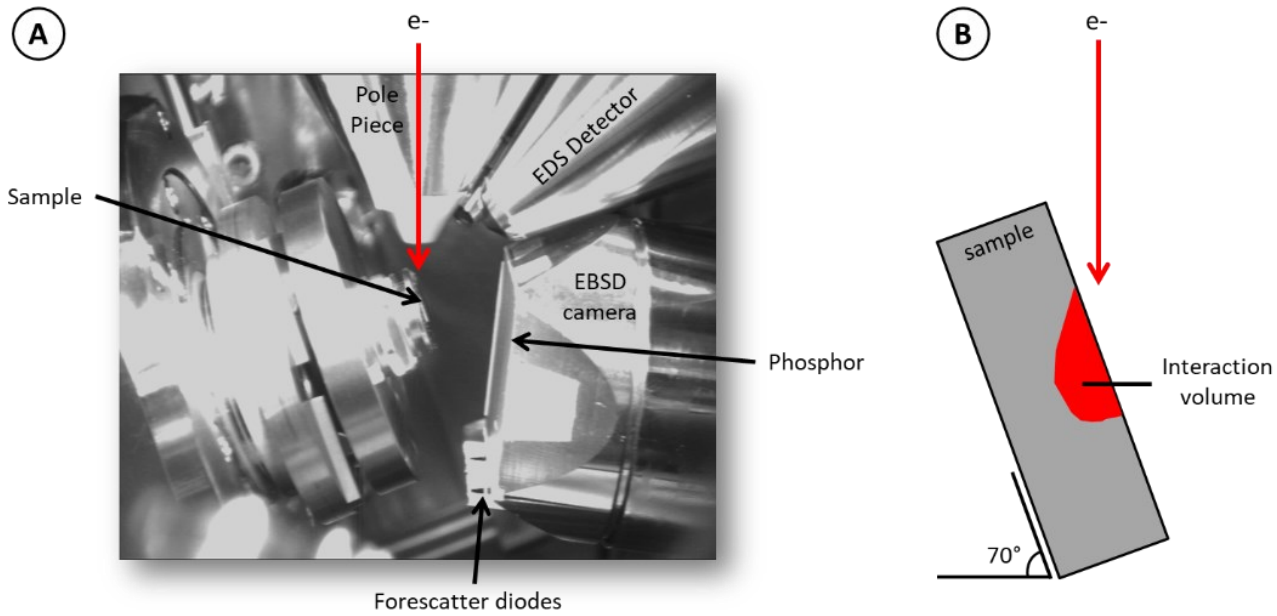


Figure 35 - EBSD: Setup. (A) Chamber view showing the relative positions of the sample and detector within the chamber. (B) Schematic showing the interaction volume of the beam with the sample in the tilted configuration. Reproduced with permission from [136].

Kikuchi bands are formed from diffracting lattice planes, and the separation of the band edges is 2θ as described using Bragg's law, as detailed in equation (2), where λ is the wavelength of the electrons, d_{hkl} is

the plane spacing and θ is the diffraction angle. Each band edge is at an angle, θ, from the lattice plane trace.

$$n\lambda = 2d_{hkl}\sin(\theta) \quad (2)$$

In 3D, this leads to a cone of diffracted electrons for each plane. EBSD patterns are imaged using a flat screen (typically a phosphor). Each pattern is made up of a series of Kikuchi bands, where the band edges are described as conic section lines originating from the electron-sample interaction (the pattern centre). This is shown schematically in Figure 36.

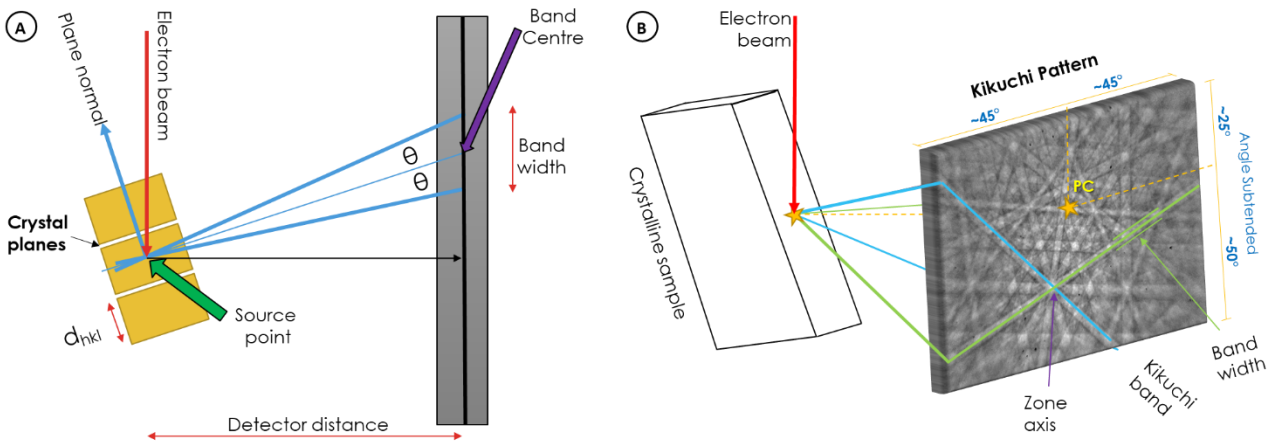


Figure 36 - EBSD: Pattern formation. (A) Band formation in crystalline samples, based on Bragg's law (B) Formation of a Kikuchi pattern on a phosphor screen from the bands. Reproduced with permission from [136].

For a given crystal, the electrons will diffract with many planes which forms a rich pattern containing many overlapping Kikuchi bands, or a 'Kikuchi pattern' (see Figure 36 (B)) on the phosphor screen. This pattern is captured using a Charged Coupled Device (CCD) camera via a series of optical lenses. The CCD camera is connected to a computer which synchronises beam movement with pattern capturing to form a map.

Typically, online processing is used to determine the phase and crystal orientation for each measurement point. The phase can be determined due to the presence (and absence) of different diffracting bands and the interplanar angles associated with these diffracting planes. The crystal orientation can be determined as the EBSD pattern is a direct projection of the unit cell, i.e. as the crystal rotates the pattern rotates with it.

2.7.4.2 Pattern analysis

The raw patterns contain both the diffracted pattern and other (non-diffracted) backscattered electrons from the sample. To index the patterns, they first need to be 'background corrected' to remove anisotropic scattering and increase the orientation and phase contrast found within the Kikuchi bands. Although there are several methods to do this, commonly a static background pattern is captured and the raw pattern divided by this to get the final pattern, as shown in Figure 37.

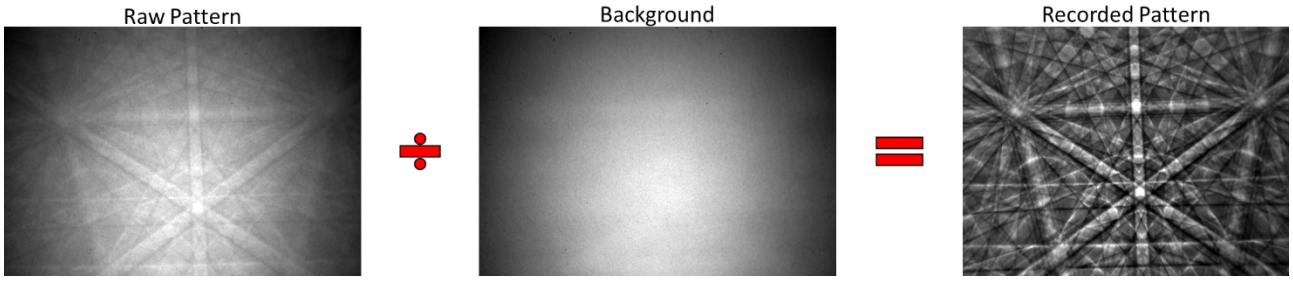


Figure 37 - EBSD: Background correction. The raw pattern is often background corrected by dividing by a diffuse background pattern to form the recorded pattern. Reproduced with permission from [136].

At this point, the bands in the pattern need to be identified and indexed to determine the crystal orientation. The process for this is outlined in Figure 38.

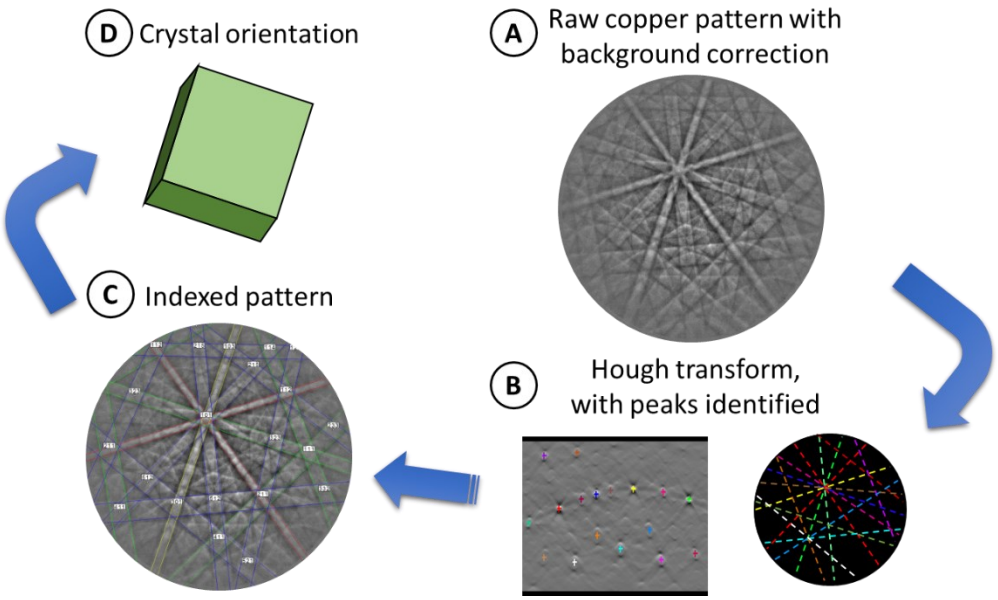


Figure 38 - EBSD: Pattern indexing. Steps to get from the raw (background corrected) pattern (EBSP) to a crystal orientation. (A) Raw copper pattern with background correction; (B) Pattern converted to Hough space and peaks identified; (C) Indexed pattern (D) crystal orientation identified. Reproduced with permission from [136].

The first step is to convert the (background corrected) pattern to Hough space using the Hough transform (equation (3)), where ρ is the length of a normal from the origin to the pattern line and θ is the angle of this line with the x axis.

$$y = -\left(\frac{\cos\theta}{\sin\theta}\right)x + \left(\frac{\rho}{\sin\theta}\right) \tag{3}$$

Once in Hough space, the peaks (now points rather than lines) can be easily identified and indexed. Phase classification can be performed if more than one crystal type is used to compare the measured and expected list of interplanar angles (formed in a look up table, LUT). Indexing can be performed by measuring the interplanar angles from each band and pattern centre (i.e. the projection centre of the diffraction pattern, which is the source position of the electron-sample interactions). Once the bands are indexed, the crystal orientation can be determined by measuring the orientation of the bands found within

the experimental pattern with band positions expected in a reference crystal with a known orientation. This rotation matrix can be described in a number of ways (e.g. matrixes, axis/angle, quaternions) but it is commonly recorded to disk in the form Euler angles, in the form ZXZ'.

In addition to the orientation data, quality information can be recorded. The pattern quality is a measurement of the sharpness of the bands found within the Hough transform, and a lower value of pattern quality is typically associated with poor quality indexing and/or other features such as grain boundaries. The angular deviation of the interplanar angles measured and the interplanar angles expected can be captured in the form of the mean angular deviation (MAD). A low value of MAD indicates good quality indexing, and a threshold value can be used to determine a so-called 'hit rate'.

2.7.4.3 Map creation

A map is created by scanning across the surface of a sample and capturing a pattern at each point. Each point is labelled with data obtained from the experiment, and typically this includes: raster point number, X and Y position on the sample, pattern quality (band contrast, image quality, or Radon quality – depending on the instrument manufacturer), indexing success (e.g. the MAD), phase identified, and crystal orientation.

Using the position and orientation information obtained from the online software , an output orientation map created. The indexed map can then be processed either within the software, or exported and processed externally, for example using MTEX in MATLAB. These microstructural maps can be further analysed to determine grain boundary location and character, as well as more sophisticated microstructural assessment.

2.8 Aims and objectives

This literature review highlights that it would be useful to:

(1) Reconstruct prior-β grain structure routinely, to reveal the role of prior-β grain structure on subsequent microstructural evolution and performance.
(2) Understand the microstructural evolution of Zircaloy-4 cladding materials following post-weld heat treatments, using *in situ* and *ex situ* microstructural characterisation.
(3) Explore hydride-matrix deformation fields at the µm length scale, including characterisation of the stress fields, to help understand how hydrides will influence component performance and why some but not all grain boundaries are decorated with hydrides.

These three objectives are addressed within this thesis.

3 Experimental Methods

The aim of this chapter is to outline the experimental methods used in this thesis. It includes details of the materials used and sample preparation methods, followed by details of analysis techniques used and a sample log.

3.1 Materials

Zircaloy-4 was supplied by Rolls-Royce in the form of rolled sheet and electron beam welded samples. This alloy has a nominal composition of Zr-1.5Sn-0.2Fe-0.1Cr (wt%) [137]. The material was used with two different microstructures in this work:

- **Fine grain α samples**. These were cut from rolled and recrystallised sheet. This sheet has a 'split basal' (α) texture, where the basal planes are oriented at ±30° to the normal direction (ND) towards the transverse direction (TD) after rolling, as shown in Figure 39. The average grain size for the as-received material is ~11 µm, measured using the linear intercept method.

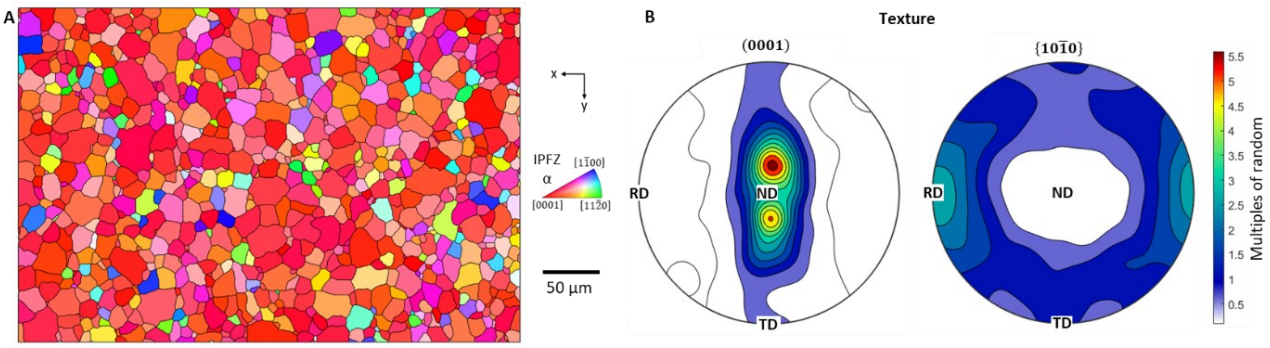


Figure 39 - Fine grain as-received material. A: Crystal orientation map coloured according to the IPF-Z colour key; B:Texture - (0001) and {10-10} pole figures for the IPF map. The map contains 862 grains as processed using MTEX with 4° grain boundary threshold and 5 pixel minimum grain size. The texture is plotted with a FWHM of 10 and range 0.1-6.0 multiples of random.

- **Electron beam (EB) welds**. These samples consisted of two pieces of β-quenched Zircaloy-4 electron beam welded together. A representative microstructure is shown in Figure 40, with three distinct regions identified.
    - Above the weld, there is a fine lath microstructure, with the parent grains clearly identifiable by looking at the different colours in the IPFZ map at Figure 40 (C) for the different parent grain regions, along with the straight lines between these regions.
    - Below the weld there β quenched microstructure is formed of coarser α laths (due to a slower cooling rate) – the entire region in the IPFZ map in Figure 40 (E) comes from the same parent grain.
    - In the weld region, the microstructure is more complex, as can be seen in the polarised optical micrograph at Figure 40 (A) and the IPFZ map in Figure 40 (B). This microstructure is the result

of the rapid heating and cooling that forms part of the EB welding process and is the region of interest for this work.

For more information on similar EB welds, see [44].

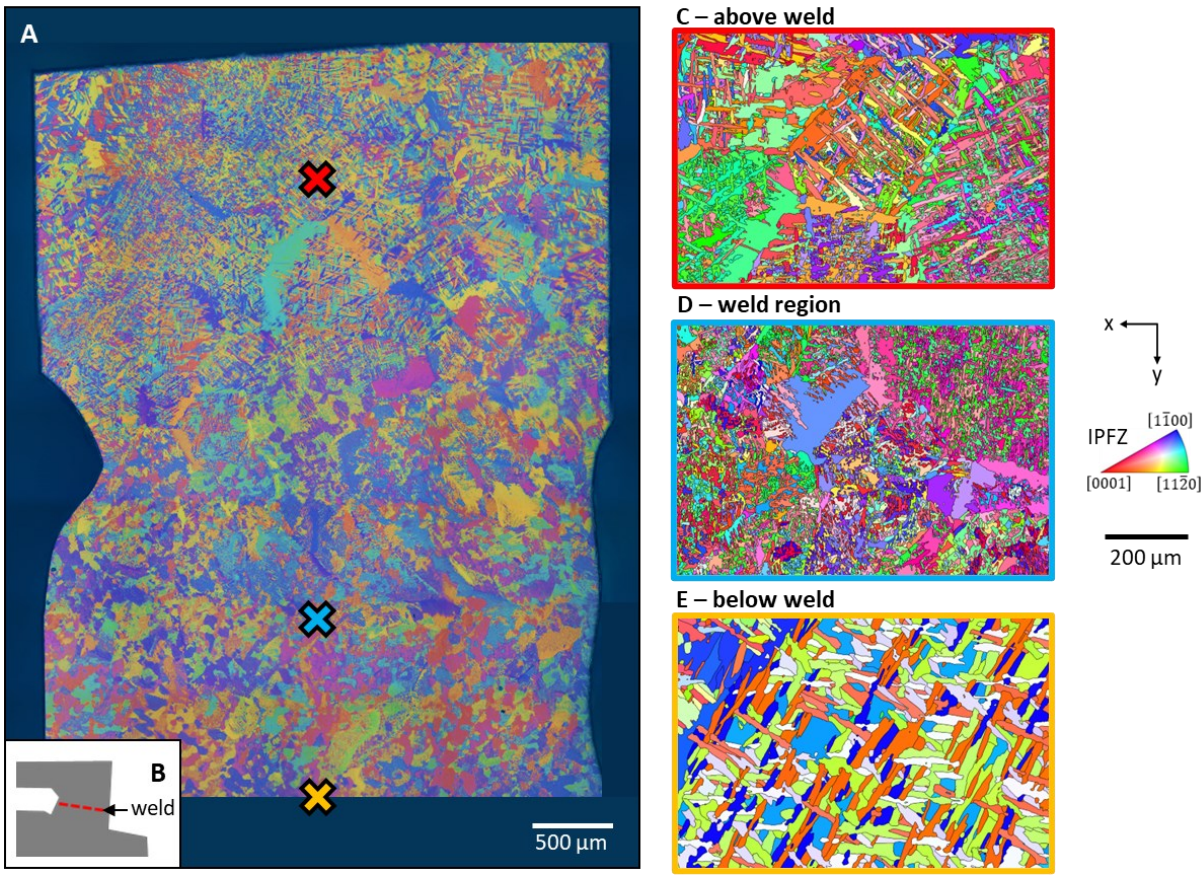


Figure 40 - Weld microstructure overview. A: polarised optical micrograph showing top half of a weld sample - the coloured 'X's correspond to IPF(Z) maps C-E; B: schematic showing weld geometry; C: representative IPFZ map for above the weld; D: representative IPFZ for weld region; E: representative IPFZ map for below weld region (sample bulk). Note: all IPF maps are at the same scale.

The weld sample was manufactured by colleagues at Rolls Royce plc to represent the joint between two structural components. A high energy density, autogenous electron beam weld was performed between a thin, flexible member and a thick component to provide a large heat sink effect leading to fast cooling and relatively high residual stress.

3.2 Initial sample preparation

Details of initial sample preparation techniques:

- **Cutting.** Samples were cut down to the required sizes using a Buehler Isomet 1000 slow saw (gravity fed) with a 0.3 mm diamond cut-off wheel (MOD 10). A slow saw was used to reduce sample waste during cutting and reduce surface damage. Typically, cuts were made at wheel speeds of $\leq$150 rpm with a mass of 50-100 g and water as a lubricant/coolant.
- **Sample mounting.** For mechanical grinding and polishing, samples were mounted using VersoCit-2 cold mount, with the exception of the initial weld slices that were mounted using Bakelite. The Bakelite

mounting was carried out using a Struers CitoPress-20 mounter, set to cure at 180 °C for 3 minutes at 25 bar pressure, with a 2 minute cooling time.

Prior to PECS-based broad ion beam (BIB) polishing (see section 3.5.1), samples were mounted on 12.5 mm Al pin stubs using silver paint ready for SEM analysis. These stubs can then be secured directly into one of the PECS sample holders (see Figure 41) for polishing. The exception to this was for the *in situ* experiments, where the samples were mounted on the Gatan Murano heating cartridges (which fit into the heating stage – see section 3.6.1.1) using high temperature carbon paste. Note that an alternative mounting system had to be designed for securing the heating cartridges to a PECS sample holder, since the heating cartridge is fragile and is easily damaged if stuck to the PECS sample holder using carbon tape. In this case, small metallic offcuts were stuck to the PECS holder to wedge the heating cartridge into place (these must be thinner than the heating cartridge & sample otherwise they may interfere with the polishing), as shown in Figure 41.

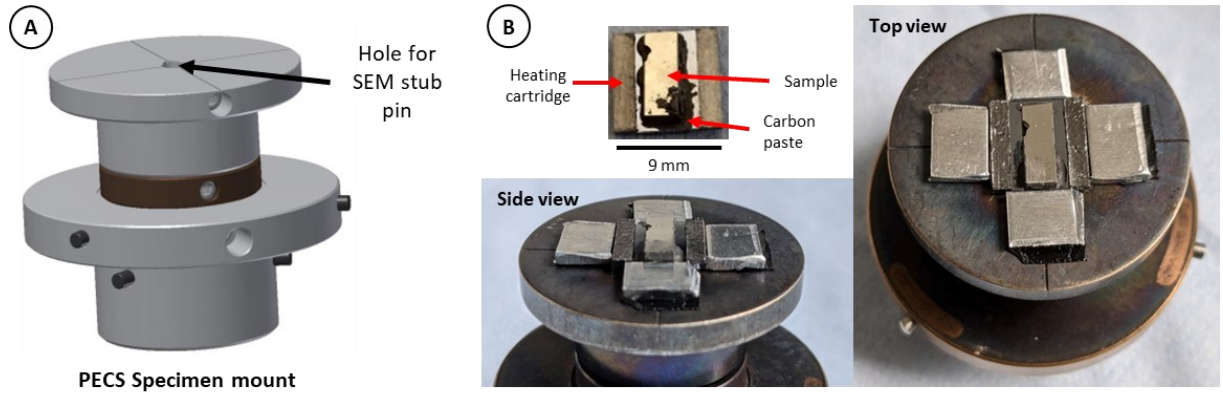


Figure 41 - Specimen mounting for BIB polishing. A: PECS specimen mount for SEM stubs (height adjustable). B: setup for Murano heating cartridges - secured by wedging between small offcuts that are stuck to the specimen mount using carbon tape.

- **Grinding.** Samples were hand ground on a wheel using SiC papers using 800, 1200 & 2000 grit sizes, with an increase in time between grinding steps. The wheel was lubricated with water.
- **Mechanical polishing.** Samples were mechanically polished for 1.5-4.5 hrs using an MD-Chem polishing pad and an OPS based polishing solution mixed at ratio of 5 OPS : 6 H_2O : 1 H_2O_2. This ratio results in a neutral pH – if this is not the case, pitting of the surface may occur during polishing, particularly for the relatively long polishing times used for Zr alloys.

3.3 Heat treatments

To avoid oxidation during subsequent heat treatments, samples were encapsulated in quartz tubes and backfilled with argon gas. *Ex situ* heat treatments were performed using Lenton box furnaces in the Engineering Alloys shared lab. A sample monitoring thermocouple was used to confirm the sample (quartz tube) temperature during heat treatment, as the hot zone has a different temperature to the temperature recorded on the Eurotherm furnace controller. Details of each individual heat treatments are detailed in section 3.9 , however two specific heat treatments are outlined below.

- **Large grain (blocky-α) material**. Large grained samples were prepared from the fine grain α using a 2-week heat treatment at 800°C followed by an air cool (as per the recipe given in [48], [138]). This results in grains >200 µm in average size, an example microstructure is shown in Figure 42.

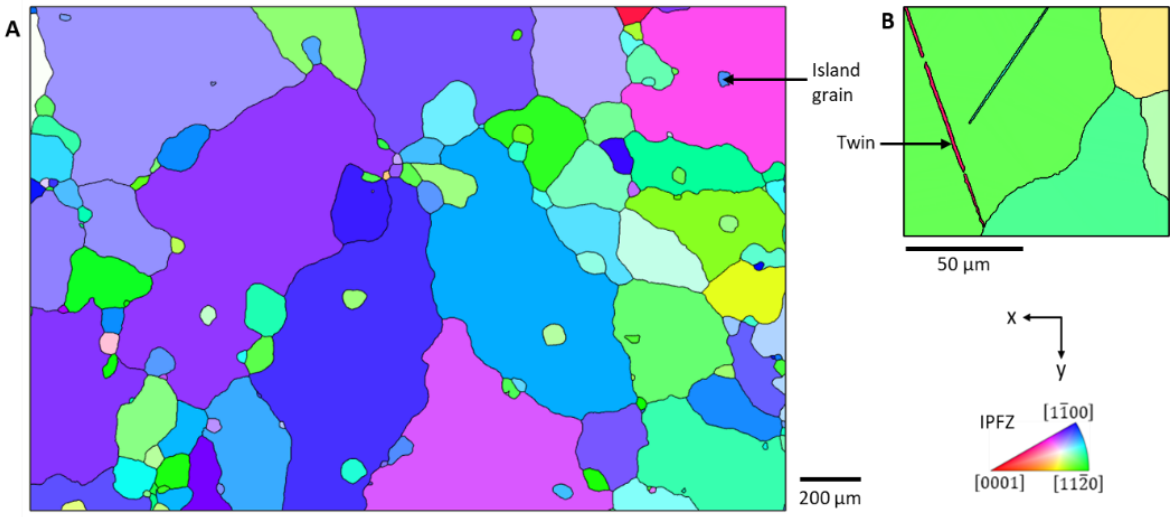


Figure 42 - Blocky-α microstructure - A: IPFZ map showing the large grain microstructure with island grains remaining; B: example showing twinning.

As shown, the grain growth process often leaves smaller island grains among the blocky-α grains. Common features of the microstructure are relatively coarse secondary phase particles (SPPs), which are usually $Zr(Fe, Cr)_2$ and Zr_2Fe [26] and a propensity for sample preparation induced deformation twinning as shown at Figure 42 (B).

3.4 Hydriding

Samples were individually electrolytically hydrided using dilute sulphuric acid (1.5 wt%). The method is described in [54] and is briefly reproduced here for completeness.

3.4.1 Setup

The electrochemical hydriding apparatus is shown schematically in Figure 43. The sample is held as part of an electrochemical cell in an acid solution, and the cell is set up to generate hydrogen ions at the sample surface. The sample is mounted as the anode and a large area Pt mesh is mounted as the cathode. A high current power supply provides a fixed voltage. The electrodes are immersed in a sulphuric acid solution which is heated to 65 °C using a hot plate. Hydriding typically takes 20 hours to create a saturated surface layer [139] and so to reduce evaporation the solution is heated in a flask with a condenser tube.

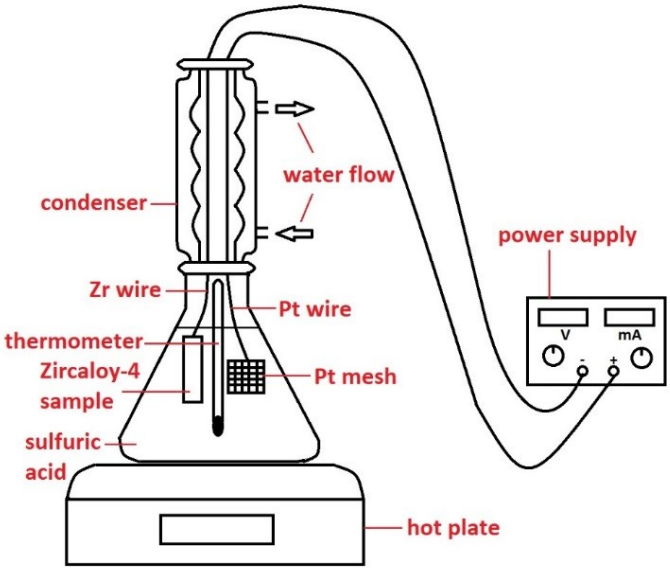


Figure 43 - Schematic of the hydriding rig (Reproduced with permission of Elsevier [54]*).*

Hydriding of Zr for >20 hrs results in the formation of surface hydride layer of fixed thickness (~20 um [139]) where the material is in contact with the solution. After hydriding, this hydride layer is diffused into the bulk via a second homogenisation step.

In this electrochemical charging route, the concentration of hydrogen in a sample can be controlled by adjusting the exposed surface area and volume of zirconium. This is possible as the hydriding forms solid hydride precipitates in the surface layer and the thickness of this layer is limited by the process

The surface area of zirconium exposed to the acid solution is adjusted by coating the surface with a polymer (lacomit) coating and leaving a window unpainted. The applied current (I) required is calculated using the exposed surface area (A) using (1). A fixed current density (J) of 2 kA/m^2 was used in all cases.

$$\mathrm{I} = J \times A \tag{4}$$

All samples were hydrided on one side for 24 hrs unless otherwise stated. In previous work [54], using differential scanning calorimetry (DSC), it was determined that for a 4 x 3 x 3 mm^3 sample hydrided on one side (total surface area 12 mm^2), this results in a hydrogen content of approx. 150 wt ppm.

3.4.2 Hydrogen content

The hydrogen content can be approximated using the thickness of the hydride rim (saturated layer after hydriding) and the volume of the sample, according to equations *(5)-(9).* This approximate value is then used to calculate the annealing temperature and time required for homogenisation of the hydrogen in the Zircaloy-4 material. Symbols used in this section are tabulated in Table 8.

.

Table 8 - Symbol definitions for hydrogen content calculation.

Symbol	Definition	Units
[H]	Hydrogen content	ppm
$V_{hydride}$	Volume of hydride layer	m^3
V_{sample}	Volume of sample	m^3
$V_{\varepsilon\text{-}ZrH}$	Volume of epsilon hydride unit cell (tetragonal)	m^3
$V_{\alpha\text{-}Zr}$	Volume of α-Zr unit cell (HCP)	m^3
n_H	Number of H atoms per ε hydride unit cell	-
$n_{\alpha\text{-}Zr}$	Number of Zr atoms per α-Zr unit cell	-
M_H	Atomic mass of H	-
M_{Zr}	Atomic mass of Zr	-
$t_{hydride}$	Thickness of hydride layer	m
t_{sample}	Thickness of sample	m

To determine the approximate hydrogen content (in ppm), the relative amount of hydrogen atoms in the rim vs. Zr atoms in the bulk are used. The hydride phase for the rim was determined by X-ray diffraction to be ε phase [54] so the hydride parameters are based on this. The hydride unit cell volume ($V_{\varepsilon-ZrH}$) and number of hydrogen atoms per unit cell (n_H) are therefore based on this.

$$[H] = \frac{\frac{V_{hydride}}{V_{\varepsilon-ZrH}} \cdot n_H \cdot M_H}{\frac{V_{sample}}{V_{\alpha-Zr}} \cdot n_{Zr} \cdot M_{Zr}} \tag{5}$$

This rearranges to become a ratio of the hydride volume ($V_{hydride}$) to sample volume (V_{sample}) multiplied by a constant.

$$[H] = \frac{V_{hydride}}{V_{sample}} \cdot \frac{n_H \cdot M_H \cdot V_{\alpha-Zr}}{n_{Zr} \cdot M_{Zr} \cdot V_{\varepsilon-ZrH}} \tag{6}$$

This is equivalent to the hydride layer thickness ($t_{hydride}$) divided by the sample thickness (t_{sample}) multiplied by the constant, A.

$$[H] = \frac{V_{hydride}}{V_{sample}} \cdot A = \frac{t_{hydride}}{t_{sample}} \cdot A \tag{7}$$

Where A is:

$$A = \frac{n_H \cdot M_H \cdot V_{\alpha-Zr}}{n_{Zr} \cdot M_{Zr} \cdot V_{\varepsilon-ZrH}} \tag{8}$$

Using an epsilon phase hydride (ε – ZrH) and α zirconium (α Zr), with lattice parameters identified at Table 9, the value of constant A is 3.4489×10^{-2}.

Table 9 - Lattice parameters for α-Zr and epsilon phase hydrides.[140]

Unit cell	Lattice Parameters		No of Zr atoms in unit cell	No of H atoms in unit cell
	a (Å)	c (Å)		
α Zr	3.2276	5.1516	6	-
ε – ZrH	4.9689	4.4497	4	8

The final equation for hydrogen content (in ppm) is therefore:

$$[H] = 3.4489x10^{-2} \cdot \frac{t_{hydride}}{t_{sample}} \cdot 1x10^{6} \quad (9)$$

Note that for a more accurate determination of the hydrogen content, techniques such as differential scanning calorimetry (DSC) [54] or specific hydrogen analysers (e.g. LECO hydrogen analyser [141]) can be used.

3.4.3 Annealing time

The time and temperature required to diffuse the hydrogen evenly throughout the sample can be calculated using equations (10)-(13). The time and temperature are related and can be adjusted depending on requirements (e.g. if you go to a higher temperature it will be quicker, but there may be microstructural changes, for example grain coarsening, at these temperatures).

The minimum temperature required is calculated using the approximate hydrogen content (in ppm) and equations (10) and (11). Symbols used in this section are tabulated in Table 10.

Table 10 - Symbol definitions for annealing time calculation.

Symbol	Definition	Unit
C_{TSSd}	Hydrogen content at TSSd	ppm
TSSd	Temperature of terminal solid solubility on dissolution	K
T	Temperature	K
[H]	Hydrogen content	ppm
D	Diffusivity constant	cm^2s^{-1}
D_0	Arrhenius constants	cm^2/s
Q		cal/mol
R	Universal gas constant	cal mol^{-1} K^{-1}
L	Furthest distance the H needs to travel through the sample.	Cm

The relationship between hydrogen content and temperature ($C_{Tssd}(T)$) is taken from the experimental work by Vizcaino et al. [140]. This captures the experimental relationship between hydrogen concentration and the temperature of terminal solid solubility on dissolution (TSSd) and is detailed in equation (10).

$$C_{TSSd}(T) = [H] = 263024e^{-4728/T} \quad (10)$$

This can be rearranged to equation (11).

$$T\,(K) = \frac{-4728}{ln\left(\frac{[H]}{263024}\right)} \quad (11)$$

The time required can be determined using equation (12), where L = the furthest distance the H needs to travel [139]. For a sample hydrided on 1 side this would be the sample thickness, whilst for a sample hydrided on two opposite sides this is half sample thickness.

$$time = \frac{1.5 \cdot L^2}{D} \quad (12)$$

The diffusivity constant (D) can be calculated using the required temperature calculated (in Kelvin) and the values at Table 11 in equation *(13)* [139]. The molar gas constant R is 1.987 cal mol^{-1} K^{-1}.

$$D = D_0 exp - \frac{Q}{RT} [139] \quad (13)$$

Table 11 - Values of Arrhenius constants, D_0 and Q for Zircaloy-2, -4. From [142]

Direction through sample*	D_0 (cm^2/sec)	Q (cal/mole)
Longitudinal	7.73×10^{-3}	10830
Transverse	5.84×10^{-3}	10290
Through-thickness	7.90×10^{-3}	10730

*If the direction is unknown, use the value which gives the most conservative value.

The time and temperature can then be adjusted as discussed above using the relationship between equations (11) & (12). It is advisable to use a conservative (slightly higher than calculated) value for the temperature and a slightly longer annealing time for larger samples or where the furnace temperature is known to vary which could lead to an un-even distribution.

As an example, a 3 mm thick sample hydrided on 1 side with a hydride layer approximately 20 µm thick hydride rim could be annealed at 350 °C for ~30 hrs, or 450 °C for ~9 hrs. Annealing time details for my samples are found in the sample log in section 3.9 .

3.4.4 Cooling rate.

The cooling rate after the annealing heat treatment determines both the type and position of the hydrides that form [54], [143]. Generally, slower cooling results in thicker (δ) hydrides located mainly along the grain boundaries, with faster cooling resulting in intragranular hydride formation. For more details see [54] and section 3.9 for specific details of the cooling rate used for each sample.

3.5 Ion beam polishing

The zirconium surface layer was prepared using broad ion beam polishing as a final step for all samples in the project prior to SEM analysis.

3.5.1 Broad ion beam (BIB) polishing

Broad ion beam (BIB) polishing was carried out using a Gatan PECSII machine [144]. The PECSII machine uses two miniature penning ion guns to produce broad argon (Ar+) ion beams that etch the surfaces of the sample. The guns are adjustable from 0-8 keV and 0-18 ° incidence angle (to the surface). An investigation to optimise polishing parameters was carried out in conjunction with Ning Fang, for more details see [145]. Depending on holder and recipe, the PECSII machine can be setup for planar or cross-sectional polishing.

3.5.1.1 Planar polishing

Planar, or surface, polishing creates a polished region on the top surface of the sample. The size of this polished region will vary with gun incidence angle (lower angle = greater area) and voltage but can be up to 4 mm^2. Generally, samples are polished whilst attached to SEM stubs, as shown in the schematics in Figure 44 A and B. Figure 44 C shows a special case where the sample (attached to a Murano heating cartridge) had to be held in place on the PECS sample holder using small pieces of metal in order to carry out planar polishing during the *in situ* experiment. In all planar polishing recipes used in this work, the gun modulation was set to 'no modulation' i.e. both guns are always on, as shown in Figure 44 B.

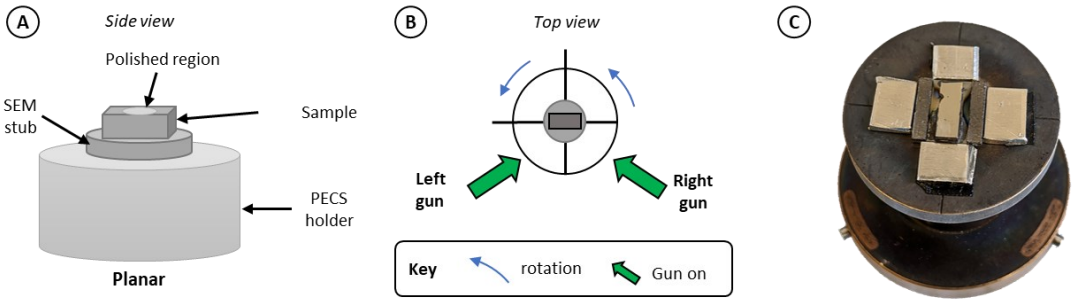


Figure 44 - Planar BIB polishing. A: schematic showing sample mounted on SEM stub with polished region indicated; B: Top view showing gun operation during planar polishing; C: special case - setup for polishing weld samples that are already attached to a Murano heating cartridge.

3.5.1.2 Cross-sectional polishing

An alternative polishing setup is cross-sectional – this creates a small, polished region that cuts into the top surface of the sample, up to ~70 µm deep. In this setup, the sample is mounted on the back of a Ti blade, and the top surface that protrudes above the edge of the blade is cut into. The blade and cross-sectioning geometry are shown schematically in Figure 45 along with a secondary electron image of the top surface of a cross-sectioned example.

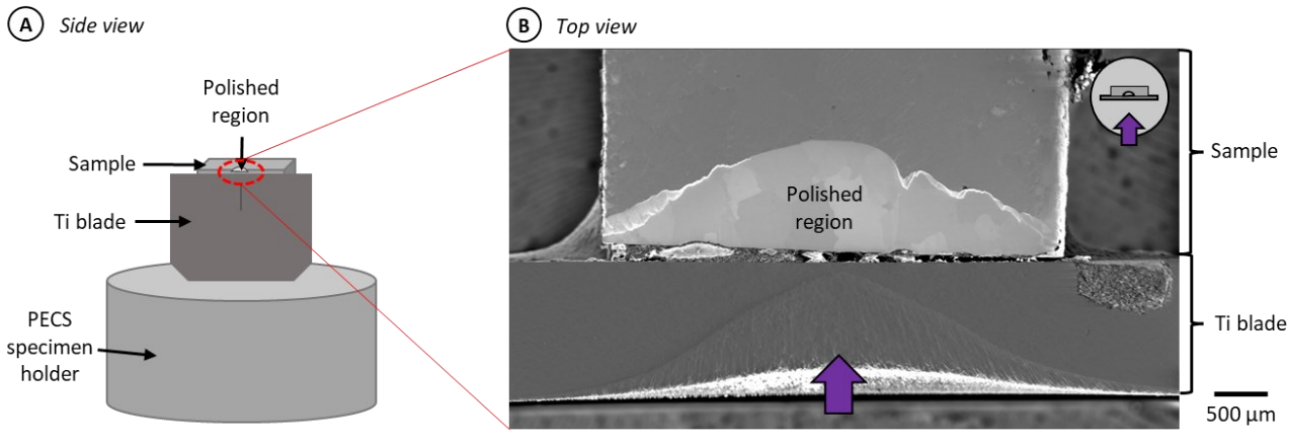


Figure 45 - Cross section BIB polishing. A: schematic showing sample behind Ti blade with polished region indicated (side view); B: top view setup for polishing (SE image). The purple arrow indicates the ion beam polishing direction.

The ion beam guns for this process are aligned at 0° angle, and the aim is for the widest part of each gun beam to hit the top edge of (angled) Ti blade (i.e. 50% of the beam hits above the blade edge), cutting sideways into the sample. The sample is still rotated during the polishing, but the guns are run in single modulation mode, using a 90° sector. A schematic for single modulation is shown in Figure 46 – essentially this means that each gun is only on whilst the Ti blade is facing it, within the desired sector, so each gun polishes the sample independently (alignment is important!).

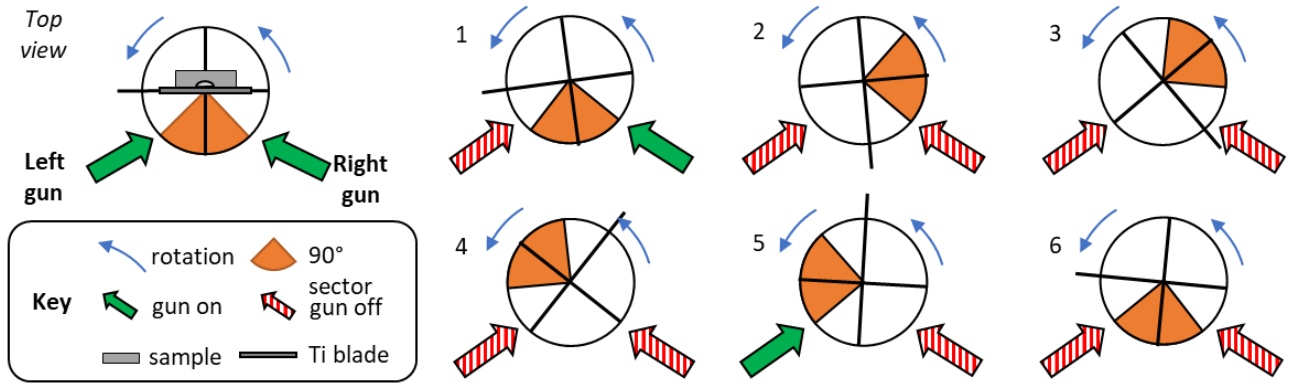


Figure 46 - Schematic showing how single modulation works: The top view of the setup is shown on the left; the relative position of the sample and gun on/off are shown in 1-6, which are chronological as the sample rotates – adapted from figure 3-76 in [8].

The polishing time is approximately 6 hrs – the limiting factor being the Ti blade – as soon as the top edge adjacent to the sample is damaged, the quality of the polished region decreases dramatically, as shown in Figure 47.

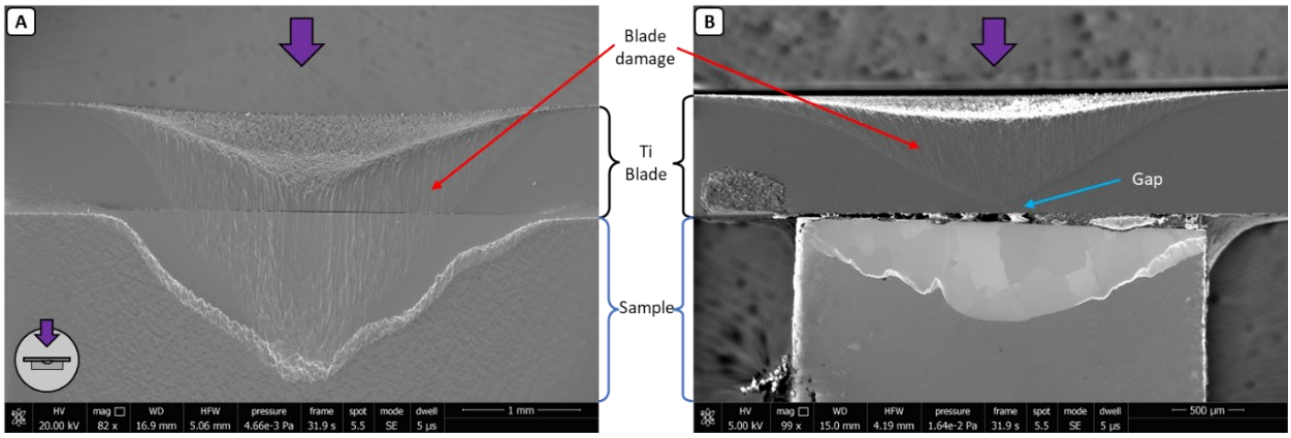


Figure 47 - Cross section polishing quality – (A) Poor quality when the edge of the Ti blade adjacent to the sample has been damaged (B) good quality polished region when the edge is intact (gap in damage vs. blade edge indicated by blue arrow). Blade damage is indicated by the red arrows.

3.5.1.3 Cold BIB Polishing

An adaption to both polishing methods is to use liquid nitrogen to cool the sample in the chamber and eliminate (localised) sample heating issues during polishing. Cold polishing generally leads to a more uniform surface finish and better EBSD pattern quality, even at lower voltages and gun angles than would be used at room temperature. The impact of cold polishing was investigated in [145]. Running cross-sections cold has also proven to be an effective way to retain and polish zirconium hydrides rather than remove them as so often occurs during room temperature polishing (cross section or planar).

This method adds approx. 1.5 hrs to the polishing process: 0.5 hrs to cool the chamber; 0.5 hrs to then cool the sample when added to the cooled chamber; and 0.5 hrs to heat the sample prior to removal from the chamber to avoid condensation on the sample. The PECSII nitrogen dewar needs topping up every 5-8 hrs.

3.5.1.4 Recipes

Typical polishing recipes used are detailed at Table 12, with recipe A the most commonly used for planar polishing. For more information about optimising BIB parameters, see [145].

Table 12 - Standard broad ion beam polishing recipes used

Recipe	Type	Temperature	Voltage (keV)	Gun angle (°)	Duration (mins)	Modulation Type	Rotation speed (rpm)
A	Planar	RT	8	8	15	None	1
B	Planar	RT	6	6	15	None	1
C	Planar	Cold	8	8	15	None	1
D	Planar	Cold	6	6	15	None	1
E	Cross section	Cold	8	0	360	Single - 90° sector	1
F	Cross section	Cold	8	0	600	Single - 90° sector	1

3.5.2 Focussed ion beam (FIB) polishing

For this thesis, cross sections of Zircaloy-4 containing zirconium matrix and zirconium hydrides were created using a plasma focussed ion beam (pFIB) instrument to enable site specific preparation of cross sections that contain zirconium hydride plates. A Thermofisher Scientific Helios Hydra DualBeam

instrument fitted with a cryo-stage was used, and the sample preparation recipes are described in Table 7. This experiment was one of the first experiments performed using cryo-pFIB at Imperial College London, with the kind assistance of Dr James Douglas. Due to the nature of preliminary experimentation the conditions reported in Table 7 are described with the best of our knowledge of how the instrument was set up. The specific uncertainty is the sample temperature in step 2. Due to the nature of ion-beam induced hydride formation in Zircaloy, the polishing step (Step 3) was confirmed to be performed in cryo conditions.

Table 13 - pFIB polishing recipe details for hydrided Zircaloy-4.

Step		Aim	Details
1	Rough mill	Setup for polishing	• 30 kV 2.5 µA Xe for rough mill • Deposit Pt at 12 kV at 60 nA for 5 µm thick
2	Initial mill	Find ROI grain boundary region	• Mill at 30 kV Xe at 0.5 µA
3	Polish	Cryo-final polishing	• Switch to Ar plasma • Tilt to 53° • 30 kV and 0.5 µA • 12 kV and 200 nA for polishing • 12 kV and 28 nA for polishing • 12 kV and 14 nA for polishing

The final polishing steps were performed at cryogenic temperatures to reduce ion-surface damage and secondary formation of hydrides (a known issue for Zr- and Ti-alloys, see [146], [147]).

One challenge of cryo-milling is to ensure the sample temperature is maintained during milling, and in this experiment a cryo-suitable copper spring clip microtip stub in a specimen puck [148] holder was used. The sample was attached to the holder using silver paint and also held in place with the clip. This holder (Figure 48 A) enables a cross section to be performed with the polishing face to be at normal incidence to the plasma ion beam. The holder was then transferred to the Quanta 650 instrument and mounted on a 20° pre-tilted stage (Figure 48 B) so that the polished face is presented at 20° to the incident electron beam. The polishing geometry and EBSD analysis geometry are shown in Figure 48 C.

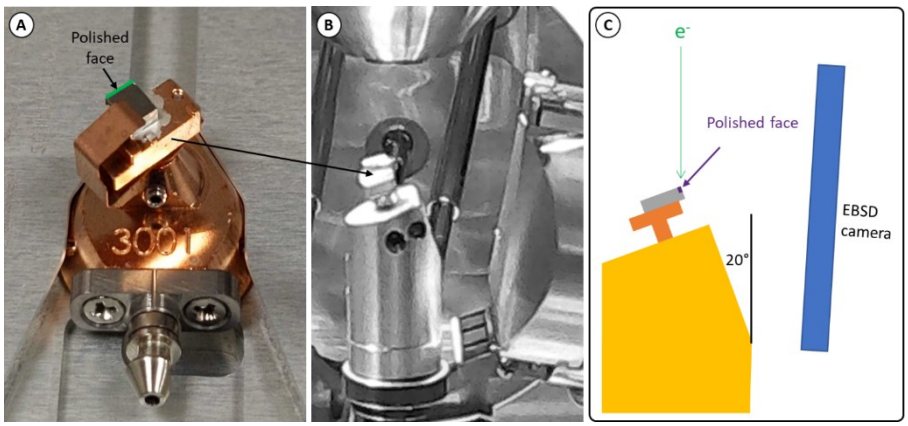


Figure 48 - Sample holder and EBSD analysis conditions for pFIB cross sections. (A) Cryo-suitable copper spring clip microtip stub in specimen puck [148] *containing the sample for pFIB polishing. The sample is held under a clip and affixed to the holder with silver paint. (B) EBSD setup – chamber view showing sample in the chamber with the ebsd detector inserted. (C) schematic showing how the holder and sample are loaded for EBSD.*

3.6 *In situ* heating experiment

The setup for the *in situ* heating experiment used for investigating grain growth in electron beam welded microstructures (see chapters 5 ,6 and 7) is detailed in this section.

3.6.1 Equipment

The *in situ* heating experiment setup contains multiple parts, both internal and external to the SEM chamber, as detailed below.

3.6.1.1 Murano heating stage

A Gatan Murano heating stage [149] was used for the *in situ* experiment. This stage can heat samples to 950 °C (as measured on the internal thermocouple) using ramp rates of >100 °C/s (temperature dependent). It consists of a number of sections:

- Heating carriage (Figure 49) – this is the main unit for the Murano stage – it both heats the sample and controls the temperature (for more details on temperature control see chapter 1 5). Samples (9 x 3 x 2 mm) are inserted into the heating carriage on consumable heating cartridges (semiconductor hot plates), to which they are attached with high temperature carbon paste. An EBSD shield was used for these experiments to protect components inside the microscope from the effects of light emission and radiative heating [149].

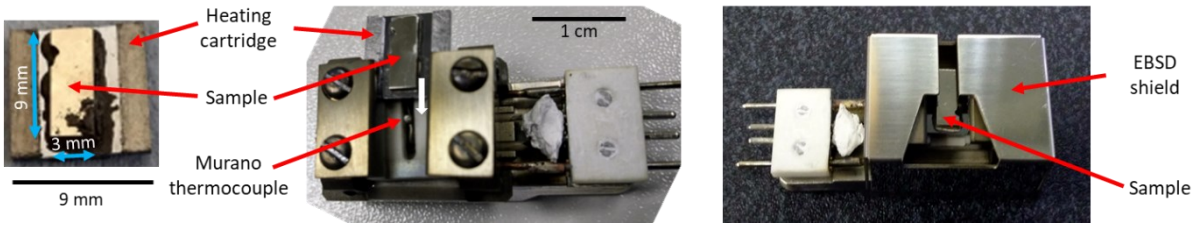


Figure 49 - Murano heating carriage. LEFT: heating carriage with (sample on) heating cartridge partially inserted (it slides in, as indicated by the direction of the white arrow). RIGHT: heating carriage with sample and EBSD shield installed.

- Heating module (Figure 50) – the Murano stage has two potential setups – flat for imaging or pre-tilted (70°) for EBSD. For this experiment, the pre-tilted version was used throughout.

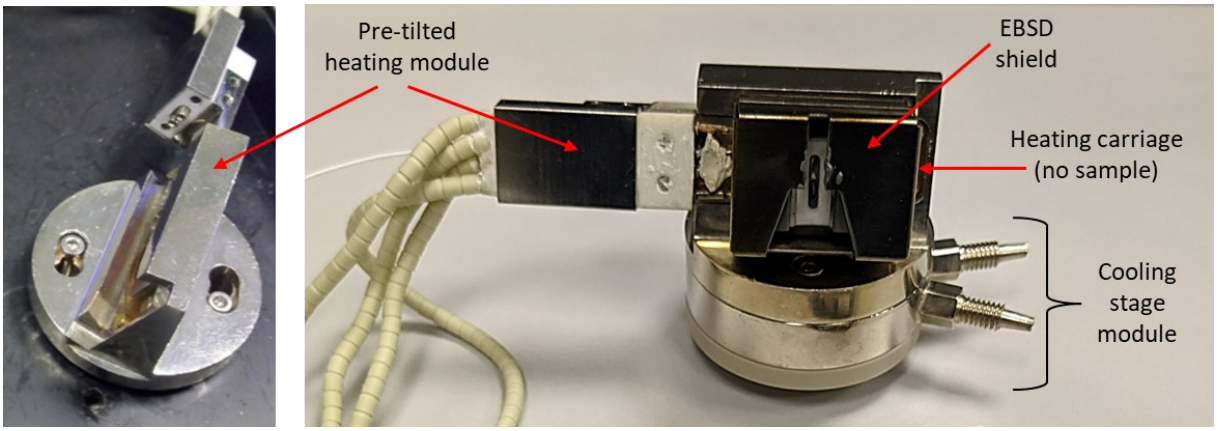


Figure 50 - Pre-tilted heating module. LEFT: slide view showing the tilted setup. RIGHT: pre-tilted heating module with heating carriage in place, installed on cooling stage module.

- Cooling stage (Figure 50) – The stage is cooled using a water jacket which connected to an external chiller, via the Murano flange. The cooling stage module is shown in Figure 50. This is a closed loop system filled with de-ionised water that is used to cool the sample.

3.6.1.2 High temperature phosphor

A Bruker high temperature EBSD phosphor with an Al coating on the surface was used for this experiment (Figure 51 (A)). Note that this will deteriorate after prolonged exposure at high temperatures, as shown in Figure 51 (B) and discussed in chapter 1 5 .

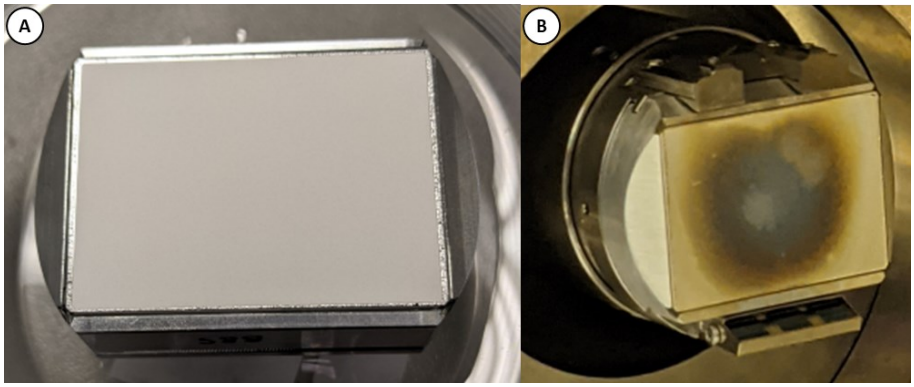


Figure 51 - High temperature (HT) phosphor. A: new HT phosphor; B: Installed HT phosphor showing significant deterioration after trials at high temperature.

3.6.1.3 Flanges.

Two specific flanges are required for this experiment:

- Murano flange (Figure 52) – this attaches the cooling loop, power, and temperature control to the Murano stage in the chamber. It also has a gas inlet if required and bias control for the stage (used for imaging).

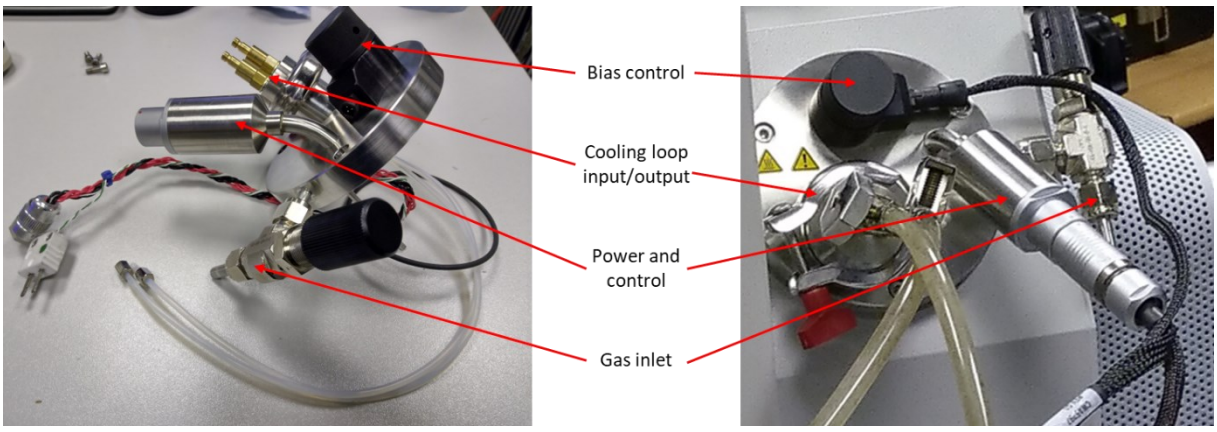


Figure 52 - Murano flange with external connections labelled.

- Thermocouple flange (not pictured) – This is a simple pass through flange that allows additional thermocouple(s) to be used in the chamber and read externally. An additional thermocouple was used for testing and to monitor the sample surface temperature throughout the experiment.

3.6.1.4 External connections.

To control the Murano heating stage and monitor the temperature, a number of external connections are required. The main components are identified in Figure 53 – these are: a power booster unit to enable the stage to heat to 950 °C; a chiller unit for the cooling loop and a USB controller, which has inputs from the chiller and power unit and feeds into the Murano control laptop. In addition to this, any additional thermocouples added via the thermocouple flange feed into a datalogger which can either store the data for later download or be fed directly into another laptop.

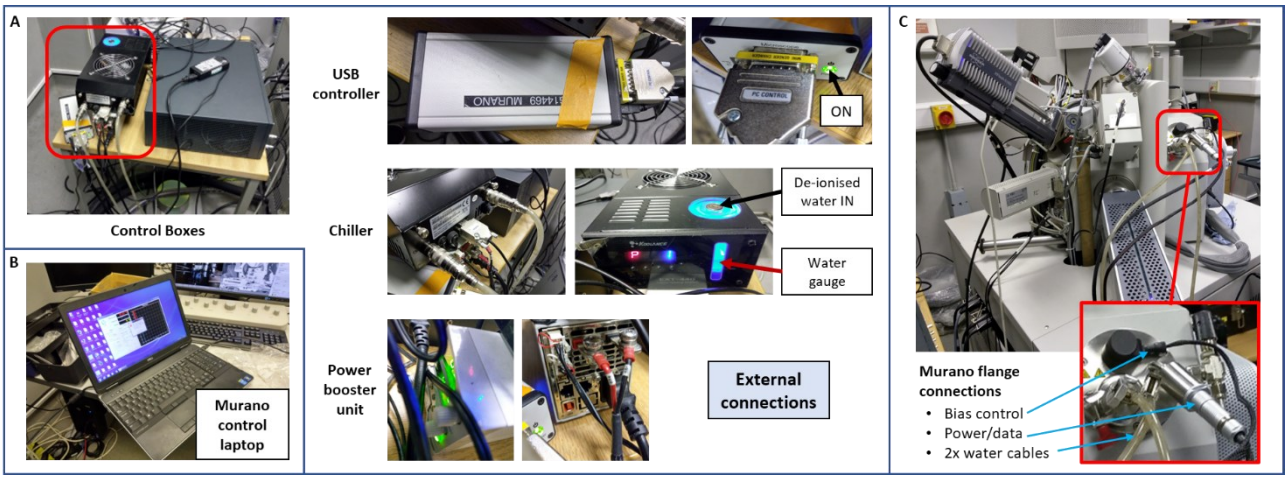


Figure 53 - External connections for the Murano stage. A: cooling system control: chiller and control boxes; B: Laptop for Murano stage control; C: External connections on installed Murano flange.

3.6.2 Final setup

The final setup for the Murano stage (with additional thermocouple of the surface) is shown at Figure 54 (A) along with an in chamber view with the EBSD detector inserted. Discussion of the additional thermocouple that is used to monitor the sample surface temperature can be found in chapter 1

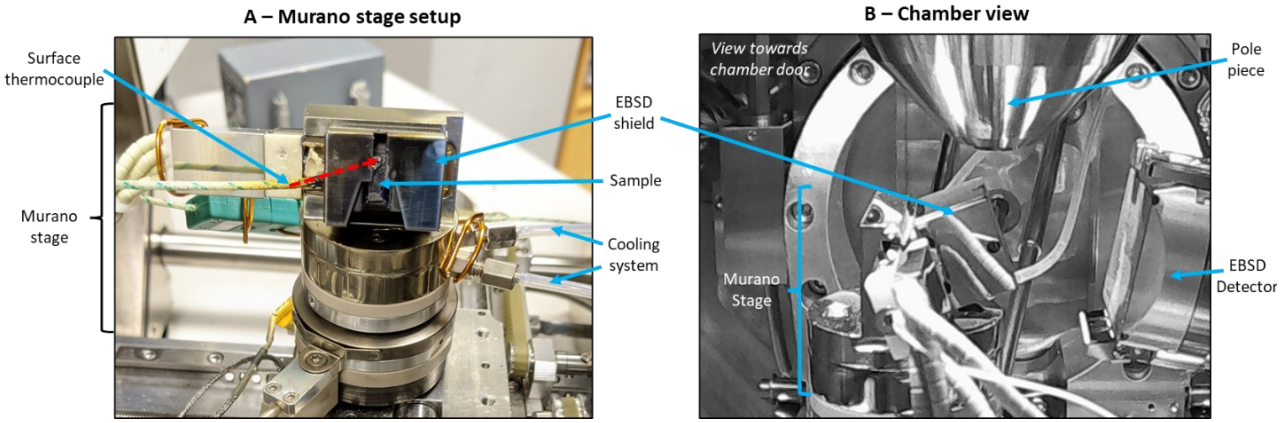


Figure 54 - In situ experiment setup. A: Murano stage assembled (with additional thermocouple) and (B) chamber view with the EBSD camera inserted.

3.6.3 Heat treatment & data collection

The exact heat treatment and data collection schedule for each sample is detailed in Table 14, however a representative example is found in Figure 55. Three data types are collected: temperature; forescatter imaging and EBSD.

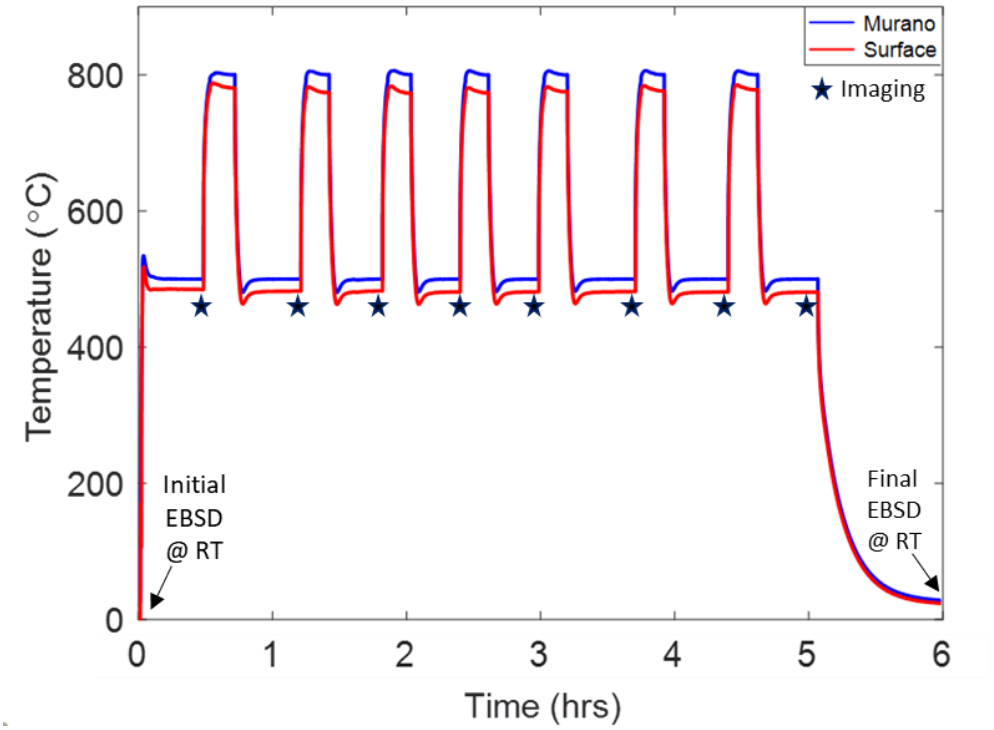


Figure 55 - Representative heating cycle and data collection points for the in situ heating experiment.

An interrupted heating cycle is used, with 10 min holds at temperature (800 °C on the Murano thermocouple, >760 °C surface temperature) interspersed with holds at 500 °C (Murano thermocouple) to enable forescatter imaging of the surface. EBSD maps are taken *in situ* at the start and finish of the experiment at room temperature (RT). The number of cycles used varied but for reference, Lusby [125] showed full coverage of blocky-α in the weld region after as little as 2 hrs. Note: an additional BIB planar polish may be required prior to the final EBSD map depending on the level of oxidation.

A full discussion of the decisions that led to this solution can be found in chapter 1 5 .

3.7 *Ex situ* heating experiment

One weld sample was sectioned from the weld and prepared for EBSD mapping, using standard metallographic routes and final polishing with (cold, planar) BIB. The sample was mapped, and then encapsulated in a quartz tube that was evacuated and then backfilled with Argon. The tube was heated at 760 °C for 4 hrs and air cooled. The sample was subsequently removed from the quartz tube and repolished using planar BIB polishing and mounted for EBSD mapping.

As this was a relatively large sample (approx. 12 x 8 x 1.5 mm), BIB was carried out on multiple areas. This was achieved by mounting the sample on an SEM stub using a small amount of carbon tape and moving the sample on the stub between polishes. The recipe used for these polishes was 6 keV, 6 °, 1 rpm, no modulation, 20 mins, cold (cooled with LN_2). The results for this sample are presented in chapter 6 6 .

3.8 Analysis Techniques

Analysis of microstructural evolution in Zircaloy-4 has focussed on polarised light optical microscopy and scanning electron microscopy (SEM). For SEM, three types of imaging were employed: secondary electron imaging; forescatter electron imaging; and electron backscatter diffraction.

3.8.1 Polarised light optical microscopy

Polarised optical microscopy reveals the grains within the Zr samples that are not visible in an optical light microscopy bright field image. Figure 56 shows a weld sample imaged with and without polarisation, along with a processed version of the polarised image. In the latter case, the image has been processed in ImageJ to balance and stretch the colours, allowing easier observation of the grains present (unfortunately this makes the stitching artifacts more obvious). In this example, these micrographs enable easy observation of the different regions across the weld, highlighting the changes in grain size and morphology across the imaged region.

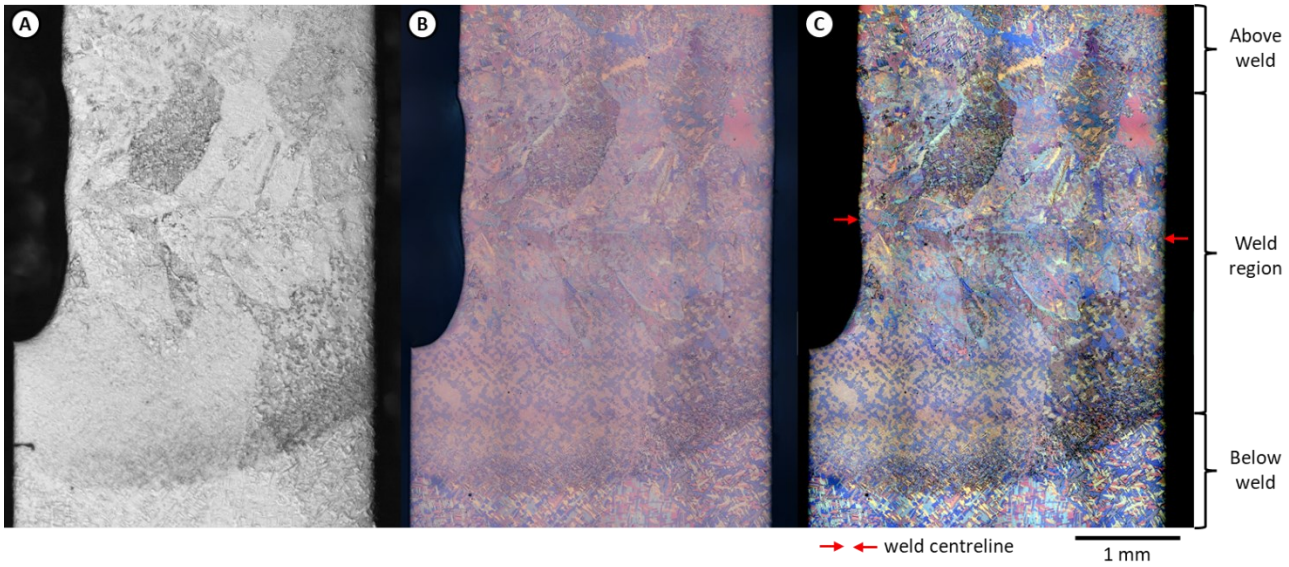


Figure 56 - Polarised optical microscopy example. Initial weld microstructure (Zircaloy-4) imaged (A) without polarisation (B) with polarisation and (C) after image processing. Using polarised optical microscopy, the grains are clearly identifiable. Note: B and C are stitched images – the grid results from stitching artefacts.

For this thesis, all optical microscopy was carried out using an Olympus BX51 light microscope. For more information on polarised optical microscopy see [150], [151] and specific to HCP materials [130], [131].

3.8.2 Forescatter electron (FSE) imaging

The Bruker ARGUS imaging system [134], [152], used for FSE imaging in this work, consists of three diodes which are attached underneath the phosphor screen of the EBSD detector. Each diode captures a different part of the diffracted signal and is assigned a colour (red, green, blue). The software (Esprit) then creates a false colour image based on the input to each of the three channels. Changes in grain orientation cause subtle variations in signal variation (largely due to channelling-in effects [135]), changing the signal collected and allowing an image to be created to display the changes to the user.

Changing the detector distance for FSE imaging switches between giving more information about surface topography at shorter detector distances to more grain contrast at higher distances. The grain contrast can also be optimised by tilting the detector to adjust how contrast is formed (for more details on optimising scanning electron channelling contrast for imaging see [135]).

Figure 57 shows how different micrographs can be captured by adjusting the detector positioning. (C) was taken using a detector distance of 17 mm and tilt of 9.5 ° whereas (D) was captured using a (longer) detector distance of 27 mm and tilt of 10.6 °. In (C) the surface topography is clear – with grains easily identifiable due to the surface gradients at grain boundaries (caused by different orientations polishing at different rates). In comparison, (D) gives more information about grains using a false colour image, and surface topography is minimised.

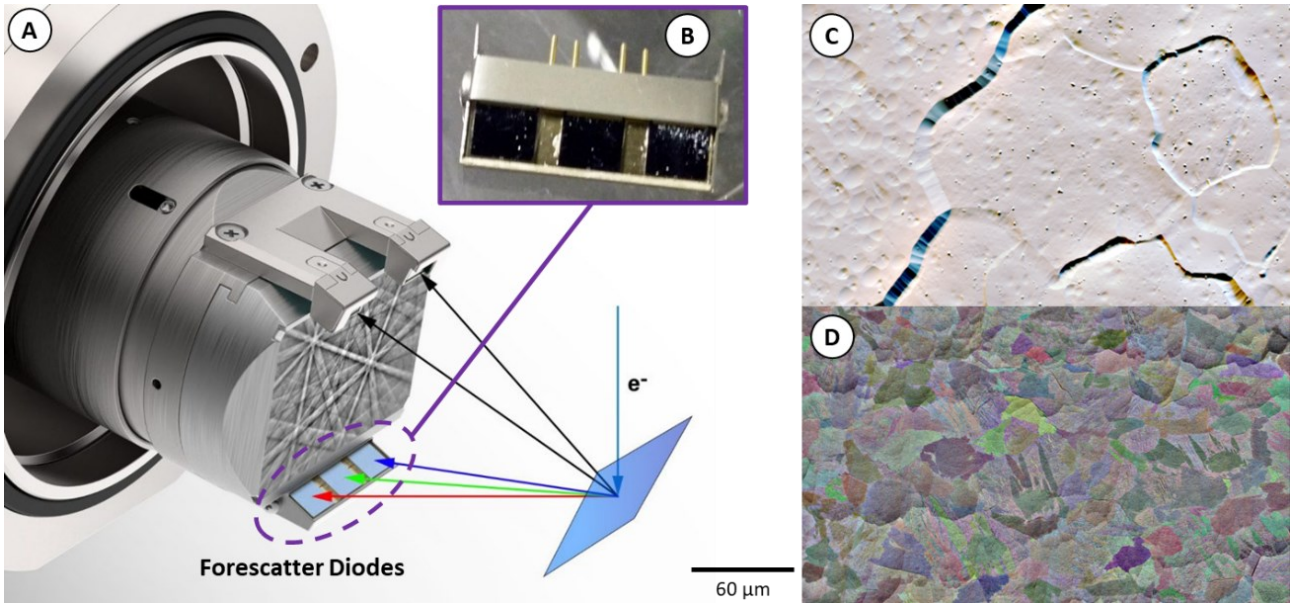


Figure 57 - Forescatter imaging examples. (A) Bruker ARGUS FSE/BSE imaging system showing path of electrons to forescatter diodes in the tilted sample configuration [reproduced from [134]*]; (B) Photo of the forescatter diodes removed from the detector; (C) FSE image of large grain Zircaloy-4 taken at a detector distance of 17 mm and showing surface topography; (D) FSE image of β-quenched Zircaloy-4 taken at a detector distance of 27 mm and showing grain contrast.*

3.8.3 Electron backscatter diffraction (EBSD)

For this work, typically EBSD data was collected using an FEI Quanta FEG 650 SEM equipped with the Bruker eFlashHD2 EBSD detector. Collected electron backscatter diffraction patterns (EBSPs) were processed online in the Esprit [153] software to determine the orientations prior to further processing using MATLAB [154]. Note that it is important to use the correct axes for the setup and software (see [155]) in order to usefully describe the sample orientations.

3.8.4 High angular resolution electron backscatter diffraction (HR-EBSD)

Some data was analysed using a mixture of EBSD and high angular resolution EBSD (HR-EBSD), as follows.

Conventional (online) EBSD was used to measure the crystal orientations and determine the phase for each point. This data was used for conventional analysis within MTEX which was then used for labelling to run

the polycrystalline high angular resolution EBSD (HR-EBSD) with the XEBSD software code, developed by Britton and Wilkinson [156]. EBSD maps were captured with patterns stored to disk at 2x2 binning (i.e. 800 x 600 pixels) with a step size of 0.08 µm, an estimated probe current of ~10 nA, and an exposure time of 150 ms.

HR-EBSD analysis was performed offline, and in brief the XEBSD code will automatically select reference patterns (of high pattern quality, and far from the grain boundary) and cross correlate each pattern within the grain to measure the (type 3) deformation tensor that maps the reference to the test crystal. This is achieved using region of interest-based image correlation, with filtering in the Fourier domain to remove high spatial frequency noise and low frequency long range background gradients. Two passes of cross correlation were used to enable measurement of subtle variations in elastic strain (i.e. stress) in the presence of larger lattice rotations. After the first pass, the pattern was remapped using an interpolation of the diffraction pattern intensities once a finite rotation was applied (i.e. following the method of [156]).

Lattice strains and the stress tensor were extracted and separated using crystal orientations of the hydride and matrix phase and the following elastic constants (and anisotropic Hooke's law) assuming an out of plane traction free boundary condition (i.e. $\sigma_{zz} = 0$).

The density of geometrically necessary dislocations (GNDs) was calculated using Nye's framework and the approach described by Wilkinson and Randman [157]. Six lattice curvatures are used to calculate six terms of the Nye tensor, and then the dislocation densities are calculated by minimising the line energy assuming that the energy is proportional to b^2 for screw and $(b^2/(1-\upsilon)$ for edge dislocations (where b is the Burgers vector and υ is Poisson's ratio) [158]. For the zirconium phase <a> basal, prism, and pyramidal slip systems, as well as <c+a> 1st order pyramidal slip systems were used. For the hydride, it was assumed to be FCC(-like) and <111>{110} slip systems were assumed.

3.9 Sample Log

Details of the samples, relevant experiment and heat treatments are shown in Table 14.

Table 14 - Sample log

Experiment		Sample ID	Microstructure (start)	Sample dimensions L x W x D	Heat Treatment(s)	Hydriding
In situ	Experiment 1	*In situ* 8	Weld	9 x 3 x 1.7 mm	*In situ* heating cycle[6]: 10 mins @ ~780°C [HT] ~15 mins @ ~480°C [imaging temp] No of cycles: 7 Total time at HT temperature: 70 mins	N/A
	Experiment 2	*In situ* 9 EBW3a_A	Weld	9 x 3 x 1.5 mm	*In situ* heating cycle[1]: 20 mins @ 790 °C [HT] ~15 mins @ 500 °C [imaging temp] No of cycles: 1 Total time at HT temperature: 20 mins	N/A
	Experiment 3	*In situ* 9 EBW3a_C	Weld	9 x 3 x 1.5 mm	Part 1 *In situ* heating cycle[1]: 10 mins @ 765 °C [HT] ~15 mins @ ~480 °C [imaging temp] No of cycles: 3 Total time at HT temperature: 30 mins Part 2 *In situ* heating cycle[1]: 10 mins @ ~790 °C [HT] ~15 mins @ ~480 °C [imaging temp] No of cycles: 2 (10 min + 20 min) Total time at HT temperature: 30 mins	N/A
Ex situ Trial		EBW3a_E	Weld	Slice – approx. 12 x 8 x 1.5 mm	4 hrs @ 760 °C Air cool	N/A

[6] Measured surface thermocouple temperatures

Experiment	Sample ID	Microstructure (start)	Sample dimensions L x W x D	Heat Treatment(s)	Hydriding
Hydride stress field	2.5H	Fine grain α	4 x 3 x 1.5 mm	Blocky-α HT: 2 weeks @ 800 °C / air cool Hydride anneal: 7 hrs @ 475 °C Cooling rate: slow furnace cool	No of sides: 1 Time: 24 hrs
	2.9H	Fine grain α	20 x 3 x 3 mm	Blocky-α HT: 2 weeks @ 800 °C / air cool Hydride anneal: 3 hrs @ 460 °C Cooling rate: 5°C/min (furnace cool)	No of sides: 2 Surface area hydrided: 120 mm^2 Current: 240 mA Time: 24 hrs
Reconstruction code testing	WQ10min *(experimental example)*	Fine grain α	9 x 3 x 3 mm	β colony HT: Temperature: >1000 °C Hold: 10 mins Cooling: Water quench	N/A

4 Reconstruction Code

4.1 Overview

This chapter introduces the development and testing of a new parent grain reconstruction code (i.e. reconstruction of the parent β grains that were present at an elevated temperature processing step, prior to cooling into the α-phase field), which includes post processing analysis that is useful for Zr alloys. Parent grain reconstruction can be used to understand the impact of processing routes on the final microstructure and the post processing analysis provides further detail on the final microstructure (e.g. α variants).

This chapter introduces the development the 'ParentBOR' code, followed by testing (simulated and experimental datasets) and then comparison with an alternative code.

This chapter reproduces material written up in my paper entitled 'Effective structural unit analysis in hexagonal close-packed alloys – reconstruction of parent β microstructures and crystal orientation post-processing analysis' [1].

4.2 Symmetry and crystallography of the Burgers orientation relationship (BOR)

The OR for the BCC/HCP phase transformation in zirconium alloys (as reported by Burgers [13]) is:

$$(0001)_\alpha // \{110\}_\beta \text{ and } \langle 11\bar{2}0\rangle_\alpha // \langle 1\bar{1}1\rangle_\beta \tag{14}$$

4.2.1 BCC to HCP

For any initial β grain, the transformed α orientation can be one of 12 unique variants, as described by the BOR and this is shown in Figure 58. In this figure, an initial orientation of the β phase (BCC) has been selected and each of the six $\{110\}_\beta$ planes highlighted in turn, in a different colour. Each of these $\{110\}_\beta$ planes contain two different $\langle 1\bar{1}1\rangle_\beta$ directions, e.g. for $(110)_\beta$, the two directions are $[1\bar{1}1]_\beta$ and $[\bar{1}11]_\beta$. For each cube shown, one of the two $\langle 1\bar{1}1\rangle_\beta$ directions contained within has been highlighted with a dashed pastel coloured/black line. The corresponding hexagonal prisms (α orientations - which do change) are shown in the columns adjacent to the cubes. In each case, the $(0001)_\alpha$ plane is highlighted with the same colour as the plane that it matches in the BCC orientation and the $[11\bar{2}0]_\alpha$ direction has the same pastel coloured/black dashed line as its corresponding $\langle 1\bar{1}1\rangle_\beta$ direction in the BCC orientation. This information is shown on the pole figure plots for the BCC/HCP planes and directions. In this case, the BCC orientation (including symmetry) is shown with the small black dots, and the larger dots are the HCP planes & directions. The overlapping, coloured, point is the shared plane or direction, and the colours correlate with the prisms. Note that all prisms and pole figures have the same axes.

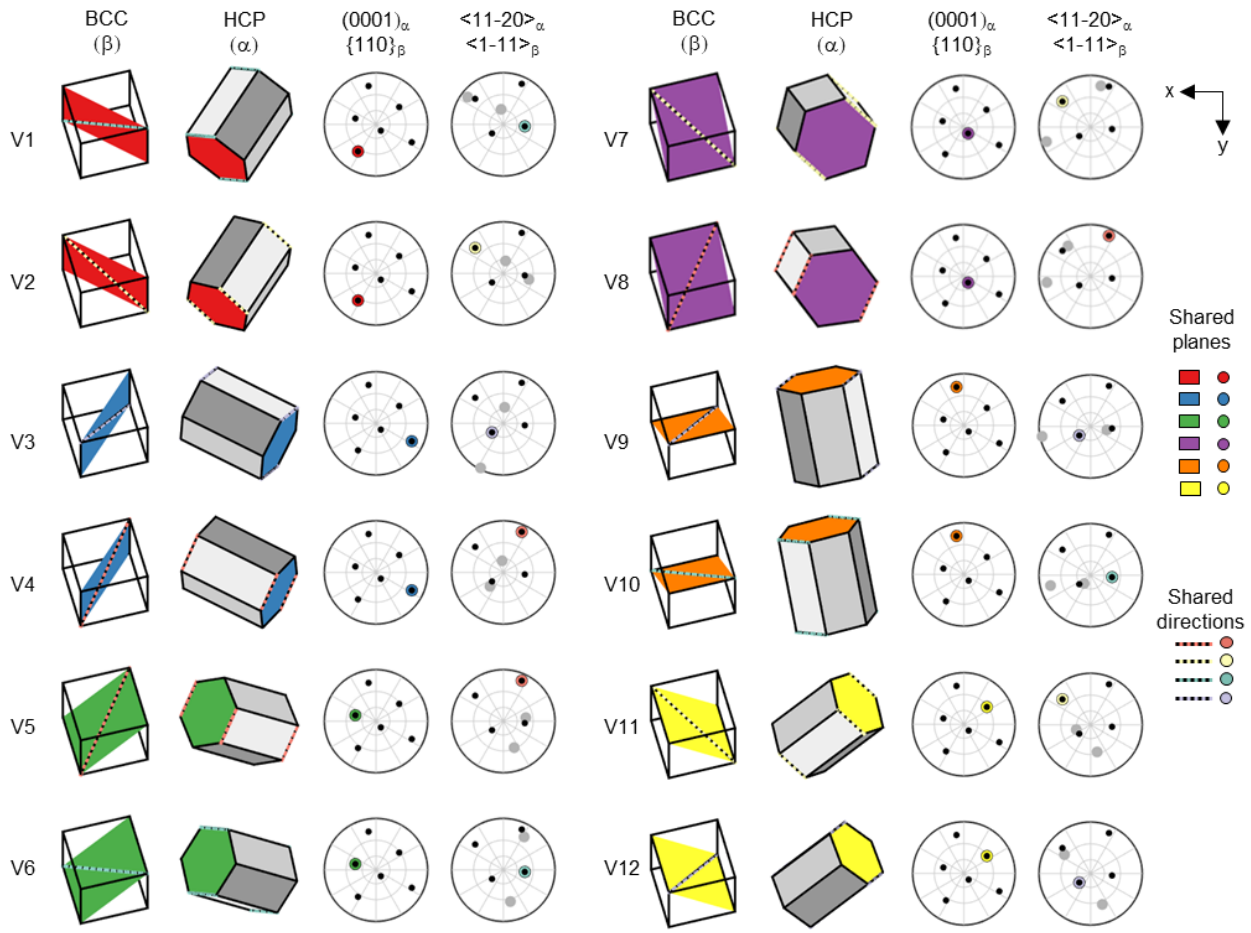


Figure 58 - β → α BOR shared planes and directions example. 12 unique α variants (V1-12) for a fixed β orientation of (0,30,15) showing the corresponding planes and directions between the BCC and HCP orientations via prisms and pole figures. For the prisms: shared planes between variants are indicated by the colour of the plane and shared directions between variants are indicated by the coloured + dashed directions. For the pole figures, the shared plane or direction is shown by the coloured dot, the other HCP points by the larger grey dots and the BCC orientation is shown by the smaller black dots. Reproduced from [159].

As can be seen in Figure 58, there are common shared planes and directions between the 12 unique α variants that can result from an initial parent grain orientation. There are four groups of variants that share the same shared direction, as shown by the colour of the directions in the figure, e.g. V1,6 & 10 have a common shared direction. Similarly, there are six pairs of α variants with the same shared plane, e.g. V1 & V2.

4.2.2 HCP to BCC

When the situation is reversed, any start HCP orientation gives rise to 6 potential unique BCC orientations, as illustrated at Figure 59. The HCP crystal is aligned with the $< c >$ axis out of plane and one $< a >$ direction pointing upwards, as per our chosen convention of the reference crystal orientation for HCP. For each $< a >$ direction parallel with a $< 1\bar{1}1 >_\alpha$ in the BCC phase, there are two orientations of the BCC crystal. This can be explained as for each HCP/BCC orientation alignment, such that $< a_1 >$ (which is parallel to $< b_1 >$ in the β phase) is aligned with a common $-\frac{1}{3}[\bar{1}2\bar{1}0]_\alpha$, then each of the two related variants the $< a_2 >$ and $< b_2 >$ relationship (which is 10.52° misaligned) switches from $-\frac{1}{3}[2\bar{1}\bar{1}0]_\alpha$ to

$-\frac{1}{3}[\bar{1}\bar{1}20]_{\alpha}$. Six variants in total are generated, as this is repeated three times for each of three HCP $< a >$ directions.

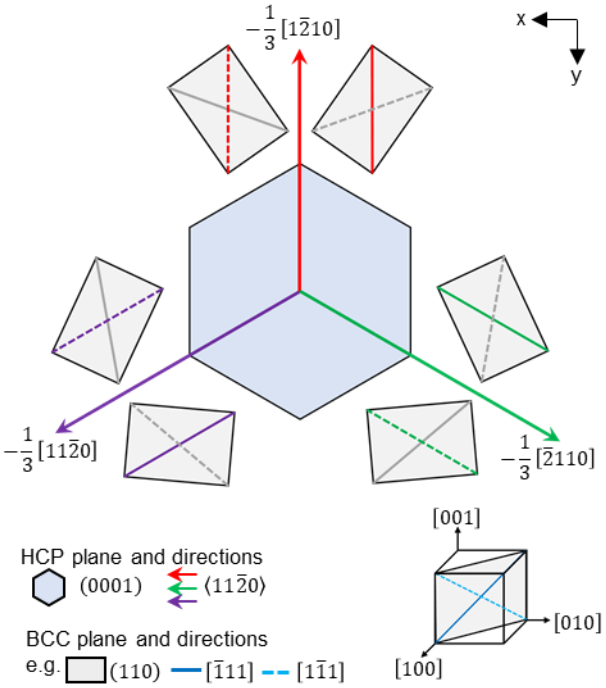


Figure 59 - α → β BOR shared planes and directions example. 6 potential unique parent β orientations for a start α reference orientation. Parallel directions are indicated using the <a> direction colouring. Reproduced from [159].

4.3 Reconstruction algorithm & microstructural post processing

I have developed an MTEX [154] based code in MATLAB, called ParentBOR. This code is available via GitHub at https://github.com/ExpMicroMech/ParentBOR and an example dataset can be found via Zenodo (DOI:10.5281/zenodo.4632039). This code can be broken down into two sections: (A) Initial reconstruction and (B) post processing.

4.3.1 Initial reconstruction

This section of the code is adapted from work by Nyyssönen et al. [103], [108], [109]. The Nyyssönen algorithm is used to reconstruct the parent austenite microstructure from a child martensite microstructure found in steels. To adapt this code for the BCC to HCP (β→α) phase transformation in HCP alloys, both the phases and OR have been updated (which includes consideration of the reference orientations of the α and β phases). I follow the conventions described by Britton et al. [155] where the b axis of the reference HCP unit cell is aligned along the b axis of the reference BCC unit cell, and use the BOR described in equation (1).

As discussed, using this OR, there are 12 potential unique α variants for any start β orientation. In reverse, there are 6 potential unique β variants for any start α orientation [160]. This is important in the initial reconstruction and post processing algorithms.

The algorithm for the initial reconstruction section is shown schematically at Figure 60 and contains 4 main steps:

(1) setting up the OR;

(2) identifying grain boundary types;

(3) applying the MCL algorithm;

(4) reconstructing the parent β microstructure.

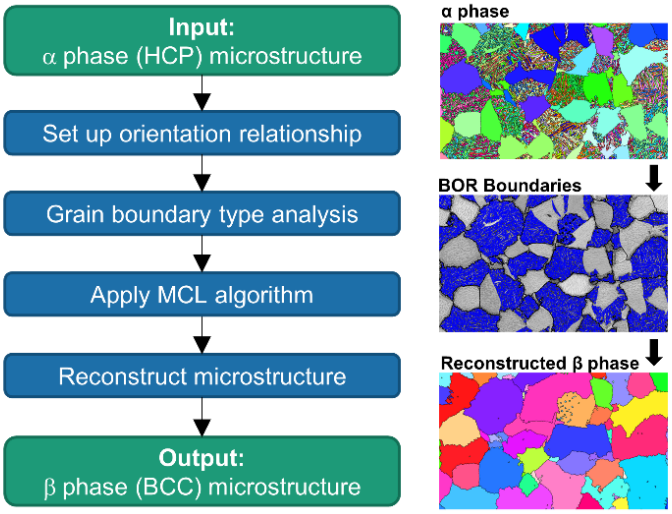


Figure 60 - Initial reconstruction code overview – steps to go from the input α phase microstructure (HCP) to the reconstructed β phase (BCC) microstructure, with microstructure schematics. Reproduced from [159].

4.3.1.1 Setting up the orientation relationship (OR)

Firstly, the OR is established for the β → α transformation. The transformation matrix ($T_{(\beta\rightarrow\alpha)}$) is set up using an initial pair of orientations (α_{init} (0,45, 24.7) and β_{init} (0,0,0)) that meet the BOR. The BOR relationship links the BCC to HCP orientations, and how one of the $\langle 010\rangle_\beta$ direction matches onto the HCP unit cell and different EBSD indexing algorithms change these relationships. Again, following Britton et al. [155] with $\langle 1\bar{2}10\rangle_\alpha$//Y and $\langle 010\rangle_\beta$//Y for the reference orientations[7] .

$$T_{\beta\rightarrow\alpha} = \alpha_{init} \cdot (\beta_{init})^{-1} \tag{15}$$

This is then expanded to include symmetry:

$$T_{\beta\rightarrow\alpha}^{1-24} = S_\beta^{1-24} \cdot T_{\beta\rightarrow\alpha} \tag{16}$$

where S_β^{1-24} are the 24 symmetry matrices for the BCC phase. This allows the potential α variants (α^{V1-24}) to be calculated for any starting β orientation (β) using:

$$\alpha^{V1-24} = \beta \cdot T_{\beta\rightarrow\alpha}^{1-24} \tag{17}$$

Note that due to symmetry, only the first 12 are unique, the second 12 are repeats.

[7] Please note that Britton et al. use a convention where <b> is parallel to the Y axis, and in the HCP unit cell <b> is one of the <a> directions.

4.3.1.2 Identifying grain boundary types

The OR is then used to identify parent grain boundaries on the α grain map. A set of α variants is calculated and the misorientations between the variants found. Due to symmetry, the list of misorientations can be minimised to a short list of angle/axis pairs [96], [160] as detailed at Table 15.

Table 15 - Misorientation between potential α variants. Minimised list of angle/axis pairs for α-zirconium that can exist between α variants from the same parent β grain (as determined from the code, but similar to Gey et al. [96]*, and Karthikeyan et al.* [160]*). Reproduced from* [159]*.*

ID	Angle (°)	Axis			
		h	k	i	l
1	10.53	0	0	0	1
2	60.00	-1	2	-1	0
3	60.83	-12	7	5	3
4	63.26	-2	1	1	1
5	90.00	-7	12	-5	0

These angle/axis pairs are used to evaluate whether each grain boundary segment is a parent grain boundary or not. In the experiment, the misorientation across an α-α boundary may not be exact, both due to measurement uncertainty and rotation away from transformation strain. A threshold of 4 ° is set as default. Boundaries which are not described by the special relationships in Table 15 (within the selected threshold) are classified as non-BOR i.e. typically a parent grain boundary.

4.3.1.3 Applying the MCL algorithm

At this point, the Markov clustering algorithm (MCL) [104] is applied to identify discrete clusters of closely related α grains that will be used for the reconstruction step. The aim of using a clustering algorithm is to quickly identify the child grains that originated from the same parent grain and speed up the reconstruction process. In brief the MCL enables groups of related BOR α grains to be clustered together for parent β orientation determination. Similar approaches exist [97], [101], but often require further steps to incorporate grains not included in the initial analysis (due to threshold conditions).

The algorithm creates a network based upon the closeness of grain boundaries to the potential grain boundaries. This network is then put through a series of expansion and inflation steps until a discrete network of clusters is established. For more discussion of the MCL algorithm, please see [103]. An advantage of this algorithm is the single factor for adjusting it – the 'inflation power'. In practice this term can change the number of parent β grains that are found. A smaller inflation power decreases the number of discrete clusters identified, i.e. The user is advised to explore variation of the inflation power and the output reconstruction (which is assisted by the post processor, described later).

4.3.1.4 Reconstructing the parent β microstructure

Once clusters of α-grains are joined together to describe one parent β grain, it is now valuable to determine the parent β-grain orientations. The reconstruction step combines (1) and (3), with each discrete cluster of α grains treated individually. For each α grain within the cluster, the potential β grain orientations are calculated (using $T_{\beta\rightarrow\alpha}$). When this is completed for every α grain within the cluster, a density function is used to find the most intense orientation – this is allocated as the β orientation for that cluster. Once completed for all discrete clusters, an EBSD map for the parent β phase can be plotted. The code then processes the grains for the β phase ready for the post processing section.

4.3.2 Post processing

Once the parent β grain boundaries are determined, it is possible to evaluate:

(1) Uniqueness of the determined β orientation.
(2) The shared $< a >_{\alpha}$ directions within the parent β grain.
(3) The shared $\{0001\}_{\alpha}$ planes within the parent β grain.

The additional information generated in this section of the code can then be used to look at the influence of grain boundary types and variant selection.

4.3.2.1 Certainty of the β-orientation and the associated α variants

The α variants are calculated on a grain by grain (β) basis – this allows for comparison of α variants within each β grain, but not between (β) grains. The process used to analyse the α variants present begins by setting the β grain orientation to the fundamental zone ($\beta_{ori} \rightarrow \beta_{ori}^{FZ}$) and then using this to calculate the potential α variants (α_{calc}^{V1-12}):

$$\alpha_{calc}^{V1-12} = \beta_{ori}^{FZ} \cdot T_{\beta\rightarrow\alpha}^{1-12} \tag{18}$$

The minimum misorientation between each of the calculated α variants and the parent β orientation (β_{ori}^{FZ}) are then calculated and stored as the 'ideal' misorientations:

$$Miso_{ideal}^{1-12} = \left(\beta_{ori}^{FZ}\right)^{-1} \cdot \alpha_{calc}^{V1-12} \tag{19}$$

Next, the experimental β→α misorientations ($Miso_{exp}^{1-12}$) are calculated for each α grain present (α_{1-n}) within the parent β grain (β_{ori}^{FZ}):

$$Miso_{exp} = \left(\beta_{ori}^{FZ}\right)^{-1} \cdot \alpha_{1-n} \tag{20}$$

Finally, each experimental misorientation is compared with the list of ideal misorientations – the number of the closest match is taken to be the α variant ID for that grain.

4.3.2.2 β certainty

The number of potential β orientation options (β certainty) for each parent grain identified depends on the number and type (whether there are shared planes or directions) of unique α variants present. For

example, if there is only one α grain, it is not possible to determine which of the 6 potential β orientation options is the parent β orientation.

To fully determine the parent β orientation, the number of unique α variants required depends on the type of variants present (shared basal plane, which I call (c) in this chapter; or shared <a> direction; or neither). In the case where there is a shared plane, three of the β options will be the same, whilst for a shared direction, two options will be the same between variants. The minimum number of unique α variants required for a unique β-parent is 2 and the maximum is 4 in the case where three of the variants have a common <a> direction. The algorithm used for determining the number of β options is described in Figure 61.

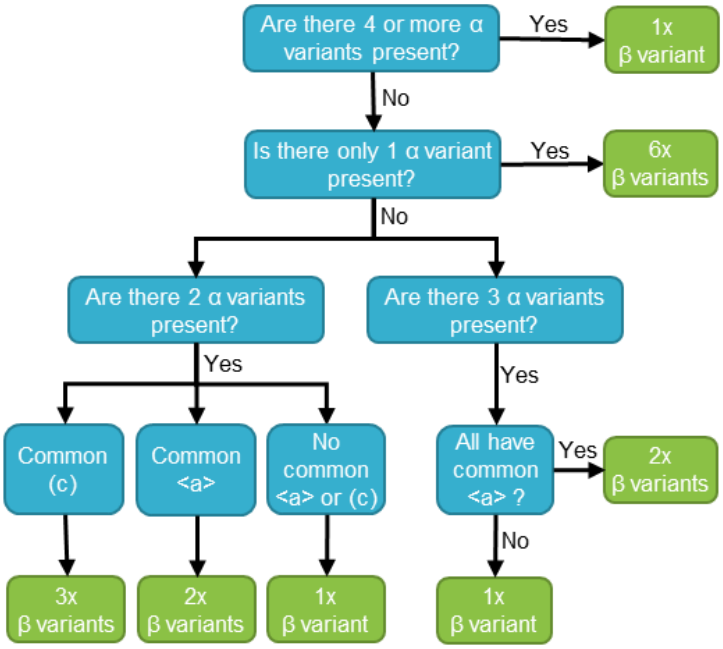


Figure 61 - β grain orientation certainty flowchart. Decision flowchart for the number of potential unique parent β grain orientations, depending on the number and type of unique α variants present with the parent β grain. Reproduced from [159].

4.3.2.3 β orientation options

As part of the step to calculate the β certainty, all potential parent β orientation options (β options) are stored, as calculated from the associated α grains within the parent β grain. For uniquely determined β grains, this is a single orientation, but where there is uncertainty different orientations can be represented. Additionally, the number of potential β orientations can be reported.

4.3.2.4 Analysis of the structural units within the α-phase: shared planes and directions

With the α variants identified for each parent β grain, variants with shared planes or directions can be identified. Within the set of 12 unique α variants, there are several combinations that share a common plane or direction, as illustrated at Figure 58 for a set of α variants calculated from a start β orientation of (0,30,15). This enables the α grain map to be plotted coloured by variant number (coded with respect to each parent β grain), as well as the shared $\{0001\}_\alpha$ planes, or shared $< a >_\alpha$ directions within each parent

β grain. Analysis of the relationship between the α-phase domains within the parent β grain is similar to the analysis of parent austenite grain (PAG) block and packet analysis, as explored in [161]. Note that the variant numbering for α-domains may be different within two adjacent parent β-grains.

4.4 Simulated dataset

To validate the algorithm, a simulation was performed. A dataset consisting of 6 β grains was created with a 'checkerboard' morphology to test whether the algorithm would determine the exact parent β microstructure and whether the uncertainty was correctly evaluated. This data set is shown in Figure 62.

From this β-grain structure, an α microstructure was then created from this by assigning an α variant number to each of the 12 sub-grains contained within each parent grain.

To test varying the number of unique α variants present and the effect of shared planes or directions, the assigned α variant numbers were carefully selected for the simulations for each parent grain, as detailed at Table 16. The potential α variants for each parent grain orientation were then calculated and the appropriate orientation assigned to each α sub grain. The resultant α microstructure was then used as the input for the algorithm.

Table 16 - Details of simulated dataset. α variant population choices for each grain and the number of potential parent β orientations that can be found based on these. Reproduced from [159].

Grain no.	No of unique α variants	Details	No of potential parent β orientations
1	12	All 12 variants present	1
2	3	2 common <a> + 1 random	1
3	3	All common <a>	2
4	2	No commonality	1
5	2	Both common (c)	3
6	1	Only 1 variant	6

The simulated dataset and the corresponding reconstructed parent β microstructure are shown at Figure 62 (and are provided in the supplementary data). As can be seen in Figure 62 (C), the parent grain boundaries are correctly identified (red boundaries), as are all the α-α boundaries within each grain (blue boundaries). The reconstructed parent grain microstructure is correct for each of the 'known' (1 potential β orientation) parent grains. However, as expected, there is uncertainty for the remaining grains. The chosen parent grain options can be selected to match the original parent β orientations, but the output may not select this (as there is a random selection of the represented β grain from the uncertain candidate orientations). For each uncertain grain, the alternative β orientation options are presented as the small circles within each grain in Figure 62 (D).

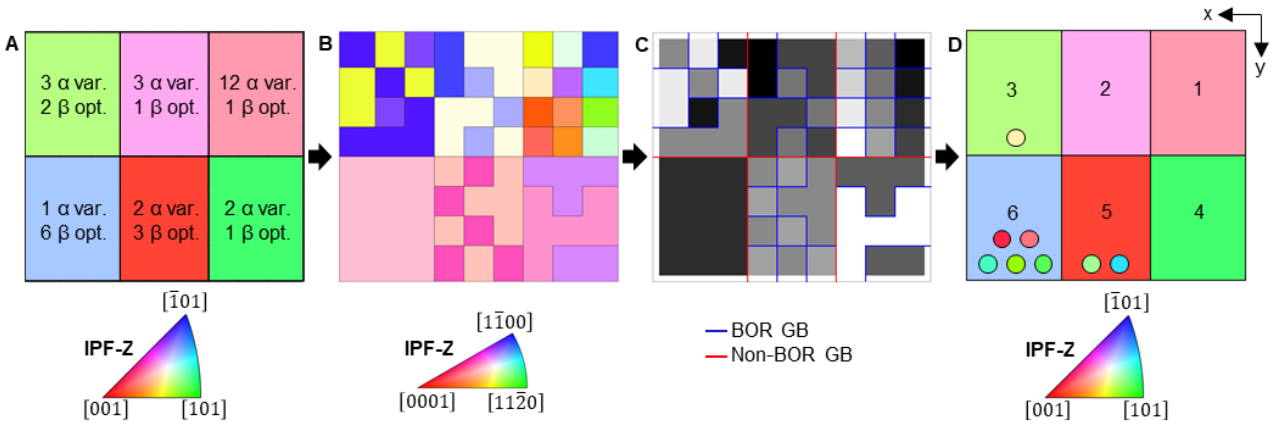


Figure 62 - Simulated dataset reconstruction example. Simulated dataset in (A) β phase (IPF-Z) and (B) α phase (IPF-Z). (C) Grain boundaries identified by type on a greyscale variant number background – red = parent grain boundary, blue = α/α grain boundary. (D) The reconstructed parent grain microstructure (IPF-Z) – where there are multiple β grain orientation options, the alternative orientations are shown in the circles overlaid on the grains. The grain numbers on (D) correspond with the those reported in Table 16. Reproduced from [159].

4.5 Experimental materials & method

For the experimental example, a Zircaloy-4 sample with a grain size approx. ~11 µm was used (from the same batch of materials as used by Tong & Britton [48]). The sample was encapsulated in a quartz tube, backfilled with Ar, and heated to >1000 °C (i.e. super transus) for 10 mins and then water quenched. The sample was then ground using 800-2000 grit SiC papers followed by a 4.5 hr polish with OP-S. Finally, the sample was broad ion beam polished using a Gatan PECSII machine for 15 mins at 8 keV, 8° tilt, 1 rpm, no modulation.

EBSD data was captured using a Quanta FEG 650 SEM equipped with the Bruker eFlashHD2. Data was processed using Bruker ESPRIT software and data exported to .h5 prior to analysis in MATLAB (R2018b) using MTEX version 5.4. EBSD patterns were captured using a 20 kV beam with a working distance of 15 mm and 70° sample tilt. The patterns were captured at a resolution of 320 x 240 pixels using a 34 ms exposure time and 0.14 µm step size.

4.6 Results

The reconstruction of this experimental data is shown in Figure 63, which includes the α orientations, grain boundary map with labelling of the BOR boundaries, and associated parent β microstructures. For the parent β microstructures, the initial reconstruction output (Figure 63 (3)) is based on the α grain groupings identified using the MCL algorithm [104] - the grain boundaries present are the non-BOR boundaries

identified at step 2. The reprocessed map (Figure 63 (4)) takes the orientations from the initial reconstruction map and processes the grains.

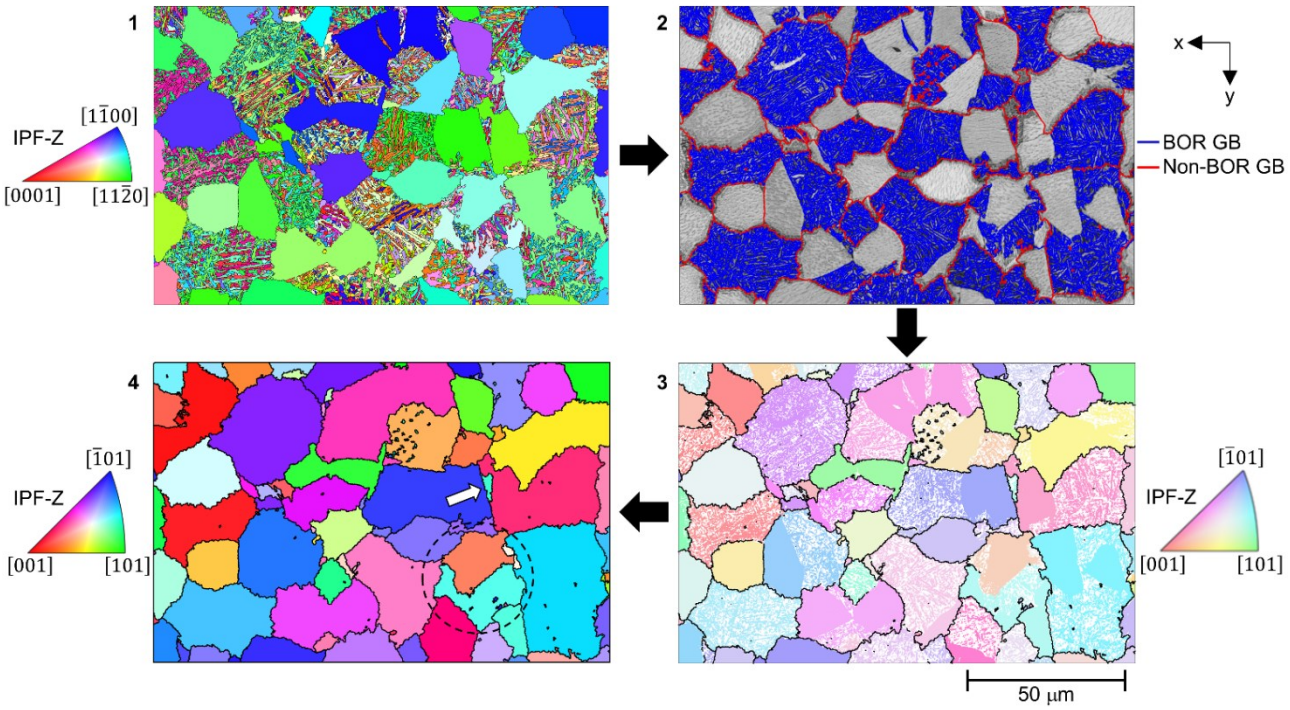


Figure 63 - Experimental example – initial reconstruction results. Reconstruction of an EBSD map from a β quenched Zircaloy-4 sample showing [1] Initial α microstructure (IPF-Z) [2] Pattern quality map with overlaid grain boundaries, identified by type: RED = parent grain boundaries; BLUE = α-α (or BOR) grain boundaries [3] Initial reconstruction output – β phase (IPF-Z) [4] Reprocessed parent β grains (IPF-Z) with an arrow showing the location of the grain selected for further analysis. The grain pair within the dashed circle is explored in 4.6.2 . Reproduced from [159].

4.6.1 Microstructure

This microstructure has (large) globular α domains, which have an approximate diameter of 20 µm. The origins of these globular domains is unclear. The microstructure observed here is similar to many Ti-6Al-4V microstructures [162], where the global α-grains are thought to originate due to recrystallisation of α-laths in the α+β phase field. In my experiment, this globular α-nucleation and growth could occur as the sample is taken from the furnace and dropped into the quenching fluid. While the precise mechanism of this process is out of scope of the present work, it is interesting to note that often these globular grains have an orientation that is related to the neighbour α-lath region.

Between these globular regions, there is a fine scale secondary α lath microstructure with multiple different α variants. The size and shape of these regions containing secondary α regions is of similar size to the globular α, but the α laths tend to have a width of ~1 µm. Analysis of the grain boundary map shows that the globular α and variants of α within the transformed secondary α domains are often from the same parent β orientation, and this is shown within the reconstructed parent β orientation maps in Figure 63.

4.6.2 Split grain

An artifact was revealed in this reconstruction, as highlighted by the dashed circle in Figure 63 stage 4. In the reconstruction shown, this is labelled as two parent β grains.

An investigation of this grain showed that it can be reconstructed either as a single parent β grain, or two (main) parent β grains, as shown in Figure 64. This uncertainty is caused by a closely aligned $\{110\}_\beta$ plane between the two parent β grains as shown in this case. Whether it reconstructs as one or two grains depends on the number of discrete clusters formed prior to reconstruction, in other words, the inflation power. This is demonstrated in Figure 64 where a smaller region from the larger map has been selected and reconstructed using a range of inflation powers.

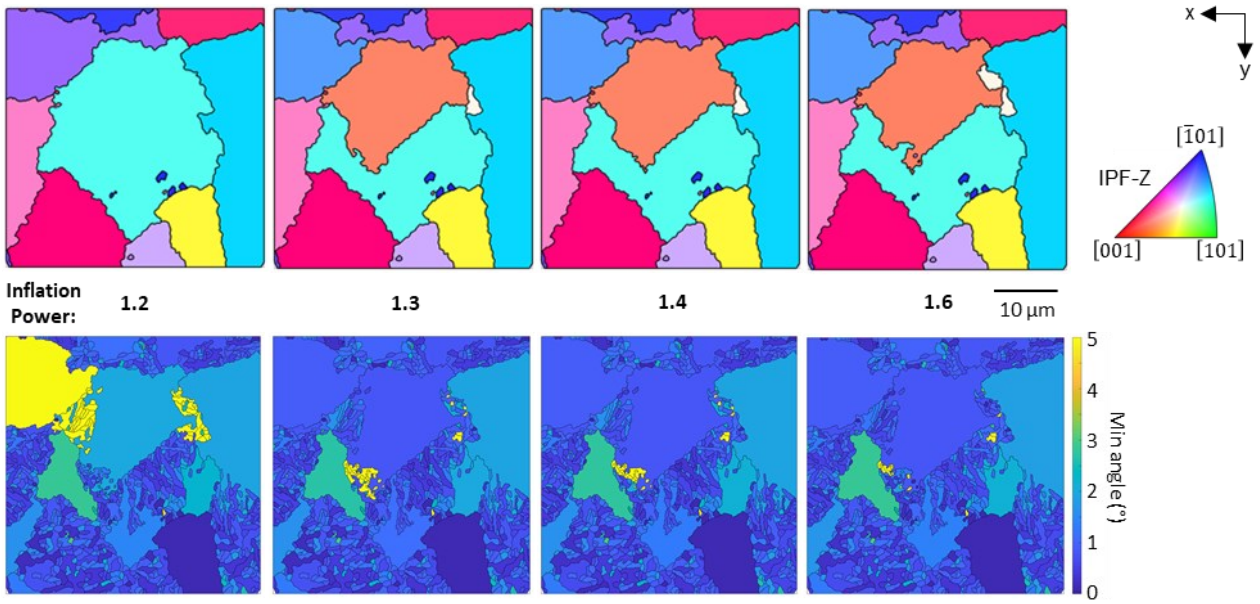


Figure 64 - Split grain investigation – inflation power. Reconstruction of smaller region into one or two (main) parent β grains - effect with changing inflation power from 1.2 to 1.6. In this figure, the upper row shows the reconstructions as coloured using the IPF-Z colourmap, and the bottom row shows the calculated misorientation of the (as measured) α grains from the ideal α orientations determined from the parent β grain orientation. Reproduced from [159].

Looking at the two β grain option, the two potential orientations have a shared $\{110\}_\beta$ plane, with a 1.34° angle between the two $\{110\}_\beta$ planes and a total misorientation of 47° between the two crystals (i.e. they are rotated about the shared $< 110 >_\beta$). This is shown visually in Figure 65 (A) where the two parent grain orientations have been plotted as overlapping cubes, with the common planes indicated by the solid colours. The consequence of this shared plane is that there are α variants which would match either parent grain orientation – this is where the ambiguity in the reconstruction occurs.

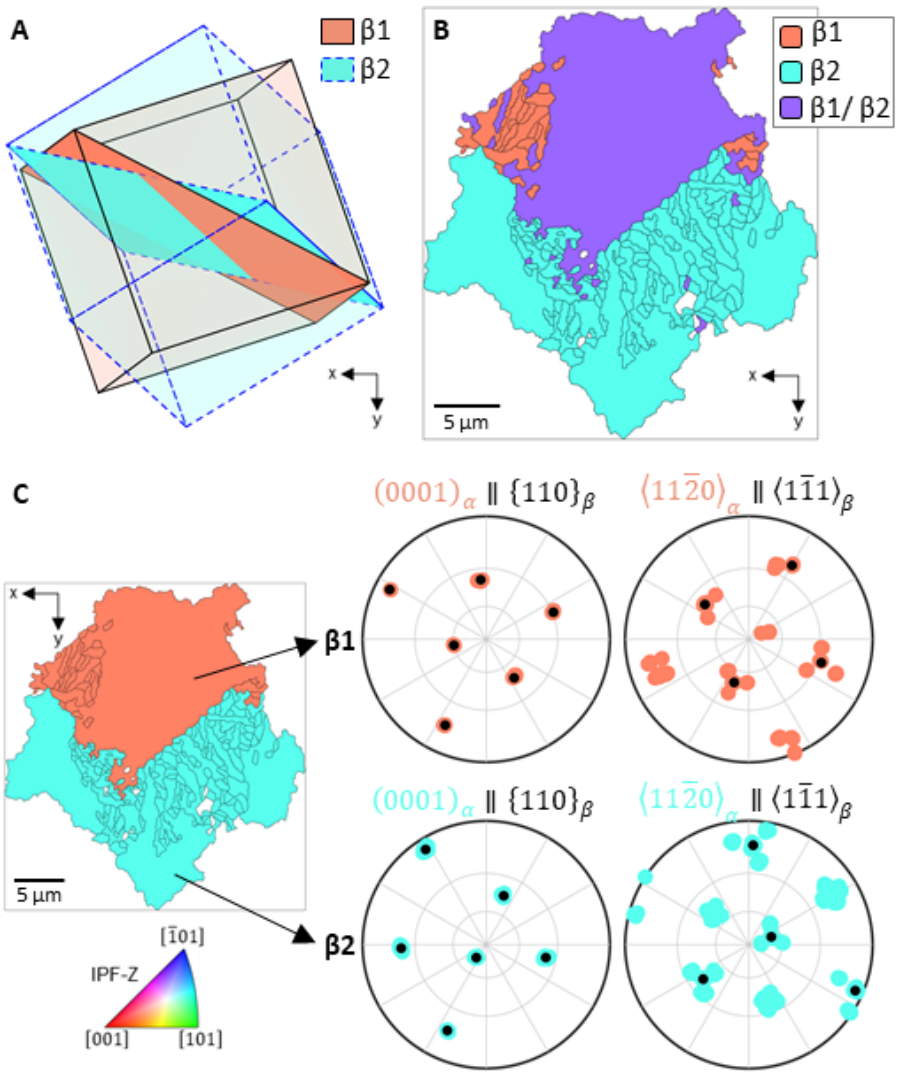


Figure 65 - Split grain investigation – manual sorting. (A) Comparison of the two β grain orientations, showing the shared planes for each using solid colour (corresponding to the IPFZ map colours for each grain). (B) α grains for this region coloured by parent grain orientation β1, β2 or uncertain (β1/β2). (C) manually sorted α grains, coloured by parent β grain assigned (IPFZ colouring) – along with the pole figures for each parent β grain region, with the α orientations the coloured dots and the α orientations the black dots in each case. Reproduced from [159].

A manual analysis of the α grains contained within this region, in Figure 65 (B), shows the issue more clearly, with uncertain grains shown in purple. The region could plausibly be reconstructed as a single parent grain, although there would be regions (orange grains in Figure 65 (B)) that do not match this parent grain well – these could potentially be other parent β grains. However, a better reconstruction (comparing the α and β orientations on pole figures) can be achieved using the split grain option, as demonstrated by Figure 65 (C). It is therefore likely that the 2 parent β grains, with a shared $\{110\}_\beta$ plane is a valid reconstruction.

4.6.3 Reconstruction certainty

To explore the certainty of the parent β reconstruction, one region was extracted from the map in Figure 63 (4) and the ORs are plotted in Figure 66. In this example, the α phase structure includes 8 variants of α phase, and so the parent β orientation is over determined. However, the stereographic relationships can be

analysed between the α variants and parent β orientation to show which combinations of α variants which are required to determine a unique parent β orientation.

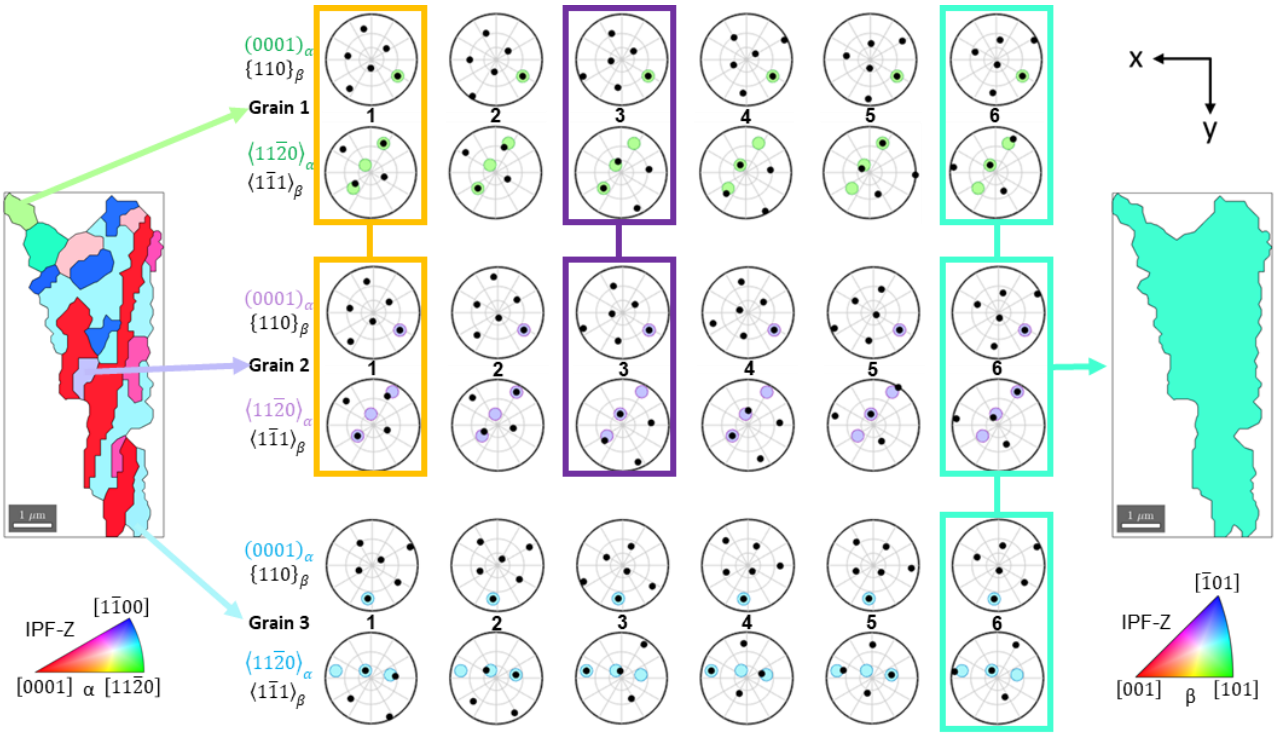


Figure 66 - Impact of the no. of unique α variants. Example showing how the β orientation certainty is affected by the number unique α variants present. There are three potential β variants (shown by the coloured & linked boxes) with just α grains 1 and 2, whereas with all three grains this reduces to one orientation (β variant 6 for all grains). α grain orientations are shown by the coloured dots in the pole figures, whilst the 6 potential β orientations for each of these are shown by the black dots in the pole figures. Reproduced from [159].

Three variants are highlighted, with the stereographic projections of the final (i.e. correct) β and α phase crystal planes and directions which are involved in the BOR. The combination of grain 1 (light green) and grain 2 (lilac) results in three potential parent β crystal orientations, as they have a shared basal plane. This ambiguity is immediately resolved when a third variant is identified from the same parent β grain if this (new) variant does not share the same basal plane.

Examination of the other 5 α orientations (not shown in figure) confirms that the β orientation determined is consistent with all the child α variants found in this region.

4.7 Post processing

The parent β reconstruction algorithm enables us to explore the relationship between the α grains within the complex microstructures. As I have demonstrated that the parent β microstructure can be determined using this algorithm, it can now be used to explore the relationship between microstructural units within the α phase map.

In terms of mechanistic understanding, it is useful to report on four relationships:

(1) The number of potential parent β orientations, i.e. the uniqueness of the parent β reconstruction.

(2) A labelled map of each α variant within each β grain.

(3) Sharing of the basal plane within each parent β grain.

(4) Sharing of the <a> direction within each parent β grain.

For example, four maps for these relationships (using the experimental dataset) are shown in Figure 67. These maps are related to each other, and also can be insightful depending on the microstructural analyses required.

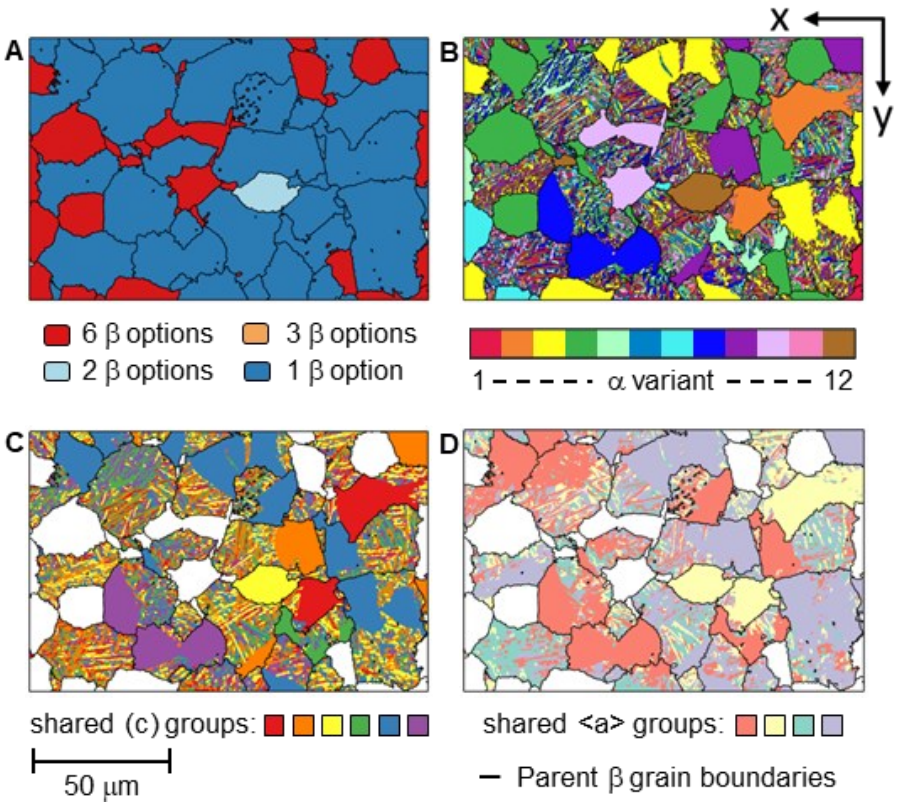


Figure 67 - Experimental example – post processing results. Post processing outputs for β quenched Zircaloy-4 samples [A] β orientation certainty map showing the number of potential β variants for each parent β grain [B] α variant map – all 12 variants shown [C] α variant map coloured by α variants with shared (c) planes [D] α variant map coloured by α variants with shared <a> directions. Note: for [B]-[D] comparisons can only be made directly within the grains as it is calculated on a grain by grain basis. Reproduced from [159].

Uncertainty of the parent β orientation is dependent on the number α variants generated from each parent β, combined with whether these variants share <a> directions and basal planes. This is shown pictorially in Figure 66. This ambiguity was also explored within the simulated data set shown in Figure 62. The uncertain cases, and the reason why they are uncertain (e.g. due to shared basal planes or shared <a> directions, can be inferred from the associated other figures in Figure 67, such as for the pale blue region (in Figure 67 (A)) where there are 2 two β options. In this case, there are two α variants present (the second grouped variant is a smaller grain not visible on the figure) which share a common <a>, hence the ambiguity.

The map of variants, shown in Figure 67 (B), can be useful to evaluate the size and shape distribution of variants within a parent β grain. For example, where the large globular α and lath α reconstruct to the same parent grain, the globular α variant type and the fine scaled transformed α can be compared (different or similar variants). The colour coding as presented plots the variants with respect to each parent β grain

structure, as you cannot read the relationship between α variant numbering from one parent β grain to the next.

The map of shared basal planes is likely to be useful when considering properties that will extend across microstructural regions, such as any property that is transversely isotropic in the zirconium system (e.g. elastic stiffness). This map could also be useful to help navigate arguments in the literature on failure under fatigue loading and the formation of facets [163]. Again, similar to the variant analysis, this map must be interpreted with respect to the parent β grain structure, as a similarly coloured shared basal plane in this map across with two β grains is unlikely to have a common plane normal.

Finally, the map of shared <a> directions echoes the idea of the shared basal plane map, but now is true for the <a> directions. This map could be important when considering the propagation of slip through the microstructure and the relative transparency of different α/α grain boundaries. Furthermore, if there is a transformation strain associated with the β→α OR, potentially analysis of this map could assist in understanding transformation strain heterogeneity and variant selection [164].

4.8 Comparison with an alternative algorithm within MTEX

In the process of developing my algorithm, a reconstruction algorithm was developed within MTEX.

The MTEX reconstruction was performed using MTEX 5.7.0. The following recipe was used:

- Calculate (α) grains (4° threshold used for direct comparison), remove quadruple points and remove small grains (less than 5 points);
- Compute parent orientations from triple junctions (& probabilities);
- Use a voting system (threshold 0.7) to determine which grains are converted to parent grains;
- Grow parent grains at grain boundaries;
- Merge parent grains;
- Merge inclusions.

A comparison of the reconstruction between the ParentBOR code and the MTEX reconstruction is shown in Figure 68. Of note, the MTEX reconstruction algorithm does not include any of the post processing analysis that I have described for the ParentBOR code. In practice, this could be included in the MTEX algorithm, but it would need some subtle (but important) changes with respect to how the variants are numbered and the results are described within the MATLAB variable arrays.

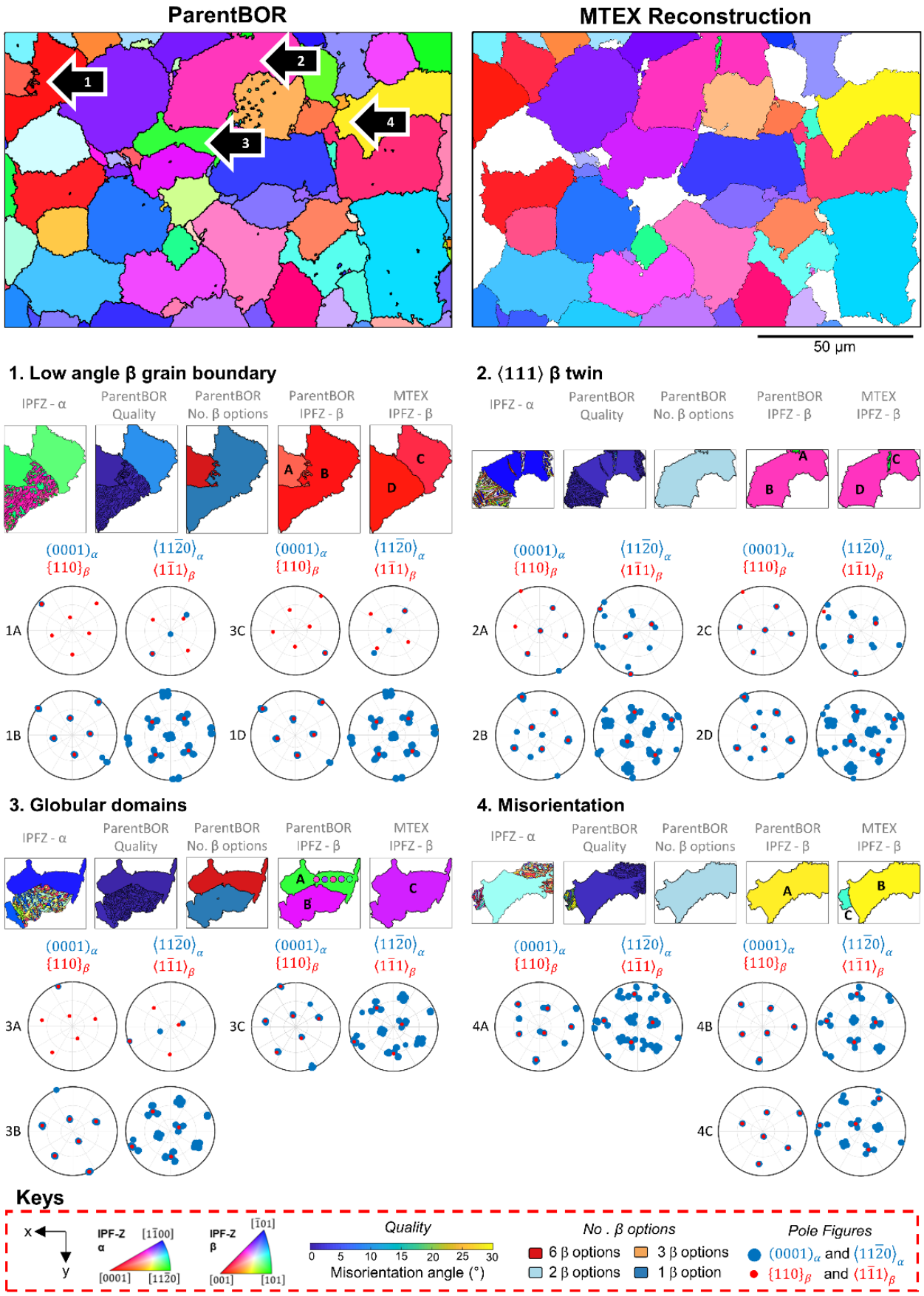


Figure 68 - Comparison of ParentBOR reconstruction and MTEX 5.7.0 reconstruction. Reproduced from [159].

The MTEX reconstruction does not reconstruct regions where there are more than one parent β grain orientations, and these are shown as white regions in Figure 68. In addition to these (apparently unsolved) regions, there are four other types of difference between the two reconstructions shown in Figure 68:

4.8.1 Type 1: Low angle β grain boundary

The MTEX reconstruction and the ParentBOR reconstruction differ in how the parent grain domains are identified. In the MTEX reconstruction, the orientation of the potential parent β-grains are evaluated and considered at triple junctions in the α microstructure and a voting system is used to determine the grouping for the parent grain domains. In contrast, in the ParentBOR reconstruction domains are reconstructed using clusters identified from the MCL algorithm. In region 1, the large 'red' grain (i.e. near [001] out of plane) is broken down with two different sub-grain boundaries. In practice these regions are closely aligned, and they could be post processed to be joined together within the same large region of parent β structure.

4.8.2 Type 2: <111> β twin

There is a small region within the pink grain which has a different orientation (in the parent reconstruction) to the neighbourhood. Analysis of the β pole figures reveals that this region is a <111> type twin in the parent β orientation. The orientation relationship between these two regions in the β phase, and the associated inheritance of this OR through the α domain, results in a slight confusion in the size and extent of the parent β grain size (and the very small grain within this parent β domain).

4.8.3 Type 3: Uncertainty of globular domains

The MCL clustering regime tends to grow domains outwards from clusters of similar orientation. Spatial regions which include a single variant can cause issues when the reconstruction is performed. Here it can be seen that there is a region (A) which does not have a certain parent β orientation, but the candidate orientations of this region include both the green (the ascribed colour) as well as the purple orientation (closely aligned to region B, and similar in orientation to the MTEX domain, labelled C). This highlights that the ParentBOR code could be extended further to post process the parent β map, for regions that are less certain, to consider whether they belong to nearby regions.

4.8.4 Type 4: Misorientation

For this region, the ParentBOR reconstruction shows one parent β grain and the MTEX reconstruction reveals two separate parent β domains. Analysis of the pole figures shows that region A (the ParentBOR grain) has the same β orientation as region B (the large area from the MTEX reconstruction). In region A however, there is a region which has a high angular deviation for the left-hand shoulder (which MTEX describes as a different β grain). The poor reconstruction of this area is shown as a high value (i.e. bad) in the quality map. It is likely that the MCL algorithm clusters these two regions together despite there being a small misorientation between the α variants (and associated small angular deviation for the β grains).

4.9 Discussion

In this chapter, I have presented an evolved form of parent β-grain analysis, together with some new post processing capabilities.

Using the MCL algorithm to group the α grains parent to reconstruction provides a good balance of speed and accuracy, whilst the single coarsening parameter (inflation power) provides the opportunity to easily adjust the number of discrete clusters identified. This has benefits and disadvantages as there is the potential to add parent grain orientations if there are too many clusters identified. The inflation variable can average small sub-groups of grains within each parent, and this risks adding ambiguity to the analysis. The MCL algorithm approach is also implemented as an option within MTEX, and released as open source, which may promote wider use and further developments of the method.

In the reconstruction, I have selected to use all α grains present for our code, but this leads to uncertain parent grain orientations in cases where there are insufficient variants present. The post processor for the approach will subsequently label these regions and provide suggestions for the alternative β orientations which may be selected, as per the users' needs.

The simulated dataset (with code included in supplementary data) allows us to validate the reconstruction and test the post processing, and it can be adapted to different sized datasets. In development of our approach, the simulation has been useful to explore specific scenarios e.g. where there is uncertainty as to why a parent β grain reconstructs as two grains or an α grain flips between two parent β grains with changing inflation power. Application of the code to experimental data revealed further nuances, such as the ORs within the parent β structure that can cause confusion within the reconstruction.

I have also evaluated the ParentBOR code against recently available code within MTEX (see Section 4.8). While there are (understandable) differences between these reconstructions, it is also useful that there are now two analysis methods available that are constructed within the same overall framework. This enables us to understand how reasonable (or unreasonable) the reconstruction is with regards to specific algorithm induced artifacts. The relevance of these artifacts will depend on how the parent β grain structure is interrogated. This comparison highlights that the ParentBOR code reconstructs a significant fraction of the map equally to the MTEX implementation, and that there are specific regions which are reasonably reconstructed in ParentBOR and vice versa. This implies that a hybrid approach could be implemented, such as the recently described methods of [123] which include orientation relationship refinement, orientation coalescence and regional voting.

Recent advances using pattern matching by [165] of overlapped BOR related patterns offer the chance to index finer scaled microstructures, where there may be two or more overlapping patterns within the interaction volume. Fortunately, our microstructure mapped sufficiently well (>83% success) and there is no retained β in this material.

From a materials engineering perspective, it is expected that the post processing analysis is likely to prove useful for understanding variant selection during thermomechanical processing of alloys with a BCC to HCP allotropic phase transformation, such as titanium, zirconium, and hafnium. For the future, it may also be useful to explore the relative effectiveness of different grain boundaries for specific materials properties, such as the effective slip length in during deformation.

4.10 Conclusion

In this chapter, I have:

- Introduced a HCP→ BCC parent phase reconstruction method and demonstrated this on simulated and experimental zirconium material data.
- Created a post processor to reveal the uniqueness of the parent β grain orientations and shared crystallographic relationships within the parent β grains.
- Compared the ParentBOR performance to an MTEX in-built code and highlighted the usefulness of using different approaches.

The ParentBOR code will be used as part of the data analysis throughout the rest of the thesis, particularly the grain growth analysis chapters where it is used to understand growth of large α-grains formed from solid state grain growth.

5 *In Situ* Experiment Development

5.1 Aim

The purpose of this chapter is to outline development of a new experimental approach to obtain information about the evolution of microstructure during an *in situ* heating experiment where Zircaloy-4 samples are held at high temperature (up to a stage temperature of 950°C) while being observed using a scanning electron microscope. For Zircaloy-4 weld samples, the *in situ* temperatures of interest are related to: the α→β phase transformation at 800-900 °C; the SPP dissolution temperature ~800 °C [166]. In practice, for the early stages of microstructural evolution to occur, typically these temperatures must be held for time scales on the order of an hour.

This chapter outlines challenges in obtaining data at high temperatures and assessment of risks to the instrumentation. Highlights of this chapter include: (1) development of forescatter electron imaging at elevated temperatures; (2) challenges in obtaining electron backscatter data at high temperature; (3) understanding temperature control of the stage and the temperature of the sample.

This chapter blends method development and preliminary results to provide context for data collection in subsequent chapters where details of the phase transformations and grain structure evolution are characterised in detail.

5.2 Introduction

The objective was to develop an experimental method to capture and investigate grain growth within the weld region for the Zircaloy-4 electron beam welded samples.

An *in situ* experiment was chosen to observe the grain growth in a specific region with a controlled heating regime and static position. The ideal scenario would be to continually map the weld region during the heat treatment and observe the grains growing, using either EBSD or forescatter imaging. However, the initial approach for this experiment sought to capture the onset of growth in a meaningful way that could be used for further investigation. To enable mechanistic insight, given the constraints of an *in situ* experiment, two techniques were chosen for analysis:

- **Forescatter Imaging.** To observe the grain growth during the experiment, the initial chosen mechanism was forescatter imaging, which allows the observation of grains using electron channelling contrast (see [135] for more details). If successful, the microstructure changes with time should be observable throughout the course of the experiment. Forescatter imaging has the benefit of a very fast capture time, as compared to most EBSD, with the potential for orientation based grain contrast.
- **EBSD.** Capturing initial and final microstructures using EBSD to allow further analysis using the ParentBOR code (see chapter 81) was the minimum output for this experiment, alongside the

temperature data. The feasibility of high temperature mapping during the experiment would also be explored as part of initial trials.

5.3 Setup

The equipment used for this *in situ* experiment was:

- FEI Quanta FEG 650 SEM
- Gatan *Murano in situ* heating stage capable of heating small[8] samples up to 950 °C (as measured using the stage thermocouple)
- Bruker eFlashHD2 EBSD detector equipped with ARGUS FSE diodes and a high temperature phosphor

Figure 69 shows the experimental setup, with the Murano heating stage on the left and the SEM chamber view (view towards the chamber door) with the EBSD detector inserted on the right.

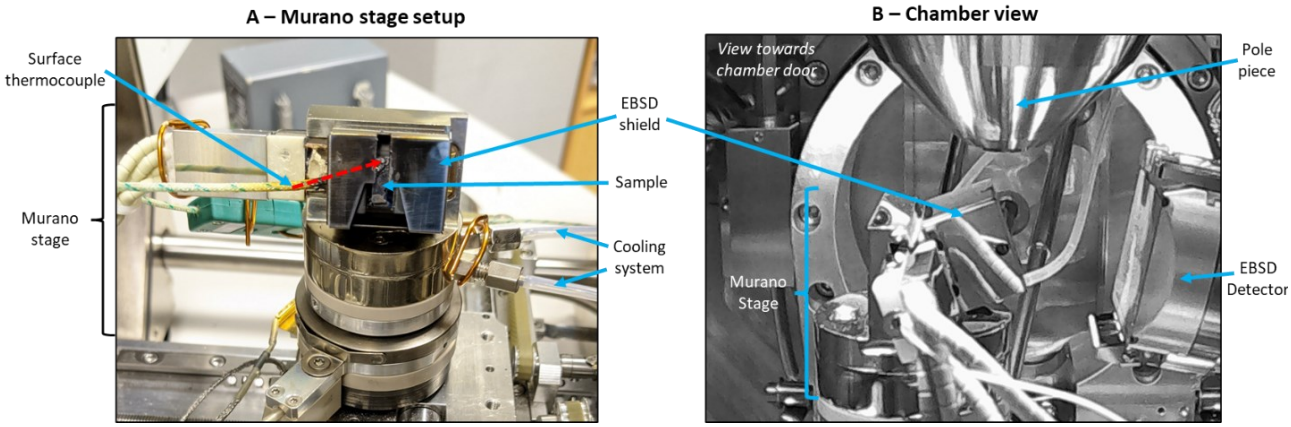


Figure 69 - In situ experiment setup. A: Murano stage assembled (with additional thermocouple added to the sample surface) and (B) chamber view with the EBSD camera inserted.

As this experiment leads on from prior work [44], [125], the target temperature for the heat treatment was 760 °C (max 800 °C as this is the start of the range for the β transus and SPP dissolution temperature), and the target duration around 1 hr to ensure some grain growth is seen.

5.4 Potential issues

It is important when planning a high temperature experiment to avoid damaging the equipment, and carry out preliminary trials to ensure the experiment is viable. With this in mind, a number of potential issues were identified and these are detailed in Table 17. Each of these issues are discussed in turn in section 5.5 .

Two main preliminary trials were also carried out:

- **High temperature forescatter imaging.** A trial to investigate the feasibility of carrying out forescatter imaging at elevated temperatures, up to the heat treatment temperature (760 °C).

[8] up to a volume envelope of 5 x 10 x ~5 mm (W x L x D) – though not all of the surface will be visible if using the EBSD shield – the aperture gives ~ 3mm width.

- **High temperature EBSD.** A trial to investigate the feasibility of high temperature EBSD during the experiment.

Table 17 - Potential issues identified for the in situ experiment.

ID	Topic	Potential Issue
1	Temperature measurement	Sample temperature different to the Murano stage control thermocouple so the sample does not stay within the heat treatment temperature range and grain growth does not occur.
2		Murano temperature cannot be accurately controlled due to timing or control loop issues.
3	Heat damage	Temperature too high for forescatter diodes causing long term damage.
4		High temperature EBSD phosphor life too short at high temperatures for the experiment.
5	Forescatter imaging	Light from the sample at high temperatures floods the forescatter diodes and imaging not possible.
6		Drift occurs during heating making it difficult to image the same area throughout.
7	Sample	Sample oxidises and no results are possible to gain during the *in situ* experiment (only start + end points).
8	Stage/setup related	Maintenance issues with the setup lead to inaccurate results or experiment failure.

5.5 Issue investigations

To investigate the potential issues identified and in preparation for the full experiment, iterative preliminary trials were carried out on similarly dimensioned (to the weld samples) fine grain Zircaloy-4 samples, and an initial weld piece. The sections below outline key results for the issues investigated.

5.5.1 Temperature measurement

This section deals with installation of a thermocouple to monitor the sample surface temperature and the effectiveness of the Murano stage temperature control.

5.5.1.1 Surface temperature

The grain growth experiment relies on being able to monitor and control the sample surface temperature in order to ensure that the desired heat treatment is applied. Unfortunately, this cannot be directly monitored using the Murano stage and the in-built control thermocouple is located underneath where the sample is mounted. The exact position of the thermocouple is shown in Figure 70, and its position leads to a difference in temperature between the sample surface temperature and the Murano thermocouple reading. For this reason, an additional thermocouple was attached to the sample surface to measure the exact sample surface temperature (see Figure 73).

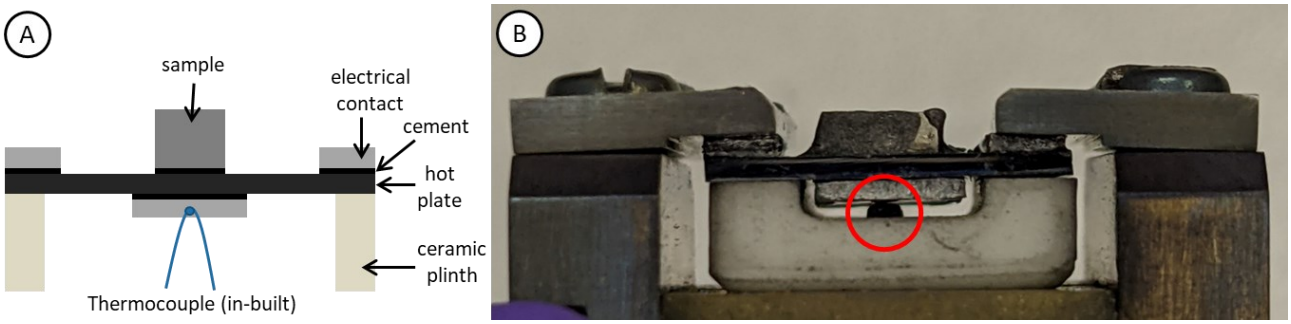


Figure 70 - Murano (in built) thermocouple position. (A) Schematic of the central part of the heating carriage with thermocouple positions labelled (from figure 8 in [149]*). (B) Photo showing the Murano (in-built) thermocouple in contact with the heating cartridge.*

While attaching a thermocouple to the surface of the sample appears very simple, i.e. spot welding a thermocouple to the surface prior to installation, in practice this is challenging especially for Zircaloy-4 as thermocouples do not weld easily to this material. A series of spot welding conditions were trialled, with some success, but ultimately they all fell off prior to full installation in the chamber (as subsequent adjustments to the sample to load it into the system were required). An additional challenge being that once the sample is attached to the heating cartridge (using high temperature carbon paste), if the thermocouple detaches, it can not easily be re-spot welded on as the heating cartridge acts as an insulator.

To overcome the challenges with spot welding, high temperature carbon paste was explored as an adhesive to attach the thermocouple to the sample surface, an approach which was semi-successful in initial trials.

Using either mounting method, one of the complications is the way that the sample is installed in the Murano heating stage. This is shown in Figure 71 where the steps are:

1) Sample is attached to heating cartridge using high temperature carbon paste;
2) Carbon paste is cured[9] for optimal electrical and mechanical properties according to [167];
3) The heating cartridge is slid into the heating carriage (can be installed without sliding but its more challenging);
4) The EBSD shield is installed over the top of the heating carriage;
5) The heating carriage is slid into the Murano stage in the chamber.

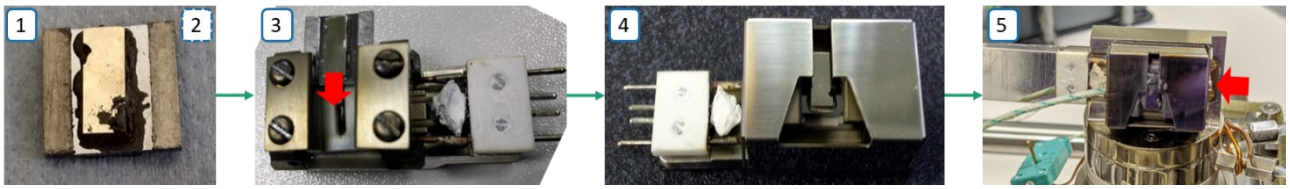


Figure 71 - Sample installation in Murano stage. Red arrows indicate sliding movement. See section 5.5.1.1 for further details on the steps and numbering.

[9] This step was omitted as it did not have a noticeable effect in this experiment.

The thermocouple may detach at any point in the installation process if not firmly attached to the sample. This is particularly likely in steps 3 and 5 where the sample (and heating carriage) is slid into position, or at step 4 when the EBSD shield is installed on top.

The design and positioning of the thermocouple is particularly important in this geometry since it is easy to block the electron beam and impact the ability to carry out imaging or EBSD. This is nicely illustrated in Figure 72 where the sample is fully blocked by the thermocouple (this setup was used for the initial sample surface trials – data only). Note that the thermocouple outer coating fibres also can cause significant of image distortion if they fray (as they charge under the electron beam), and this is evident especially at elevated temperatures.

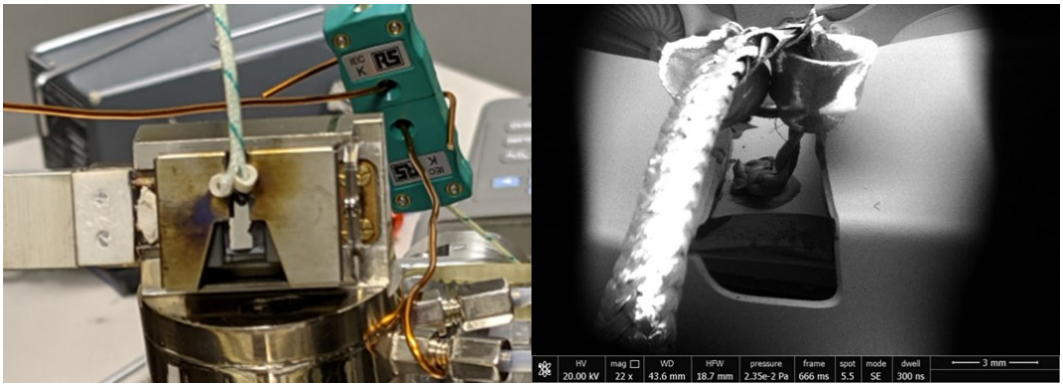


Figure 72 - Thermocouple positioning issue. Thermocouple setup from surface temperature trials (temperature data only). LEFT: photo of thermocouple positioning; RIGHT: SE image with sample blocked by the thermocouple.

This eventually led to the decision to install the thermocouple when the sample and stage are installed in the SEM chamber, using the high temperature carbon paste to attach it. The optimal positioning was found to be through the side of the EBSD shield (the gas inlet hole) to the top of the sample, as shown in Figure 73.

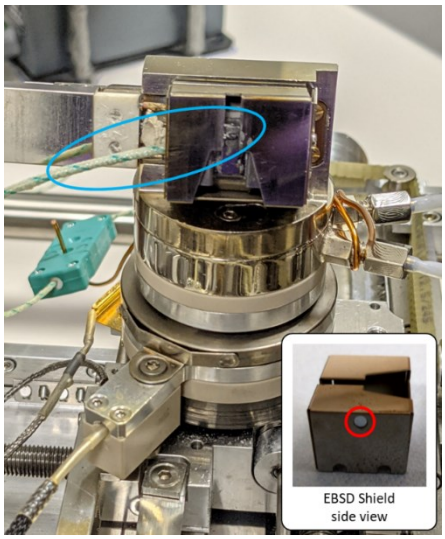


Figure 73 - Final thermocouple solution. The thermocouple (blue ellipse) is inserted through the side of the EBSD shield and attached to the top of the sample using (high temperature) carbon paste - installed in situ. INSERT: side view of EBSD shield with gas inlet hole (through which the thermocouple is inserted) identified by a red circle.

5.5.1.2 Murano temperature control

The stage temperature (and therefore sample temperature) is controlled using the Murano control software ('Temperature control software v2.2.0' from Gatan) and this is informed using the Murano thermocouple, which is embedded in the stage and below the sample (see Figure 70). Further to establishing the sample surface temperature (section 5.5.1.1) difference to the Murano thermocouple reading, the effectiveness of the control loop needs establishing, which is split into two sections below.

Start-up cycle

The sample needs to be pre-heated using a relatively low temperature in order to degas the sample/setup. This is important for any trapped gas and, in the case of use of a high temperature adhesive, if there is any gas evolved during the final stages of curing. If this not carried out, when the sample is heated, the sample will degas, and the microscope's safety systems will close the gun and the electron beam will turn off. A program was used to carry out this heat treatment, initially with 100 °C (Murano reading) as the maximum temperature, and later using 120 °C as the maximum temperature, as illustrated at Figure 74. The change in maximum temperature was made as there were still issues with degassing when ramping straight to 500 °C after using the lower maximum temperature – this is likely due to the temperature delta between the Murano thermocouple and the sample. Furthermore, Figure 74 shows a delay when using a program between changing the set point and the Murano thermocouple reading changing. This is accounted for in the (updated) control program used, where the aim is to reach the set temperature and stabilise. The overshoot is approx. 5 °C or 7 °C for the 100 °C and 120 °C max programs respectively and temperature stabilisation time <5 mins in both cases. The magnitude of the overshoot here is small, and as can be seen later in Figure 75 and Figure 76, remains relatively small at all temperatures. For the *in situ* experiment, the overshoot would only become significant if it put the sample temperature above 800 °C at the heat treatment (maximum) temperature.

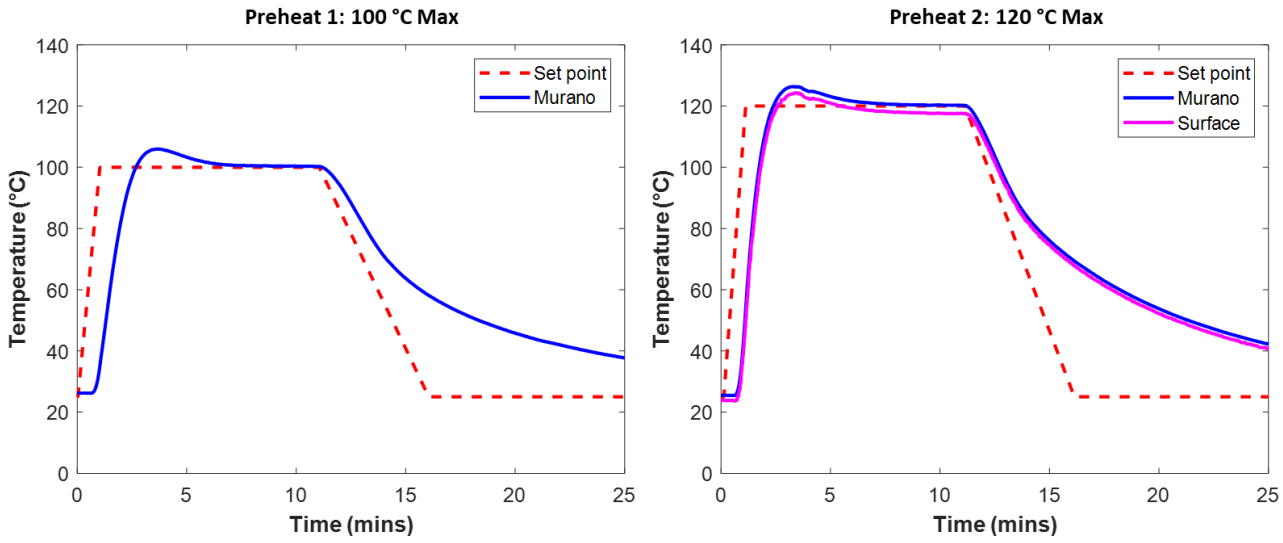


Figure 74 - Preheat cycles. LEFT: preheat 1 – 100 °C max with Murano thermocouple data only. RIGHT: preheat 2 – 120 °C max including Murano and surface thermocouple data.

Control

The effectiveness of the control loop was established throughout the initial testing phases. The main questions to be answered were:

- What it the magnitude of any overshoot or undershoot in temperature compared to the set temperature?
- What is the maximum heating/cooling rate?
- How long does it take for the temperature to stabilise?

In terms of the overshoot/undershoot, this varies with temperature, but the temperature stabilises in around 10 mins in all cases during heating. During cooling the stabilisation time is generally longer and the magnitude of the undershoot 2-3x as large. As an example, Table 18 covers temperature overshoot and duration (stabilisation time) for temperatures in the range 500-850 °C. For this experiment, the heating segments are more significant as the time at the heat treatment temperature needs to be recorded accurately – for the temperature ranges trialled, the overshoot magnitude and duration was consistent for the heating segments.

Table 18 - Temperature overshoot and stabilisation times for the range 500-850 °C.

Start (°C)	Setpoint (°C)	Time to hit set point (mins)	Time to return to setpoint (mins)	Overshoot duration (mins)	Undershoot duration (mins)	Maximum over/undershoot (°C)
500	750	2.78	10.92	8.14		5.14
500	800	2.64	10.59	7.96		6.61
500	850	3.03	10.03	7.00		6.10
850	500	1.83	15.75		13.92	10.65
800	500	1.92	14.17		12.26	13.89
750	500	2.08	15.56		13.48	17.85

The heating rate can be predicted and used as a program for the final experiment, but there are limits to the ability of the stage to meet the set temperature, and as the program follows the timing schedule, the exact time at the set temperatures may not be the planned amount. This is illustrated in Figure 75 where the heating program asks for a 15 min hold at the maximum temperature (see red dashed line), yet this is not achieved as it takes the stage longer than planned to reach the maximum temperature.

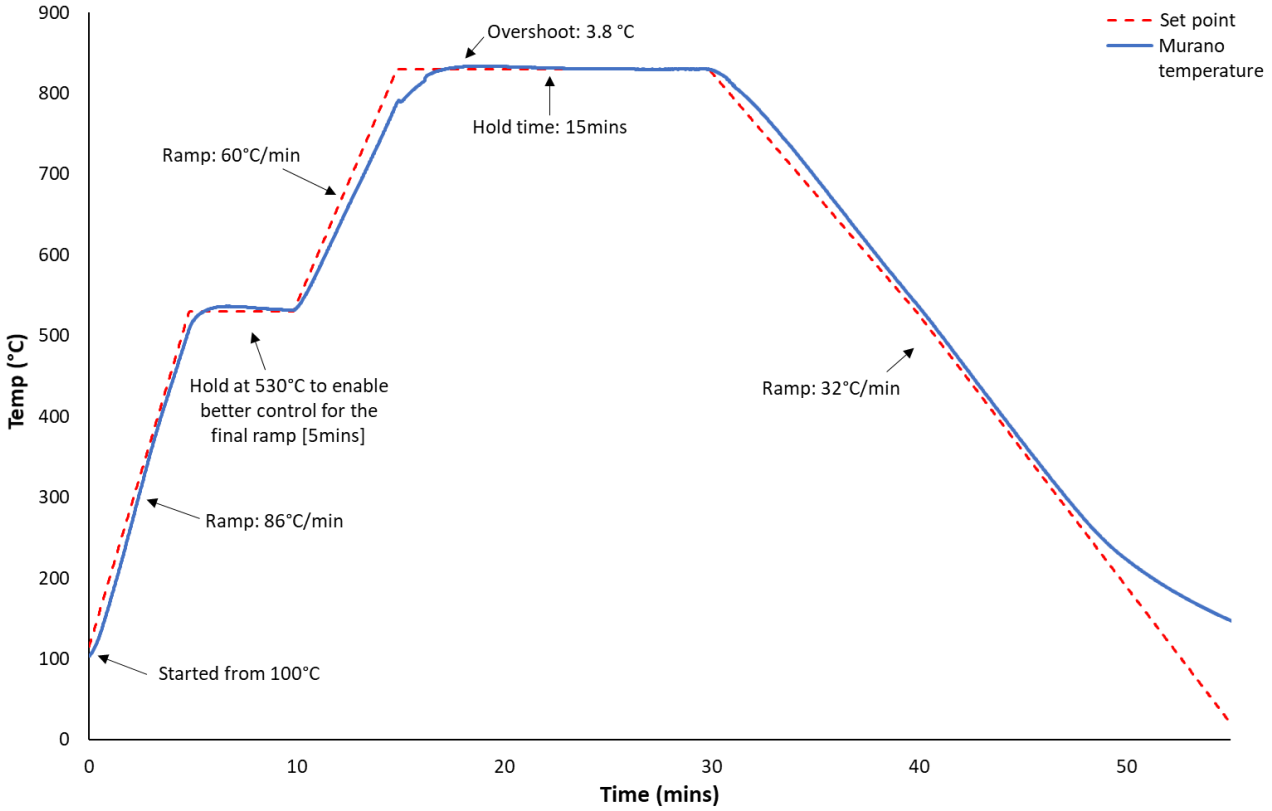
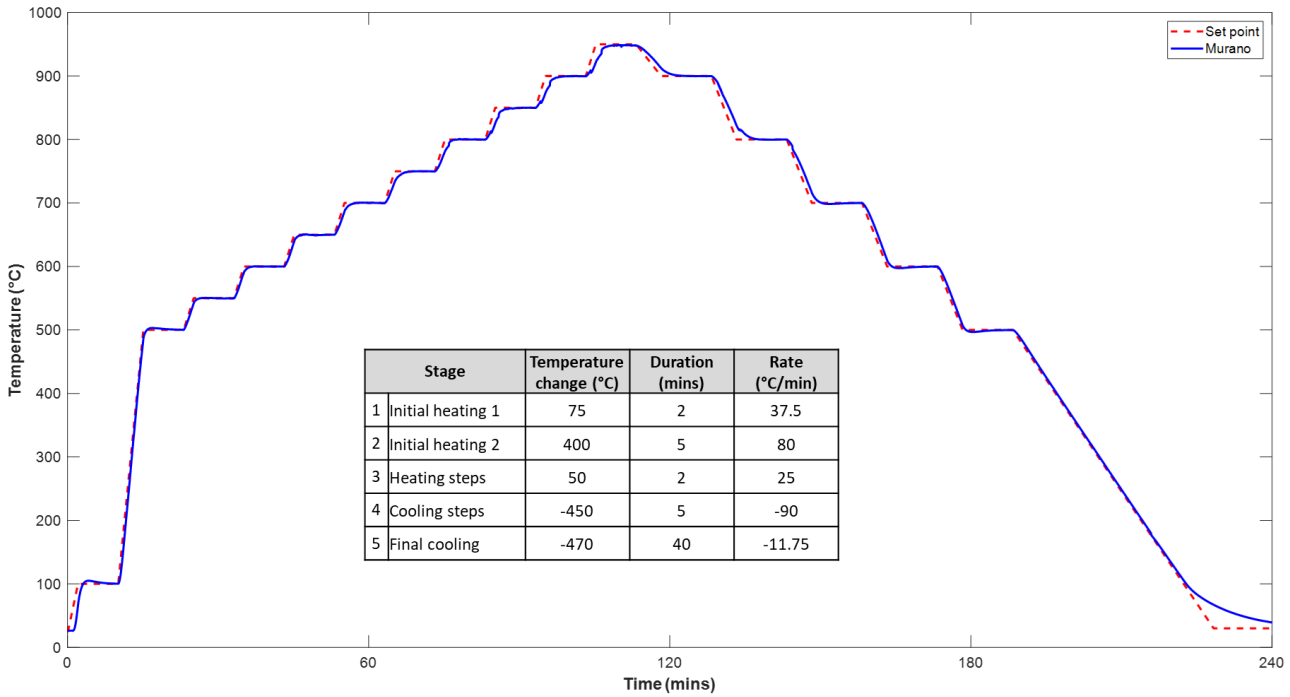


Figure 75 - Trial heating program for LG sample showing the Murano thermocouple data (solid blue line) and the programmed set point (red dashed line), with comments on ramp rates.

The ramp rates in Figure 75 are controlled using the program, but the Murano fails to achieve the 60 °C/min rate set for the transition between 530 and 830 °C (max temp), with the set temperature (red dashed line) and measured temperature (solid blue line) diverging as the temperature increases. To consider using a program for the full experiment (i.e. no manual control of the Murano stage temperature during the experiment), a heating and cooling trial was carried out using ramp rates based on preliminary results where there Murano temperature and the set temperature did not deviate significantly. For the trial, consistent ramp rates for each heating step (25 °C/min) and cooling step (90 °C/min) were used above 500 °C, with a hold time of 8 mins at each step. The results are shown in Figure 76 where it can be seen that although the Murano temperature matches the set temperature well at lower temperatures, there was a lag at higher temperatures. This is an issue as the program changes temperature at specific time intervals, rather than using a closed loop based on temperature, so the time at the hold temperature is often shorter requested amount of time.



	Stage	Temperature change (°C)	Duration (mins)	Rate (°C/min)
1	Initial heating 1	75	2	37.5
2	Initial heating 2	400	5	80
3	Heating steps	50	2	25
4	Cooling steps	-450	5	-90
5	Final cooling	-470	40	-11.75

Figure 76 - Program controlled heating cycle. Murano thermocouple (blue solid line) and setpoint (red dashed line) temperatures for the heating cycle defined in the table. Hold times for temperature stabilisation were 8 mins throughout.

There are two things to note with the control software:

1) The maximum temperature is entered when the software is started up – if the maximum temperature is reached, the stage heating will turn off and the software will require a restart
2) If the program is stopped for any reason, temperature control will be temporarily lost – it will drop or spike (depending on how it's interrupted)

As a result of the various trials, the decision was made to only use a program for the start-up cycle, which would be using a maximum (Murano) set temperature of 120 °C. During the experiment, the temperature would be controlled manually, since rapid heating and cooling were required, and this allowed for any delays or issues during the experiment to be addressed without losing temperature control.

5.5.2 Heat damage issues

Due to the high temperatures used for this experiment, it was important to ensure that equipment was not damaged by the heat. The areas of concern were the forescatter diodes (FSD) and the high temperature EBSD phosphor.

5.5.2.1 FSD temperature

An FSD temperature trial was designed to check that the radiative heating from the stage and sample would not damage the diodes. In order to do this, the FSD (Figure 77(A)) were removed from the EBSD detector and replaced with a blanking plate. A thermocouple was spot welded onto the blanking plate (prior to installation), as shown in Figure 77(B & C) and used to monitor the temperature throughout the trial.

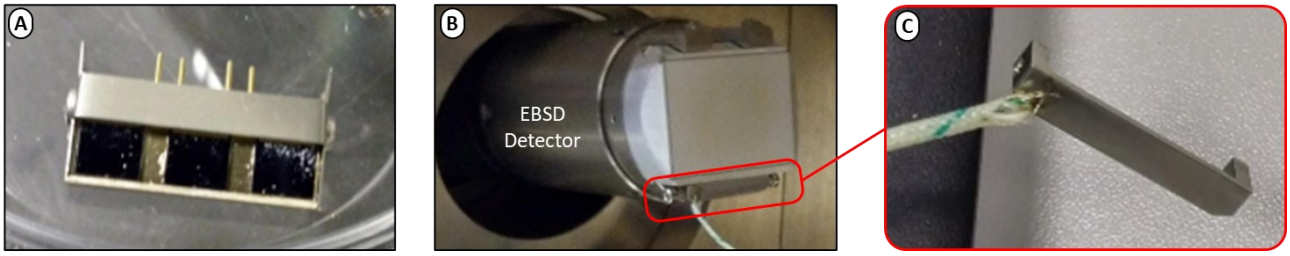


Figure 77 - Forescatter diode (FSD) trial. A - FSD removed from detector; B - EBSD detector with FSD removed and blank in place, with thermocouple attached; C - close up view of blanking plate with thermocouple attached.

The in-chamber setup is shown in Figure 78 with the EBSD detector at a distance of ~28 mm from the sample, which is a distance typically used for forescatter imaging of the Zr samples.

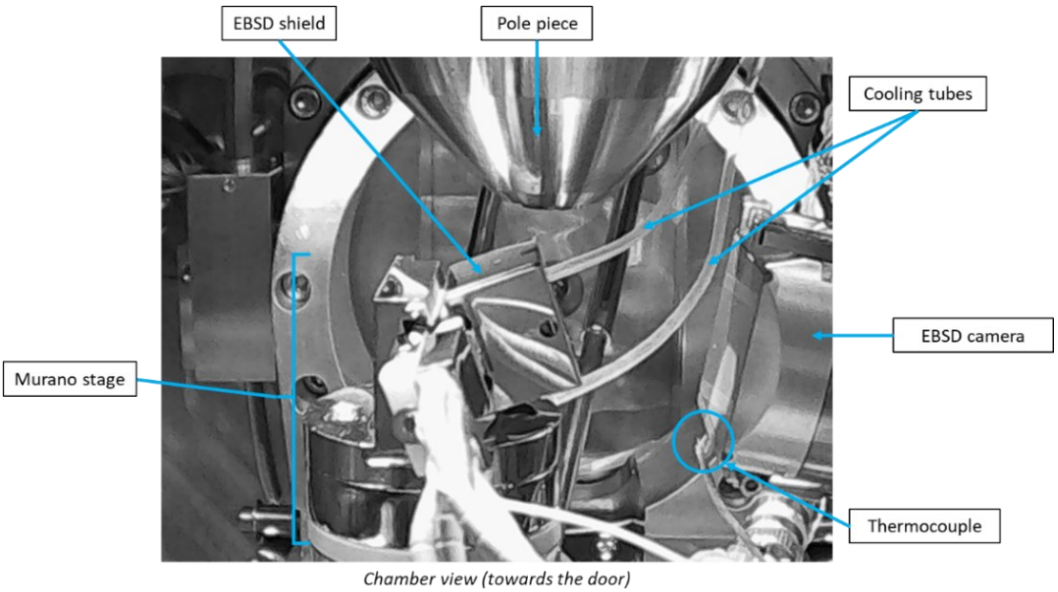


Figure 78 - Chamber view for the FSD temperature trial showing the EBSD detector with the FSD removed and replaced by a blank with a thermocouple. EBSD detector distance ~28 mm from sample.

The trial consisted of heating a similarly dimensioned (fine grain) Zircaloy-4 sample in the Murano heating stage at 830 °C (slightly higher than the planned temperature for the experiment) – as measured by the Murano thermocouple – for approximately 1 hr, or until it was considered that the temperature was unlikely to dramatically change further. The exact setup used is detailed in Table 19.

Table 19 - Setup details for FSD temperature trial

Attribute	Value
Detector distance	28 mm
Detector tilt	10.9 °
Working distance	20 mm
Beam acceleration voltage	20 kV
Maximum set temperature	830 °C
Hold time at max temperature	58 mins

The temperature results are shown at Figure 79, where it can be seen that the inbuilt thermocouple in the Murano heating stage ('Murano' / blue line in Figure 79) closely follows the set point temperature that was

used to control the Murano heating stage. The FSD thermocouple ('FSD' / green line in Figure 79) clearly stays below 50 °C throughout the trial, with no significant upwards trend.

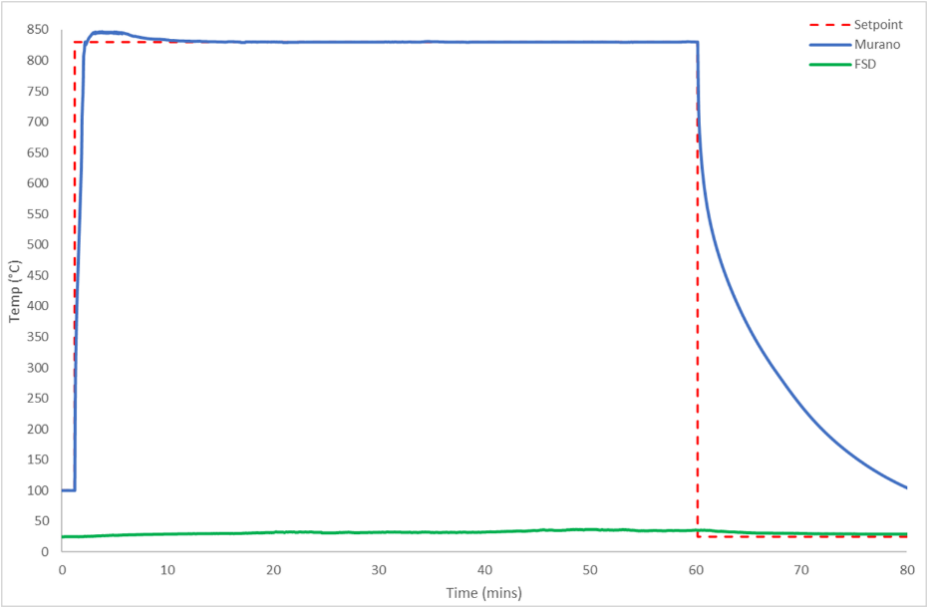


Figure 79 - FSD temperature trial results. Red dashed line = set temperature; Blue solid line that closely follows the dashed line = Murano in built thermocouple temperature; Green line at the bottom = temperature at FSD position.

More details on the temperatures reached are shown in Table 20. As can be seen, the FSD thermocouple temperature peaked 10 mins prior to the end of the trial, and did not exceed 36.7 °C.

Table 20 - Temperatures reached during the FSD temperature trial.

Temperatures	**Thermocouple**	
	FSD	**Murano**
Maximum temperature	36.7 °C @ 48 mins	847 °C @ 4 mins
Mean temperature	31.4 °C	-

There is a slight limitation to the trial, as the FSD protrude from the front of the EBSD camera. The FSD are therefore ~5-10 mm closer to the sample when the camera is inserted. However, it is not expected that this would make a significant difference and the maximum temperature is sufficiently low that even a relatively large temperature increase (e.g. 30 °C) is not expected to cause damage.

Based on the results of this trial, it is unlikely that the FSD will reach temperatures likely to damage them during the *in situ* heating experiment thanks to the air gap/vacuum and the angle at which the FSD are to the sample.

5.5.2.2 Phosphor deterioration

The high temperature EBSD phosphor fitted to the EBSD camera is a consumable item as it will deteriorate with use. It is the Al coating that deteriorates with use as shown visually in Figure 80 where the high temperature phosphor was imaged between experiments for the first 13 hrs of service. Full details of the heating conditions and detector to sample distances are found in Table 21.

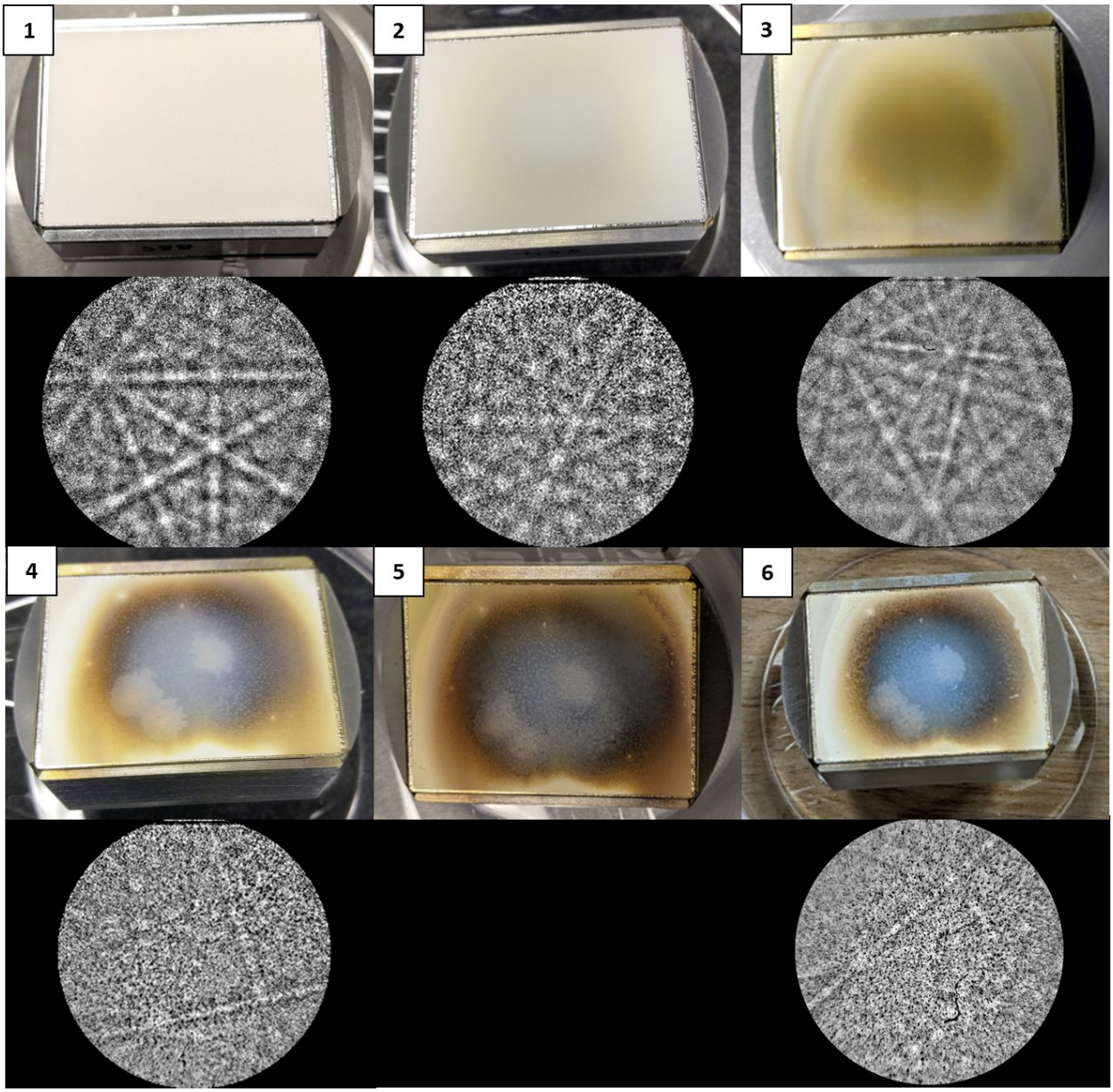


Figure 80 - HT phosphor deterioration and EBSP quality. Rows 1 & 3: Progressive deterioration of the high temperature phosphor over the course of the first 6 trials - time at temperature and distance to sample are detailed at Table 21. Rows 2 & 4: Example EBSPs for the phosphor states in rows 1 & 3, all room temperature examples. Note: no EBSD was carried out in experiment 5, so there is no example EBSP.

Table 21 - Heat treatment details for the high temperature phosphor.

Experiment	Image taken before/ after experiment	ARGUS distance (27mm)	EBSD distance (~17mm)	Max temperature* (°C)
1	Before	-	-	-
2	After	-	1 hr 30	720
3	After	1 hr	1 hr 50	865
4	Before	3 hrs	-	950
5	After	2 hr 20	-	950
6	After	3 hr 20	-	950

*As measured using the Murano thermocouple

Figure 80 shows heat damage on the surface of the phosphor screen as function of time. The damage is focussed on the centre of the phosphor (roughly where the EBSP pattern centre would be). The effect on the EBSPs is also illustrated in Figure 80, where an example EBSP for each of the phosphor states is shown underneath the image for each. Some indexing is possible even with the quality at Figure 80 (6), however the time required to capture the EBSPs increases (the resolution for this EBSP is 1600 x 1200) and indexing is generally poor.

It is worth noting that the deterioration between Figure 80 image (3) and (4) occurred *ex situ*, probably as a result of the phosphor not being fully cooled prior to putting it away. It is recommended that the phosphor is allowed to cool to room temperature in the chamber before being removed and packed away.

Discussion with Bruker suggests that high temperature EBSD should be possible at ~750 °C for 30 mins [168]. This temperature is below the temperature planned for this experiment and this combined with the general deterioration seen even when not running high temperature EBSD, led to the decision not to run high temperature EBSD mapping during the experiment.

The phosphor was replaced prior to the main experiment and showed minimal damage (close to (2) in Figure 80) after the experiments using the final setup where the detector was kept at a distance of ~27 mm for FSD imaging during the high temperature phase.

5.5.3 Forescatter imaging issues

Specific considerations for forescatter imaging at elevated temperatures are discussed below, with further details in the high temperature imaging trial at section 5.6.1

5.5.3.1 Light

As the sample heats up, the chamber light levels increase, as demonstrated in Figure 81, which affects the ability to collect forescatter images as the forescatter diodes get flooded by photons. This limits the maximum temperature at which forescatter imaging can be carried out, which is investigated in more detail in section 5.6.1.3 .

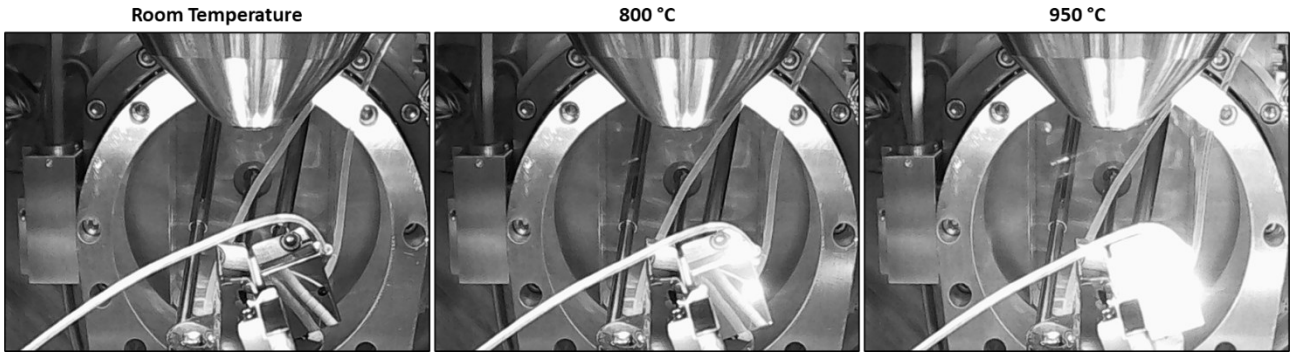


Figure 81 - Chamber light levels at elevated temperatures. The two extremes (LEFT: room temperature (~23 °C) / RIGHT: maximum Murano stage temperature (950 °C)) and the set temperature for the in situ experiment (800 °C). Note: all temperatures are Murano thermocouple temperatures.

It is possible that the issue could be helped by using a modified shield or additional filter, but for this project the solution chosen was to limit the temperature for FSD imaging to <600 °C. The increase in stability of the experiment means that imaging is significantly easier, especially as this lower temperature hold will not result in significant microstructural evolution. In practice, this means that larger micrographs with more points can be taken without the FSD being flooded. These images take longer but result in a higher quality micrograph that is easier to interpret (including more successful colour balance across the image by the Esprit software).

5.5.3.2 Drift

During temperature changes, and until the temperature has stabilised, the image is likely to drift. This makes it difficult to continue to image the same area. However, if the temperature is allowed to stabilise for longer (~10 mins) the image is generally more stable, although there will still be some shift at elevated temperatures compared to room temperature. This shift reduces after the initial heating step (i.e. there is less change between higher temperatures (e.g. 500 to 800 °C) than RT to 500 °C. For an example, see section 5.6.1.2

5.5.3.3 Bias control

There is an option on the Murano stage to apply a voltage (+6V to -6V) to the top shield plate (with respect to the earth potential) [149]. The aim is to aid extraction of secondary electrons or repel thermionic electrons that may interfere with imaging [149]. A trial was conducted to evaluate the effectiveness of changing the bias control for the Murano stage on improving the forescatter imaging quality at elevated temperatures.

In the trial, forescatter images were taken at temperatures from 200-600 °C at 100 °C increments. At each temperature, an image was taken with the bias control set to -6V (fully anticlockwise), 0V (neutral) and +6V (fully clockwise). The detector position was kept constant throughout at a distance of 26.6 mm and detector tilt 10.7 °, with a sample working distance of 20.9 mm, beam acceleration voltage of 20 kV and magnification 2000x. A selection of the results are shown in Figure 82.

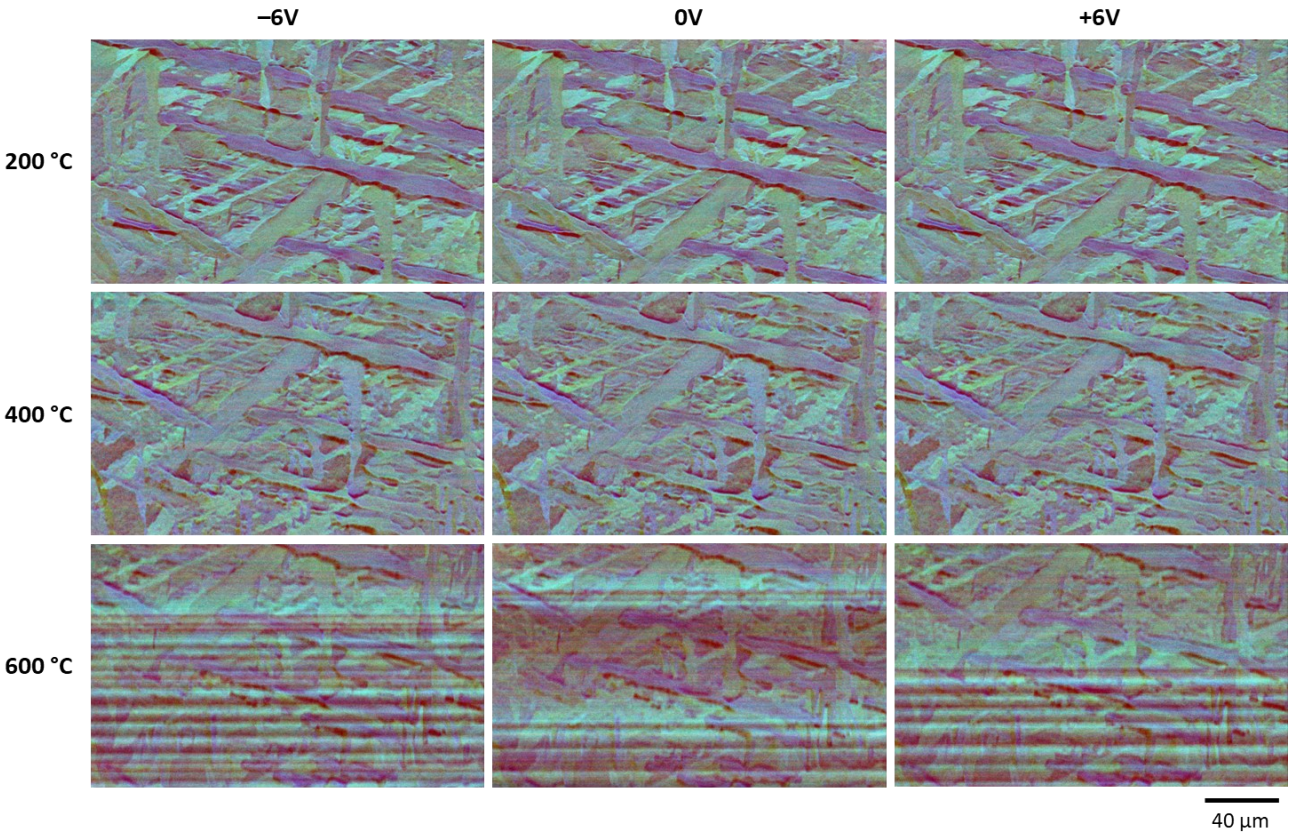


Figure 82 - Bias control trials - effect of changing the bias control from -6V to +6V at 200, 400 & 600 °C on FSD imaging quality. Imaging settings: working distance 20.9 mm; detector distance 26.6 mm; detector tilt 10.7°; image resolution 2000 points; beam acceleration voltage 20kV.

As can be seen in Figure 82, there is limited difference in the FSE imaging at each temperature when a voltage (bias) is applied. There is a very slight shift of the image up or down, but the impact is minimal. All three bias states still struggle at 600 °C. Overall, there is no clear evidence that changing the bias state affects the FSD imaging quality, therefore a neutral state is chosen for the main experiment.

5.5.4 Sample and stage considerations

Sample and stage issues are discussed in this section, including general maintenance observations from the initial trials.

5.5.4.1 Oxidation

As Zr has a high affinity for oxygen, as demonstrated by the 2-5 nm thick oxide layer that usually forms at room temperature [63], it is perhaps unsurprising that at high temperatures we see oxidation of the sample. For example, Figure 83 shows the progression of oxidation in a fine grain Zircaloy-4 sample during an initial trial of ~2 hrs whilst heating incrementally to 760 °C (Murano), with a 15 min hold at temperature before cooling incrementally again. Small white spots can be seen in the SE images from 500 °C onwards. It is likely that these spots are oxidised SPPs given the frequency and size. These white spots then become clearer and more defined as the sample is held at the maximum temperature. During this hold, grain boundaries also become clear (white lines on the images). Both of these are signs of oxidation. Whilst useful to see the grain boundaries, the concern was that the oxidation would pin the grain boundaries and

not allow growth to occur.

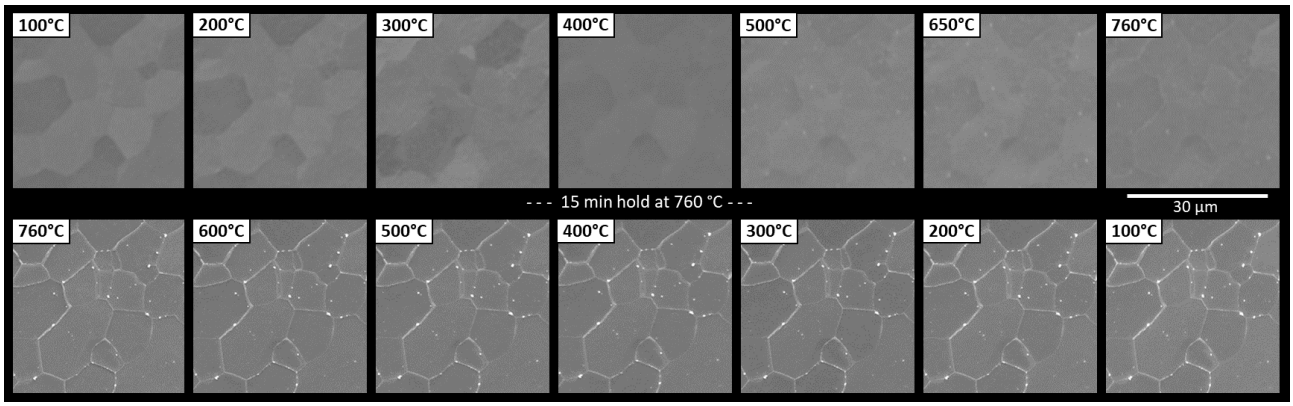


Figure 83 - Oxidation at elevated temperatures. Progression of oxidation during an initial SE imaging experiment heating from 100 to 760°C with a 15 min hold before cooling to 100 °C in 100 °C intervals. Temperature and image were allowed to stabilise before imaging at each temperature – total experiment time 113 mins.

Figure 84 shows a further example, this time at 830 °C in a weld microstructure, where it can be clearly observed that the oxide is protruding from the sample surface. Again, this occurs mainly along the grain boundaries, with speckling throughout the grains.

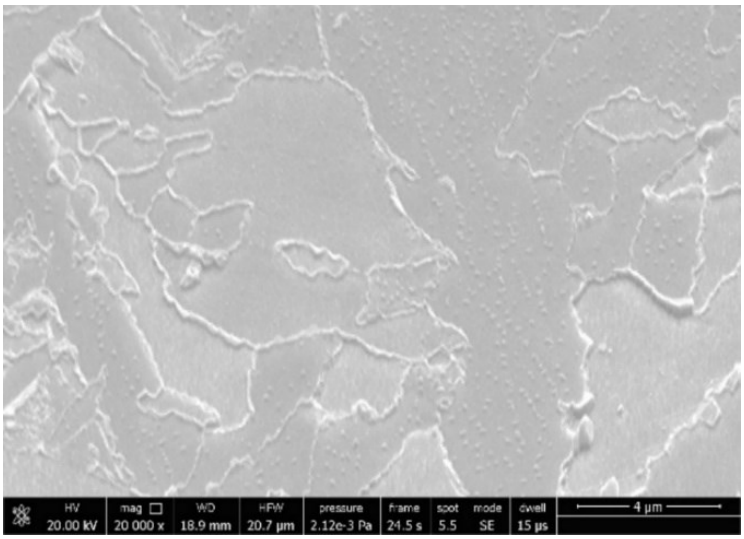


Figure 84 - Oxidation at 830 °C in a weld microstructure. Oxide growth is clearly on (protruding from) the surface, and mainly located along grain boundaries, with smaller dots speckling the grains.

A number of adaptions to the experiment were trialled to minimise the extent of oxidation, including:

- Additional PECS broad ion beam polishing prior to installation
- Waiting overnight after setup to improve the vacuum in the chamber
- Cleaning the Murano stage prior to installation (and after each experiment)
- Plasma cleaning of chamber and sample once installed
- Sample pre-heat cycle (necessary to degas the sample)
- Baking the Murano stage without the sample in place (using an old heating cartridge)

These adaptions helped to a certain extent – with oxidation occurring after 2-3 heating cycles rather than almost immediately, but in my experiments oxidation of the zirconium samples was not fully avoidable. The impact of the oxidation on the data collected was two-fold, as illustrated in Figure 85.

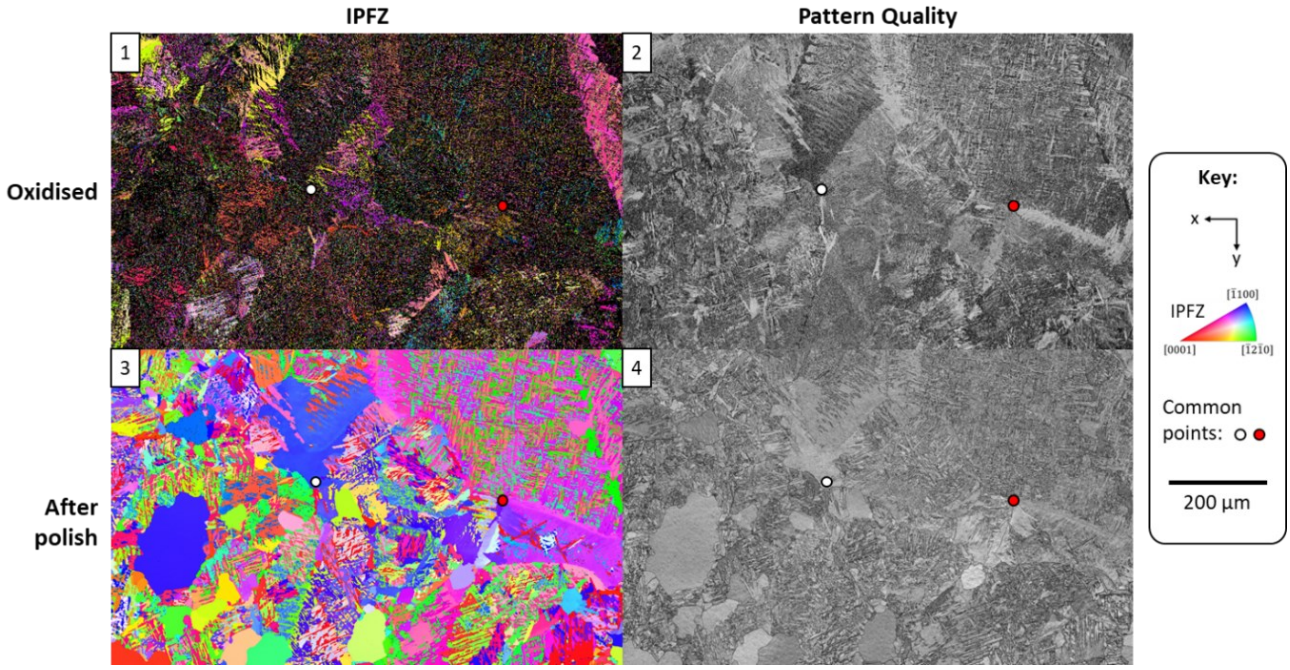


Figure 85 - Effect of oxidation on EBSD. IPFZ and pattern quality for a weld sample after the heat treatment (with surface oxidation) (1 & 2) and after a short BIB planar polish to remove the oxidised layer (3 &4). Two common points across the maps are identified with red/white dots to aid comparison.

Firstly, after heating and due to surface oxidation the indexing quality is very poor – this is due to the oxide causing overlapping patterns that are challenging to index (i.e. the pattern contains diffraction data from the oxide and the α-Zr matrix). This also affects the mapping time, for example, the 'oxidised' map in Figure 85 took ~8 hrs and only indexed at a rate of 34% compared to the re-polished map that took ~2 hrs and was 99% indexed.

Secondly, the oxidation appears to have pinned the grain boundaries at the surface, as can be seen in the pattern quality images in Figure 85. These two examples (2 & 4) are the same sample, before and after a BIB polish. The grains that grew are not evident in the map at (2) but are obvious at (4), leading to the conclusion that the oxidation pins the grains at the surface. The BIB polishing removes the oxide and a very small amount of the layer below, revealing the grain growth.

To address this issue in the final experiment, an additional BIB polish was included prior to the final EBSD mapping, as well as keeping the adaptions discussed above.

In the future, an oxygen getter could be included as part of the setup, and/or an alternative microscope setup with a cleaner chamber could be used. Alternatively, the gas inlet on the Murano flange & stage could be considered with an inert gas in an attempt to minimise oxidation. A potential setup could be similar to that used by Stolbov et al.[169] for thermal analysis where an oxygen getter is placed next to the sample and the heating carried out in a helium gas flow to minimise oxidation.

5.5.4.2 General maintenance

Further to the above, it is worth mentioning that some of the components require regular maintenance for optimal results. These include:

- EBSD shield – the central edges of the shield (i.e. above the sample) may get contaminated with carbon paste during the installation of the surface thermocouple. Failing to clean up these edges (it can be scraped off even if baked on) will reduce the field of view. The inside of the shield will get affected by the heat and may also need some clean up. Further to this, due to the design, the sides of the shield are relatively flexible and can bend in to the point where the shield will not fit so should be checked prior to setup.
- Electrical contacts – the screw down electrical plates that keep the heating cartridge in place (see Figure 86) need to be cleaned up to remove any oxide or surface contamination. This will ensure good contact and avoid non uniform heating or inability to reach the setpoint temperature (see manual for more details [149]).

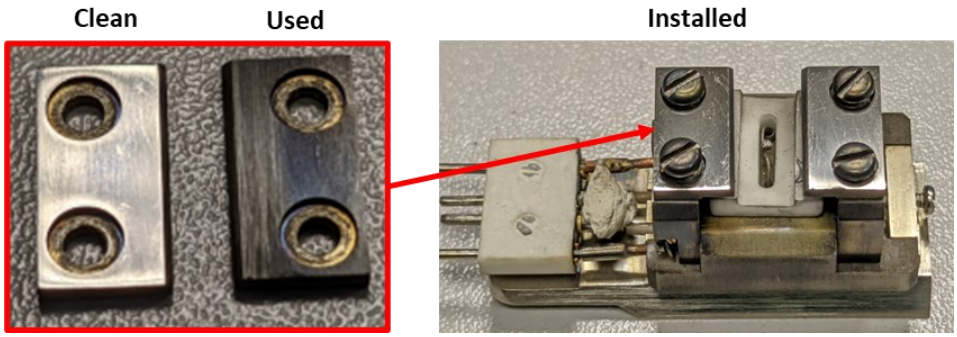


Figure 86 - Maintenance of Murano stage - electrical contacts. Screw down electrical contacts for the Murano heating carriage - shown both before and after use.

5.6 High temperature trials

This section captures the two main preliminary trials: high temperature forescatter imaging and high temperature EBSD. These trials were both to test the operation of the setup and to see what was feasible for the main experiment.

5.6.1 High temperature forescatter imaging

The high temperature imaging trial was designed to check the FSD imaging feasibility and conditions at elevated temperatures. For this trial, a weld sample was heated to 800 °C (Murano temperature) in 100 °C increments, with FSD images of the same area taken at each stage and then compared.

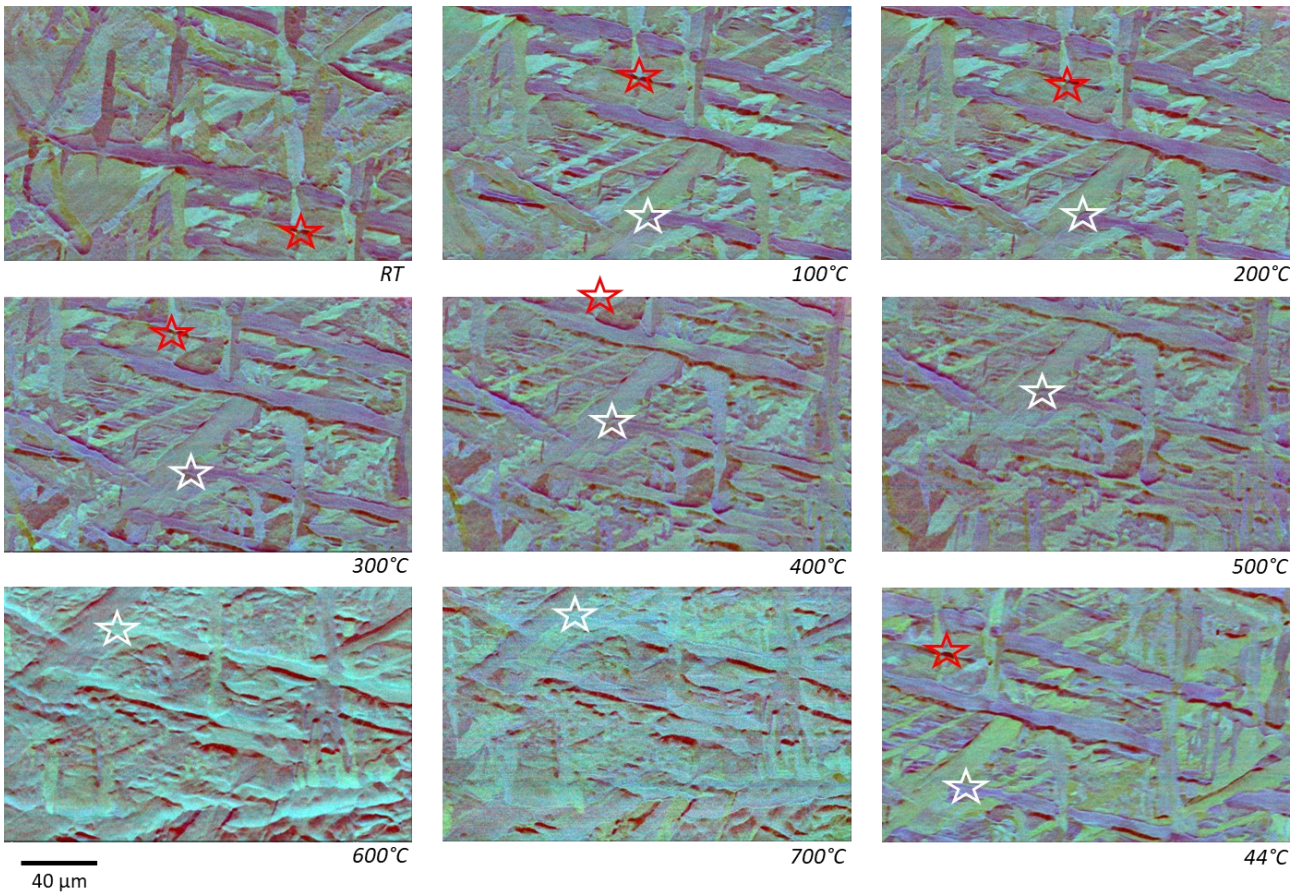


Figure 87 - High temperature FSD imaging: FSD imaging of the same area at temperatures from room temperature to 700 °C. Images taken at RT-500 °C used a detector distance of 26.6 mm and detector tilt 10.7 °; for 600-700 °C and 44 °C a detector distance of 28 mm and detector tilt of 8.8 ° were used. All images taken at 2000x magnification and 2000 px resolution, with a working distance of 20.9 mm and beam accelerating voltage 20 kV. The red and white stars indicate the same positions within the microstructure and indicate the change in position of the imaging with temperature.

The outcome of this trial is shown in Figure 87, where imaging conditions were kept constant for room temperature (RT) to 500 °C then changed for the remaining images in order to continue imaging, as detailed at Table 22.

Table 22 - FSD imaging conditions for high temperature imaging trial

Conditions	Setup 1	Setup 2
Temperature range	RT-500 °C	600,700 & 44 °C
Magnification (x)	2000	2000
Resolution (px)	2000	2000
Working distance (mm)	20.9	20.9
Detector tilt (°)	10.7	8.8
Detector distance (mm)	26.6	28

FSD imaging was possible temperatures up to 700 °C, with varying levels of effectiveness. The ideal solution involves high grain contrast with lower levels of topographical detail.

5.6.1.1 Detector position

In general, changing the detector (and thus FSD) position affects the relative amount of topography or grain contrast seen in the FSD images - it is the electron channelling-in contrast that is optimised for the colourful FSD images (for more details see [135]). At higher temperatures, the FSD were flooded by photons so the detector position and angle had to be adjusted (moved back and down) to achieve a high contrast image. However, this also led to an increase in topographical detail and a decrease in grain contrast. For comparison, the 600 °C images in Figure 82 show the same region as the 600 °C image in Figure 87, but at the closer distance which leads to a distorted image as shown. It is possible that with experimentation a more optimal angle/distance could be established for very high temperature imaging, although the detector angle is limited so it may not be possible.

5.6.1.2 Drift

The imaged area clearly shifts with increased temperature, as indicated by the stars in Figure 87 which indicate the same microstructural position within the sample. These images were taken as soon as the temperature had stabilised (i.e. after the overshoot or undershoot when the Murano temperature matched the set temperature). If the temperature is allowed to stabilise for longer (~10 mins) the image is generally more stable, although there will still be some shift compared to room temperature.

5.6.1.3 Light levels

The final topic to discuss is the impact of the sample heating on light levels in the chamber and the ability to continue to capture FSD images. Figure 88 shows the issue more clearly – as can be observed, chamber light levels increase as the sample heats up. This is observable initially in the 600 °C image via the hole in the EBSD shield (see red circle in Figure 88**)** , and increases past the point where the EBSD shield can contain it at 800 °C. The resulting light floods the FSD and an image is not obtainable.

Overall, the FSD imaging limitations at high temperature require the experiment to be interrupted, with imaging carried out at a lower temperature (500 °C) than the heat treatment (800 °C)[10] at a constant detector distance and tilt for consistency. A temperature stabilisation time of 10 mins (measured from the point the Murano thermocouple first measures the set temperature) was also included for optimal imaging.

[10] Murano temperatures

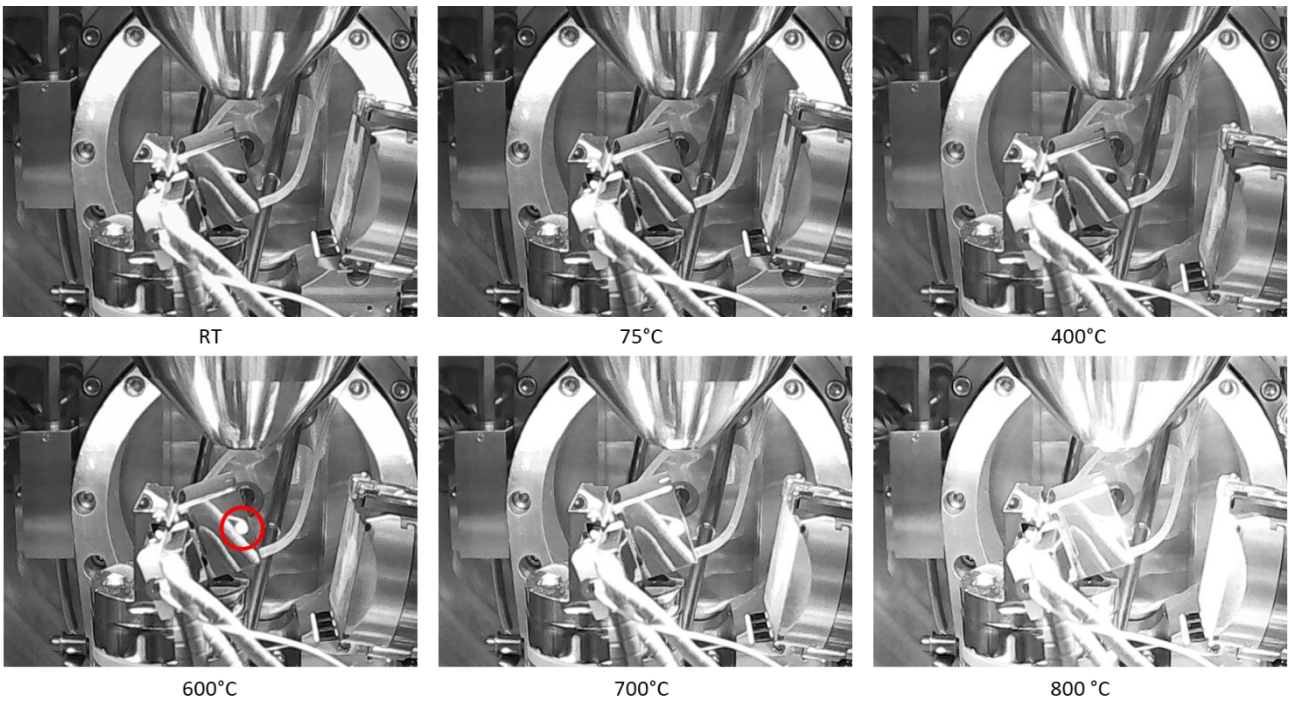


Figure 88 - Chamber view for FSD high temperature imaging trial. Images show chamber view (towards the door) for temperatures from room temperature to 800 °C showing the increasing light levels in the chamber. The red circle highlights the increasing light level within the EBSD shield. (RT = room temperature)

5.6.2 High temperature EBSD

The feasibility of EBSD mapping at high temperature was also considered in the initial trials. In these trials high temperature EBSD maps were captured at 500 °C, 720 °C and later at 850 °C (Murano temperature) using a spare weld sample. The maps at 500 and 720 °C were taken of the same area (i.e. no manual adjustment to position made in between maps) for comparison, as shown in Figure 89.

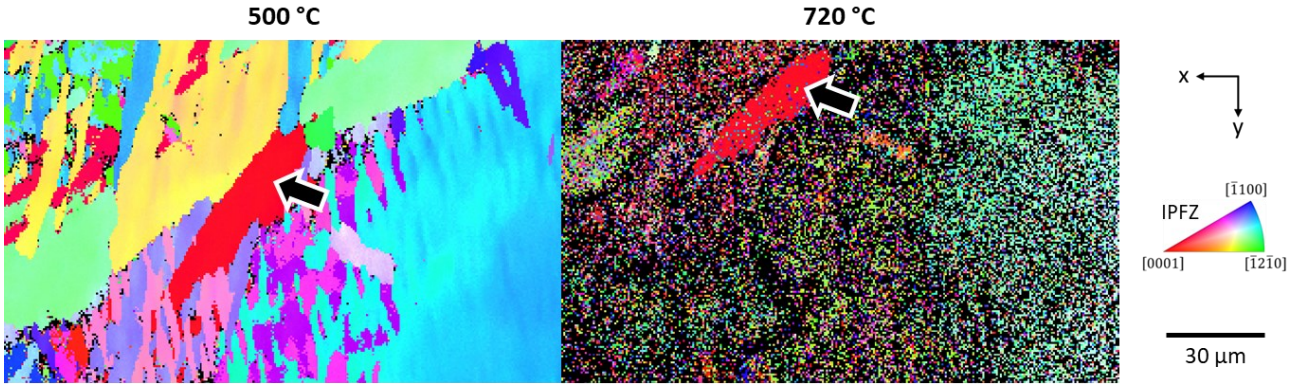


Figure 89 - High temperature EBSD mapping at 500 and 720 °C. The 500 °C map EBSPs were collected at 320x240 resolution with an exposure time of 20 ms giving a total map time: 18m29s. The 720 °C map EBSPs were also collected at 320x240 resolution, but with an exposure time of 9.3 ms, giving a total map time of 8m49s. Setup for both: working distance ~18 mm, detector distance 17 mm, detector tilt 9.8°, beam accelerating voltage 20 kV, magnification 2500x. The arrows show the position of a grain that can be tracked across both maps.

As can be seen in Figure 89, EBSD mapping at 500 °C is possible – the map here has 97.7% indexing. However, at the higher temperature, the mapping quality decreases significantly – this map has 28.1%

indexing[11]. It is notable that certain orientations map better than others, for example there is a (red) grain (shown by the arrows in Figure 89) that is clearly identifiable in both maps – this grain has c axis out of plane (i.e. in Z direction, hence red in this IPFZ map). This is also a useful grain to show the drift as the temperature increases – the setup was kept constant for this trial, but the area mapped clearly changes. This may be minimised slightly with increased stabilisation time at temperature, although further trials would be required.

In terms of EBSP quality, this will vary with the setup chosen, however it is likely that high temperature mapping for an *in situ* experiment would need to be relatively quick (e.g. 1-2 hrs), with a lower exposure time in order to capture microstructural changes over time. Figure 90 shows example EBSPs from the maps in Figure 89. For the quicker exposure time, the EBSP quality decreases, but is generally still indexable. If the EBSPs are of sufficient quality, further clean up using MTEX based codes [170] may help with the indexing.

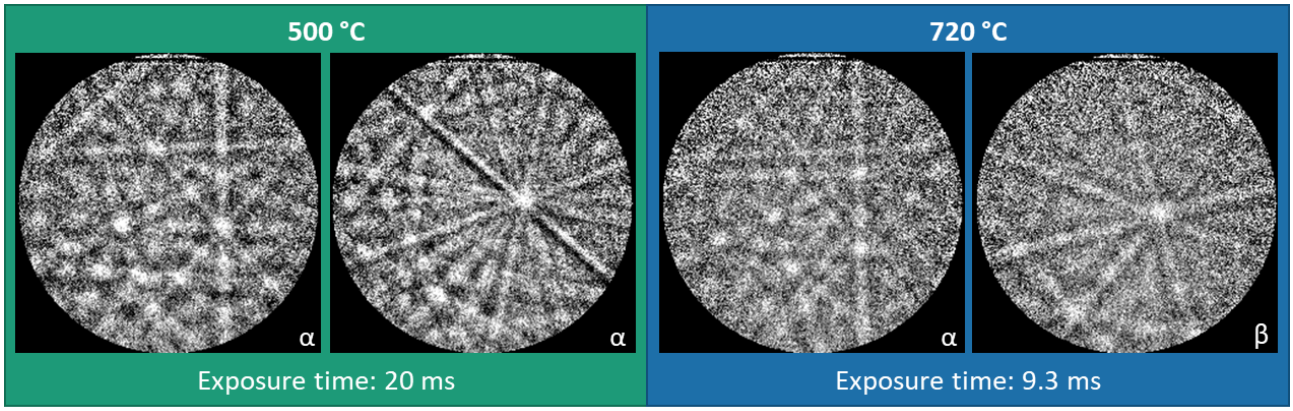


Figure 90 - EBSP examples at 500 and 720 °C – these are example EBSPs for the maps in Figure 89, taken at different exposure times but with the rest of the setup (working distance & EBSD detector position and angle) kept constant. The phase (α-Zr or β-Zr) that the EBSP indexes as is indicated by the symbol in the lower righthand corner of each EBSP. The leftmost example for both temperatures is from the grain indicated by the arrows in Figure 89.

Moving to the higher temperature, 850 °C, this map is likely to contain β-Zr as the sample temperature may be above the β transus. Figure 91 shows a very small sample map but gives an indication of what might be possible at high temperature. However, the exposure time for these EBSPs is 125 ms, which means that for this tiny area (13.38 x 12.33 µm / 125 x 117 pixels), the mapping took 31 mins. There is also very little resemblance between the SE image and the phase map – it is likely that some drift occurred during the mapping time. This mapping is proof that it is possible to get EBSD data at high temperatures, but further investigation would be required to optimise time/EBSP quality/area mapped.

[11] 28.1% when indexed as all α phase Zr – this can be increased to 77% by including β-Zr, but the temperature should not be high enough for the sample to be in the β phase. The exact sample surface temperature was not monitored for this trial.

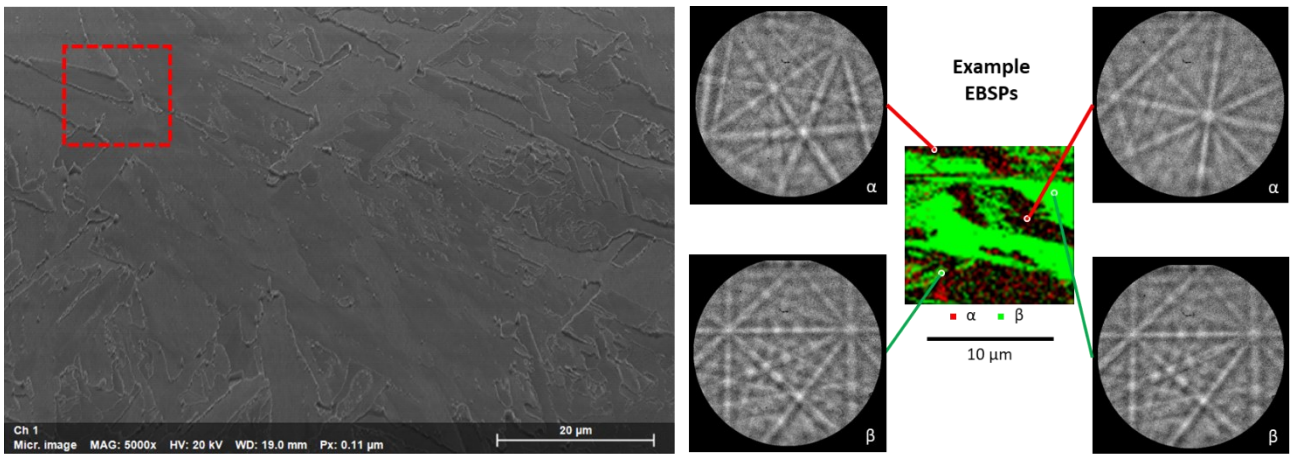


Figure 91 - EBSPs at 850 °C for a weld sample (slightly oxidised). A small region from the SE image at (A) was mapped using EBSD, as shown by the phase map at (B), with example EBSPs shown. EBSP resolution 800 x 600, exposure time 125 ms, working distance 19 mm, detector distance 17 mm, detector tilt 9.15°.

Overall, whilst high temperature EBSD is clearly feasible, there are a few hurdles to overcome, not least phosphor deterioration, as discussed in the next section. High temperature EBSD will not be included in this experiment, however it could be used in a further iteration of the experiment. Questions to be addressed to do this would be:

- *Can we achieve a well indexed map at the heat treatment temperature?* Initial trials have shown good mapping at 500 °C so this could be used for an interrupted heat treatment, but for continuous mapping at temperature mapping quality still needs investigating.
- *What size map would be useful?* – the smaller the map the quicker the mapping, however this may not capture grain growth well.
- *How much drift?* – will mapping the same area be feasible if there is drift at high temperature?
- *What frequency of mapping would be useful?* – depends on how quickly the grain growth occurs,
- *Can a likely area for grain growth be predicted prior to the experiment?* – the area mapped is likely to be limited so targeting a key area would be useful.
- *How long will the phosphor last and could an adaption (e.g. an additional shield) be useful for its longevity?* – following the grain growth for up to 4 hours continuously at temperature would be useful.

5.7 Summary

To summarise the outcomes of the initial trials, an updated version of Table 17 is found in Table 24, , with comments against each potential issue. The sections that follow then capture best practice for similar experiments based on my experience, and specific decisions made for my *in situ* experiment as a result of these trials.

Table 23 - Potential issues: revisited - comments and solutions for the potential issues previously identified.

ID	Topic	Potential Issue	Comments & Solutions
1	Temperature measurement	Sample temperature different to the Murano stage control thermocouple so the sample does not stay within the heat treatment temperature range and grain growth does not occur.	Add a surface thermocouple to monitor the sample temperature. Set the Murano temperature to account for the temperature delta.
2		Murano temperature control cannot be accurate controlled due to timing or control loop issues.	Preliminary trials found the system to be responsive, with the limitations on ramp rate and likely overshoot/undershoot durations captured and used to adapt the final heating schedule.
3	Heat damage	Temperature too high for forescatter diodes causing damage or destruction.	Not an issue – see section 5.5.2.1
4		High temperature EBSD phosphor life too short at high temperatures for the experiment.	The high temperature phosphor does deteriorate over time (see section 5.5.2.2) but not within the timescale of an experiment. To minimise the deterioration, the distance to the sample should be increased and high temperature EBSD minimised.
5	Forescatter imaging	Light from the sample at high temperatures floods the forescatter diodes and imaging not possible.	Adjusting the EBSD detector (and therefore FSD) position can alleviate this issue to some extent, but there is still a maximum temperature (700 °C) for forescatter imaging. See section 5.6.1 for more details.
6		Drift occurs during heating making it difficult to image the same area throughout.	Allowing the temperature to stabilise prior to imaging (~10 mins) reduces drift caused by temperature changes.
7	Sample	Sample oxidises and no results are possible to grain during the *in situ* experiment (only start + end points).	There are ways to minimise oxidation (see section 5.5.4.1) but this remains an issue.
8	Stage/setup related	Maintenance issues with the setup lead to inaccurate results or experiment failure.	Details of suggested maintenance tasks are captured in section 5.5.4.2

5.7.1 Best practice

This next part contains advice for anyone carrying out a similar experiment based on my experiences.

5.7.1.1 Temperature control

Due to the Murano stage thermocouple position, if the exact sample temperature is required, an additional thermocouple(s) should be added. Ideally this should be prior to installation and securely attached using spot welding for example. This may be challenging for some samples, e.g. Zr alloys, but gluing the thermocouple to the surface (*in situ*) using high temperature carbon paste is generally successful. Take care not to block the beam with the thermocouple.

The Murano stage can be programmed with a temperature cycle, but prior testing would be required to determine the temperatures (sample vs. Murano thermocouple), overshoot/undershoot durations and achievable ramp rates. It is also worth noting that changing the parameters during the temperature program briefly results in loss of temperature control (usually a sharp temperature drop).

5.7.1.2 Forescatter imaging

For high temperature forescatter imaging, a filter may need to be designed to avoid flooding the diodes when the sample glows as it gets hot. The detector position (distance/tilt angle) and potential imaging duration (e.g. no of points per image/total time for each image) will need to be adjusted as the temperature is increased. I have demonstrated it is possible to image up to 700 °C, but it may be possible to go higher with further trials/adaptions.

In general, the temperature needs to be allowed to stabilise to reduce issues with drift, so continuous imaging is unlikely to be feasible. A small change in imaging area is still likely between room temperature and elevated temperature, but this drift reduces with stabilisation time and when changing temperature above this level.

5.7.1.3 High temperature EBSD

High temperature EBSD is possible, but the high temperature phosphor will deteriorate with use at high temperature and when the detector position is close to the sample during heating – it may be wise to keep the EBSD detector further away during heating and then move closer just for the EBSD duration. There is also a tension between EBSP resolution (and therefore exposure time) and time at temperature with respect to phosphor deterioration. Without further shielding, it is likely that a shorter term experiment would be better suited to high temperature EBSD, particularly as it will not be possible to change the phosphor mid experiment (this requires opening the chamber).

5.7.1.4 General advice

For all samples, but particularly samples likely to oxidise, a high level of cleanliness should be maintained throughout. To reduce issues, the following recommendations are made:

- ‘Bake’ prior to use – e.g. use a spare/old heating cartridge in the Murano stage after setup and heat to 350 °C for 20 mins.
- Plasma clean the chamber once the stage and sample are installed.
- Pre-heat the system (with sample) to 120 °C max (10 min hold) to de-gas the sample.

Setting up the system (with sample) and leaving overnight for the system to settle is also recommended – note that turning the cooling system on/off affects the stability so stabilisation time should be factored in for this if leaving it on overnight is not an option.

Furthermore, equipment maintenance should be carried out prior to the experiment. This should include: a visual check of all equipment, including flanges (and screws), and cleaning of the heating plates and EBSD shield on the Murano stage.

5.7.2 Experiment decisions

Finally, this section details specific decisions made for my *in situ* experiment as a result of the initial trials. This includes the decision to carry out an interrupted heat treatment so that forescatter imaging was possible, and the choice to carry out EBSD mapping only at the start and end of the experiment to protect the high temperature phosphor. A full summary of the key decisions made because of the investigations and preliminary trials is found in Table 24.

Table 24 - Summary of experimental decisions made as a result of preliminary trials

ID	Trial or Issue	Experiment Adaption
1	FSD temperature	➢ FSD can be installed & used during the experiment
2	High temperature imaging	➢ Maximum (Murano) temperature for imaging 500 °C → interrupted test ➢ Hold at temperature for ~10 mins to stabilise image ➢ Detector distance ~27 mm
3	Bias control	➢ Keep bias control neutral (0V)
4	Temperature control	➢ Initial heating cycle to be used to address sample degassing (120 °C max, as measured using Murano thermocouple) ➢ Programme control not to be used during the full experiment
5	Surface thermocouple	➢ Additional thermocouple to be added to the sample surface via the gas hole in the EBSD shield. It is to be attached using high temperature carbon paste and installed *in situ*.
6	EBSD	➢ No high temperature EBSD during these trials. Could be re-visited in the future.
7	Phosphor deterioration	➢ No high temperature EBSD ➢ Keep EBSD detector at a greater distance from the sample (e.g. 27 mm for FSD imaging vs. 17 mm for EBSD)
8	Oxidation	➢ Oxidisation minimisation mechanisms to include: final BIB polish prior to setup; plasma cleaning; pre-heating cycle ➢ To deal with oxide build up during experiment: BIB polish prior to final EBSD; option for intermediate cleaning step (split experiment)
9	Maintenance	➢ Electrical contacts to be cleaned prior to use of Murano to avoid uneven heating ➢ Murano EBSD shield to be cleaned to ensure maximum field of view

6 Macroscopic Observations of Blocky-α Grain Growth

6.1 Aim

This is the first of two results chapters where grain growth in electron beam welds in Zircaloy-4 is explored. This chapter takes a macroscopic approach to investigating grain growth in the weld region. The following chapter builds on these findings to focus on the nature of microstructural evolution at a local level using detailed *in situ* EBSD analysis.

To understand macroscopic trends in grain growth, results for the *ex situ* experiment are presented in this chapter. Initially, evolution of macroscopic microstructure is observed using optical and electron microscopy. This is followed by grain orientation and grain structure analysis with EBSD mapping. Highlights from this chapter include: (1) observations about grain growth in different regions of the weld; (2) comparison of the reconstructed initial microstructure with the final microstructure after grain growth.

6.2 Introduction

The objective for the grain growth experiments was to observe how the initial weld microstructure influences the final microstructure, and thereby will influence the performance of the welded part. Of particular interest was any potential link between the prior-β microstructure for the initial weld and the final weld microstructure after grain growth.

The *ex situ* experiment was designed to replicate one of Lusby's trials [125] and enable a more detailed analysis of the microstructure before and after heat treatment. To enable these experiments, the entire weld region was mapped before (pre-HT) and after (post-HT) the 4 hr heat treatment (HT) at 800 °C using imaging (optical and forescatter) and EBSD.

6.2.1 Initial weld microstructure

In this chapter, the weld is spatially segmented into three regions (bulk, heat affected zone, fusion zone) as microstructural evolution is different in these regions between initial and final microstructures.

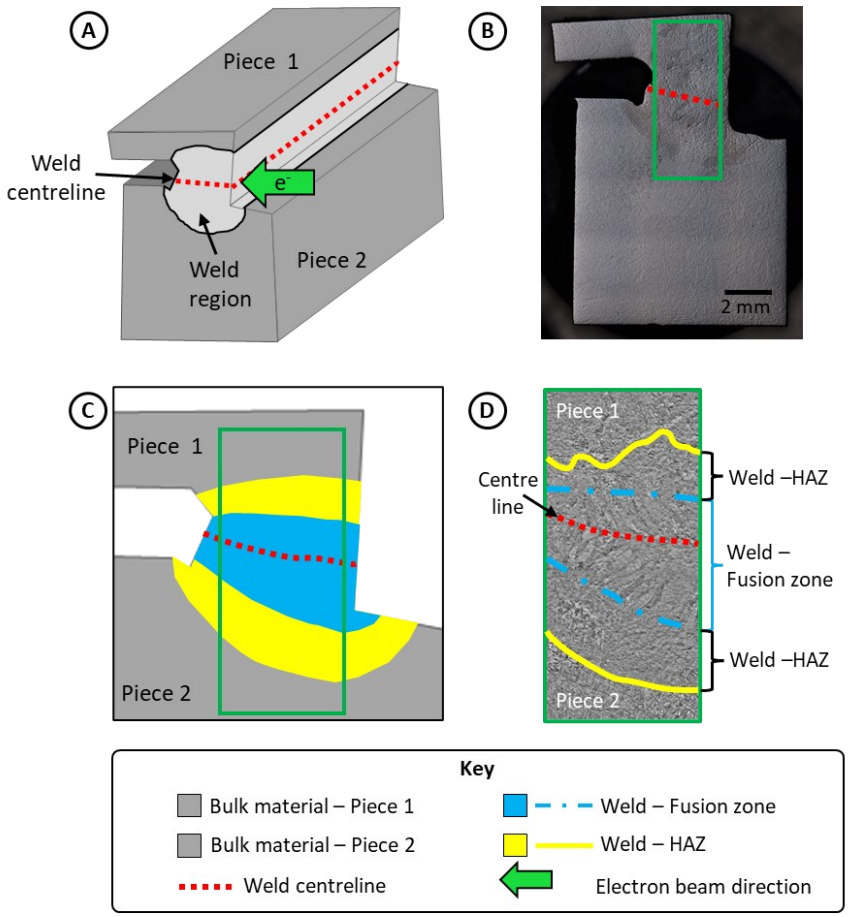


Figure 92 - Weld region schematics. (A) schematic of bulk weld sample – thin piece (1) is welded to a thicker piece (2); (B) optical micrograph showing a weld slice with region for (C) indicated by the dashed green line; (C) schematic showing weld regions and weld centreline; (D) greyscale FSD image of weld region with outlines for the different weld regions indicated.

These regions are shown in Figure 92 and can be detailed as:

- **Bulk.** This is the original microstructure in each of the pieces being joined. For this sample, both pieces are β-quenched Zircaloy-4 with two different initial α lath sizes. The region above the weld has a finer α lath size with smaller prior-β grains. The region below the weld contains coarser α laths due to a slower cooling rate.
- **Weld – HAZ.** This is the outer region of the weld where the microstructure has changed due to the heat, but this material has not melted in the welding process. It can identified easily in the post heat treatment microstructure, but in the as welded (pre heat treatment) microstructure it is challenging to uniquely identify. In this weld example, due to the geometry and cooling rates, the HAZ is less clearly defined in the half of the weld attached to the thin member (top half). Below the weld centreline is closer to that investigated by Taylor et al. [44]. It has a clearly defined edge and two distinct regions of HAZ (with different grain sizes) that are easy to observe.
- **Weld – Fusion zone.** This is the central region of the weld, from the weld centreline to the HAZ on both sides of the weld. The fusion zone contains elongated prior-β grain structures within the

centre, and some elongation can also be seen in the α grains. A clear α lath microstructure is not observable throughout this region.

Note that due to the geometry of this weld (thin piece and thick pieces welded together), the relative size of the weld on either side of the centreline differs. Above the centreline, with the thin member, the distance from the centreline to the edge of the weld is smaller, and the edge of the weld is less defined.

6.3 Results: Imaging observations

Figure 93 shows an overview of the weld region for the *ex situ* sample before (pre-HT) and after (post-HT) the 4 hr heat treatment at 760 °C using forescatter imaging. The microstructure of the entire weld region has transformed in the post-HT image, with a range of blocky-α grain sizes across this region. There is a clear definition between the weld region and the bulk material, which is easier to observe at the lower edge of the weld. The bulk material itself appears unchanged after the heat treatment.

Within the weld region, the different regions of the weld can still be identified on the two maps, with the weld centreline particularly clear. For example, the elongated grain structures in the fusion zone become elongated blocky-α grains in the post-HT microstructure. The grain sizes are smaller within the fusion zone and larger in the HAZ, particularly in the lower half of the weld where there was originally more definition in the HAZ. These results strongly suggest a link between the weld microstructure and the post-HT microstructure.

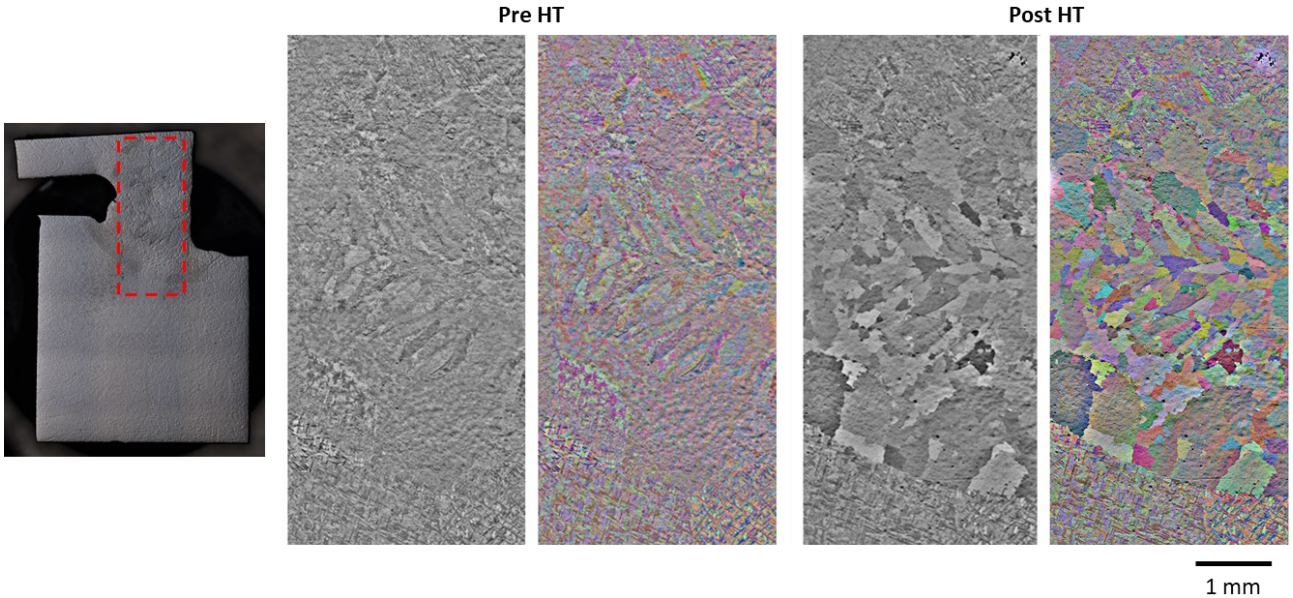


Figure 93 - Ex situ FSD overview. Pre and post-HT FSD images (greyscale & false colour) stitched together for the approximate area indicated on the overview image. Note that due to image distortion the scalebar is approximate.

6.4 Results: EBSD analysis

Macroscopic EBSD mapping of the two areas shown in Figure 93, using four subregions to span the welded regions. The pre-HT and post-HT maps were aligned reasonably between scans to enable the maps to be overlaid for a comparison of the microstructural regions. The mapping conditions are described in Appendix A.

To identify and classify changes in the microstructure, regions from the weld have been labelled as follows in Figure 94: (a) bulk – above weld; (b) upper half of weld (fusion zone & HAZ); (c) lower half of weld – central region; (d) lower half of weld – HAZ; (e) bulk – below weld. This allows a more detailed analysis of the grain growth in each region. These regions have been identified from changes in the microstructure between the pre-HT and post-HT maps, the FSD micrographs, and the β-reconstruction.

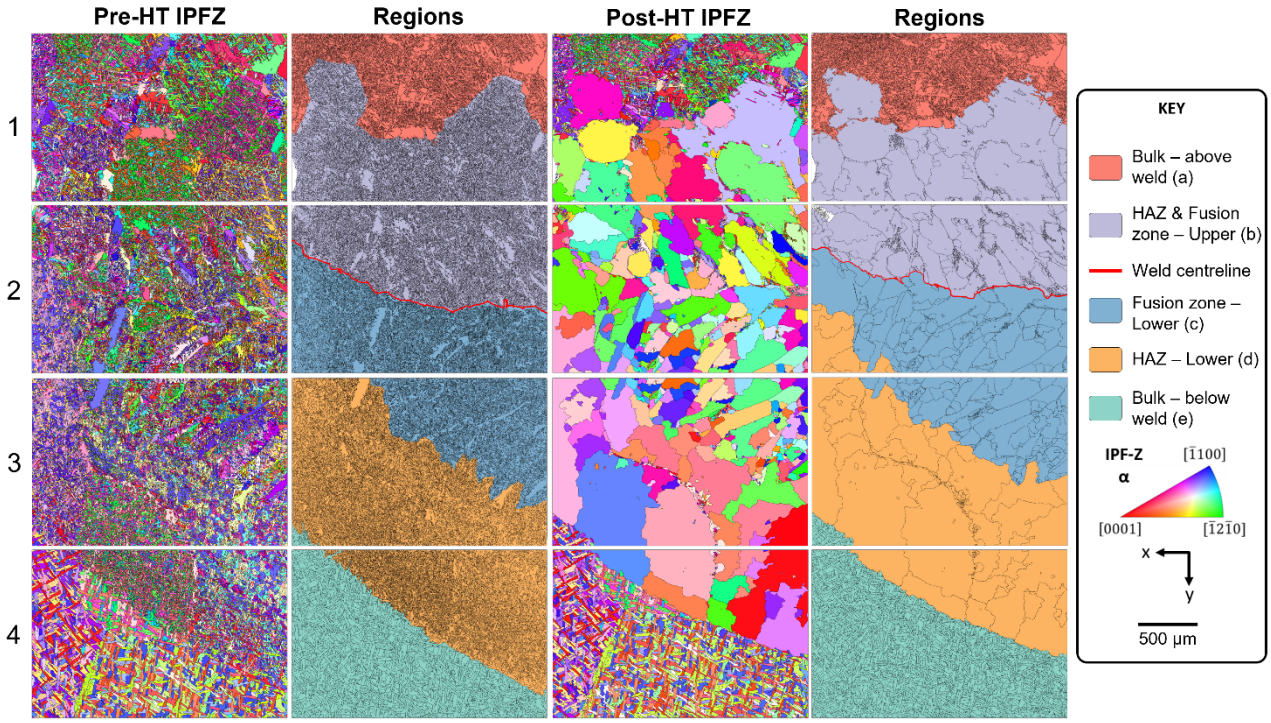


Figure 94 - Ex situ data segmented. Pre-HT and post-HT data using IPFZ colouring (columns 1 & 3) and the same maps coloured by region (columns 2 & 4). Regions: (a) bulk – above weld; (b) upper half of weld (fusion zone & HAZ); (c) lower half of weld – central region; (d) lower half of weld – HAZ; (e) bulk – below weld.

A more complete representation of the EBSD mapped areas is shown using pattern quality, crystal orientations as coloured with the IPF X and Z colour keys, and the α-α grain boundary map (boundary angle > 4 °), shown for pre-HT and post-HT in Figure 95 (A and B respectively). Prior β-reconstruction was performed using the ParentBOR code for both sets of maps and the output maps are shown in Figure 96 (C: pre-HT, D: post-HT).

In the pre-HT maps (Figure 95 A and Figure 96 C) the weld and heat affect zones can be observed due to the change in grain shape and pattern quality. There are regions of common α orientation which reconstruct to large prior-β grains. The α and prior-β grain shape and texture in different regions changes from the top base material, through the upper HAZ, fusion zone, lower HAZ and the lower base material.

In the post-HT maps (Figure 95 B and Figure 96 D) these different regions are more easily observed, and very large grain growth of the α-phase is observed in the HAZ. The α grain size has changed significantly in the HAZ and fusion zone, and this change in grain size and the grain shape spatially varies with respect to the weld line. The grain shape and texture within the base material does not strongly vary.

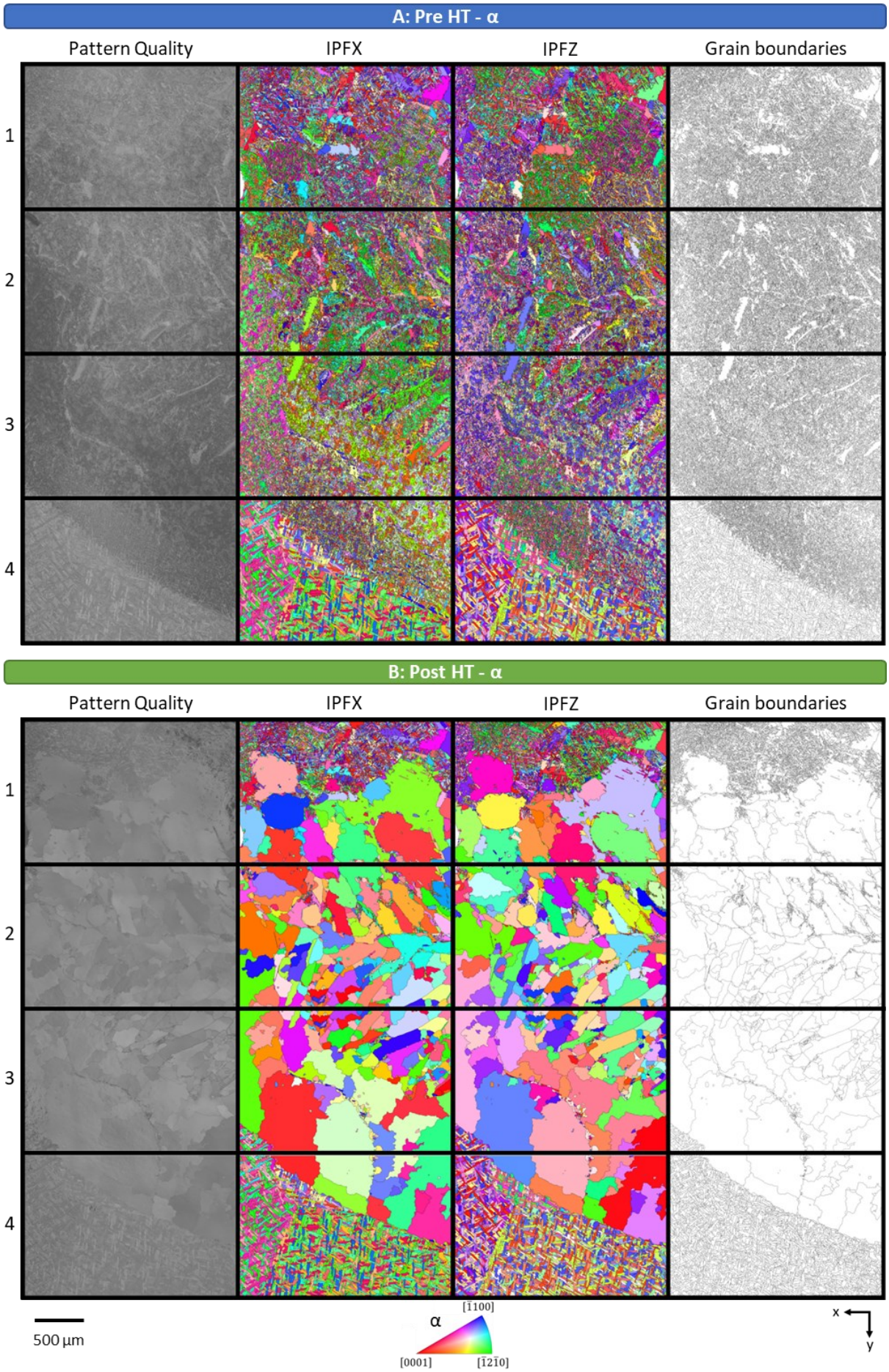


Figure 95 - Ex situ EBSD results – α. Maps of pattern quality, crystal orientation (IPFX, IPFZ coloured) and grain boundary outline map (gB > 4°) for A: Pre-HT and B: Post-HT.

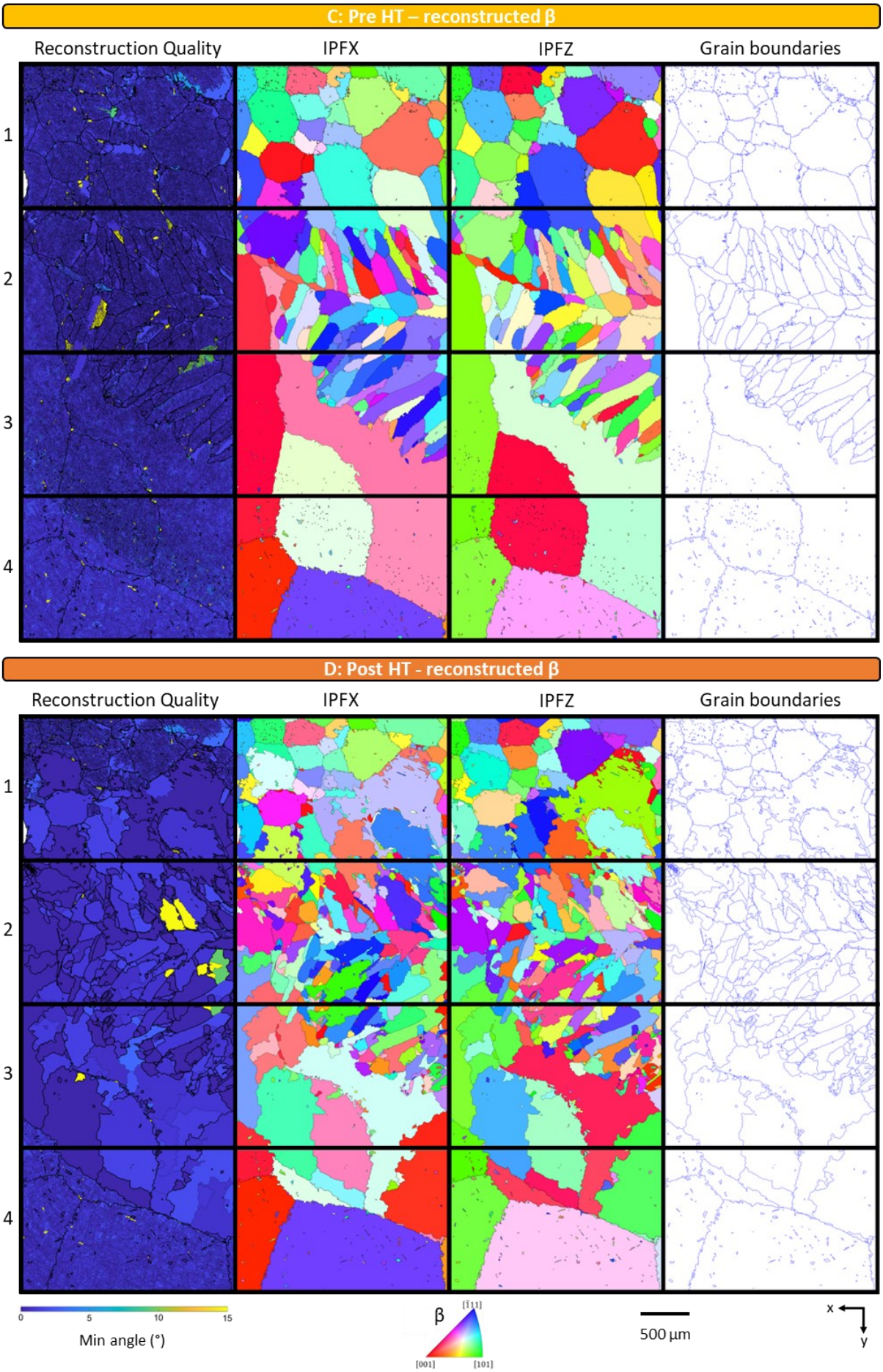


Figure 96 - Ex situ EBSD results – reconstructed β. Maps of reconstruction quality, crystal orientation (IPFX, IPFZ coloured) and grain boundary outline map (gB > 4°) for C: Pre-HT and D: Post-HT. Reconstruction details in Appendix A.

6.4.1 Bulk material

The microstructure in the bulk regions above (a) and below (e) the weld region do not change significantly with the heat treatment (see maps 1 & 4 in Figure 95 and Figure 96). The α lath orientations are recognisable in terms of grain shape and orientation between the pre-HT and post-HT maps for these regions, as evidenced by the α lath dimensions in Table 25. The mean length and width of the α-grains were calculated in MTEX using the fitEllipse function, after removing the edge grains and the large grains that are constant across both maps. These results show that there is no significant difference in the lath dimensions for these regions after heat treatment, i.e. the microstructure in these regions is stable.

Table 25 - α lath dimensions[12]

α laths	Pre-HT		Post-HT	
	Map 1	Map 4	Map 1	Map 4
Mean length (µm)	9.4	21.9	9.5	20.8
Mean width (µm)	3.2	7.4	3.2	7.1

This result is echoed in the reconstructed β maps for the regions (Figure 96) where the same parent grains (shape & orientation) are reconstructed both pre-HT and post-HT. There is a small amount of variation in the β phase orientations for the lower region (map 4) which is likely due to slight differences in sample tilt during mapping pre-HT and post-HT.

6.4.2 Heat affected zone

The size and definition of the HAZ in the weld differs on both sides of the weld centreline due to the relative thickness of the two pieces that were welded together, and this affects the flow of heat away from the fusion zone. For this reason, the HAZ in the two halves of the weld (above & below the weld centreline) are discussed separately. For the upper half of the weld, the fusion zone and HAZ are not identified separately in Figure 94 (blue region, maps 2+3). However, for the lower half of the weld (Figure 94 maps 2 and 3), the HAZ and fusion zone are identified separately (HAZ = yellow; fusion zone = blue).

6.4.2.1 Upper half of weld

The upper half of the weld has less definition between the regions, with a wavy edge to the weld region and a less defined HAZ. For this discussion the section between the elongated grains in the fusion zone and the bulk material is selected as the HAZ. It is easier to identify this region within the grain boundary maps (α and reconstructed β), as this region contains larger prior-β grains. In the post-HT microstructure, the α grains in this region are relatively large, similar to the prior-β, but there are more retained α grains within this region, and smaller grains that grew but the growth was exhausted.

6.4.2.2 Lower half of weld

The lower half of the weld has a more defined HAZ in the initial microstructure (see maps 3 & 4 for the initial microstructure in Figure 96) and is closer to that described in Taylor's work [44]. Where the initial

[12] Map 4 laths: Edges removed; Map 1 laths: Edges and large grains (grainsize>5000) removed

microstructure appears to have layers of different grain sizes within the HAZ, there is no longer any subdivision after grain growth. The region transforms as a complete area, with no discernible difference in the region between the bulk and the elongated grains in the fusion zone. The largest blocky-α grains grow in this region, which is expected if the prior-β microstructure is influencing the grain growth (see Figure 96 C) where the initial microstructure for this region reconstructs to very large prior-β grains. However, whilst the grains are largest in this area, they are significantly smaller than the reconstructed β grains.

An interesting exception to this is the trail or necklace of smaller grains that are retained after grain growth, as shown in Figure 97. These appear to be along a prior-β grain boundary (see Figure 96 C map 3). These small grains appear to be different orientations from the larger grains in this region, suggesting that some orientations are less likely to grow.

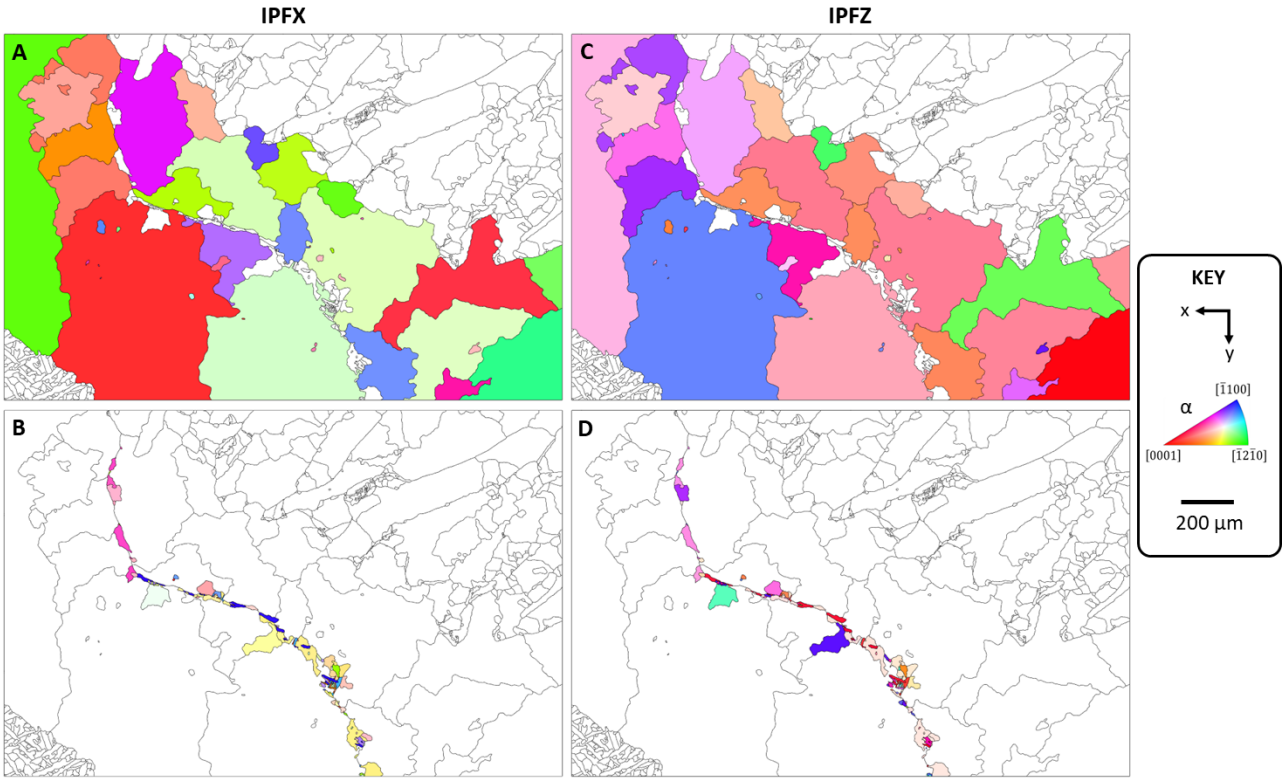


Figure 97 - HAZ grain size differences post-HT (map 3). A & C: HAZ grains post-HT with the small grains removed. B & D: the trail or necklace of small grains running along a prior-β grain boundary. Maps A & B maps use IPFX colouring and maps C & D use IPFZ colouring.

6.4.3 Fusion zone

The centre of the fusion zone retains the columnar domains identified in the pre-HT microstructure (clearest in the reconstructed β map – Figure 96 maps 2 & 3) in the post-HT microstructure, where large ~columnar grains occur. This is most clearly seen by looking at the reconstructed β pre-HT microstructure (Figure 96 C map 2) and comparing this to the post-HT α (Figure 95 B map 2).

Post HT there are a lot of smaller grains within this region, as well as the larger elongated blocky-α grains. This is likely due to competitive growth in the region. However, the region remains easily recognisable.

The line of prior-β grains along the weld centreline in the reconstructed β map for the initial microstructure (compare Figure 96 C map 2 with Figure 96 D map 2) is not present in the post-HT microstructure. Instead, the (reconstructed) grains in this region are subdivided and grouped with other β either side of the weld centreline. This subdivision and/or growth into adjacent prior-β regions is found consistently across the entire map, and motivates further investigation.

6.4.4 Parent microstructure vs. grain growth

To compare the prior-β microstructure and the post-HT microstructure, the prior-β grain boundaries (as calculated from the initial microstructure using the ParentBOR code) can be overlaid on the post-HT (α) microstructure. An example of this is shown in Figure 98 for *ex situ* map 2.

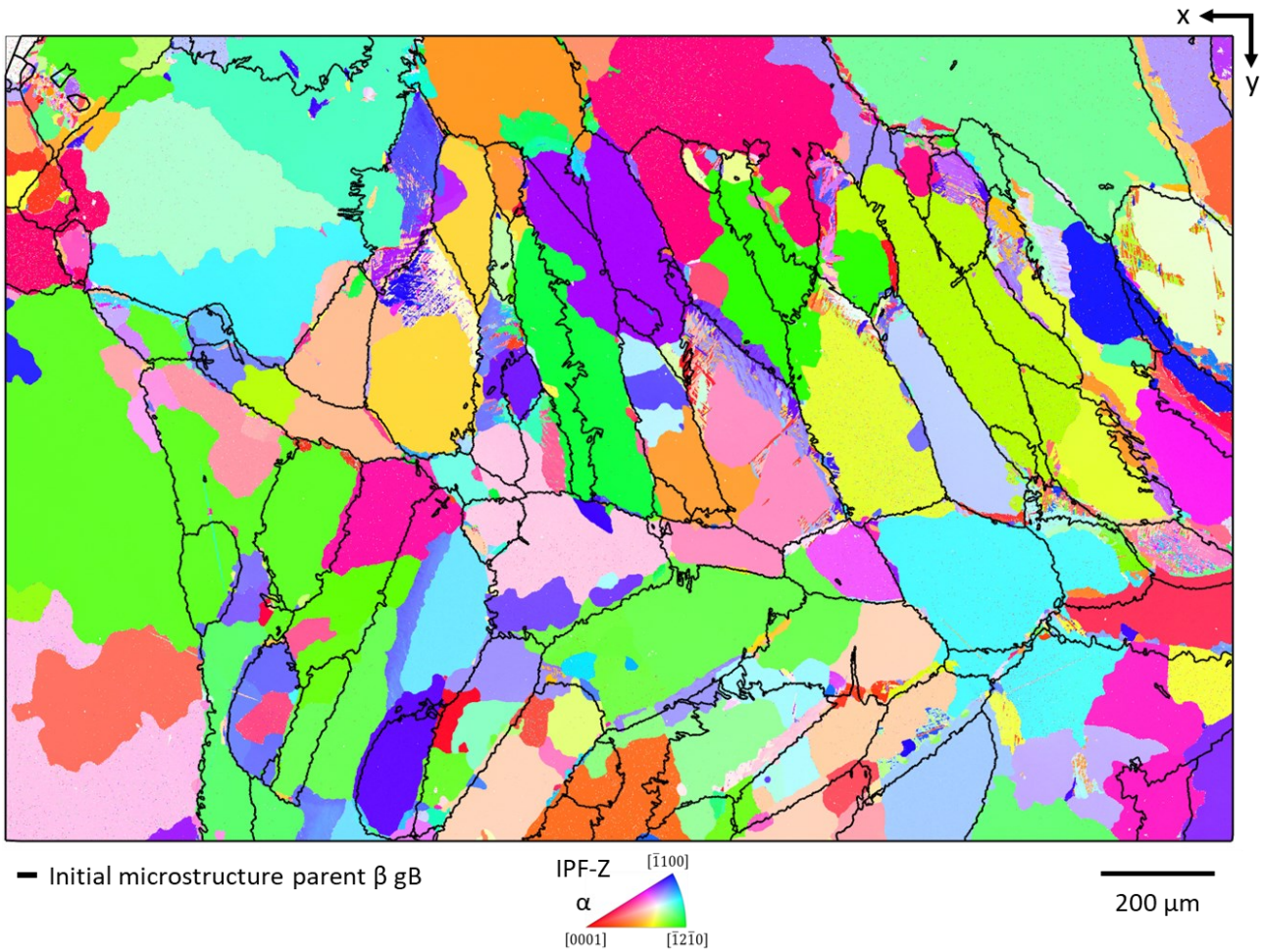


Figure 98 - Initial parent β boundaries overlaid on the post-HT grain map enabling analysis of relative grain growth. Crystal orientation map (coloured according to IPFZ) for the post-HT microstructure - Map 2 from the ex situ experiment overlaid with the parent-β grain boundaries (thick black lines) from the same area as identified from the initial microstructure (pre-HT microstructure).

Similarities between the two microstructures suggest that the initial weld microstructure strongly influences the final microstructure. There are several areas in Figure 98 where the blocky-α grain fills a similar spatial area to the prior-β grain. However, there are also areas where the blocky-α grain covers multiple prior-β grains and subdivision of the prior-β grains is also quite prevalent across the map. Whether one of the grains in the subdivided regions would grow to fill the whole region is not determinable from this dataset, but based on Lusby's results [125], where minimal growth was reported between a 2 hr and 4

hr HT, it seems unlikely. This suggests that although the prior-β microstructure is strongly influencing the grain growth, the prior-β microstructure is not the only factor controlling blocky-α growth. This results in blocky-α that does not simply recreate α grains with a morphology that echoes the prior-β microstructure nor the orientation of a single variant from the prior-β grain.

Figure 99 shows a region that has been almost filled with a single blocky-α grain. This example is from *ex situ* map 1 and the prior-β grain spatial area (and the adjacent grain that it also grows into) is shown both as the reconstructed β (Figure 99 C & D) and the α grains (Figure 99 A & B) pre-HT and post-HT. What becomes evident from the reconstructed β is that the growing grain appears to be associated with a different parent β orientation (green grain - Figure 99 D) to the original prior-β orientation (blue grain - Figure 99 C) that is still present due to the remaining lath α at the edges. This suggests that the growing α grain (α1) was not present within the initial β1 spatial region (i.e. it was not one of the α grains that associated with β1 during reconstruction).

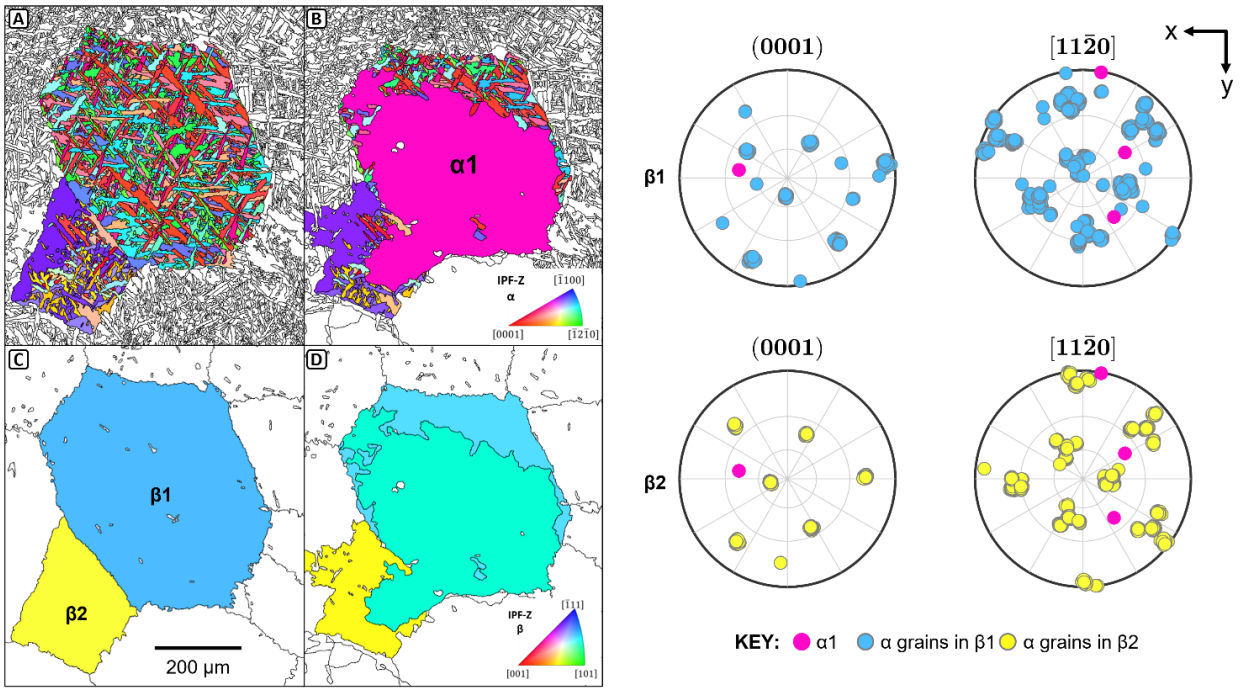


Figure 99 - Parent β vs. post-HT orientation testing. LEFT: orientation maps for (A) pre-HT α; (B) post-HT α; (C) pre-HT reconstructed β; (D) post-HT reconstructed β using IPFZ colouring. RIGHT: pole figures for the pre-HT α grains contained within spatial regions β1 (blue) and β2 (yellow) from (C), along with the growing α grain (α1) orientation (smaller pink dots), for (0001)α and <11-20>α.

To test this, pole figures for $(0001)_{\alpha}$ and $<11\text{-}20>_{\alpha}$ are plotted in Figure 99 for all the α grains contained within the blue β grain (β1) and the adjacent yellow β grain (β2) in the pre-HT microstructure (Figure 99 C). Also plotted on these pole figures is the large blocky-α orientation associated with the green parent region – this is identified as α1 in the post-HT α microstructure (Figure 99 B) and the orientation is shown on the pole figures using the smaller pink dots. If α1 grew from within one of these prior-β regions (β1 or β2), the

crystal orientation of the grown grain should match one of the original α orientations associated with the prior-β grain in this area[13].

The analysis in Figure 99 shows that the blocky-α orientation did not come from the original spatial area for that region. Analysis of other grains in the map (not explicitly shown here) reveals that this is consistent across the weld. In summary, this means the final microstructure may be related to the prior-β structure in the pre-HT microstructure but we cannot use the overlapping pre- and post-HT microstructure to directly predict the grain shape and crystal orientation without understanding the nucleation and growth of the grains that become blocky-α grains in the post-HT microstructure.

If the grain structure is not inherited from the α-grains inside a prior-β grain, then perhaps neighbouring α-grains act as nucleants. This motivates analysis of the α-variants associated with each of the neighbouring prior-β grains using a similar pole figure analysis (shown in Figure 100). Where there is an overlap between the growing α orientation, α1 (pink grain in Figure 99 B & pink dots on the pole figures), and one of the α variants, the growing grain may have originated from this cluster of α grains (parent β grain).

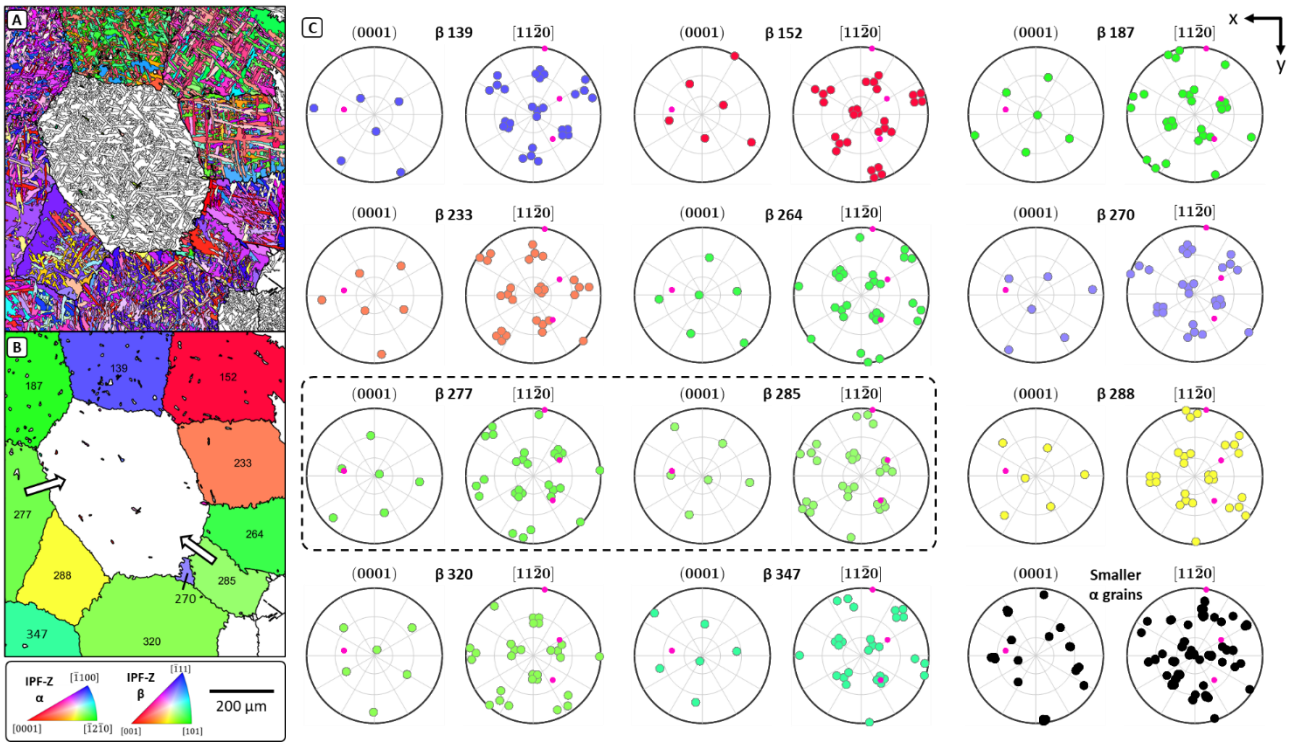


Figure 100 - Neighbouring grain orientation testing. Neighbouring grains to the parent grain region in which the blocky-α grain grows, shown as (A) α grain orientations using IPFZ colouring and (B) parent β grain orientations using IPFZ colouring; (C) pole figures (PF) showing (0001) and <11-20> for the growing α grain orientation (smaller pink dots) and the 12 potential α variant orientations for each of the parent β orientations numbered in (B), shown as the larger coloured dots (IPFZ β colouring). The exception is the last plot which contains the smaller α grains across this region that are not grouped with the larger numbered β grains (black dots). The dashed black rectangle outlines two potential β grains that the growing α grain (α1) may have originated from.

[13] Note that as both of these regions contain all 12 potential α variants for each β orientation, it was not necessary to calculate any additional potential α variant orientations that could have been hidden subsurface for these grain areas.

For this blocky-α grain, there are two potential grains that it may have grown from, (β 277 & β 285 as indicated by the dashed line in Figure 100). This 2D section suggests that the growing grain could be more likely related to β 285, but below the surface there may be nucleation from grains that belong to β-277. Furthermore, while it looks like there may be a special relationship between these prior-β grains, i.e. a 60° about <111> relationship for the prior-β reconstruction, measurement of the misorientation angle and axis reveals it is 58.2° about <-1.81,1.77,2.62> which is 10.7° from 60° about <111>, and the reconstruction has a much lower angular uncertainty with median angle of ~2°.

While the exact nucleant grain of this blocky-α can not be uniquely identified, analysis of this *ex situ* data suggests that an α grain from a prior-β region moves into a neighbouring prior-β region as the blocky-α grows. This motivates the *in situ* study described in the next chapter.

6.5 Summary

In this chapter, a macroscopic view of blocky-α grain growth in EB welds in Zircaloy-4 was presented using the *ex situ* grain growth experiment results. Overall, these observations of blocky-α grain growth seen aligns well with prior work by Lusby [125] and Taylor et al. [44]. Notably, the blocky-α grain growth affects the entire weld region after holding at 760° for 4 hr (i.e. ~100° sub-transus), with a clearly observable distinction in the grain structure between the weld region and the bulk material.

Looking at the different regions within the weld area between the pre- and post-HT microstructures:

- **Bulk -** The α lath microstructure within the bulk material does not change significantly in terms of orientation or morphology.
- **HAZ -** The HAZ contains the largest blocky-α grain growth across the weld region. The cooling rate for the welding affects the size of the HAZ and this in turn impacts the maximum size of the blocky-α grains, as seen by the (generally) smaller grains in the HAZ of the top half of the weld. There are also smaller grains that are retained after grain growth, for example, the trail or necklace of smaller grains along a prior-β grain boundary in the lower half of the weld. These smaller grains generally have different orientations to the blocky-α in this region, and indicate that there is competitive growth with certain orientations more likely to grow.
- **Fusion zone** - The fusion zone morphology most closely resembles the reconstructed β microstructure from the pre-HT map. The post-HT fusion zone microstructure is characterised by elongated blocky-α growth starting from the centreline. Again, smaller α grains that have not grown are also contained within the region.

The differing grain growth patterns in the different regions means that the likely grain growth pattern can be predicted from the pre-HT microstructure. Practically this means that if you can control the weld microstructure (for example, minimising the HAZ size via different cooling rates), it is likely that you can control the post weld heat treatment microstructure.

Comparing the reconstructed β microstructure from the pre-HT maps to the post-HT α microstructure, some interesting observations are made:

- The post-HT microstructure is related to the prior-β microstructure as it is recognisable from optical and electron microscopy microstructural mapping.
- The prior-β microstructure is not recreated exactly in the post heat treatment microstructure, as subdivision and/or growth into adjacent prior-β regions occurs. This is found consistently across the entire map.
- The blocky-α grain that grows in a prior-β spatial area does not originate from one of the (pre-HT) α grains within this prior-β grain.
- It appears that blocky-α grains grow from a neighbouring prior-β grain.

These observations motivate the next chapter, where *in situ* experiments look at the onset of grain growth and microscopic observations.

7 Microscopic Observations of Blocky-α Grain Growth

7.1 Aim

This is the second of two results chapters where grain growth in electron beam welds in Zircaloy-4 is explored. This chapter focuses on the nature of microstructural evolution at a local level using detailed *in situ* EBSD analysis, building on the macroscopic findings of the previous chapter. Results here focus on observations about the initial onset of grain growth through detailed EBSD analysis of the *in situ* experiment results, and uses the full ParentBOR code to analyse microstructural evolution, including α variant analysis for the growing regions.

Highlights from this chapter include: (1) observations about the initial on set of blocky-α grain growth, with respect to the weld region and prior-β grain boundaries; (2) factors affecting grain growth, both initial and during growth in the new region; (3) a potential grain growth hypothesis using the α variant analysis.

7.2 Introduction

The *in situ* experiments were designed to capture the initial onset of grain growth within the weld region, allowing access to information such as: where the grains initially grow; how the grains grow with respect to the parent grain boundaries; factors that affect how the grains grow.

Building on the previous chapter, areas of focus include: detailed crystallographic analysis of where/how the grains grow with respect to the prior-β grains and evaluation of the grain orientations to determine where the growing grain orientation originates from. Further to this, the ParentBOR code is used (including post processing section) to look at how the α variants and α/α grain boundaries affect the grain growth. Finally, a blocky-α grain growth model is proposed as a result of this analysis.

This chapter is split into two main sections, the first covers the initial onset of grain growth, whilst the second focusses on how the grains grow.

7.3 Part 1: Onset of grain growth

This section looks at where the blocky-α grains initially form, both spatially across the weld region and with respect to the prior-β grain boundaries. Factors that help predict where the grains may grow are also investigated.

Figure 101 gives an example of the EBSD results from *in situ* experiment 1 where grain growth is seen across the mapped region. This region is focused on the weld centreline and the fusion zone (see Figure 92 on page 127). The focus of the grain growth appears to be the central region and the outer edges and the HAZ (see section 7.3.1). Similar to the *ex situ* results (Figure 95 on page 130 and Figure 96 on page 131), the reconstructed microstructure for both the pre- and post-HT maps (Figure 101 C and D) highlights the relationship between grain growth and the prior-β grains. In each case, the grains appear to be growing out of one prior-β domain into another (see section 7.3.2).

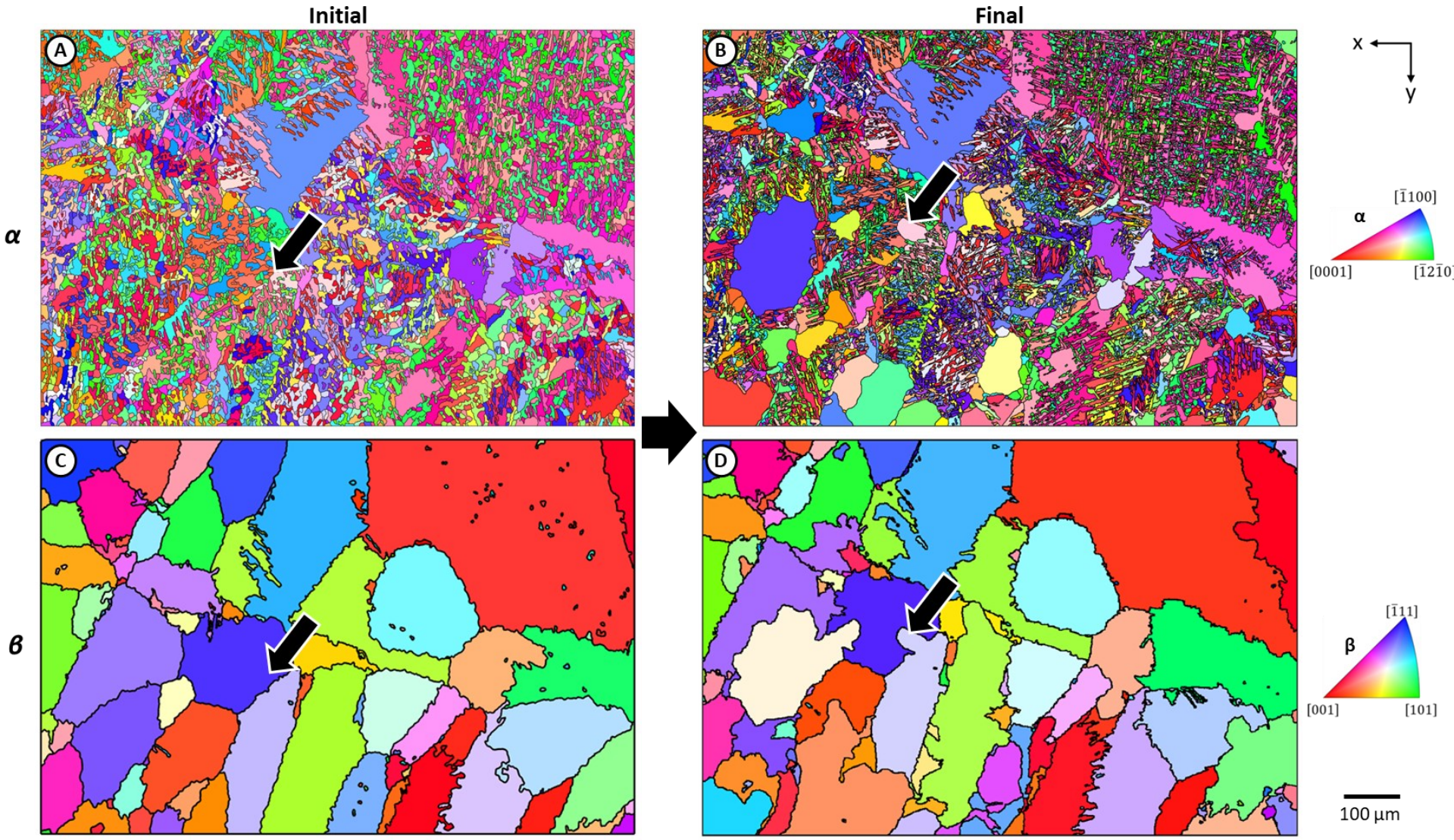


Figure 101 - In situ evolution of grain growth, highlighting how one variant from a neighbour parent β grain grows inwards to form the new blocky-α grain (A) Initial orientation map (α); (B) Final orientation map after onset of grain growth (α); (C) reconstructed parent β map for the initial map (β); (D) reconstructed parent β map for the final map. The annotation arrow points out one area where growth occurs (similar point on all maps). All maps use IPFZ colouring.

7.3.1 Initial growth location – weld region

As discussed in the Literature Review (section 2), prior work [44], [52] suggests that the HAZ is a starting point for grain growth in the weld region, with full coverage of the HAZ within ~1 hr at 760 °C. In the same timescale, Lusby's work shows growth across the entire weld region [125], whilst my initial trials suggest that the weld centreline is also important (see chapter 5). Given that there appears to be an order to the grain growth that occurs, there are three potential growth hypotheses proposed, as shown in Figure 102. These are: (1) grain growth starts at the outer edge of the weld region (i.e. the edge of the HAZ) and growth continues inwards; (2) grain growth starts at or near the weld centreline and growth continues outwards; (3) a combination of (1) and (2), where growth occurs across the region, but with a focus on growth inwards from the HAZ edge and outwards from the weld centre.

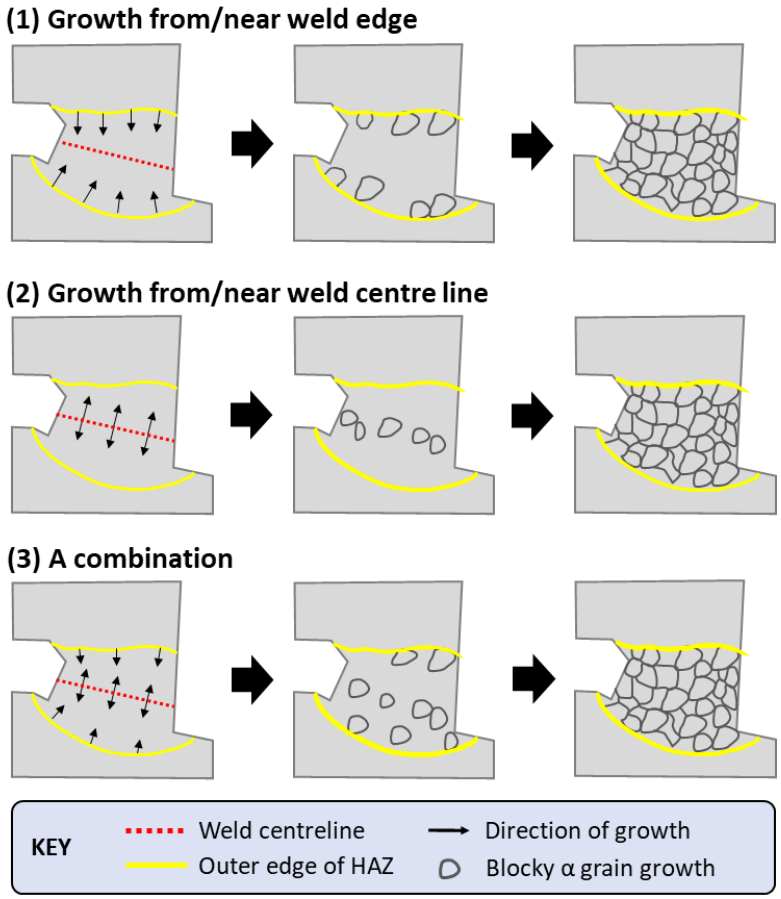


Figure 102 - Blocky-α grain growth hypotheses across the weld region. (1) Growth begins from/near edge of the weld (edge of HAZ); (2) Growth begins at/near the weld centreline; (3) A combination of growth from the outer edge and the weld centre occurs.

Figure 103 shows pre- and post-HT polarised optical micrographs for part of the weld region for an *in situ* experiment. The *in situ* experiment was designed to capture the onset of grain growth in the central weld region, and so unfortunately the lower HAZ is not captured fully, but the HAZ in the upper half of the weld (this half being smaller) is mostly captured within the map. This experiment has an interrupted heating schedule (see Figure 55 on page 75), so while the time at temperature is 70 minutes, it is difficult to relate this directly to the prior work of Lusby [125] or Taylor [44] in terms of the fraction of blocky grains, but this experiment can provide insight into the mechanisms and locations of blocky-α grain growth.

The overview provided within in Figure 103 shows grain growth near the weld centreline, in the HAZ of the upper half, in the fusion zone (mainly lower half) and along the edges of the sample. Blocky-α can be seen in all three regions, with more blocky grains observed within the lower HAZ as compared to the upper HAZ and no blocky-α growth within the parent material (i.e. similar to the *ex situ* results shown in Chapter 6).

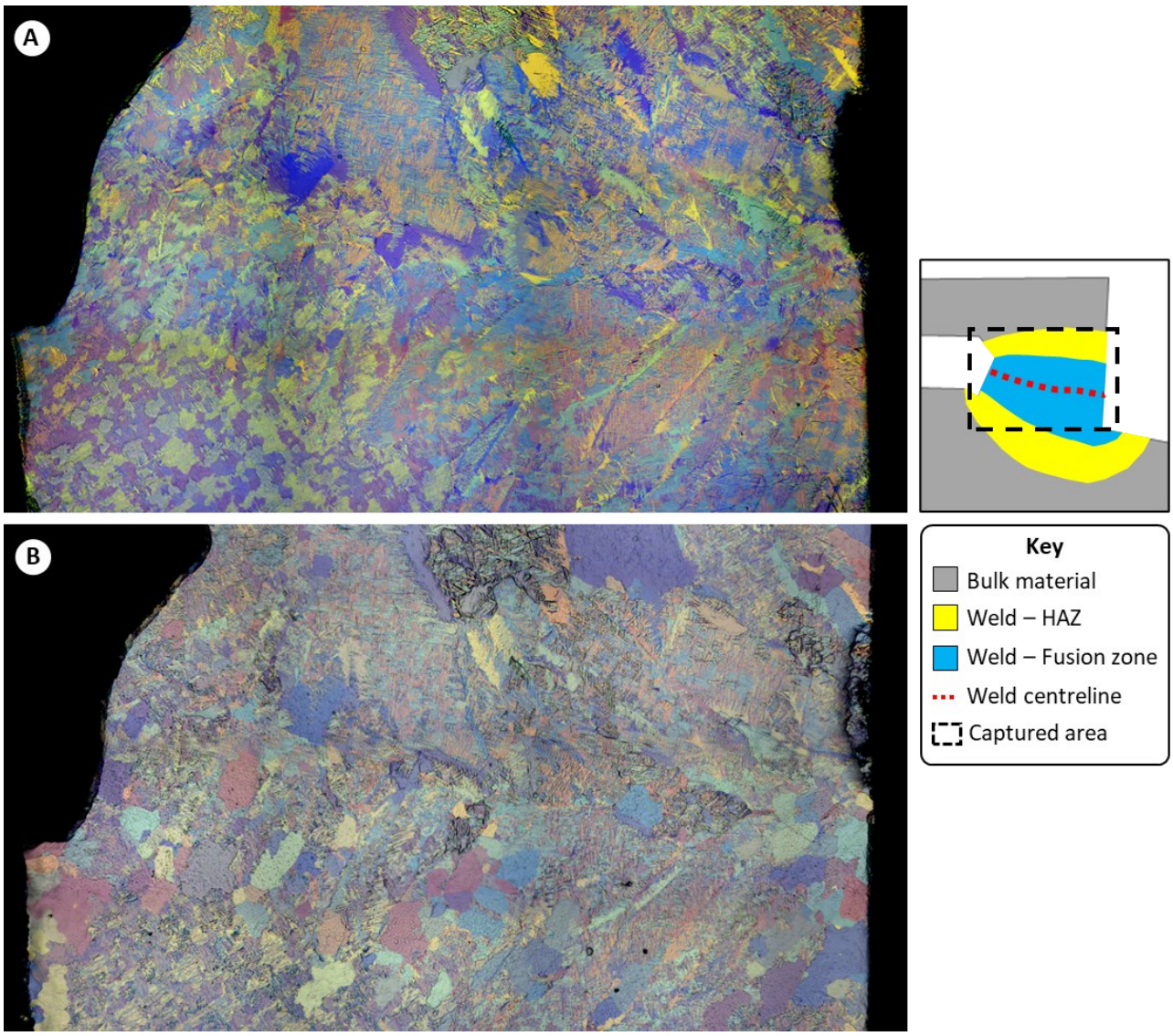


Figure 103 - Onset of grain growth across weld region. Polarised optical micrographs showing (A) pre-HT microstructure and (B) post-HT microstructure for an in situ experiment sample (in situ – experiment 1). Total time at ~760 °C for this sample was 70 mins over 7 heating cycles.

The locations of (new) blocky-α growth would suggest that hypothesis (3) seems most likely, with grain growth seen both in the HAZ and at/near the weld centre. However, it is not clear which occurs first based on these experimental results. Limitations in this analysis are shared with prior literature as although Taylor et al. [44] focussed on the HAZ, grain growth can be seen in the fusion zone in their micrographs for times <1 hr.

7.3.2 Initial growth location – prior-β grain boundaries

We know from the *ex situ* results (Chapter 6) that the prior-β microstructure is an important factor in grain growth, yet the situation is more complicated. The prior-β grain structure provides a skeleton which the new blocky-α structure is related to, but the grain orientations and final grain shape are not described well.

The *in situ* observations extend this to reveal in Figure 101 that the grain growth appears to protrude out from one prior-β domain into another (see Figure 101 C & D). This motivates a focus on subregions of Figure 101, as shown now in Figure 104, to explore this in more detail.

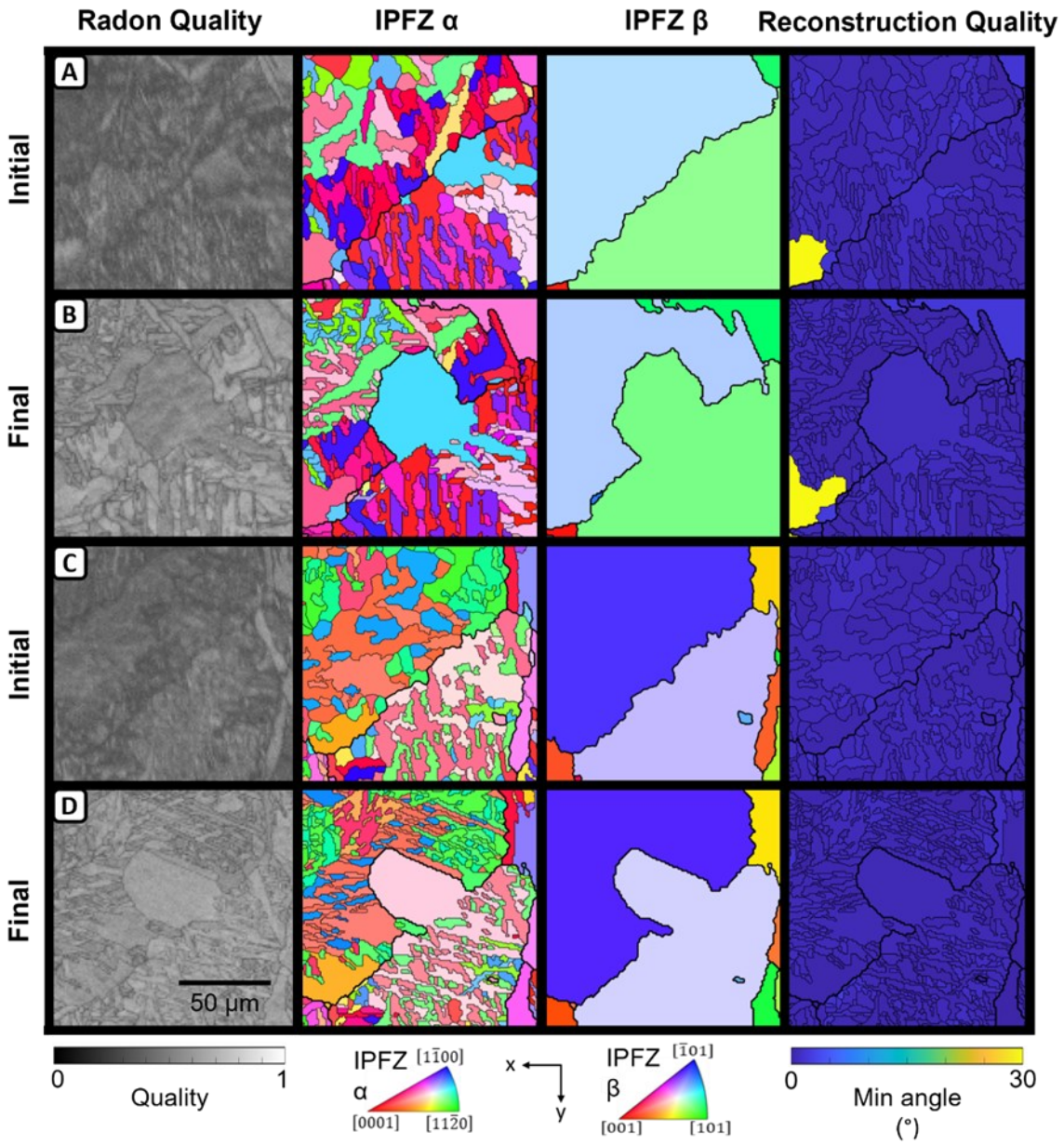


Figure 104 - In situ grain growth - small map examples (experiment 1) . Radon quality, orientation maps for α and reconstructed β using IPFZ colouring, and reconstruction quality for (A) small area 1 – Initial; (B) small area 1 – final; (C) small area 2 – Initial; (D) small area 2 – final.

In every case, the grain growth occurs adjacent to the position of a prior-β grain boundary, and this is seen in all three *in situ* experiments, i.e. at no point did a blocky-α grain form in the middle of a prior-β grain. The importance of the prior-β grain boundary for the onset of grain growth, combined with observations about the direction of growth between prior-β grains, suggests that α domains grow from the edge of prior-β boundaries, into new prior-β domains as shown schematically in Figure 105.

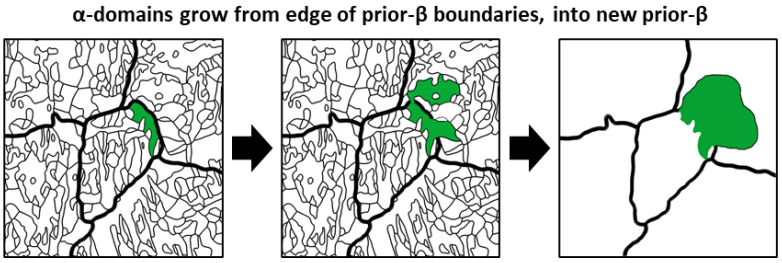


Figure 105 - Microscopic grain growth mechanism

One example to demonstrate growth of blocky-α from one prior-β into an adjacent prior-β grain is shown in Figure 106. This is an example from experiment 1 (the same region is shown in Figure 104 rows C & D). Here the pink α grain in Figure 106 (A & C) appears to grow from the lilac β grain (β_2) into the blue β grain (β_1) (see Figure 106 (B & D)). This is confirmed using pole figure analysis in Figure 106 (E & F).

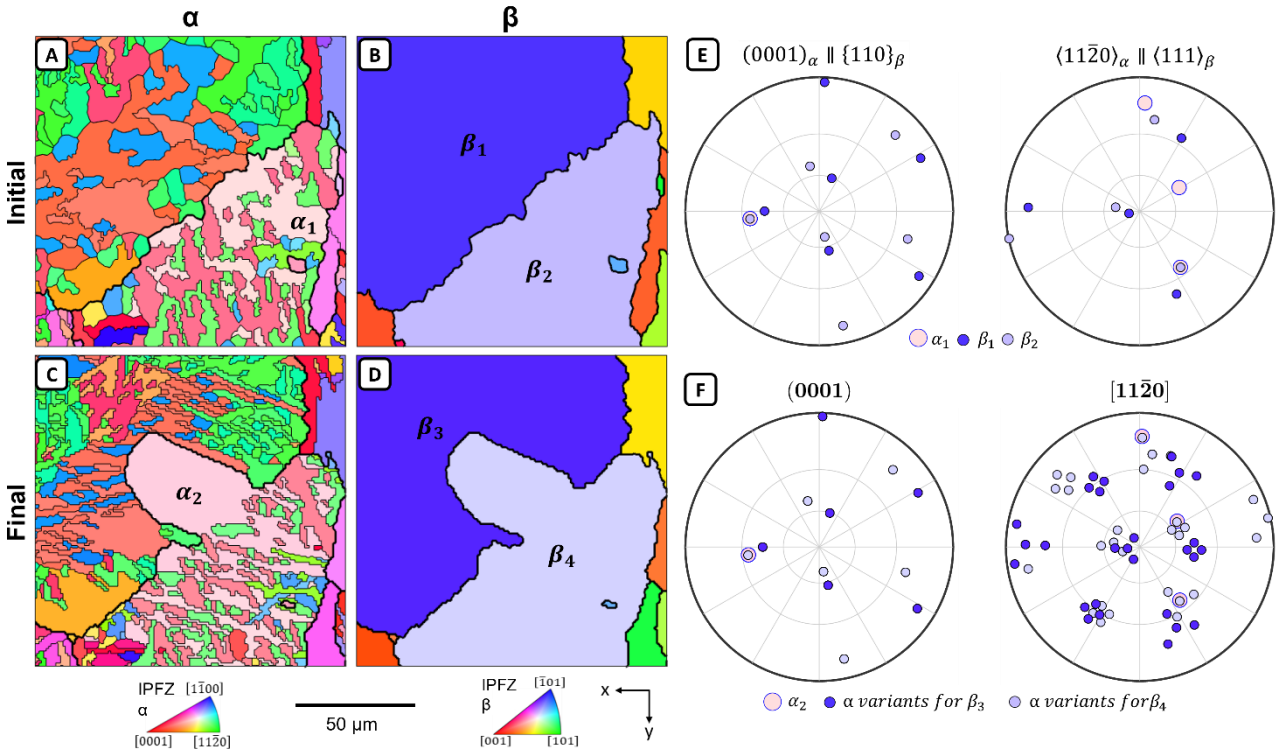


Figure 106 - Testing grain growth mechanism. Initial (A) and final (C) α orientation maps along with their respective reconstructed β maps (B & D), all using IPFZ colouring and with key grains labelled. Testing the β reconstruction is valid: (E) pole figures for the (BOR planes and directions) for α_1 (growing α grain) and the two β grains; (F) pole figures for $(0001)_\alpha$ and $<11\text{-}20>_\alpha$ comparing the grown grain orientation (α_2) with the potential α orientations for each of the β grains in (D).

This validates the *ex situ* analysis (see section 6.4.4), this time with the growing grain clearly identified, and supports the grain growth mechanism proposed, where the α grain grows out of one prior-β domain into another. This analysis was repeated for all grain growth examples and in each case growth of the blocky-α grains from the edge of one prior-β domain into the neighbour was seen.

7.3.3 Factors affecting the initial onset of growth

Typically, where blocky-α grain growth is observed, the image quality for the new blocky-α is higher than the before region, i.e. patterns are sharper and there are fewer/less strain gradients within the interaction volume. Often the new blocky-α originates grows into a region of lower image quality, i.e. regions with

higher strain gradients in the (pre-HT) transformed microstructure which indicates that nucleation and growth could be driven in part to reduce the local stored energy. This is shown in Figure 104 and also in Figure 107, where there is a distinctly darker area into which the growing α grain grows (arrow direction indicates direction of growth). Grain growth driven by stored energy is consistent with the nucleation and growth mechanism of grain growth for blocky-α proposed by Tong et al. [48]. Tong et al. proposed that blocky-α grain growth was via strain induced grain boundary migration (SIBM), where the grains grow from regions of low strain energy into high strain energy regions.

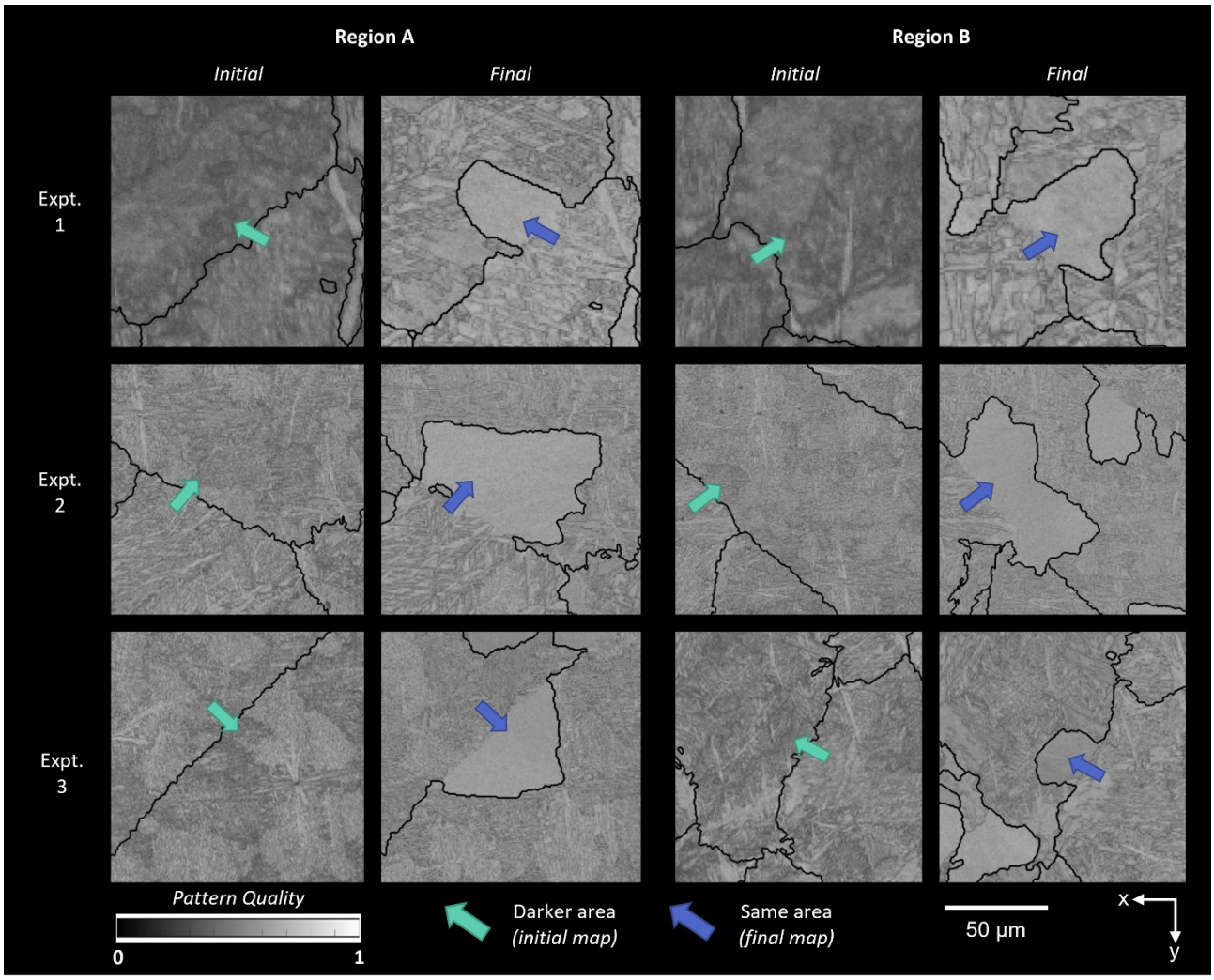


Figure 107 - Pattern quality - influence of stored energy. Two examples (regions A and B) from each of the 3 in situ experiments showing the pattern quality (radon quality) in regions where grains grow, with the darker patch indicated by a green arrow on the initial map and a blue arrow in the same place on the final map for comparison. The direction of the arrows indicates the direction of grain growth. Thick black lines = parent β grain boundaries overlaid on the maps.

7.4 Part 2: grain growth

This section looks in more detail at the growth of the α grain after it has started growing and factors that impact this growth.

7.4.1 Pinning

There are two main factors that appear to affect the grain growth inside the new domain, long straight grain boundaries and regions where the microstructure forms a 'cross' of α grains, with the two often linked.

In the α microstructure, within the prior-β regions, there is the occurrence of crosses of α grains, forming an 'x' motif which may be 'plus' shaped or 'star' shaped depending on the orientation of the parent β grain for the region and the sectioned plane. Looking at these in pattern quality (see Figure 108), in some cases, the presence of a potential SPPs can be observed in the centre of these points (indicated by a darker region of pattern quality, although these points do not index so may have been removed during the polishing process). This would fit with observations by Holt [31] (as shown in Figure 5 on page 28), where SPPs act as nucleation points (depending on material composition) for some α grains during initial lamella α formation.

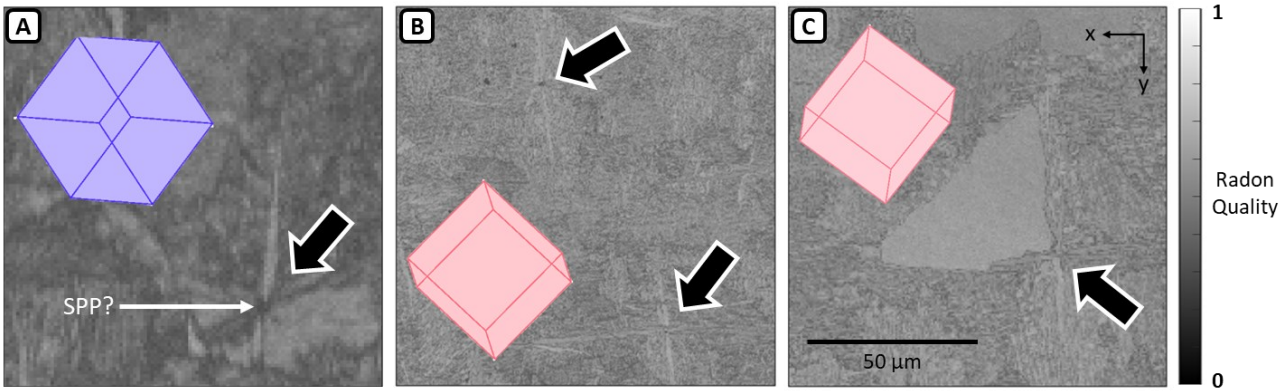


Figure 108 - Points that pin growth. Pattern quality maps showing potential nucleation points within prior-β regions for an example from (A) experiment 1; (B) and (C) experiment 2. In each case, the point(s) are indicated by arrows and the β orientation at this point is shown using the prism (IPFZ coloured – see Figure 104 for colour key). Scalebar = 50 µm.

For blocky-α growth, these points pin the growth front as seen in Figure 108 C. Looking at the grain orientations emanating from these points, there is often a variety of α variants, with few adjacent grains having shared planes or directions, which may explain the limited growth around these points (see section 7.4.3). Three examples are shown in Figure 109, where the maps are coloured by variant number and the prisms show the orientations (with shared planes/directions indicated by shared colours on the prisms).

As can be seen, in some cases, e.g. Area 2 in Figure 109, there are no shared planes or directions between the variants, whereas in other cases, e.g. Area 3 in Figure 109, there are shared directions between adjacent α grains like the purple and blue grains (α variant no. 6 & 10) which share a common direction. In microstructures with more advanced grain growth, these points are not immediately obvious. It is possible that they can be consumed from certain directions using the shared planes/directions. Where there are multiple blocky grains growing, these regions may be potential sites where the growing α grains touch and growth is halted, but further investigation would be required to confirm this.

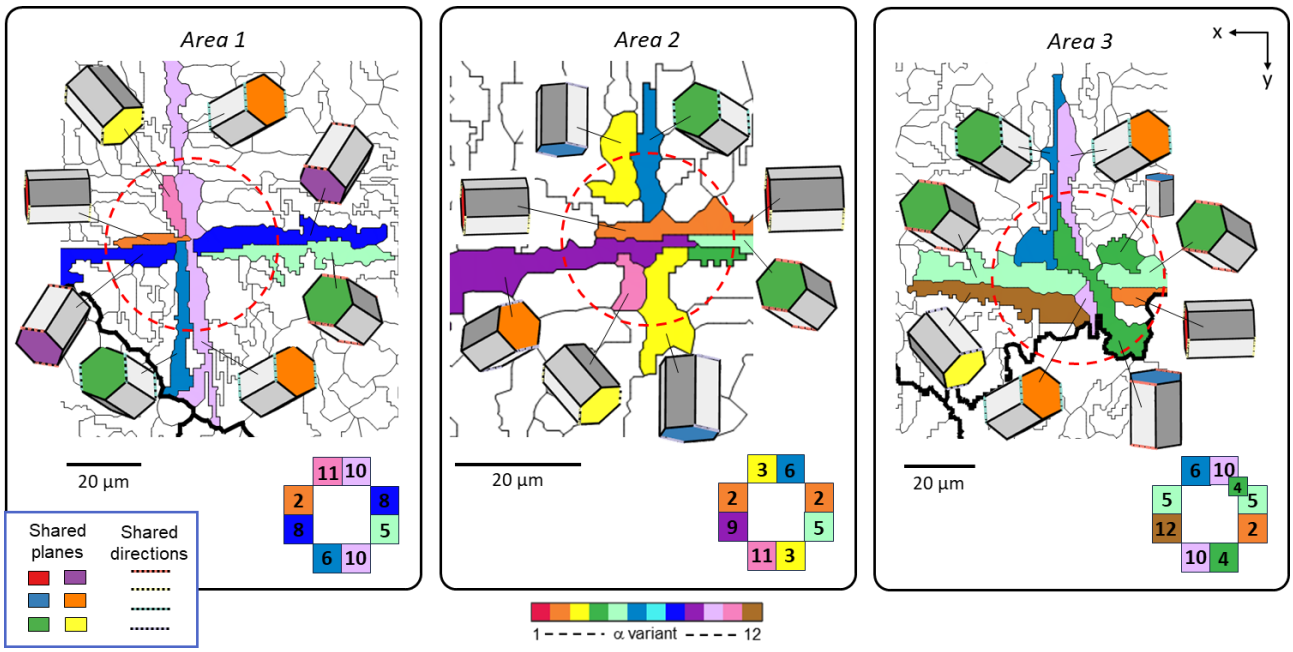


Figure 109 - 'cross' point α orientation examples. Three areas where 'cross' points exist in an experiment 3 example (from map at Figure 110). α grains coloured by variant number (number also shown in in the adjacent schematics), with orientations indicated by the prisms. Note: prism end colours indicate shared planes, whilst the dashed pastel edge colours indicate shared directions.

Growth often slows and the grain grows along (i.e. the grain boundary is retained) long straight boundaries within the microstructure, which are often connected to these 'cross' points. These grains will often have the long axis along {110} planes within the parent β grain for the region. These boundaries are more stable and lower energy than the shorter curvier boundaries where the grain grows initially (see section 7.3.3), supporting the argument that the grain grows into areas of high stored energy.

7.4.2 α variants

The α variants within each prior-β grain region were analysed using the ParentBOR post processing code. Figure 110 shows an example of this for a grain growth example in *in situ* experiment 3. Variants with shared <a> directions (Figure 110 C) are spatially co-located and there is limited spatial co-location of regions with common basal planes (Figure 110 B). This is result is common across the *in situ* microstructural evolution maps where a new blocky-α grain is shown, and it suggests that boundaries with a shared <a> direction are important in blocky-α grain growth.

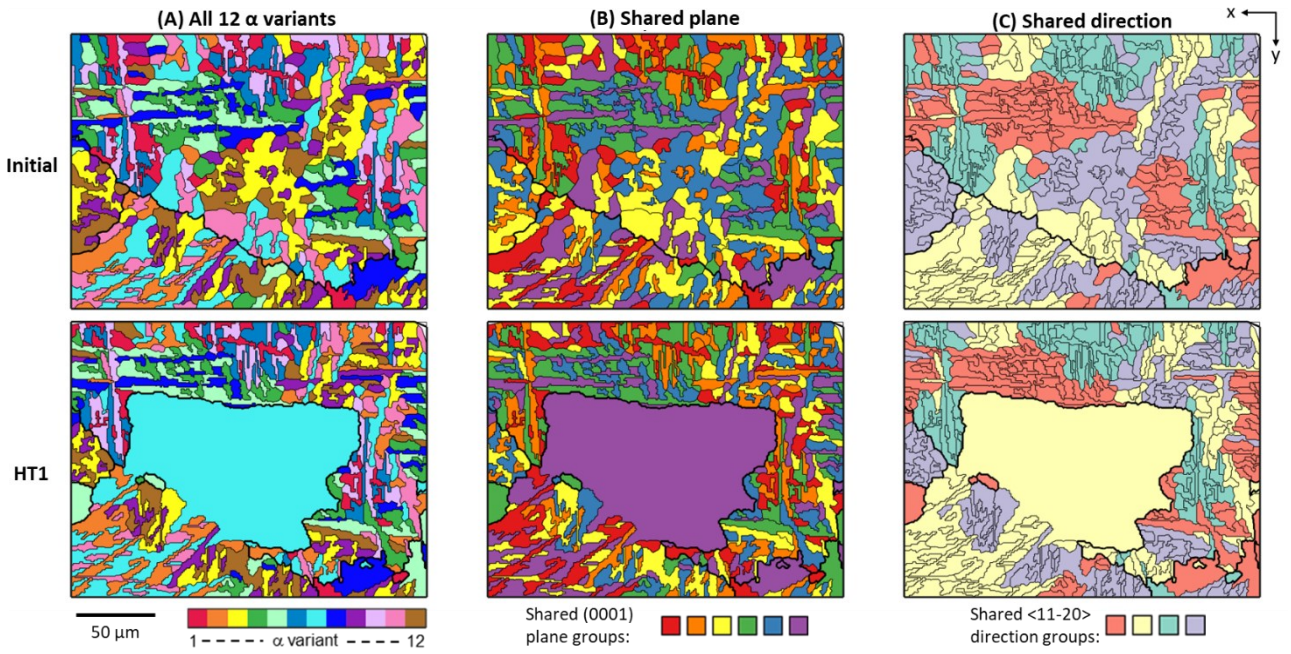


Figure 110 - α variant analysis for experiment 3 example. Initial and heat treatment 1 (HT1) grain maps for a grain growth example, using α variant colouring. (A) all 12 α variants; (B) coloured by shared (0001) plane (bright colours); (C) coloured by shared <11-20> direction (pastel colours).

7.4.3 Grain growth hypothesis

A grain growth hypothesis is proposed using the shared planes and directions between the α variants as a pathway of easy growth within the new β domain. This is described below and illustrated in Figure 111.

- **Step 1**: Cross the boundary

  α grain grows across the original β grain boundary location into the new prior-β domain.
- **Step 2**: Grow to fill shared $\langle 11\bar{2}0 \rangle$ region

  In the region where the α grain is, growth occurs between α variants with a shared $\langle 11\bar{2}0 \rangle$ direction.
- **Step 3**: Grow across shared (0001) plane grain boundary

  Growth occurs across grain boundary where the adjacent grain shares a common (0001) plane.
- **Step 4**: Repeat steps 2 & 3

  Growth continues via groups of α variants with shared $\langle 11\bar{2}0 \rangle$ directions, and moves between these groups via α grain pairs with shared (0001) planes.

A caveat to this model is that pinning takes precedence over this process, so in the example shown in Figure 112, the known pinning places ('cross' points and long straight grain boundaries) are taken into account.

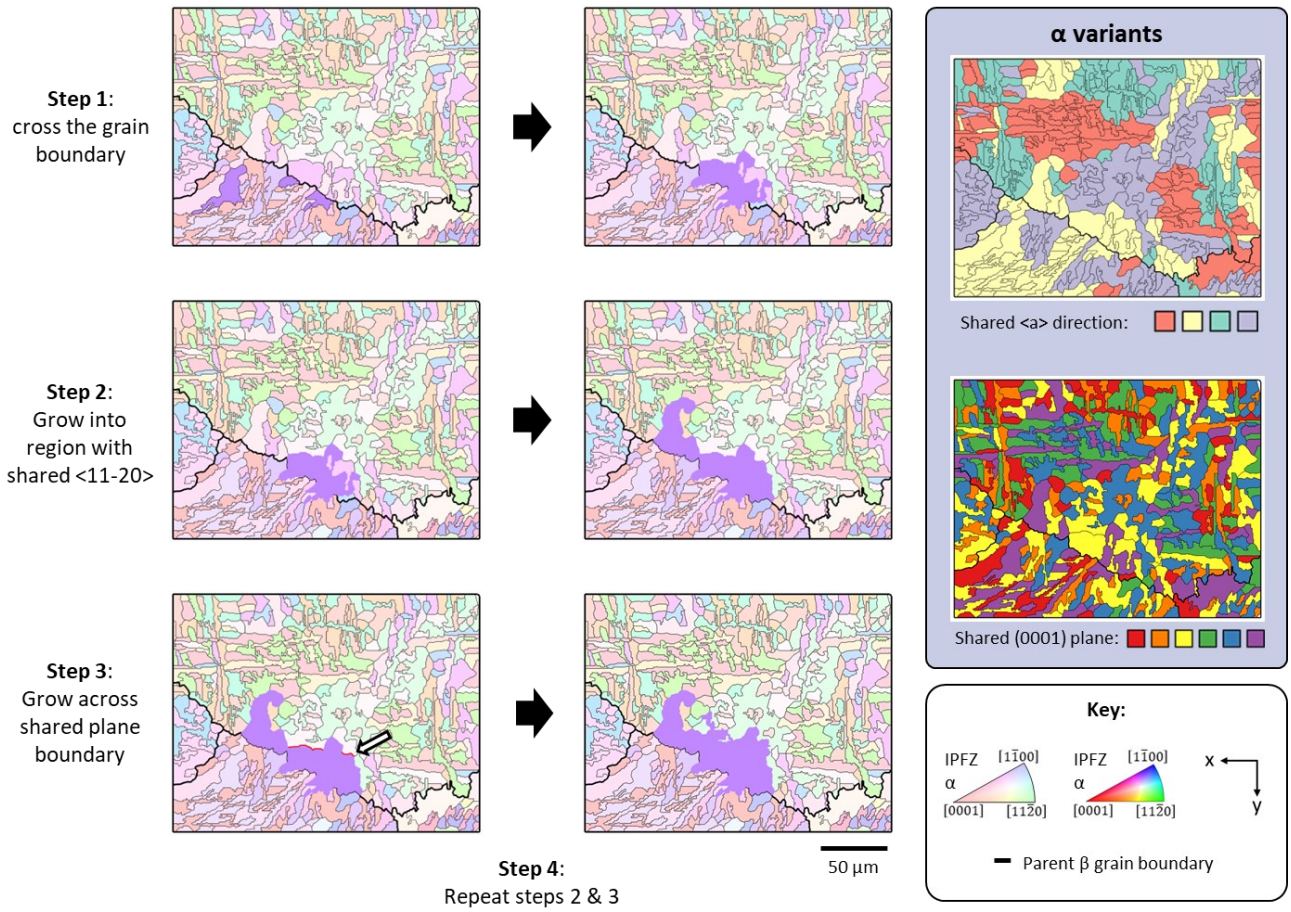


Figure 111 - Grain growth hypothesis example. The first 3 steps for an example map from experiment 3, showing how the grain growth hypothesis works, alongside the α variant maps coloured by shared direction (pastel colours) or plane (bright colours) for reference.

An example output using this model is shown in Figure 112, based on the initial map, along with the experimental results for this region. As this was an experiment 3 example, there were two heat treatments, HT1 and HT2 (details in Table 14 on page 79) and it can be seen that the model output actually fits better with the second heat treatment.

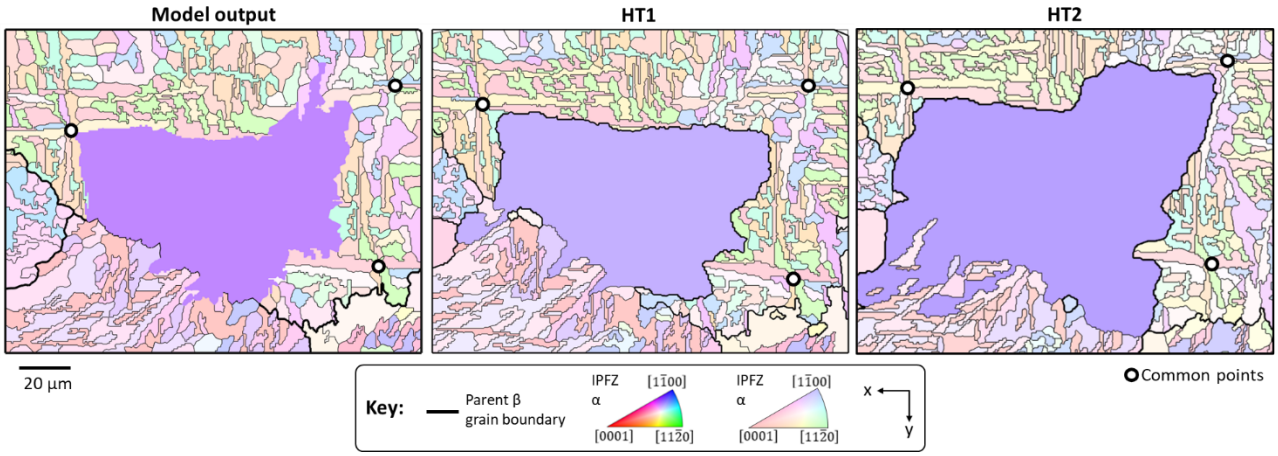


Figure 112 - Comparison of model output and heat treatment results for experiment 3 example. Model output compared with the output after the first (HT1) and second (HT2) heat treatments. Common points across the maps are marked by the white and black circles.

7.4.4 Extending observations to multiple regions within the *in situ* data sets

So far, observations from the *in situ* experiment have focussed on individual areas of interest for each of the mechanisms. Figure 113 shows the total area mapped, comparing the pre- and post- heat treatment regions to explore 17 blocky-α grains. Identification of these seventeen blocky-α regions was initially confirmed through comparison of the prior-β reconstruction maps for the post and pre- heat treatments, followed by looking for large and new regions of blocky-α microstructure in the pattern quality and α-phase IPF maps.

All seventeen highlighted regions show:

- Growth of the new blocky-α phase from an α variant in the neighbouring prior-β grain.
- Improved pattern quality for the blocky-α grain.
- The blocky-α grain tends to have a larger size than the local α variants.
- The shape of the blocky-α grain tends to be ellipsoidal (in this 2D section) as compared to the lenticular α variants.

For the larger blocky-α grains, it is challenging to determine the spatial location of the exact α variant which has grown across the boundary (and in some cases there could have even been coalescence of two growing blocky-α grains where the same variant seeds in both cases). Furthermore, as these maps are a 2D section of the 3D microstructure, the nucleation site for the initial blocky-α growth across the interface could have been subsurface.

There is one blocky-α grain (shown with an asterisk in Figure 113 post-HT α) which has grown from one initial nucleation site and has grown into more than one prior-β grain.

The forescatter micrograph in Figure 113 shows a few examples where the blocky-α grains are growing around existing α grains, leaving behind smaller ‘orphan’ grains within the microstructure. These are observed commonly within the *ex situ* maps, e.g. Figure 95 on page 130 or Figure 97 on page 133.

For the *in situ* map, there are a few blocky-α grains which have a shared interface (i.e. they touch). In these cases, the major axis of the grain ellipse extends nearly parallel to the interface, implying that growth has of the blocky-α grains has exhausted when the two blocky-α grains met. This is seen frequently in the *ex situ* experiments (Figure 95 on page 130) and can help explain anisotropy in grain shape within different regions of the weld.

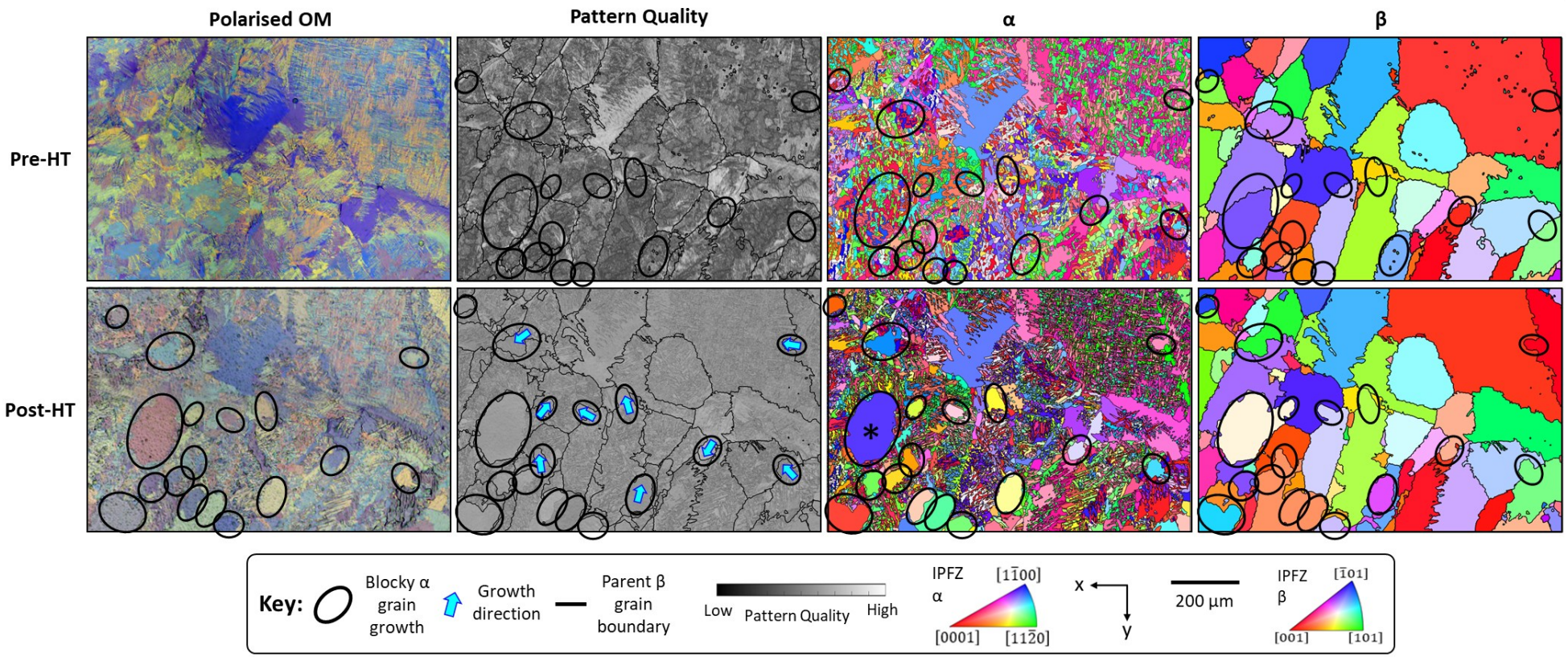


Figure 113 - Blocky-α grain growth locations and directions. Polarised OM, Pattern/radon quality, α and reconstructed β orientation maps for pre- and post-HT in experiment 1. The black ovals indicate the positions of grain growth (equivalent positions on all maps), whilst the blue arrows on the post-HT pattern quality map indicate direction of growth. The asterisk in the post-HT IPF-Z figure indicates a large blocky-α grain that has grown across multiple prior-β grains, as identified within the pre-HT map.

7.5 Summary

This chapter made macroscopic observations about blocky-α grain growth in EB welds in Zircaloy-4, using the *in situ* grain growth experiment results and built on the results of the previous chapter.

7.5.1 Onset of grain growth

Conclusions about the onset of blocky-α grain growth:

- The initial grain growth occurs across the weld region mapped in the *in situ* experiments. The *in situ* area mapped included the weld centreline, fusion zone and some of the HAZ. Although the results are not conclusive, it would appear that the grains grow both from/near the weld centre and from the HAZ.
- Grain growth is always related to a prior-β grain boundary – no evidence was found of grains growing inside prior-β domains.
- α grains grow outwards from one prior-β domain into an adjacent β domain.
- The orientation of the growing α grains can be explained using the neighbourhood orientations. This builds on analysis of the *ex situ* results, but the growing grain is clearly identifiable in some of the examples shown (not in all cases, likely due to a subsurface grain growing).
- Grains grow across the original prior-β grain boundary from regions of low stored energy to regions of higher strain energy, as evidenced by the pattern quality maps, where darker regions tend to be related to higher stored energy. This is also evidenced by the short, curvy α grain boundaries within these darker areas that are higher energy than the adjacent areas with long/straight boundaries.

7.5.2 Factors affecting grain growth

Factors affecting the grain growth once the original boundary position has been crossed into the new domain include:

- Pinning by ‘cross’ points of α laths in the microstructure. The cross points probably contain an SPP at the intersection of the α variants, and the lamella α extending from this SPP seem to inhibit further blocky-α growth.
- Pinning due to long straight grain boundaries that are lower energy and stable compared to the surrounding area.

Finally, a hypothesis for grain growth within the new prior-β domain is proposed utilising the groupings of shared planes and directions between α variants. The output of the model results in a strikingly similar shaped grain to the experimentally observed grain, when pinning due to the ‘cross’ structures is included in the model.

This chapter complements the prior chapter, as observations made at a local level extend well across the mapped region for *in situ* and tie in with observations made in the *ex situ* experiments.

8 Hydride Stress Fields

8.1 Aim

The aim of this chapter is to investigate grain boundary hydride formation in blocky-α Zircaloy-4, with a focus on exploring deformation fields near hydride/zirconium matrix interfaces. This is achieved using a combination of conventional electron backscatter diffraction (EBSD) and high angular resolution electron backscatter diffraction (HR-EBSD). The conventional EBSD gives access to grain morphology, orientations and orientation relationships between the grains whilst the HR-EBSD analysis provides insight into lattice rotations, stress fields and stored geometrically necessary dislocations (GNDs).

This chapter builds on prior work described in the literature review (section 2) which explored misfit strain between the hydride phase and the α Zr matrix, and the consequences of this in creating a stress fields around the hydrides. More specifically, the present work builds on the theoretical work of Carpenter [83], the experimental work of Kerr et al. [85] and Barrow et al.[84], and the modelling work of Reali et al. [87]. So far in the literature, investigations have focussed on small (1-2 μm) intragranular hydrides. This work looks at extending this to larger hydride packet structures near interfaces such as grain boundaries. It aims to measure the stress fields around hydrides, and evaluate their relationship to the crystallography of the parent matrix and connected hydrides.

Highlights from this chapter include: a brief comparison of the final surface preparation technique used; analysis of smooth grain boundary hydrides; analysis of grain boundary hydride that protrudes into the α Zr matrix.

8.1.1 Hydride orientation relationship (OR)

To recap, the orientation relationship between δ zirconium hydride[14] and α-Zr differs within literature ([20], [55], [63], [171]–[173]). However, they all have a common close packed direction relationship $\langle 11\bar{2}0\rangle_\alpha \parallel \langle 1\bar{1}0\rangle_\delta$. Recent work within my research group on hydrides in Zircaloy-4, has generally observed the OR to be [55] :

$$(0001)_\alpha \parallel \{1\bar{1}1\}_\delta \text{ and } \langle 11\bar{2}0\rangle_\alpha \parallel \langle 1\bar{1}0\rangle_\delta \quad (21)$$

This is the OR used for testing in this work and will be referred to as the 'hydride OR'.

8.1.2 Sample surface preparation

The final surface preparation step prior to EBSD is of particular importance for this work to provide good quality patterns for analysis, especially for HR-EBSD analysis. Ideally, both phases (δ hydride and α Zr) need to have good quality patterns, which can be a challenge as they polish at different rates and the hydride can be removed during polishing in some cases. Sources of surface roughness (e.g. strong curtaining)

[14] The hydride anneal cooling rate was chosen to get δ phase hydride – see Table 14.

should be avoided if possible to minimise unwanted effects on the results. This motivated the development of sample preparation routes to enable analysis of zirconium-hydride interfaces.

For this work, two ion beam polishing methods were used to prepare the final surface of the samples for EBSD analysis: pFIB and cross-section BIB. The final step for both methods was carried out at cryo temperatures to reduce ion-surface damage and secondary formation of hydrides (see [146], [147]).

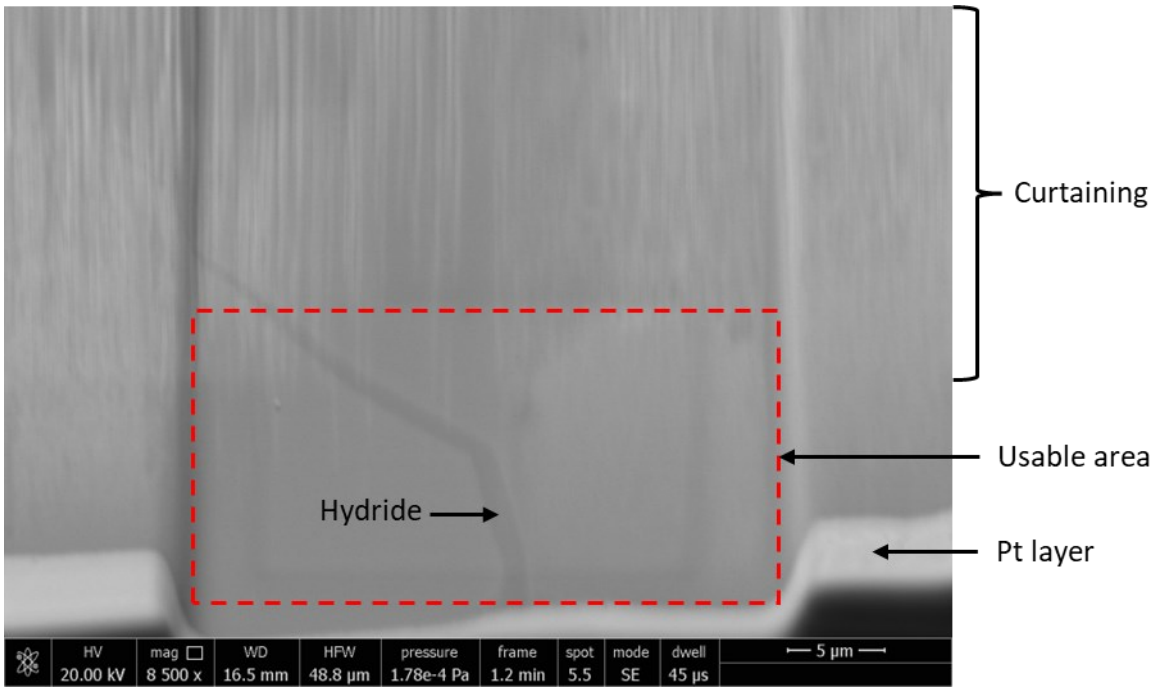


Figure 114 - pFIB hydride area overview. SE image showing the polished hydride region, with the useable area indicated by the red dashed box and the start of significant curtaining indicated. Scalebar = 5 µm.

The pFIB polishing (see Figure 114) provided a polished region of approx. 30 x 15 μm^2 (red dashed area in Figure 114). This region provided high quality patterns and indexed very well within this region (up to 100 % indexing success). Outside this area, surface roughening when cross sectioning (so called 'waterfall' effects or 'curtaining') caused significant local surface roughness. The cryo-pFIB had just been delivered to Imperial College London (< 6 months prior to this work) and so in time, there is potential that further recipe development could provide much better results. For example, a rocking stage could be used to minimise the waterfall effects.

The BIB polished sample (not shown) provided a larger area, but had a rougher surface finish than the high quality area prepared using the pFIB. The BIB polished (semi-circular) region had maximum dimensions of 2.3 x 0.6 mm, and indexing was >90%. This large area provided multiple good regions for mapping, but also contained some ridges (i.e. significant local roughness) that meant some areas were not usable for HR-EBSD analysis.

8.2 Results

This section is split into two parts, 8.2.1 hydrides that smoothly decorate the grain boundary, and 8.2.2 hydrides that protrude into the Zr matrix.

8.2.1 Smooth grain boundary hydride

There are two maps taken from where the hydride is smoothly decorating α-Zr grain boundaries, with no ingress of the hydride extending away from the grain boundary and into the matrix.

8.2.1.1 Example 1: grain boundary hydride (BIB polished)

The grain boundary hydride map, shown in Figure 115, consists of two large α grains with δ phase hydride on the grain boundary between, covering the complete length of the grain boundary imaged. The hydride thickness varies from approx. 0.5 µm to 2 µm in width, with a tapering around a (suspected) SPP, and a small amount of α-Zr (labelled α_5) contained within the hydride region.

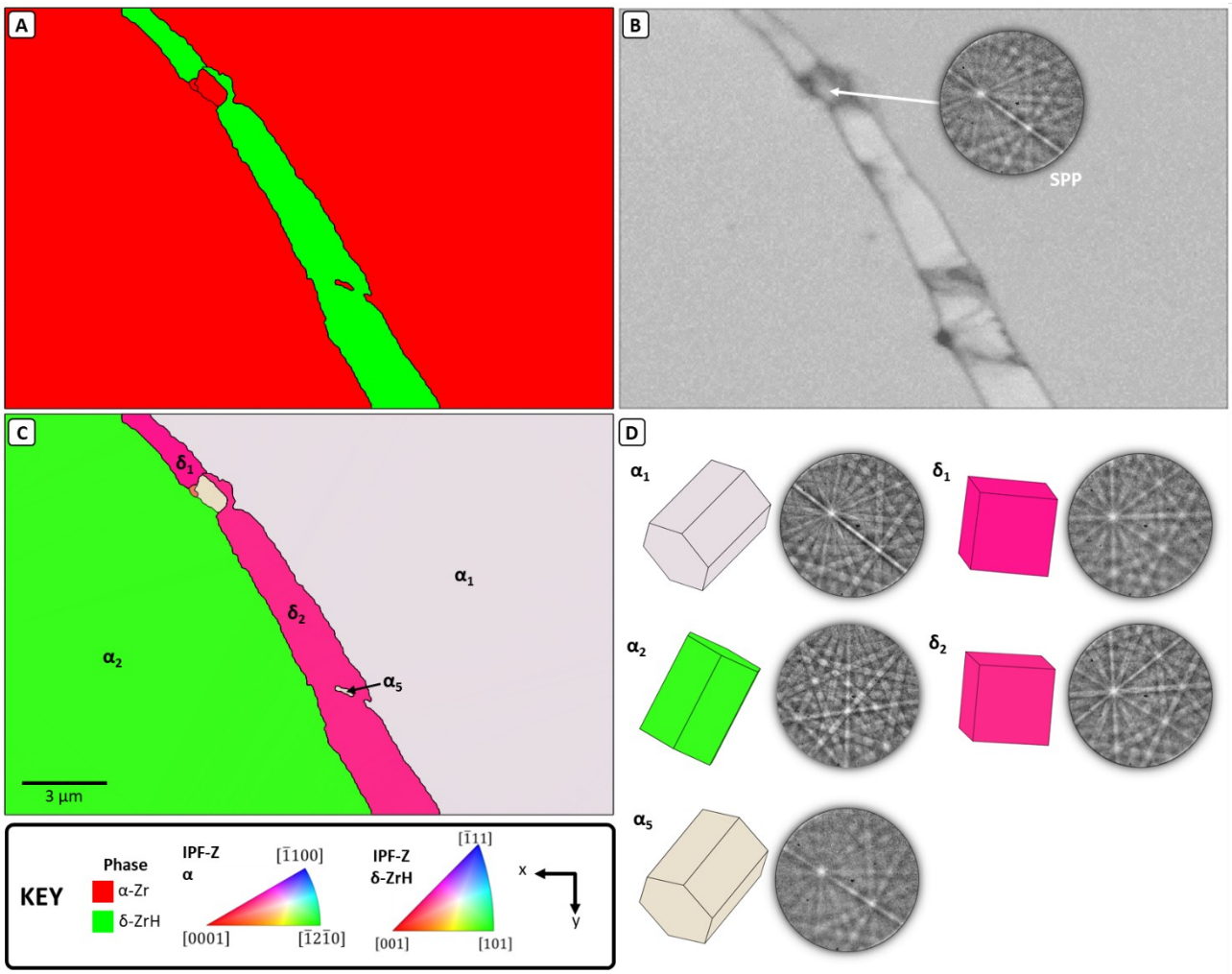


Figure 115 - Orientation analysis of the grain boundary hydride map. (A) Indexed phase map; (B) pattern quality map (with probable SPP representative pattern); (C) crystal orientation (IPFZ coloured) along with labels for key grains; (D) prisms and representative patterns for the identified grains.

Figure 115 shows an overview of the orientations in the grain boundary hydride map. From the pattern quality (Figure 115 B) there is a small region that although indexed as α zirconium matrix, is likely to be an SPP, based on the pattern quality and orientation. The crystal structure of one of the potential SPPs is HCP, and the example EBSP for this region resembles that seen in Figure 115 D for α_1 & α_5 so its orientation is related to the α_1 grain. However, it is likely that this is an FeCr SPP with a hexagonal structure [25], [174]. Also seen in the pattern quality map are a number of darker lines within the hydride, indicating the

presence of interfaces within the hydride, which is likely due to stacking of smaller hydrides within the macro hydride [20]. The small orange grain is not considered in this analysis as there is poor pattern quality at this point, which makes it difficult to tell if this is a grain and challenging to determine what phase it is.

For the α grains, α_5 has a very similar representative orientation to α_1 and is/was probably part of this grain prior to hydride formation. The δ hydride is disconnected by the SPP, but δ_1 and δ_2 have a similar orientation with respect to each other.

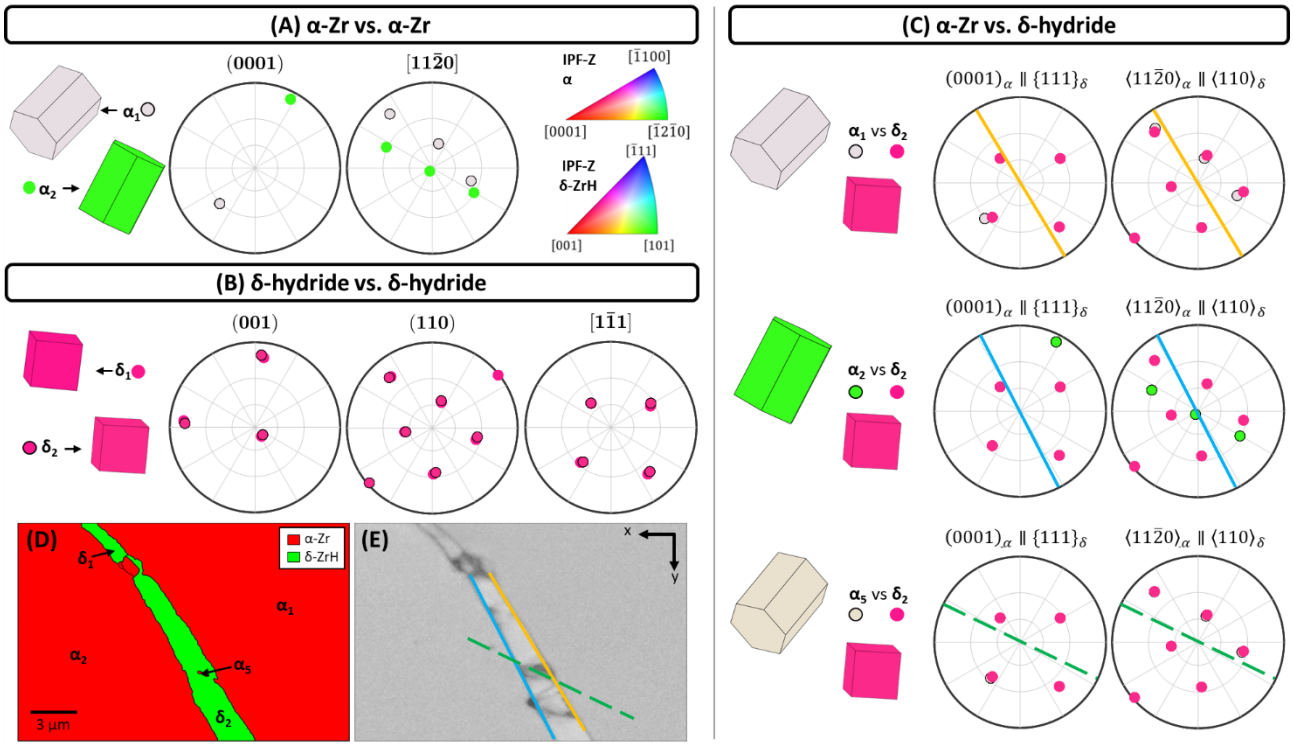


Figure 116 - Orientation relationships in the grain boundary hydride map: Pole figure analysis of (A) α-Zr/α-Zr OR;(B) hydride/hydride OR; (C) α-Zr/δ-hydride OR with grain boundary traces overlaid; (D) phase map annotated with grain labels; (E) Grain boundary traces on pattern quality map.

The orientation relationships between the α grains, δ-hydride grains and between the α-Zr and δ-hydride grains are investigated in Figure 116. There is no OR between α_1 and α_2, as shown in Figure 116 (A), and they have a <c> axis misalignment of 38 ° with the closest $\langle 11\bar{2}0\rangle_\alpha$ directions 13 ° apart. Note that due to the closeness in orientation of α_1 and α_5, only α_1 is used for the analysis in Figure 116 (A).

Figure 116 (B) shows that the two δ hydride grains are very close in orientation, and due to the poor pattern quality in the vicinity of the grain boundary (see Figure 115 (B)), these are likely part of the same hydride packet. As they are so similar, only δ_2 is used for the α vs. δ analysis in Figure 116 (C). The orientations for α_1 and δ_2 match the hydride OR, whereas this OR is not met for α_2 and δ_2. This indicates that the hydride grew from α_1. There is no discernible OR between α_2 and the hydride. Interestingly, the α region within the hydride, α_5, shows a near perfect match with the hydride OR.

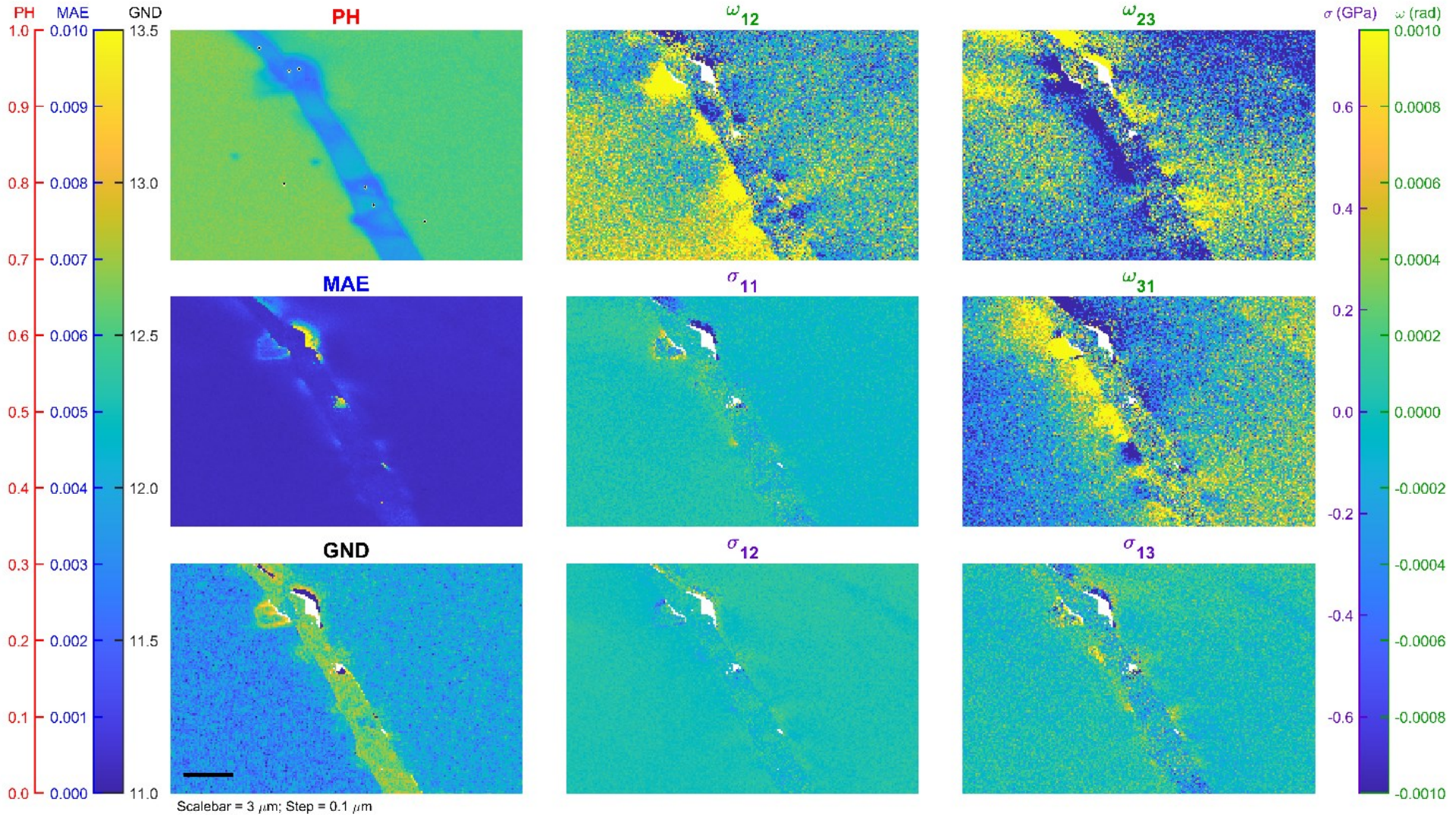


Figure 117 - HR-EBSD analysis of grain boundary hydride: PH = peak height with reference points per mapped region plotted; MAE = mean angular error; GND = sum of GND density across all slip systems; components of the rotation (ω_{ij}) and in-plane stress tensor (σ_{ij}). Maps are plotted against different colour scales. The stress tensor and rotation tensor maps are shown with respect to the reference points.

HR-EBSD analysis shown in Figure 117 of the grain boundary hydride map highlights local variations in lattice rotation, in-plane stress and stored GND density. The peak height and MAE maps show that the SPP, hydride, and neighbour regions have poorer quality patterns and that the HR-EBSD analysis was less accurate there. All the other maps have been filtered to only show reasonable values, using a filter to remove points with a PH < 0.3, and a MAE > $1x10^{-3}$.

The rotation tensor maps (ω_{ij}) show that there is a periodic variation of lattice rotation along the hydride metal interface, with notable positive and negative rotation components periodically along the hydride matrix interface. These fluctuations are seen long the interface between the hydride and α_1, with a spacing of ~2 µm. Along the interface with α_2, there is a more continuous variation in lattice rotation and the fluctuations along the interface are of smaller magnitude, except where the hydride has broken up (towards the bottom of the map) and associated with the SPP.

The stress field maps (σ_{ij}) show fluctuations of up to ~500 MPa at the interface, but these regions of high stress are limited to only ~1 µm from the interface and their spatial extent perpendicular to the interface is lower than the variations in lattice rotation.

The GND density map tells us about the stored dislocation content which can be generated from significant incompatibility (e.g. from misfit strain) which must be accommodated by the formation and storage of (geometrically necessary) dislocations. In the GND map in Figure 117 there are regions of slightly higher GND density within the metal corresponding to the periodic fluctuations in stress and lattice rotation variation, as well as a higher GND density around the SPP particle.

8.2.1.2 Example 2: triple junction grain boundary hydride (pFIB polished)

The triple junction grain boundary map (Figure 118) contains a triple junction with grain boundary hydride decorating two of the branches. The maximum hydride width at the grain boundaries is ~1 µm. In this case, the hydride is more complicated, with four δ hydride grains in total, one between α_1 and α_2, and three along the grain boundary between α_2 and α_3.

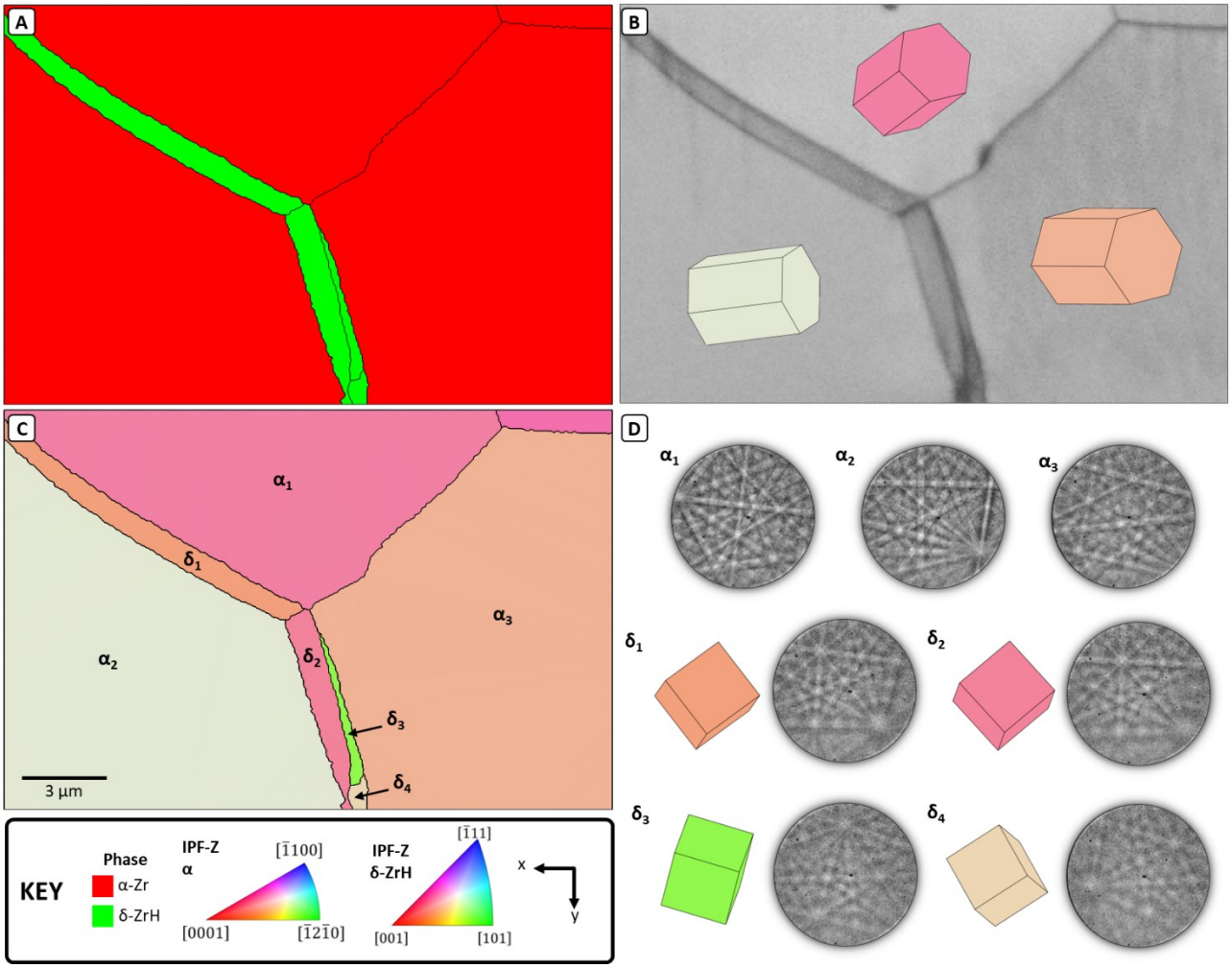


Figure 118 - Orientation analysis of the triple junction grain boundary hydride map. (A) Indexed phase map; (B) pattern quality map (with probable SPP representative pattern); (C) crystal orientation (IPFZ coloured) along with labels for key grains; (D) prisms and representative patterns for the identified grains.

The three α grains (shown in Figure 118) have relatively similar orientations, as indicated by the prisms and the IPF (Z) colouring. Two of the δ hydrides (δ_1 and δ_2) have a very similar orientation as shown in Figure 118 D, whilst the remaining δ hydrides also appear related, with a rotation seen when comparing the two EBSPs.

Analysis of the α/α and α/δ orientations in this map are shown in Figure 119. It is interesting that the undecorated α_1/α_3 grain boundary has a very closely shared $[11\bar{2}0]_\alpha$ direction, compared to the hydride decorated α_1/α_2 and α_2/α_3 grain boundaries where the α grains have a close, but not exact, shared $[11\bar{2}0]_\alpha$ direction, as detailed in Table 26.

Table 26 - Angles between α grain directions in the triple junction map – measured in degrees using MTEX.

α-grain pair	∠ between $(0001)_\alpha$ (°)	∠ between $\langle 11\bar{2}0\rangle_\alpha$ (°)
α_1 and α_2	35.4	11.9
α_1 and α_3	22.3	5.4
α_2 and α_3	24.8	13.1

Analysis of the OR between the α grains and δ hydrides compared with the hydride OR (see Figure 119 B) indicates that δ_1 and δ_2 both originate from α_2, whilst δ_3 and δ_4 originate from α_3.

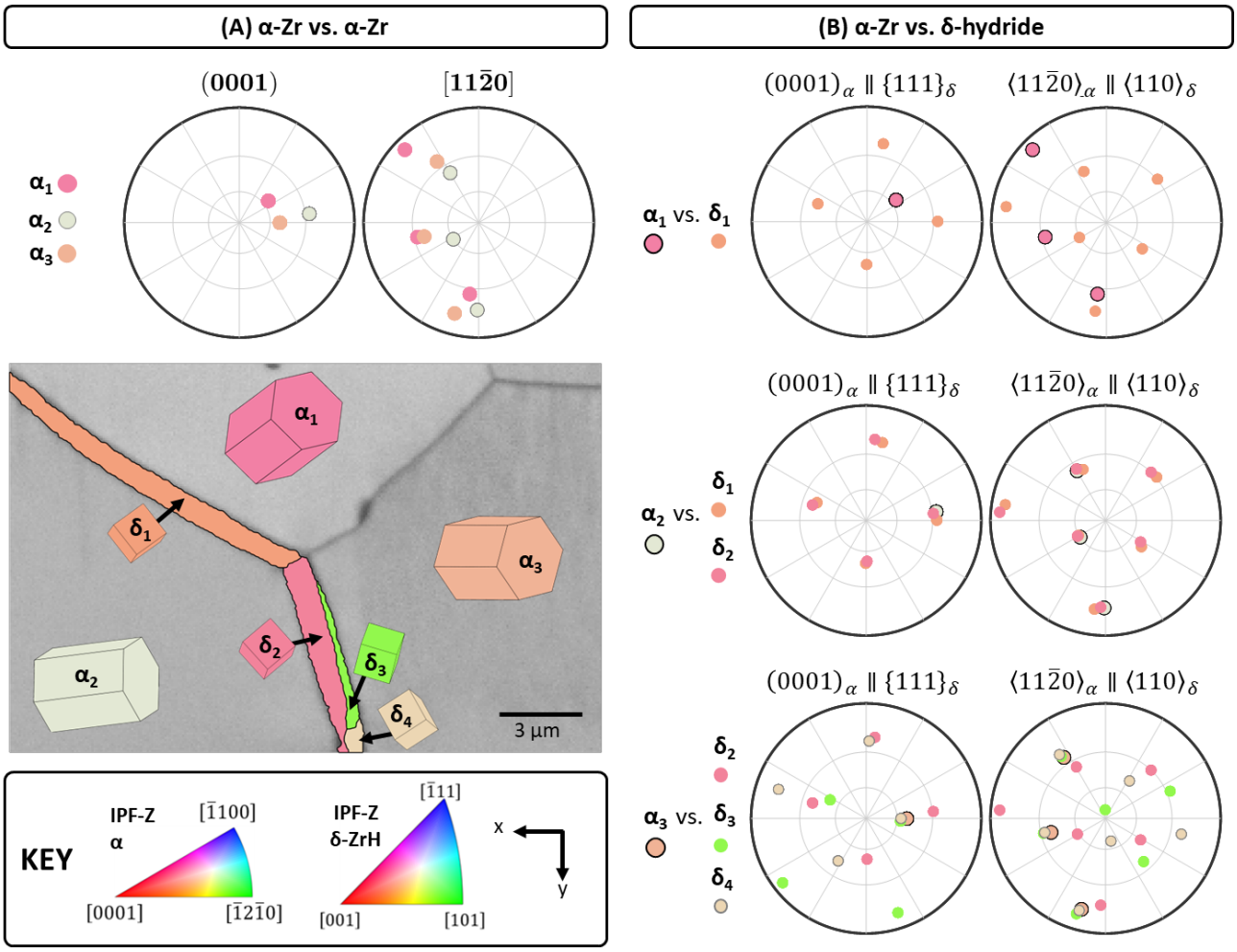


Figure 119 - Orientation relationships in the triple junction grain boundary map: Pole figure analysis of (A) α-Zr/α-Zr OR; (B) α-Zr/δ-hydride ORs. Pattern quality map with hydride grains overlaid using IPFZ colouring and labelled prisms (IPFZ colouring) are also included for reference.

It is possible also to characterise the misorientation between δ/δ (hydride) pairs, as shown in Figure 120. Here there are two cases: (1) between hydrides that originate from the same α grain (δ_1 & δ_2, δ_3 & δ_4); (2) between adjacent hydrides associated with different α grains (i.e. δ_2 and δ_3).

For the hydrides that originate from the same grain: δ_1 and δ_2 are closely aligned, with a misorientation of ~ 5 ° whilst δ_3 and δ_4 share a common $\langle 111 \rangle_\delta$ direction, and multiple $\{110\}_\delta$ planes, indicating that they are twins. It is likely that δ_2 grew from δ_1 first (hence the larger hydrides) and δ_3 grew from δ_4, with δ_3 being the accommodating hydride between δ_2 and δ_4, hence the tapering off. Looking at the trace of the grain boundary, and the perpendicular bisector, a $\langle 110 \rangle_\delta$ direction is found on the bisector line for both δ in both cases. This indicates that the habit plane between these hydrides is a $\langle 110 \rangle_\delta$ direction.

For the adjacent hydrides associated with different α grains, the only shared direction (of those evaluated) is $\langle 112 \rangle_\delta$ where there is a 4 ° difference. Looking at the grain boundary trace and the perpendicular bisector, again the $\langle 112 \rangle_\delta$ direction appears to be key, with $\langle 112 \rangle_\delta$ directions from both δ_2 and δ_3 on the

bisector line, indicating that this is the habit plane in this case. Note that the other similar pair, δ_2 & δ_4 pair is not analysed as the interface has a high degree of curvature preventing use of a grain boundary trace.

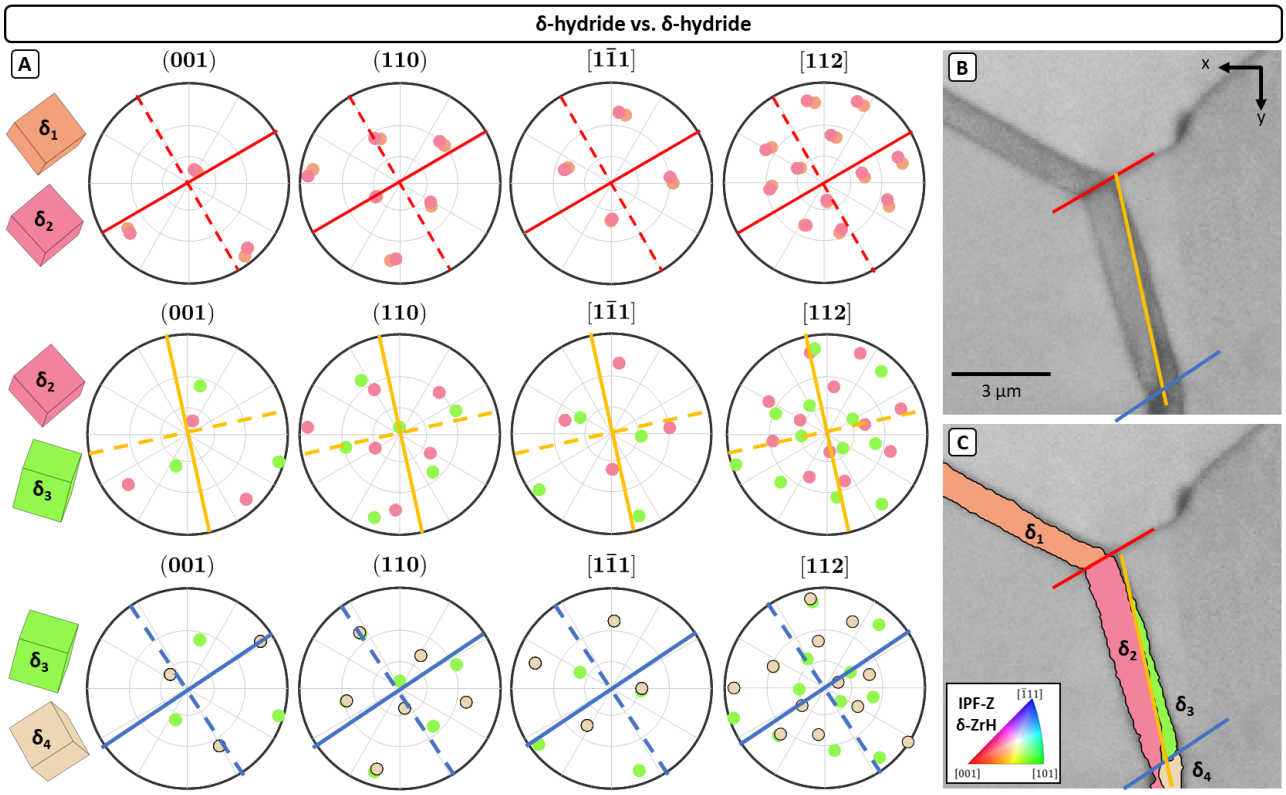


Figure 120 - δ/δ orientation relationships in the pFIB hydride map. (A) pole figures for δ_1/δ_2, δ_2/δ_3 and δ_3/δ_4, with grain boundary traces overlaid and the perpendicular bisector (which is a geometrical construction used to reveal the zone of the interface plane). Traces are solid lines and the perpendicular bisectors are dashed lines of the same colour; (B) pattern quality with inter-hydride grain boundary traces identified; (C) pattern quality map overlaid with δ hydride grains, using IPF-Z colouring.

HR-EBSD analysis is shown in Figure 121. The peak height map indicates that the hydride has poorer quality patterns than the matrix, and the righthand matrix grain has poorer quality patterns than the other two. The MAE map shows a significant concentration of deformation (indicated by poorer quality data) at the triple junction. All the other maps have been filtered to only show reasonable values, using a filter to remove points with a PH < 0.3, and a MAE > 5×10^{-4}.

The rotation tensor maps show that there is a lattice rotation associated with the hydride metal interface, and, to a lesser extent, the undecorated grain boundary. The stress field maps show a stress concentration at the top interface of the triple point, which is spatially localised to within 1.5 µm of the interface.

In the GND density map, the stress concentration has a corresponding peak region, but the hydrides also show higher (and fluctuating along the length) values than the surrounding matrix.

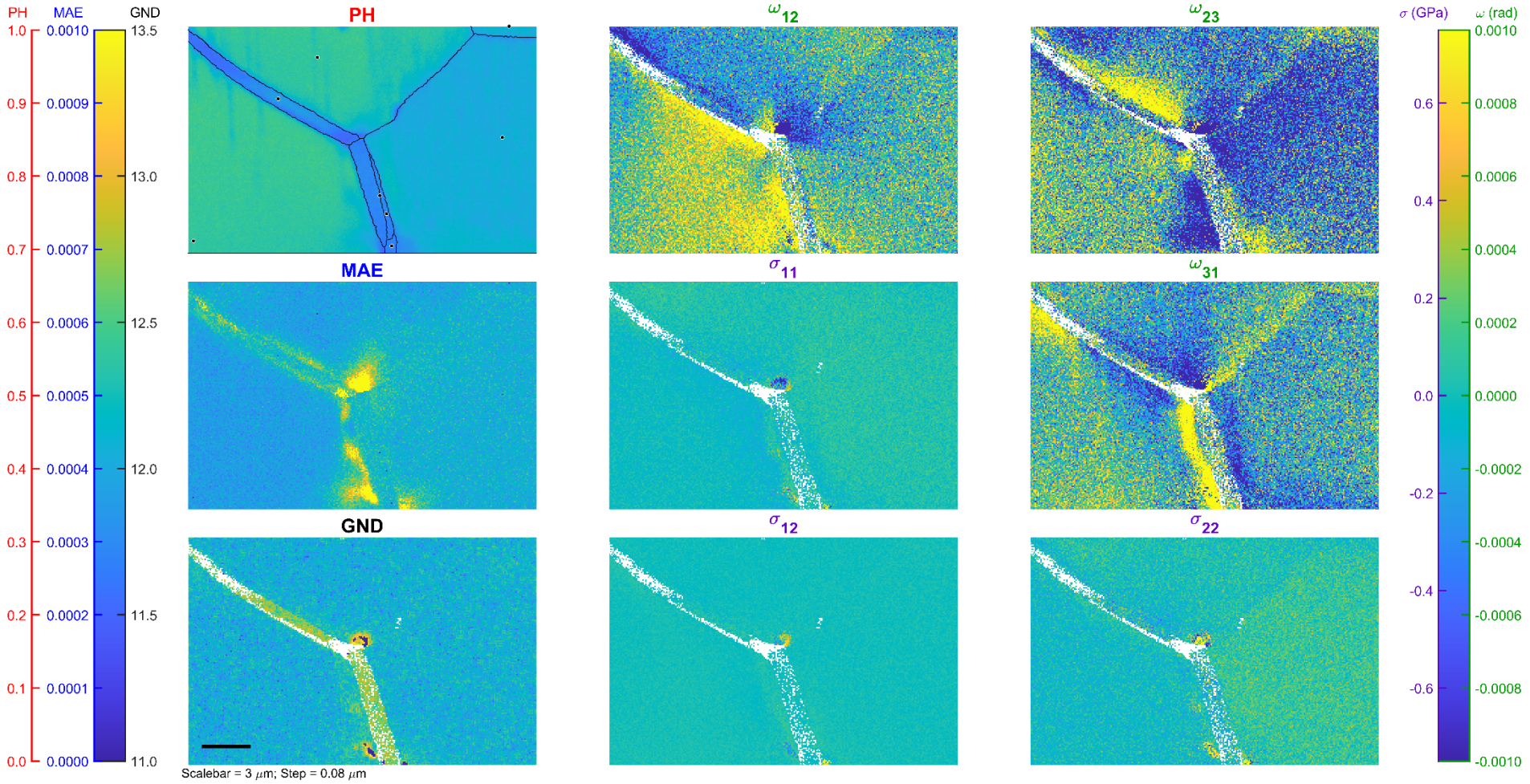


Figure 121 - HR-EBSD analysis of triple junction hydride. PH = peak height with reference points per mapped region plotted; MAE = mean angular error; GND = sum of GND density across all slip systems; components of the rotation (ω_{ij}) and in-plane stress tensor (σ_{ij}). Maps are plotted against different colour scales. The stress tensor and rotation tensor maps are shown with respect to the reference points.

8.2.2 Hydrides that protrude into the Zr matrix

Two examples where the grain boundary hydride protrudes into the matrix: pinch off from smooth grain boundary hydrides, and hydride 'spikes' protruding from the grain boundary.

8.2.2.1 Example 3: Pinch off hydride

In this map, there are two α grains with the grain boundary decorated by two hydride grains that nicely align with the grain boundary until they pinch off into the matrix at opposite ends of the hydride region (same angle into the matrix). On the righthand side of the mapped area, there is another region showing similar but less defined trends – the important point being that the hydride pinching off into the matrix is at the same angle and into the same grains. Note that the map is spatially distorted due to drift during mapping – the insert at Figure 122 B shows the undistorted forescatter image of the hydride.

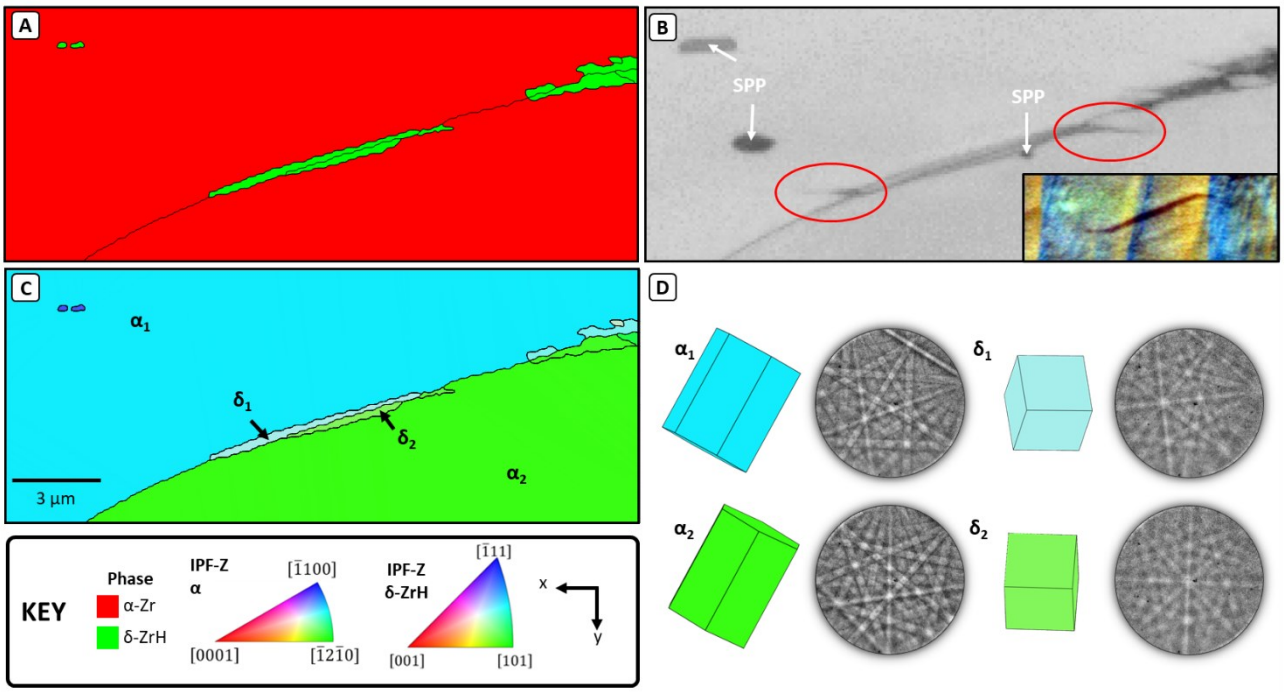


Figure 122 - Orientation analysis of the pinch off hydride map.(A) Indexed phase map; (B) pattern quality map with SPPs indicated and red ovals highlighting the pinch off sections of hydride (insert: forescatter image of the hydride); (C) crystal orientation (IPFZ coloured) along with labels for key grains; (D) prisms and representative patterns for the identified grains.

Figure 122 shows the orientations of the two adjacent α grains and the two main δ hydrides decorating this boundary. The pinch off sections are not visible on the orientation map (Figure 122 C) as they are too thin, but they are clearly identifiable on the pattern quality map due to the reduction in pattern quality compared to the matrix – they are also visible in the forescatter image. The orientations for the pinch off sections are assumed to be that of the hydride grain that they come from. The α orientations again appear close in orientation (see Figure 122 D) whilst the δ orientations also appear to be related, with a similar (001) plane orientation seen in the prisms.

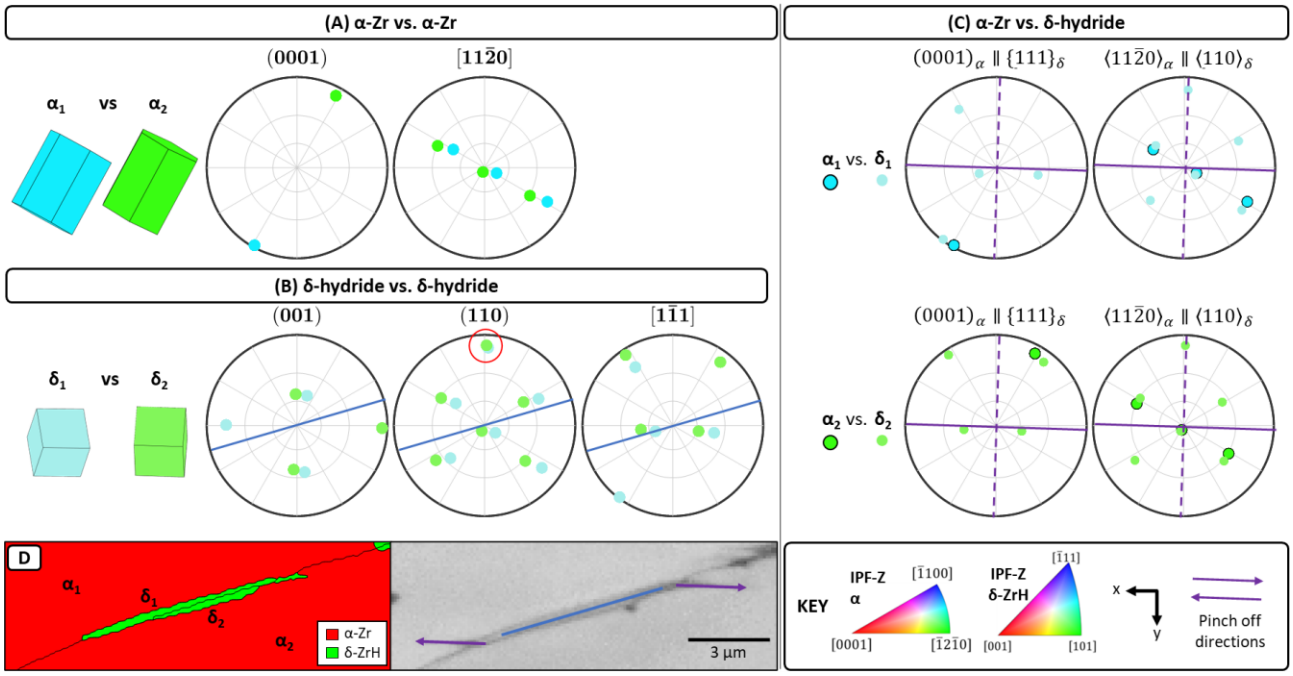


Figure 123 - Orientation relationships in the pinch off hydride map. Pole figure analysis of (A) α-Zr/α-Zr OR;(B) hydride/hydride OR – with common point indicated by red circle and grain boundary trace overlaid; (C) α-Zr/δ-hydride OR – with pinch off direction (purple solid line) and zone of interest (dashed purple line) overlaid. (D) Phase map with grain labels and pattern quality map with pinch off directions and δ/δ interface line annotated.

Analysis of the orientation relationships in this map are found in Figure 123. α_1/α_2 have a similar basal plane with a slight rotation between $\langle 11\bar{2}0\rangle_\alpha$ directions, similar to those seen in Figure 119 for the decorated α/α grain boundaries. δ_1/δ_2 have a shared $\{110\}_\delta$ plane and are rotated about this, by the same amount as α_1/α_2, suggesting that the two hydrides originate from different α grains (i.e. α_1 and δ_1 / α_2 and δ_2). In both cases, the hydride OR analysis in Figure 123 C fits well for $\langle 11\bar{2}0\rangle_\alpha \parallel \langle 110\rangle_\delta$ but not for $(0001)_\alpha \parallel \{111\}_\delta$. Future analysis will investigate alternative hydride/α-Zr ORs.

The pinch off point directions into the matrix are indicated in Figure 123 D using purple arrows, and these are overlaid on the α vs δ pole figures in Figure 123 C, along with a perpendicular line indicating the zone of interest. This analysis indicates that both δ_1 and δ_2 have a $\langle 111\rangle_\delta$ direction along the zone of interest. It is also notable that these directions are very similar to an edge in the cubic crystal (i.e. [001] direction).

Figure 124 shows HR-EBSD analysis for the pinch off hydride map. The PH map again indicates that the hydride has poorer quality patterns than the matrix, as is the case for the SPP far away from the hydride. The pinch off hydride regions are also identifiable in the PH map, showing a lower value than the surrounding matrix. The MAE map shows concentrations between the pinch off hydride and the α/α grain boundary, and extending from the tip of these points. All the other maps have been filtered to remove points with a PH < 0.3, and a MAE > $5\text{x}10^{-4}$.

There are two regions of the hydride that are interesting in the HR-EBSD maps, (1) the two hydrides along the α grain boundary; (2) the two individual hydrides as they protrude into the grains.

For the hydrides along the α/α grain boundary, the rotation tensor maps show a similar trend to the previous examples, with a lattice rotation associated with the hydride metal interface. In this case this is more notable in the lower α grain, at the interface with δ_2. Here, the peak region magnitude reaches +/- $5x10^{-3}$ rad, and spatially extends ~1 μm from the boundary. Within the hydrides, the rotation tensor maps are relatively neutral along the length.

Along the smooth hydride region, the stress field maps show fluctuations of up to ~400 MPa with the highest values localised to within <0.5 μm of the α/δ interface, again to a slightly greater extent in the lower α grain. The stress fields are of opposite magnitude relative to their reference point in the α grains above δ_1 and below δ_2. GNDs are higher in the hydrides along this region compared to the matrix.

To explore the stress fields near the tips of the hydrides as the protrude into the grains, two zoomed areas (taken from the previous map shown in Figure 124) are reproduced in Figure 125 and Figure 126 to assist in the analysis of these subtle but exciting maps.

Figure 125 shows the HR-EBSD analysis for a zoomed in area on the lefthand hydride pinch off region (end of δ_1 in Figure 122). In this region, the hydride extends away from the grain boundary at an angle of approximately 20 ° (also 20 ° from the long axis of the hydride), and approximately along the $\langle 001 \rangle_\delta$ crystallographic direction which is ~ along the x axis in Figure 125.

The PH and MAE maps in Figure 125 show that the data is reasonable for the matrix region near to the hydride, and also provide a visual indication of where the hydride tip is located.

The field map showing the density of GNDs is also spatially structured in the matrix, indicating that the GNDs may be related to the formation of low angle boundaries or slip activity on specific slip planes, related to the formation of the hydride and the shape & crystal orientation of the hydride and matrix phases. It is notable that these GNDs extend near the grain boundary, and away from the hydride tip, but they are not located in the matrix above the hydride-matrix interface (α_1/δ_1 – see Figure 122 for labelled figure).

The lattice rotation fields (ω_{ij}) show heterogeneous lattice rotation associated with the tip of the hydride that extends horizontally away from the grain boundary and into the matrix phase. Note that these fields are measured relative to the reference point, and so variations (rather than the absolute values) in these maps are important. For the rotation fields, at the tip of the hydride there are two 'lobes' of +/- lattice rotation that extend +/- 30 ° and this is most easily seen in the ω_{23} field.

The spatial gradient of the lattice rotation field can be explained by (and is used to calculate the) storage of GNDs, and with a good model, these fields can be used to explore how much accommodation strain is required around an embedded hydride that forms in the solid state at elevated temperature.

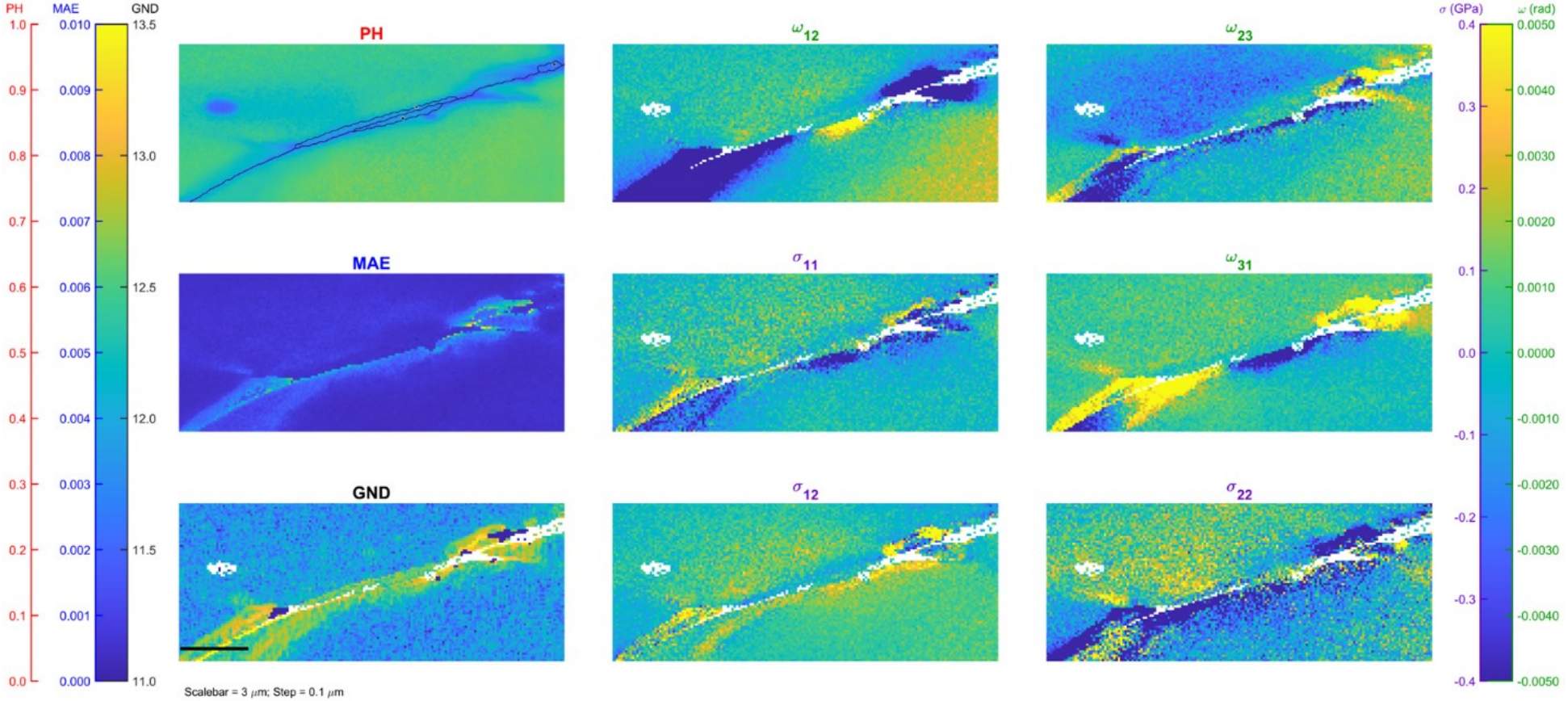


Figure 124 - HR-EBSD analysis of the pinch off hydride map. PH = peak height with reference points per mapped region plotted; MAE = mean angular error; GND = sum of GND density across all slip systems; components of the rotation (ω_{ij}) and in-plane stress tensor (σ_{ij}). Maps are plotted against different colour scales. The stress tensor and rotation tensor maps are shown with respect to the reference points.

Similar to the lattice rotation fields, the stress fields (σ_{ij}) are measured with respect to the reference pattern and so only show the (in-plane) type 3 stress variations. These stress variations are asymmetric above and below the tip of the hydride, and their extent spatially aligns with the rotation fields. For example, it is noticeable that the σ_{22} stress (i.e. the stress along the Y axis) in the upper lobe of the deformation field near the hydride tip is positive (i.e. relative tension) as compared to the lower lobe. Furthermore, the stress fields and rotation fields nearer the grain boundary are modulated strongly by the grain boundary and the presence of the hydride protrusion.

The residual stresses measured here are up to +/- 400 MPa which may be considered high for Zircaloy-4 (yield stress = between 241 and 455 MPa [9], [175]) but note that locally higher stresses may be found if there is residual work hardening (i.e. dislocation structures that increase the stored stress state prior to further plastic strain) and that zirconium has anisotropic plastic deformation, which can result in locally higher stresses (as plastic deformation can only relieve the shear stress on a specific slip plane/combination of shear stresses).

These lobes of high stress, GND activity, and lattice rotation typically extend ~1.5 μm away from the hydride tip. The distance indicated here will be slightly affected by the resolution of the method (i.e. a stress applied to an elastic solid will asymptotically approach zero far field stress) and the choice of colour scale. In future work, these fields will be quantitatively analysed by rotating components of the deformation tensor into a crystallographically significant reference frame (e.g. similar to the slip band and grain boundary work of Britton and Wilkinson [176]).

Figure 126 contains the area around the other pinch off hydride tip, this time for α_2/δ_2 (see Figure 122). The two hydrides (δ_1 and δ_2) have grown sympathetically along the grain boundary and pinch off at opposite ends, at approximately the same angle into the matrix in both cases, i.e. along the x axis. This leads to some interesting similarities and differences. The maps are spatially similar, although flipped (hydride points to the right instead of the left), with similar length into the matrix and angle relative to the grain boundary. The rotation and stress fields show the +/- lobes at the hydride tip and are of similar magnitude.

The main difference is that the +/- regions are opposite in both ω_{ij} and σ_{ij}. For example, ω_{31} in Figure 126 has a positive value between the hydride and α/α grain boundary, with negative values on the α_2 matrix side of the hydride, whereas ω_{31} in Figure 125 has the opposite. These differences are seen because the hydride that forms results in a different accommodation of the misfit strain in the α-Zr matrix. This is likely due to the difference in α grain orientation – there is a ~7 ° difference in $(0001)_\alpha$ with ~16 ° minimum angle between $\langle 11\bar{2}0\rangle_\alpha$ directions between α_1 and α_2 (see Figure 123).

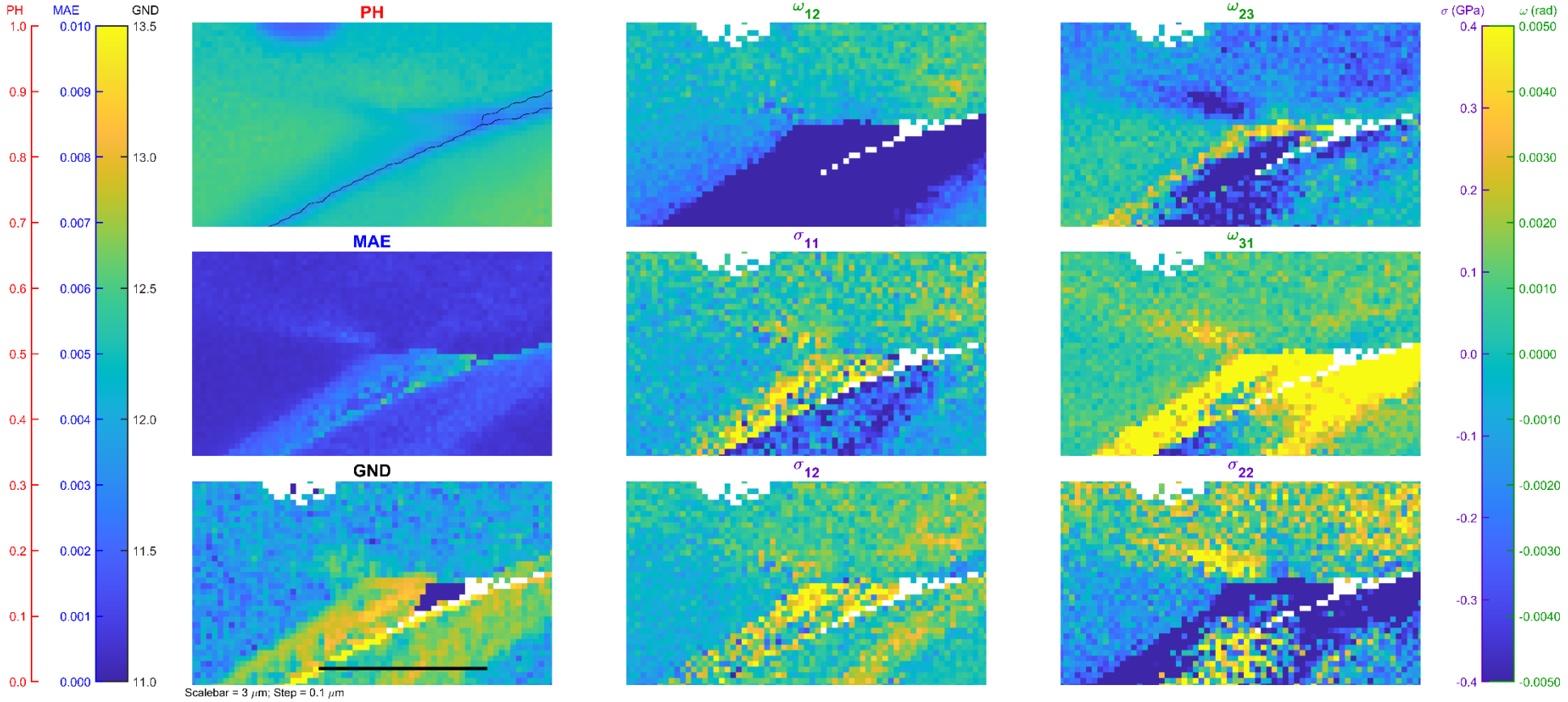


Figure 125 - HR-EBSD analysis of the pinch off hydride map – Tip 1. PH = peak height with reference points per mapped region plotted; MAE = mean angular error; GND = sum of GND density across all slip systems; components of the rotation (ω_{ij}) and in-plane stress tensor (σ_{ij}). Maps are plotted against different colour scales. The stress tensor and rotation tensor maps are shown with respect to the reference points.

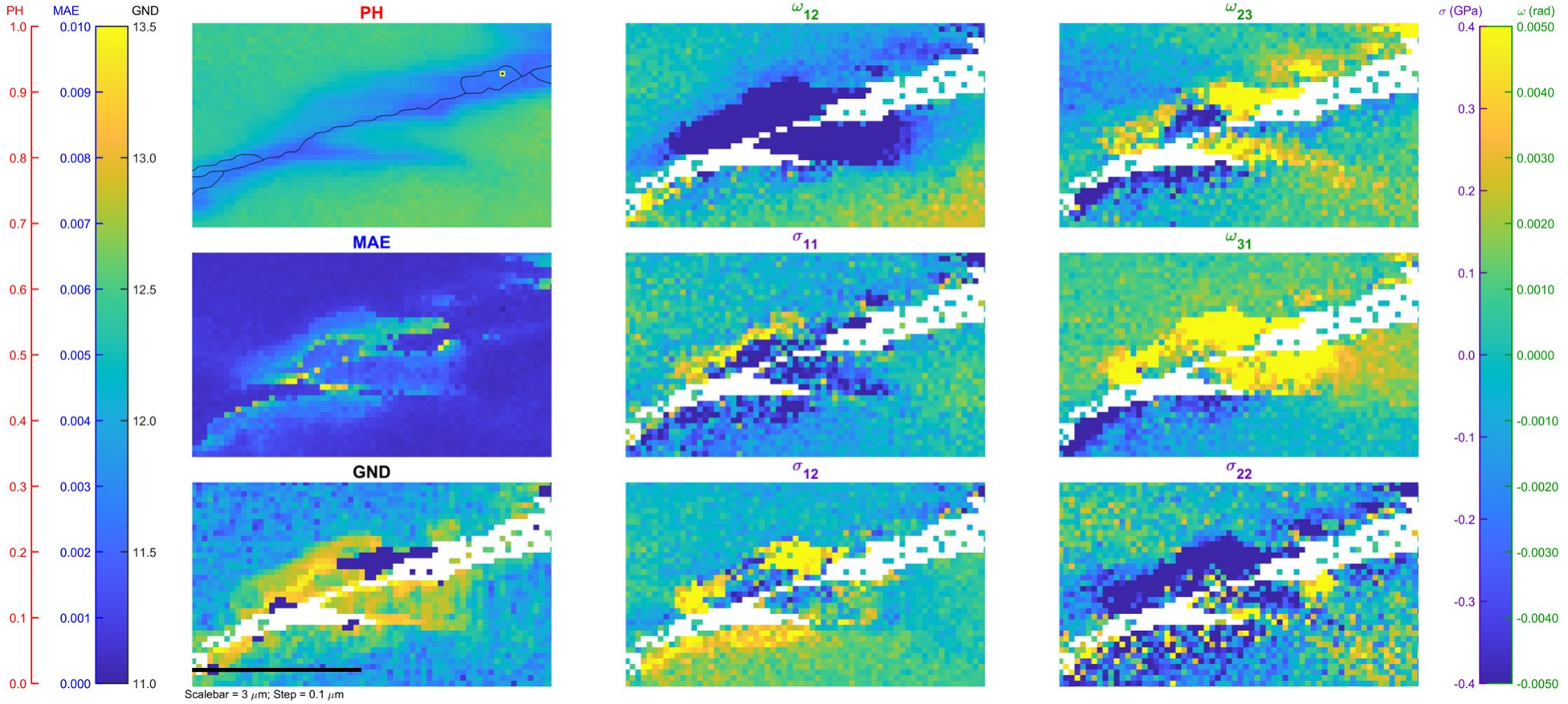


Figure 126 - HR-EBSD analysis of the pinch off hydride map – Tip 2. PH = peak height with reference points per mapped region plotted; MAE = mean angular error; GND = sum of GND density across all slip systems; components of the rotation (ωij) and in-plane stress tensor (σij). Maps are plotted against different colour scales. The stress tensor and rotation tensor maps are shown with respect to the reference points.

8.2.2.2 Example 4: Spiky hydride

The final example (Figure 127) is another region where there are thin spikes of hydride starting from the grain boundary and going into one of the two α grains. These hydrides do not show very well in the processed grain map (Figure 127 A & C) due to their size and aspect ratio, but they are visible in the pattern quality map (Figure 127 B). The hydride spikes protrude up to 13 µm into the matrix in this map at an angle of ~40 ° to the α/α grain boundary.

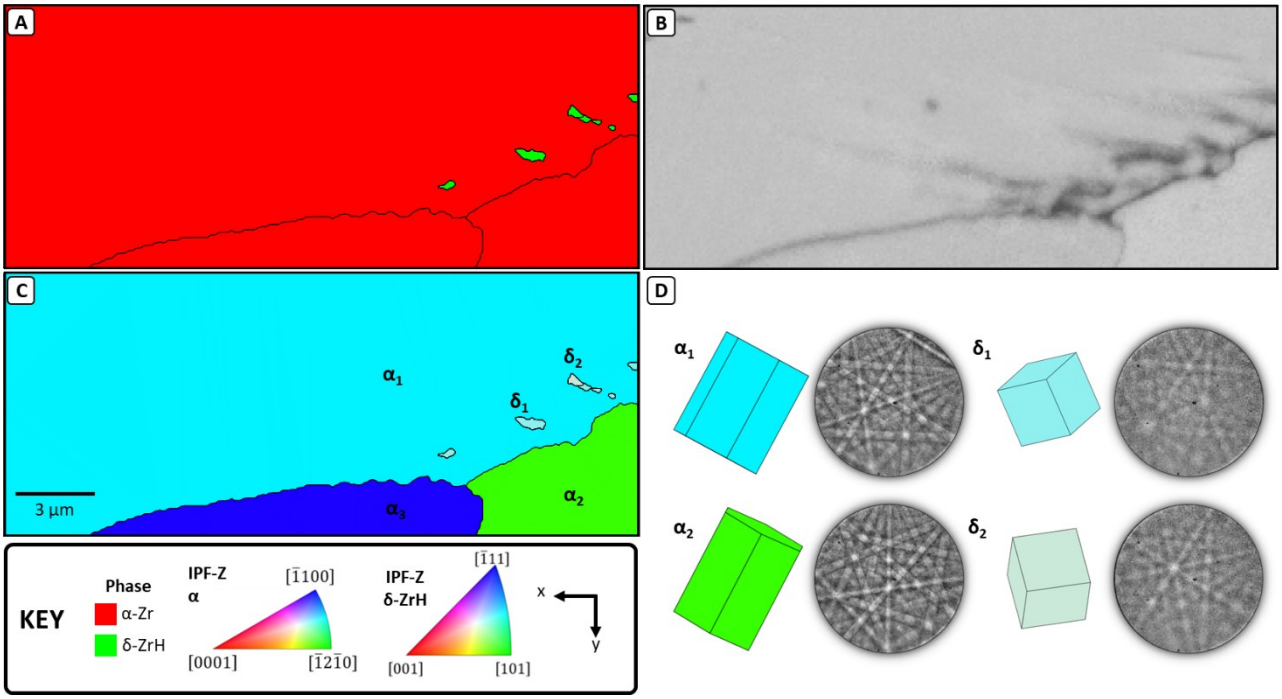


Figure 127 - Orientation analysis of the spiky hydride map. (A) Indexed phase map; (B) pattern quality map; (C) crystal orientation (IPFZ coloured) along with labels for key grains; (D) prisms and representative patterns for the identified grains.

Figure 127 contains orientation analysis for the two main α grains at this point, along with the two hydride orientations that index (in the widest sections of the hydrides). α_1 and α_2 have similar orientations, with a slight rotation (6 °) about $\langle 0001 \rangle_\alpha$ direction and similar basal planes. The δ hydrides appear to share a [111] direction about which they are rotated.

Analysis of the orientation relationships between the δ hydrides, the α grains, and the α/δ interfaces are shown in Figure 128.

The α grain pair have a common $\{10\bar{1}2\}_\alpha$ plane (2.7 ° angle between) and a similar basal plane direction (6.5 ° offset), rotated about this axis to give a 16.0 ° angle between the <a> directions. The δ grains (part of the same spikes) are twins, with a shared $\langle 1\bar{1}1 \rangle_\delta$ direction and three shared $\{1\bar{1}0\}_\delta$ planes.

Analysis of the α/δ OR (Figure 128 C) shows that both hydride phases fit very well with the hydride OR with α_1 which is expected considering both types of hydride protrude into α_1.

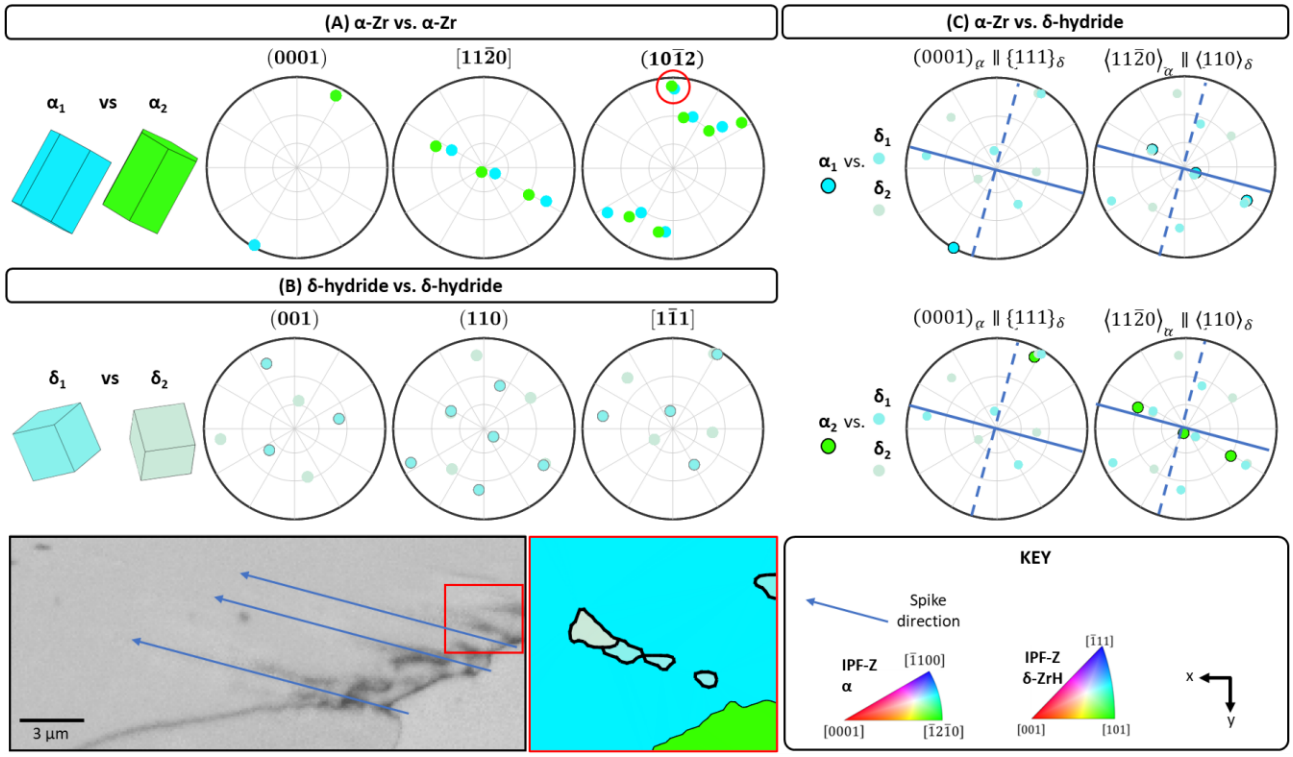


Figure 128 - Orientation relationships in the spiky hydride map. Pole figure analysis of (A) α-Zr/α-Zr OR;(B) hydride/hydride OR; (C) α-Zr/δ-hydride OR. (D) Pattern quality map with hydride directions annotated; (E) Zoomed in orientation map (IPFZ colouring) showing the two hydride orientations within a hydride spike.

HR-EBSD for the spiky hydride map is shown in Figure 129, where PH and MAE show that the data is reasonable. The PH map reveals the hydride locations, through the poorer quality patterns for the hydrides. All the other maps have been filtered to remove points with a PH < 0.3, and a MAE > $5x10^{-4}$.

Although there are multiple hydrides along this section of grain boundary which leads to come potential interactions between them, the general trends seen are similar to the previous example (Figure 124). Specifically, for the better defined hydrides, they resemble tip 2 in Figure 126 with similar trends in the lattice rotation maps (ω_{ij}) for the relative +/- regions. For the stress fields (σ_{ij}), again similarities to Figure 126 are seen, with negative stress values (relative to the reference point) observed between the hydride and the α/α grain boundary. These residual stress values are again seen locally to be +/- 400 MPa.

The biggest difference is the missing 'lobes' of +/- lattice rotation and stress in the maps in Figure 129. Although they are not immediately apparent, the zoomed in maps for one of the tips, shown in Figure 130, suggests that they are present, but much smaller in size and magnitude (see σ_{12} for example). This difference could be due to the relative hydride size, interaction of the multiple hydrides in the region, or the crystallographic orientations involved.

The map of stored GND density indicates that regions of high GND density are near the tips of the hydrides, and tend to extend ahead of each of the hydride tips. These GNDs seem to be confined to one crystallographic direction (or plane) which could be consistent with accommodation of the misfit strain ahead of the hydride.

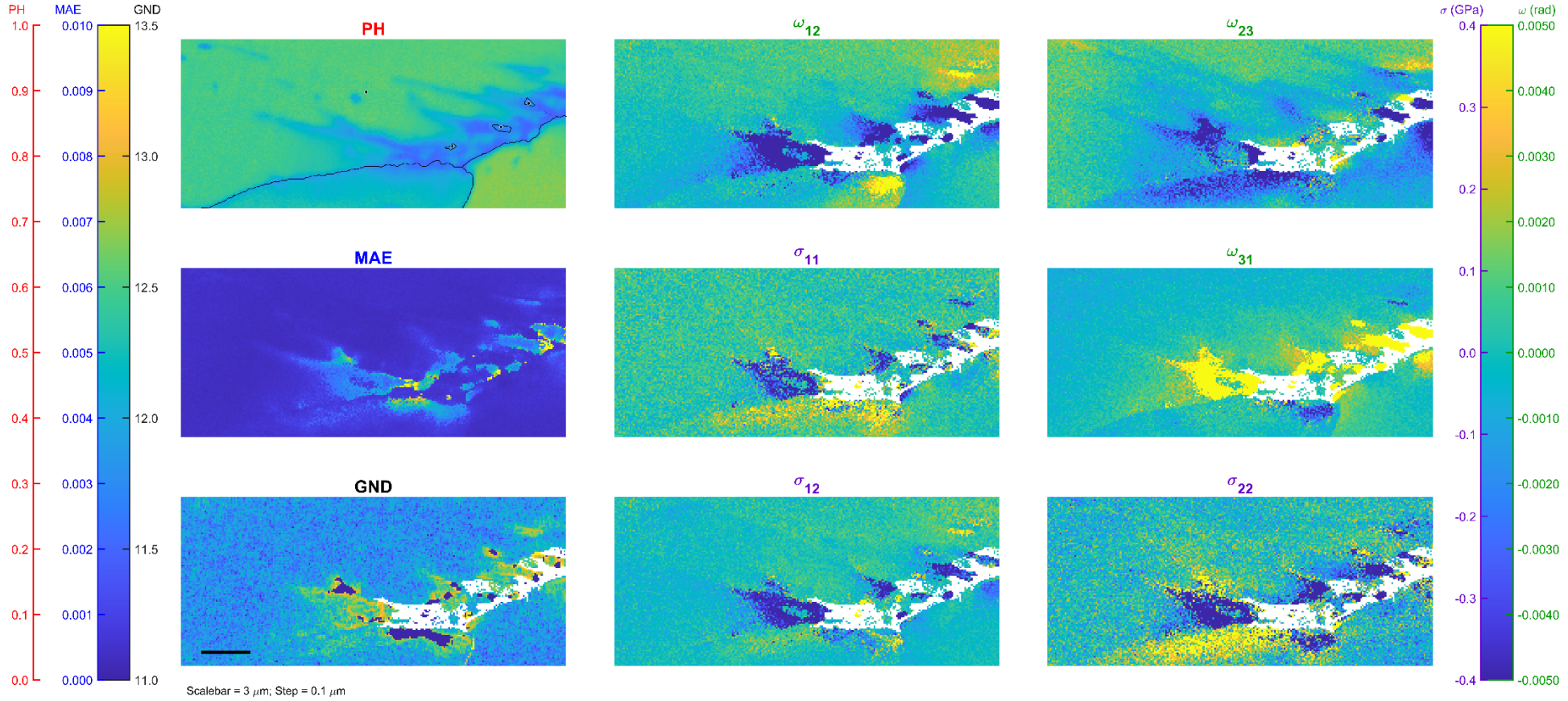


Figure 129 - HR-EBSD analysis of the spiky hydride map. PH = peak height with reference points per mapped region plotted; MAE = mean angular error; GND = sum of GND density across all slip systems; components of the rotation (ω_{ij}) and in-plane stress tensor (σ_{ij}). Maps are plotted against different colour scales. The stress tensor and rotation tensor maps are shown with respect to the reference points.

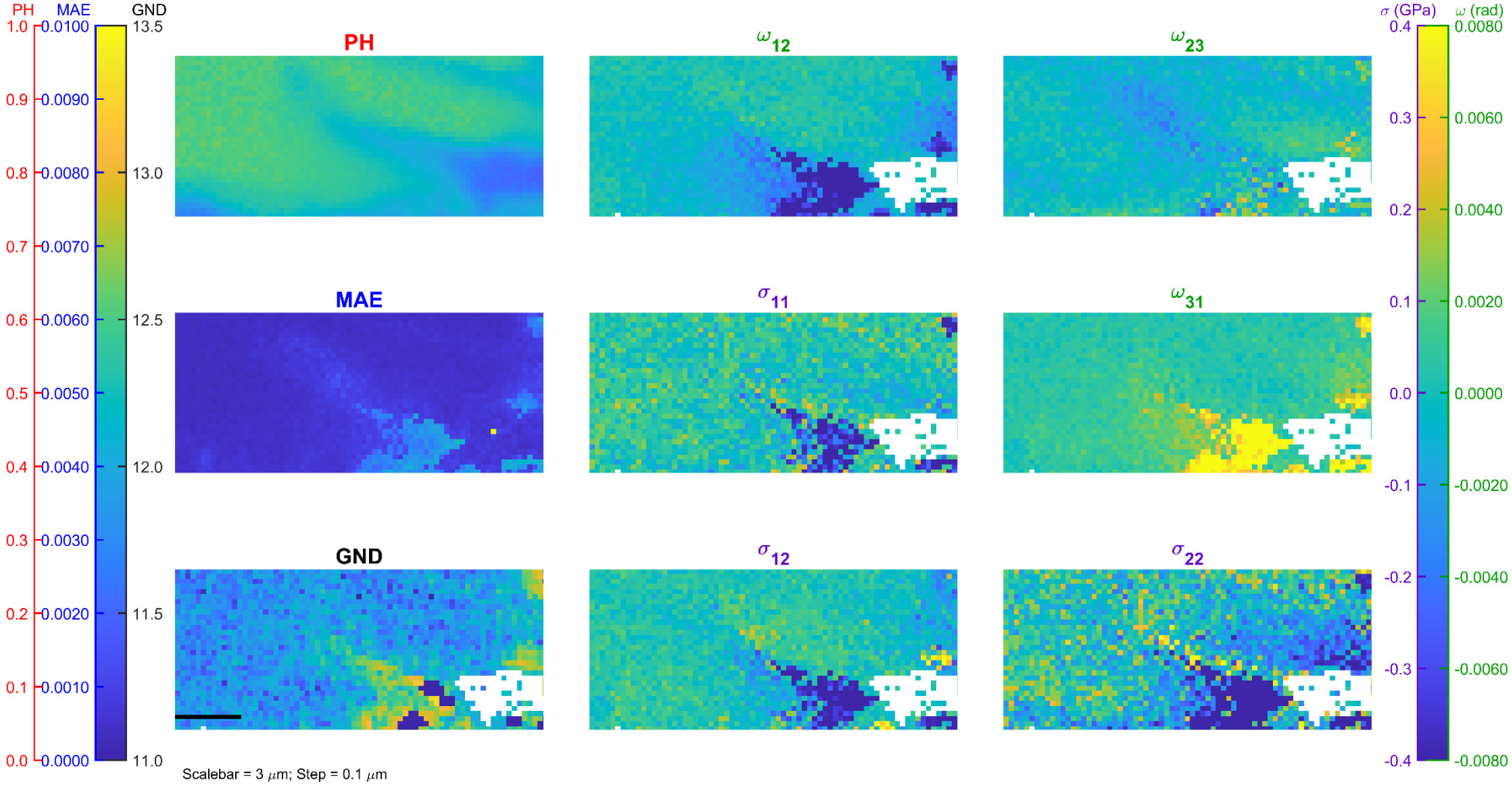


Figure 130 - HR-EBSD analysis of a section of the spiky hydride map. PH = peak height with reference points per mapped region plotted; MAE = mean angular error; GND = sum of GND density across all slip systems; components of the rotation (ω_{ij}) and in-plane stress tensor (σ_{ij}). Maps are plotted against different colour scales. The stress tensor and rotation tensor maps are shown with respect to the reference points seen in Figure 129.

8.3 Summary

EBSD and HR-EBSD mapping has been performed around α-Zr and δ-hydride interfaces. These hydrides are related to the α-Zr matrix via an orientation relationship which can be used to explain the shape and location of the hydride in each case. The hydrides investigated fall into two main types:

- **Smooth grain boundary hydride.** In the grain-boundary hydrides where the hydride smoothly decorated the α-Zr grain boundary, there are very small fluctuations near the grain boundary interfaces in stress, lattice rotation and GND density.
- **Hydrides that protrude into the Zr matrix.** In cases where the hydride extends into the matrix grain and away from the hydride, there are large stresses and stored GND density that extend ahead of the tip of the hydride.

For more complex hydride/matrix structures, and the deformation fields are consistent ahead of hydride tips of the same hydride type.

These results may enable enhanced understanding of the role of hydrides in fracture as well as stress-induced hydride reorientation, as likely found in delayed hydride cracking.

9 Discussion

The aim of this chapter is to discuss observations against each of thesis objectives, along with future work that could be insightful and add value beyond this thesis. This chapter is structured to address each of the objectives in turn.

9.1 Reconstruction of the prior-β microstructure

A reconstruction code was developed to for the α/β allotropic phase transformation in Zr using Burgers' orientation relationship. This code is available on GitHub[15] and a paper about it has been published [1]. The code is split into two sections: reconstruction and post processing.

9.1.1 Reconstruction

The reconstruction section is adapted from a steels-based code developed by Nyyssönen [108], [109] and uses grain boundary misorientations and comparison to BOR α-α variant misorientations, along with the MCL algorithm to cluster α grains together and reconstruct the parent β microstructure. Whilst there will always remain uncertainties with the reconstructed microstructure (particularly in 2D), the uncertainty is interrogable in the ParentBOR code, with alternative orientation options calculated.

It is worth noting that parent grain reconstruction was developed and incorporated into MTEX (MATLAB toolbox) along a similar timeline (slightly behind) to the ParentBOR development, with one of the three (as of Jan 2022) versions also based on Nyyssönen's work. This is useful, given that there are now multiple freely available codes where the results can be compared, and areas of uncertainty reduced.

The reconstruction section was extensively used throughout the grain growth sections, both for the *in situ* and *ex situ* results where it provided clear insight into the growth mechanism from one prior-β region into another (see chapters 6 and 7).

9.1.2 Post processing

The post processing section allows identification of the α variants associated with each prior-β grain, and then subsequent identification α variants with shared planes and/or directions. This is useful to allow further detailed analysis of microstructures, as in the case of the (initial onset of) blocky-α grain growth, where it was used to develop a grain growth hypothesis between α variants. At present it is only possible to compare α variants within prior-β domains, not across the map, so this could be considered for future development.

9.1.3 Future development

Future work may involve making the post processing section standalone to use with alternative reconstruction code outputs e.g. the in-built MTEX versions, including the latest variant graph approach version [177]. This would be particularly useful for working with larger datasets, where the ParentBOR code

[15] https://github.com/ExpMicroMech/ParentBOR

may struggle, whereas in-built MTEX codes have been optimised and can quickly reconstruct larger maps. A smaller subset of the map could still be compared using both reconstruction methods to compare, particularly where there is uncertainty.

9.2 Grain growth in weld microstructures

Complementary *in situ* (interrupted heat treatments up to 70 mins) and *ex situ* (4 hr heat treatment) experiments were carried out to investigate blocky-α grain growth within the weld region of electron beam welded Zircaloy-4 samples.

9.2.1 Grain growth location

The region where blocky-α grain growth occurs is limited to the weld region, as observed in prior work [44], [125]. Macroscopically this appears to start at the edge of the weld region, in the HAZ, and in the central fusion zone, along the weld centreline. It was also observed that the cooling rate affects the growth, with more blocky-α seen in the lower half of the weld region. This is not surprising that there are differences between the upper and lower half of the weld region in this case, due to the different cooling rates. β quenched microstructure is very sensitive to cooling rate, with microstructure type and α lath width dependent on cooling rate [32], [33] (and composition [31], [34], [39]).

There is good evidence that the blocky-α grain growth is related to the prior-β grain boundaries, which fits well with literature (e.g. [2]).

9.2.2 Grain growth mechanism

The grain growth mechanism observed in this work is growth from one prior-β grain into another prior-β grain via an α grain at the edge of the first prior-β grain (see section 7.3.2). This was observed for all samples, with no growth initiation observed away from the prior-β grain boundaries. This contradicts work by Washburn [2] who stated that growth into neighbouring prior-β grains was rarely observed. However, as Washburn's work used optical microscopy, it is likely that the same mechanism of grain growth from the prior-β grain boundaries was observed (as noted in the paper), but the origin of the grains mis-assigned.

The growth of the blocky-α is suggested [48] to be nucleation and growth, via SIBM, which fits well with the grain growth observed.

9.2.3 Onset of grain growth

This work was not able to ascertain the reason for why grain growth occurs at certain boundaries, or into certain prior-β domains.

There were two consistent observations made about this growth into the new prior-β domain: (1) the pattern quality is poor in the region where the grain grows into; (2) the grain boundaries in the region into which it grows are short and curvy. These factors indicate high energy regions into which the grain grows, lowering the energy of the region, as indicated by the significantly improved pattern quality (defect free) of the growing α grain when it grows into these regions.

It is also worth noting that the blocky-α growth initiation occurs with time, as seen in Figure 131. Here new blocky-α grain growth initiation is seen after HT2 that was not observed after HT1. Therefore multiple HT steps (and EBSD) may be required to ascertain why certain grains grow.

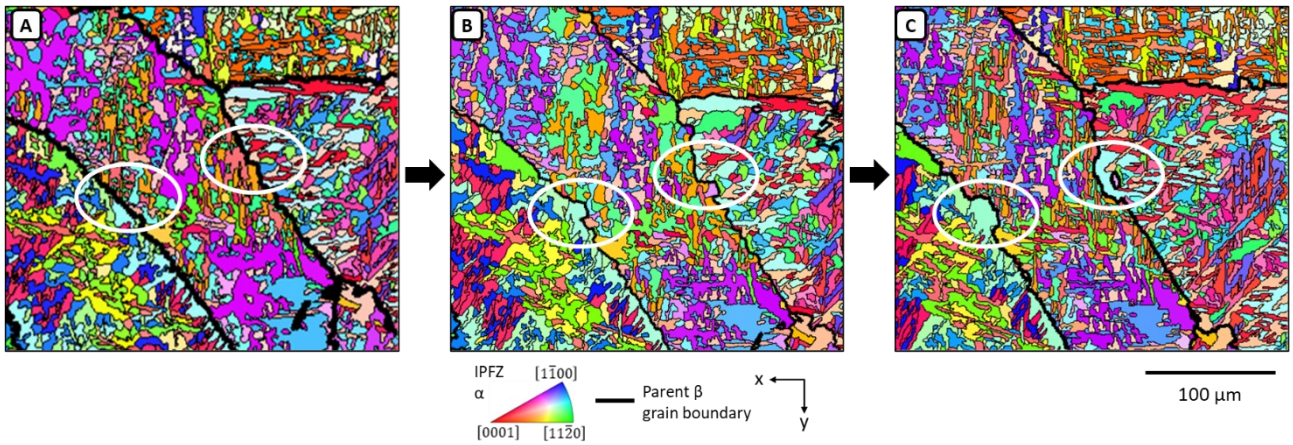


Figure 131 - Blocky-α grain growth initiation with time. Orientation maps using IPFZ colouring showing grain growth along prior-β boundaries (thick black lines) with time: (a) initial microstructure; (B) after heat treatment 1; (C) after heat treatment 2. The white ovals indicate the locations where growth occurs.

To successfully address the challenge of identifying initial nucleation sites, there will need to be greater number of heat treatment experiments to provide statistical insight in the boundaries that promote blocky-α grain nucleation, as well as snapshots of the microstructure growth as it emerges from single variants at the prior-β grain boundaries. Faster EBSD mapping and higher temperature phosphors could assist this further.

9.2.4 Factors affecting grain growth

As the grains grow within the new domain, growth is pinned by 'cross' points of α grains and long straight α grains. The long, straight α grains are likely to have lower energy grain boundaries and therefore be less favourable for growth. Again, this supports an argument that grain growth of blocky-α domains into regions is driven by the consumption of regions that have higher stored energy.

Based on literature (e.g. [31]), these 'cross' points may be nucleation points caused by SPPs within the prior-β grains, with different variants growing outwards (along $\{110\}_\beta$) from them. There is some evidence of potential SPPs at the centre of these point in the pattern quality maps (see Figure 108 on page 146) based on the decrease in pattern quality, but without knowledge of the SPP content of the material, it is difficult to say conclusively. These points may pin the growth due to the variety of unconnected (i.e. no shared plane or direction) α grains that meet/start at these points, preventing easy grain growth.

These pinning points can be overcome, though the mechanism is unclear from the data. It is possible that they can be consumed (instead of pinning) from a certain direction that shares a common plane/direction with the α grains that form part of this structure.

There is also evidence of certain directions causing pinning (e.g. see orange grain in Figure 106 on page 144) as the grains are consumed, however this needs further investigation.

9.2.5 Growth within new β domain

Analysis of the α variants within the parent β grains showed that there is often a growth pathway via shared planes and directions. A model has been proposed for growth of the α grain once it has crossed into the new prior-β domain. Specifically, this is growth in groups of α variants with shared $\langle 11\bar{2}0\rangle_\alpha$ directions, with growth between these groups via shared $(0001)_\alpha$ planes. This model works well for the small areas tested, but has yet to be tried on a whole prior-β domain. This process was done manually to take into account known sources of pinning.

9.2.6 Completion of grain growth

Completion of blocky-α grain growth would be interesting to investigate in more detail. Washburn[2] suggests that with enough time, the grains would reach their ultimate size and become equiaxed, with smooth grain boundaries. In their work, after 10,000 min (~167 hrs) at 800 °C, irregular grain boundaries and varying grain sizes across the material were seen. Tong [138] heat treated Zircaloy-4 for up to 336 hrs, to complete coverage of blocky-α, but still observed both variation in grain size and wavy, irregular boundaries. Another possibility is that the grain growth stops when blocky grains touch each other, as suggested by Tong's work. The *in situ* results for experiment 3 provide an interesting example to look at in Figure 132. In this case, there were two heat treatments[16] with EBSD mapping (at room temperature) after each which gives a view of progressive grain growth.

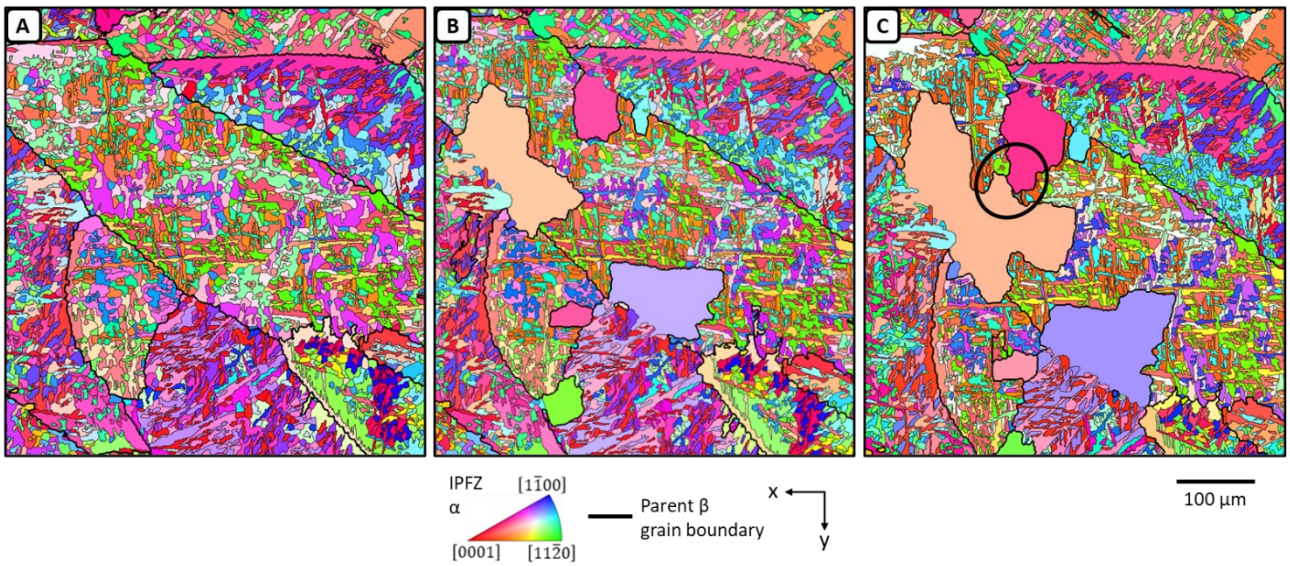


Figure 132 - Multiple α grains into same β domain. Experiment 3 example showing four (orange, pink, lilac and blue) α grains that grow into the same β domain. Orientation maps (IPF-Z colouring) shown for (A) the initial microstructure, then after (B) HT1 and (C) HT2. All maps overlaid with reconstructed parent β grain boundaries as thick black lines.

Figure 132 shows four α grains growing into one prior-β region, which grow inconsistently with the heat treatments. The orange and pink grains collide in Figure 132 C and a relatively straight grain boundary between the two is seen. This could support the argument for the grain growth stopping when blocky

[16] HT1: 3x 10 min cycles at 765 °C; HT2: 1x 10 min + 1x 20 min at 790 °C [sample surface temperature readings]

grains touch, but this would require another heat treatment to confirm.

Looking at the *ex situ* data, with the longer (4 hr) heat treatment, sub-division of prior-β domains by blocky-α grains is regularly observed (e.g. Figure 98 on page 134), this would support blocky growth stopping when the growing grains collide, since we know from the *in situ* data that multiple grains can grow into the same prior-β region.

The inconsistent growth of the α grains suggests that there is competitive growth, with some grain orientations growing quicker than others. This could potentially be due to the α grain variants present locally and/or pinning points. For example, the small blue grain that grows in Figure 132 would be expected to grow further into the local region based on the grain growth model (the region it grows into has a larger area of shared $\langle 11\bar{2}0\rangle_\alpha$ α variants). Running the model with 4 starting grains until the point where the whole β domain was covered would be an interesting experiment as it is currently only tested on the small initial regions of growth. Across the maps, there are also smaller grains that do not grow, for example the necklace of grains in the HAZ (see Figure 97 on page 133), this is not unusual for blocky-α growth, with small island grains being common [48].

An interesting point to note is that there are several cases where blocky-α grains appear to grow into multiple prior-β domains, sometimes after filling the initial β domain, and sometimes after growth is halted at another growing α grain. A better understanding of the grain growth initiation process may shed light on why this occurs in the future.

9.2.7 Further experiments

There are two potential future experiments that would be interesting:

- An *in situ* experiment with more steps (e.g. 30 min heat treatments x4 with EBSD at each step) to track the blocky growth over time. This could clarify the stopping mechanism and confirm the impact of grains colliding during growth.
- A much longer term heat treatment at 800 °C to establish whether the blocky-α grains become more equiaxed with smooth boundaries eventually (as suggested by Washburn [2]).

9.3 Hydride-matrix deformation fields

This section sought to explore hydride-matrix deformation fields at the µm length scale, including characterisation of the stress fields. This was achieved using EBSD and HR-EBSD to look at 4 examples of grain boundary hydride in blocky-α Zircaloy-4.

9.3.1 Sample preparation

Part of this work included comparison of sample preparation techniques for the final step prior to EBSD and HR-EBSD analysis. Cryo-BIB and cryo-pFIB cross-sections were trialled and both provided useable results for analysis in chapter 8 . Both techniques provided good results to work with, however, with further recipe development, pFIB polishing would be the preferred technique for optimal results due to the flatter surface

and 100% indexing in the well-polished region. Currently the area polished (approx. 30 x 15 μm^2) is only good enough to look at one or two hydrides whereas the BIB cross-section provided an area large enough (semi-circular region with max dimensions 2.3 x 0.6 mm) to contain multiple hydrides for analysis so worked well for this experiment. For targeted area analysis (e.g. to look at specific hydrides that protrude into the matrix, or specific grain boundary types), it may be useful to do a large area planar polish using BIB prior to localised pFIB polishing to locate the hydride, potentially with EBSD mapping in-between to identify grain boundary types.

9.3.2 Grain boundary hydride

Two 'types' of grain boundary hydride were evaluated: smooth grain boundary hydride and hydride that protrudes into the matrix. The latter appeared either as thin hydride 'spikes', or smooth grain boundary hydride that then 'pinched off' into the matrix.

9.3.2.1 Smoothly decorating grain boundary hydride

For smoothly decorating grain boundary hydride, HR-EBSD analysis showed very small variations in stress, lattice rotation and GND density associated with the (α/δ) grain boundary interfaces. These hydrides were much larger than previously analysed hydrides, however the behaviour is not unexpected due to both the misfit strain of the hydride (causing the stress) and the morphology of the hydride (it smoothly decorates the grain boundary).

9.3.2.2 Hydrides that protrude into the matrix

For hydride protruding into the matrix, there are large stresses and stored GND density that extend ahead of the tips of the hydride. These results show similarity to the experimental [84] and modelling [87] work on small lenticular hydrides within the α matrix.

9.3.2.3 Hydride OR

In most cases, the hydride OR used [55] fits very well with the data, however, in the case of the hydride that pinches off into the matrix, there is misalignment of the shared planes for this OR ($(0001)_\alpha$ and $\{1\bar{1}1\}_\delta$). This is not entirely unexpected as there are a few alternative ORs in the literature for α-Zr and δ-hydrides, so future work will look at alternative ORs that may fit better. Further similar examples would be required to ascertain whether this impacts the type of hydride growth seen (i.e. pinching off into the matrix).

9.3.3 Future experiments

Whilst this experiment explored a new hydride size and location for stress field analysis, this also served as proof of concept and paves the way to look at other hydride precipitation scenarios. For example, it would be particularly interesting to look at hydrided β quenched microstructures, using both the ParentBOR code to reconstruct the parent microstructure and categorise the grain boundaries, and the xEBSD code to evaluate the stress fields around the hydrides.

10 Summary

In summary, this thesis has looked at microstructural changes in Zircaloy-4 using a mixture of optical and electron microscopy. Work has focussed on two areas: grain growth in electron beam welds subjected to post-weld heat treatments; grain boundary hydride stress field and orientation relationship analysis. Supporting work to achieve this has included experimental method and code development.

Highlights include:

- Development of the 'ParentBOR' code [1] – used to reconstruct the parent β microstructure in Zr alloys, and analyse the α variants in the final microstructure.
- Development of an *in situ* heating experiment to observe the initial onset of blocky-α grain growth in the weld region using FSD imaging and EBSD.
- Recipe development for polishing Zr alloys prior to EBSD and HR-EBSD.
- Analysis of the onset of blocky-α grain growth, including location both within the weld region and with respect to the prior-β microstructure.
- Proposal of a grain growth mechanism for blocky-α growth within a prior-β domain.
- Analysis of grain boundary hydride (packets) in the μm size, with respect to orientation relationships (using MTEX) and stress fields (using xEBSD code).

Overall, this work has provided greater insight into the manufacturing and performance of Zircaloy-4 fuel cladding.

In terms of manufacturing, likely grain growth (size and morphology) can now be predicted from the initial weld microstructure. More is known about the location and mechanisms of grain growth, for example, the α grain growth is definitely associated with the prior-β grain boundaries (confirming earlier observations in β-quenched Zr alloys [2]), with the growing α grain moving outwards from one prior-β domain into another. A potential grain growth mechanism is also proposed for growth within the new β domain, although further study is required to ascertain why certain grains grow, and more information about what stops growth.

In terms of performance, a study was carried out looking at grain boundary hydride in blocky-α Zricaloy-4 using EBSD and HR-EBSD. Hydrides that smoothly decorate the α-α grain boundary interfaces and those that protrude into the matrix were investigated, with differences in the magnitude and spatial extent of stresses at the hydride interfaces seen. Whilst further analysis and/or data is required to draw solid conclusions, the measurement of the stress field, and patterns of lattice rotation and GND locations may help us to understand the role of hydrides in fracture as well as stress-induced hydride reorientation.

11 References

[1] R. Birch and T. B. Britton, “Effective structural unit analysis in hexagonal close-packed alloys – reconstruction of parent β microstructures and crystal orientation post-processing analysis,” *J. Appl. Crystallogr.*, vol. 55, no. 1, pp. 33–45, 2022, doi: 10.1107/s1600576721011584.

[2] D. F. Washburn, “Primary and secondary recrystallization of beta-quenched zircaloy-4,” 1964. [Online]. Available: https://www.osti.gov/biblio/4587077

[3] H. G. Rickover, “The decision to use zirconium in nuclear reactors,” *RPS2-EB*, pp. 9–17, 1975.

[4] T. Alam, M. K. Khan, M. Pathak, K. Ravi, R. Singh, and S. K. Gupta, “A review on the clad failure studies,” *Nucl. Eng. Des.*, vol. 241, no. 9, pp. 3658–3677, 2011, doi: 10.1016/j.nucengdes.2011.08.009.

[5] C. L. Withmarsh, “Review of Zircaloy-2 and Zircaloy-4 Properties Relevant to N.S. Savannah Reactor Design,” 1962.

[6] C. R. F. Azevedo, “Selection of fuel cladding material for nuclear fission reactors,” *Eng. Fail. Anal.*, vol. 18, no. 8, pp. 1943–1962, 2011, doi: 10.1016/j.engfailanal.2011.06.010.

[7] C. W. Solbrig, A. LaPorta, K. M. Wachs, and J. R. Parry, “Oxidation, Embrittlement, and Growth of TREAT Zircaloy-3 Cladding,” in *Nuclear Material Performance*, R. O. A. Rahman and H. E. M. Saleh, Eds. IntechOpen, 2016, pp. 57–88. doi: http://dx.doi.org/10.5772/62708.

[8] “Zircaloy-2 Zirconium Alloy,” *MatWeb Material property data*. https://www.matweb.com/search/datasheet_print.aspx?matguid=eb1dad5ce1ad4a1f9e92f86d5b44740d (accessed Jun. 29, 2022).

[9] “Zircaloy-4 Zirconium Alloy,” *MatWeb Material property data*. https://www.matweb.com/search/DataSheet.aspx?MatGUID=e36a9590eb5945de94d89a35097b7faa (accessed Jun. 29, 2022).

[10] “Zr-2.5Nb Zirconium Alloy, Nuclear Grade,” *MatWeb Material property data*, 2022. https://www.matweb.com/search/DataSheet.aspx?MatGUID=9c996807673f4208bc99c655c388072d (accessed Jun. 29, 2022).

[11] “Zirconium, Zr,” *MatWeb Material property data*. https://www.matweb.com/search/DataSheet.aspx?MatGUID=6e8936b3ad994f13bfb29923cc1506a9 (accessed Jun. 29, 2022).

[12] “Zircaloy-4(Alloy Zr4) (UNS R60804),” *AZO Materials*. https://www.azom.com/article.aspx?ArticleID=7644 (accessed Jun. 29, 2022).

[13] W. G. Burgers, “On the process of transition of the cubic-body-centered modification into the

hexagonal-close-packed modification of zirconium," *Physica*, vol. 1, no. 7–12, pp. 561–586, May 1934, doi: 10.1016/S0031-8914(34)80244-3.

[14] Y. H. Jeong, K. S. Rheem, C. S. Choi, and Y. S. Kim, "Effect of Beta Heat Treatment on Microstructure and Nodular Corrosion of Zircaloy-4," *J. Nucl. Sci. Technol.*, vol. 30, no. 2, pp. 154–163, Feb. 1993, doi: 10.1080/18811248.1993.9734463.

[15] K. V. M. Krishna *et al.*, "Microstructural and textural developments during Zircaloy-4 fuel tube fabrication," *J. Nucl. Mater.*, vol. 383, no. 1–2, pp. 78–85, 2008, doi: 10.1016/j.jnucmat.2008.08.050.

[16] Z. Wang *et al.*, "Hydrogen-induced microstructure, texture and mechanical property evolutions in a high-pressure torsion processed zirconium alloy," *Scr. Mater.*, vol. 67, no. 9, pp. 752–755, 2012, doi: 10.1016/j.scriptamat.2012.07.033.

[17] H. L. J. Yakel, "Thermocrystallography of higher hydrides of titanium and zirconium," *Acta Crystallogr.*, vol. 11, pp. 46–51, 1958, doi: 10.1107/S0365110X58000098.

[18] J. J. Kearns and C. R. Woods, "Effect of texture, grain size, and cold work on the precipitation of oriented hydrides in Zircaloy tubing and plate," *J. Nucl. Mater.*, vol. 20, no. 3, pp. 241–261, Sep. 1966, doi: 10.1016/0022-3115(66)90036-5.

[19] J. J. Kearns, "On the relationship among 'f' texture factors for the principal planes of zirconium, hafnium and titanium alloys," *J. Nucl. Mater.*, vol. 299, no. 2, pp. 171–174, 2001, doi: 10.1016/S0022-3115(01)00686-9.

[20] H. E. Weekes, N. G. Jones, T. C. Lindley, and D. Dye, "Hydride reorientation in Zircaloy-4 examined by in situ synchrotron X-ray diffraction," *J. Nucl. Mater.*, vol. 478, pp. 32–41, 2016, doi: 10.1016/j.jnucmat.2016.05.029.

[21] R. Montgomery, C. Tomé, W. Liu, A. Alankar, G. Subramanian, and C. Stanek, "Use of multiscale zirconium alloy deformation models in nuclear fuel behavior analysis," *J. Comput. Phys.*, vol. 328, pp. 278–300, 2017, doi: 10.1016/j.jcp.2016.09.051.

[22] J. B. Vander Sande and A. L. Bement, "An investigation of second phase particles in Zircaloy-4 alloys," *J. Nucl. Mater.*, vol. 52, no. 1, pp. 115–118, 1974, doi: 10.1016/0022-3115(74)90032-4.

[23] W. L. Fong and D. O. Northwood, "Identification of second-phase particles in zircaloy-4 nuclear fuel sheating," *Metallography*, vol. 15, no. 1, pp. 27–41, 1982, doi: 10.1016/0026-0800(82)90039-8.

[24] K. T. Erwin, O. Delaire, A. T. Motta, Y. S. Chu, D. C. Mancini, and R. C. Birtcher, "Observation of second-phase particles in bulk zirconium alloys using synchrotron radiation," *J. Nucl. Mater.*, vol. 294, no. 3, pp. 299–304, 2001, doi: 10.1016/S0022-3115(01)00436-6.

[25] P. A. Burr, S. T. Murphy, S. C. Lumley, M. R. Wenman, and R. W. Grimes, "Hydrogen accommodation

in Zr second phase particles: Implications for H pick-up and hydriding of Zircaloy-2 and Zircaloy-4," *Corros. Sci.*, vol. 69, pp. 1–4, 2013, doi: 10.1016/j.corsci.2012.11.036.

[26] K. Annand, M. Nord, I. MacLaren, and M. Gass, "The corrosion of Zr(Fe, Cr)2 and Zr2Fe secondary phase particles in Zircaloy-4 under 350 °C pressurised water conditions," *Corros. Sci.*, vol. 128, no. January, pp. 213–223, 2017, doi: 10.1016/j.corsci.2017.09.014.

[27] P. Chemelle, D. B. Knorr, J. B. Van Der Sande, and R. M. Pelloux, "Morphology and composition of second phase particles in zircaloy-2," *J. Nucl. Mater.*, vol. 113, no. 1, pp. 58–64, 1983, doi: 10.1016/0022-3115(83)90166-6.

[28] B. E. Zuzek, J. R. Abdata, C. A. Barlloche, C. Nacional, and D. E. Atomlca, "The H-Zr (Hydrogen-Zirconium) System," *Bull. Alloy Phase Diagrams*, vol. 11, no. 4, pp. 385–386, 1990, doi: https://doi.org/10.1007/BF02843318.

[29] R. Vogel and W. Tonn, "Über Einen Umwandlungspunkt Des Zirkons.," *Zeitschrift für Anorg. und Allg. Chemie*, vol. 202, no. 1, pp. 292–296, 1931, doi: 10.1002/zaac.19312020125.

[30] T. B. Britton, F. P. E. Dunne, and A. J. Wilkinson, "On the mechanistic basis of deformation at the microscale in hexagonal close-packed metals," *Proc. R. Soc. A Math. Phys. Eng. Sci.*, vol. 471, no. 2178, 2015, doi: 10.1098/rspa.2014.0881.

[31] R. A. Holt, "The beta to alpha phase transformation in zircaloy-4," *J. Nucl. Mater.*, vol. 35, no. 3, pp. 322–334, 1970.

[32] T. E. Perez and M. E. Saggese, "Welding structures in gas tungsten arc-welded Zircaloy-4," *Metallography*, vol. 15, pp. 43–52, 1982, doi: 10.1016/0026-0800(82)90040-4.

[33] O. T. Woo and K. Tangri, "Transformation characteristics of rapidly heated and quenched zircaloy-4-oxygen alloys," *J. Nucl. Mater.*, vol. 79, no. 1, pp. 83–94, Jan. 1979, doi: 10.1016/0022-3115(79)90435-5.

[34] G. Ökvist and K. Källström, "The effect of zirconium carbide on the β → α transformation structure in zircaloy," *J. Nucl. Mater.*, vol. 35, no. 3, pp. 316–321, 1970, doi: 10.1016/0022-3115(70)90215-1.

[35] A. Sawatzky, G. Ledoux, and S. Jones, "Oxidation of Zirconium During a High-Temperature Transient," *Zircon. Nucl. Ind.*, vol. ASTM STP 6, pp. 134–149, 1977, doi: 10.1520/stp35569s.

[36] A. R. Massih and L. O. Jernkvist, "Phase ordering under quenching: a case of Zr-alloy," *J. Phys. Chem. Solids*, vol. 65, no. 6, pp. 1193–1198, Jun. 2004, doi: 10.1016/j.jpcs.2004.01.009.

[37] A. R. Massih, T. Andersson, P. Witt, M. Dahlbäck, and M. Limbäck, "Effect of quenching rate on the β-to-α phase transformation structure in zirconium alloy," *J. Nucl. Mater.*, vol. 322, no. 2–3, pp. 138–151, Nov. 2003, doi: 10.1016/S0022-3115(03)00323-4.

[38] S.-H. JUNG and I.-S. KIM, “Effect of β-Heat Treatment on Microstructure and Mechanical Anisotropy of Zircaloy-4 Fuel Cladding,” *J. Nucl. Sci. Technol.*, vol. 26, no. 5, pp. 516–524, May 1989, doi: 10.1080/18811248.1989.9734341.

[39] R. A. Holt, “Comments on the beta to alpha phase transformation in zircaloy-4,” *J. Nucl. Mater.*, vol. 47, no. 2, pp. 262–264, 1973, doi: 10.1016/0022-3115(73)90111-6.

[40] P. Rudling, A. Strasser, and F. Garzarolli, “IZNA7 SPECIAL TOPIC REPORT 2007 - Welding of Zirconium Alloys,” 2007. [Online]. Available: https://www.antinternational.com/docs/samples/FM/11/First_chapter_-_ZIRAT12_STR_Welding_of_zirc_alloys.pdf

[41] L. J. Nayak and G. G. Roy, “Joining of zircaloy-4 of dissimilar thickness using electron beam welding,” *Int. J. Adv. Manuf. Technol.*, vol. 110, no. 9–10, pp. 2323–2340, 2020, doi: 10.1007/s00170-020-06000-7.

[42] TWI, “What is Electron Beam Welding? Process Definition and Advantages.” https://www.twi-global.com/technical-knowledge/faqs/faq-what-is-electron-beam-welding (accessed Aug. 03, 2022).

[43] C. J. Parga, I. J. van Rooyen, B. D. Coryell, W. R. Lloyd, L. N. Valenti, and H. Usman, “Room temperature mechanical properties of electron beam welded zircaloy-4 sheet,” *J. Mater. Process. Technol.*, vol. 241, pp. 73–85, 2017, doi: 10.1016/j.jmatprotec.2016.11.001.

[44] H. Taylor and S. Baker, “Blocky Alpha Transformation in Zircaloy-4 Weldments,” *JOM*, vol. 71, no. 8, pp. 2742–2748, 2019, doi: 10.1007/s11837-019-03604-7.

[45] TWI, “What is the Heat Affected Zone (HAZ)?” https://www.twi-global.com/technical-knowledge/faqs/what-is-the-heat-affected-zone (accessed Aug. 03, 2022).

[46] H. S. Kalish, “Electron beam welding of zircaloy and other materials,” 1962. [Online]. Available: https://www.osti.gov/biblio/4875206-electron-beam-welding-zircaloy-other-materials

[47] D. D. Amick, “Method of quenching zirconium and alloys thereof,” no. US patent 3847684. 1974. [Online]. Available: https://www.google.co.uk/patents/US3847684

[48] V. S. Tong and T. Ben Britton, “Formation of very large ‘blocky alpha’ grains in Zircaloy-4,” *Acta Mater.*, vol. 129, pp. 510–520, 2017, doi: 10.1016/j.actamat.2017.03.002.

[49] R. Armstrong, I. Codd, R. M. Douthwaite, and N. J. Petch, “The plastic deformation of polycrystalline aggregates,” *Philos. Mag.*, vol. 7, no. 73, pp. 45–58, 1962, doi: 10.1080/14786436208201857.

[50] G. B. Skinner and H. L. Johnston, “Thermal Expansion of Zirconium between 298°K and 1600°K,” *J. Chem. Phys.*, vol. 21, no. 8, pp. 1383–1384, Aug. 1953, doi: 10.1063/1.1699227.

[51] D. F. Washburn, “The formation of large grains in alpha zircaloy-4 during heat treatment after small

plastic deformations," 1964. [Online]. Available: https://www.osti.gov/biblio/4675033

[52] J. Echols, L. Garrison, C. Silva, and E. Lindquist, "Temperature and time effects of post-weld heat treatments on tensile properties and microstructure of Zircaloy-4," *J. Nucl. Mater.*, vol. 551, p. 152952, 2021, doi: 10.1016/j.jnucmat.2021.152952.

[53] K. Loucif, R. Borrelly, and P. Merle, "Microstructural evolution of β-quenched Zircaloy-4 during agings between 100 and 750°C," *J. Nucl. Mater.*, vol. 210, no. 1–2, pp. 84–96, Jun. 1994, doi: 10.1016/0022-3115(94)90226-7.

[54] R. Birch, S. Wang, V. S. Tong, and T. B. Britton, "The effect of cooling rate and grain size on hydride microstructure in Zircaloy-4," *J. Nucl. Mater.*, vol. 513, pp. 221–225, 2019, doi: 10.1016/j.jnucmat.2018.11.011.

[55] S. Wang, F. Giuliani, and T. Ben Britton, "Microstructure and formation mechanisms of δ-hydrides in variable grain size Zircaloy-4 studied by electron backscatter diffraction," *Acta Mater.*, vol. 169, pp. 76–87, 2019, doi: 10.1016/j.actamat.2019.02.042.

[56] W. Wan and F. P. E. Dunne, "Microstructure-interacting short crack growth in blocky alpha," *Int. J. Plast.*, vol. 130, no. February, p. 102711, 2020, doi: 10.1016/j.ijplas.2020.102711.

[57] K. Loucif, P. Merle, and R. Borrelly, "On the thermoelectric power variation according to temperature of zirconium alloys and its possible application to the estimation of the amount of solubility variations of iron and chromium in zircaloy," *J. Nucl. Mater.*, vol. 202, no. 1–2, pp. 193–196, Jun. 1993, doi: 10.1016/0022-3115(93)90042-W.

[58] V. M. Miller, A. E. Johnson, C. J. Torbet, and T. M. Pollock, "Recrystallization and the Development of Abnormally Large Grains After Small Strain Deformation in a Polycrystalline Nickel-Based Superalloy," *Metall. Mater. Trans. A*, vol. 47A, pp. 1566–1574, 2016, doi: 10.1007/s11661-016-3329-6.

[59] P. A. Beck and P. R. Sperry, "Strain Induced Grain Boundary Migration in High Purity Aluminum," *J. Appl. Phys.*, vol. 21, pp. 150–152, 1950, doi: https://doi.org/10.1063/1.1699614.

[60] J. D. Robson, "Assessment of annealing parameter approximations in zirconium alloys," *J. Nucl. Mater.*, vol. 527, p. 151814, 2019, doi: 10.1016/j.jnucmat.2019.151814.

[61] J. Bair, M. Asle Zaeem, and M. Tonks, "A review on hydride precipitation in zirconium alloys," *J. Nucl. Mater.*, vol. 466, pp. 12–20, 2015, doi: 10.1016/j.jnucmat.2015.07.014.

[62] C. E. Ells, "Hydride precipitates in zirconium alloys (A review)," *J. Nucl. Mater.*, vol. 28, pp. 129–151, 1968.

[63] S. Suman, M. K. Khan, M. Pathak, R. N. Singh, and J. K. Chakravartty, "Hydrogen in Zircaloy:

Mechanism and its impacts," *Int. J. Hydrogen Energy*, vol. 40, no. 17, pp. 5976–5994, May 2015, doi: 10.1016/j.ijhydene.2015.03.049.

[64] M. Grosse, M. Steinbrueck, E. Lehmann, and P. Vontobel, "Kinetics of Hydrogen Absorption and Release in Zirconium Alloys During Steam Oxidation," *Oxid. Met.*, vol. 70, no. 3–4, pp. 149–162, Oct. 2008, doi: 10.1007/s11085-008-9113-2.

[65] M. P. Puls, S. Q. Shi, and J. Rabier, "Experimental studies of mechanical properties of solid zirconium hydrides," *J. Nucl. Mater.*, vol. 336, no. 1, pp. 73–80, 2005, doi: 10.1016/j.jnucmat.2004.08.016.

[66] A. Steuwer, J. R. Santisteban, M. Preuss, M. J. Peel, T. Buslaps, and M. Harada, "Evidence of stress-induced hydrogen ordering in zirconium hydrides," *Acta Mater.*, vol. 57, no. 1, pp. 145–152, 2009, doi: 10.1016/j.actamat.2008.08.061.

[67] R. S. Daum, Y. S. Chu, and A. T. Motta, "Identification and quantification of hydride phases in Zircaloy-4 cladding using synchrotron X-ray diffraction," *J. Nucl. Mater.*, vol. 392, no. 3, pp. 453–463, 2009, doi: 10.1016/j.jnucmat.2009.04.004.

[68] Z. Zhao *et al.*, "Characterization of Zirconium Hydrides and Phase Field Approach to a Mesoscopic-Scale Modeling of Their Precipitation," *J. ASTM Int.*, vol. 5, no. 3, p. 101161, 2008, doi: 10.1520/JAI101161.

[69] R. E. Rundle, C. G. Shull, and E. O. Wollan, "The crystal structure of thorium and zirconium dihydrides by X-ray and neutron diffraction," *Acta Crystallogr.*, vol. 5, no. 1, pp. 22–26, 1952, doi: 10.1107/S0365110X52000071.

[70] X. Zhu, D.-Y. Lin, J. Fang, X.-Y. Gao, Y.-F. Zhao, and H.-F. Song, "New zirconium hydrides predicted by structure search method based on first principles calculations," 2017, [Online]. Available: http://arxiv.org/abs/1703.01154

[71] V. Tikare, P. F. Weck, and M. V. Glazoff, "Model for Simulation of Hydride Precipitation in Zr-Based Used Fuel Claddings: A Status Report on Current Model Capabilities," 2013. [Online]. Available: https://www.energy.gov/ne/articles/model-simulation-hydride-precipitation-zr-based-used-fuel-claddings-status-report

[72] L. Lanzani and M. Ruch, "Comments on the stability of zirconium hydride phases in Zircaloy," *J. Nucl. Mater.*, vol. 324, no. 2–3, pp. 165–176, 2004, doi: 10.1016/j.jnucmat.2003.09.013.

[73] C. D. Cann, M. P. Puls, E. E. Sexton, and W. G. Hutchings, "The effect of metallurgical factors on hydride phases in zirconium," *J. Nucl. Mater.*, vol. 126, no. 3, pp. 197–205, 1984, doi: 10.1016/0022-3115(84)90029-1.

[74] K. B. Colas, "Fundamental experiments on hydride reorientation in Zircaloy [PhD thesis]," The Pennsylvania State University, 2012.

[75] K. B. Colas, A. Motta, M. R. Daymond, J. Almer, and Z. Cai, “Hydride behaviour in zircaloy-4 during thermomechanical cycling,” in *15th International Conference on Environmental Degradation*, 2011, pp. 683–688.

[76] J. E. Bailey, “Electron microscope observations on the precipitation of zirconium hydride in zirconium,” *Acta Metall.*, vol. 11, no. 4, pp. 267–280, Apr. 1963, doi: 10.1016/0001-6160(63)90182-2.

[77] K. B. Colas *et al.*, “In situ study of hydride precipitation kinetics and re-orientation in Zircaloy using synchrotron radiation,” *Acta Mater.*, vol. 58, no. 20, pp. 6575–6583, 2010, doi: 10.1016/j.actamat.2010.07.018.

[78] B. A. Cheadle, C. E. Coleman, and M. Ipohorski, “Orientation of Hydrides in Zirconium Alloy Tubes,” *Zircon. Nucl. Ind. Sixth Int. Symp. ASTM STP 824*, pp. 210–221, 1984.

[79] E. Tenckhoff, “Review of Deformation Mechanisms, Texture, and Mechanical Anisotropy in Zirconium and Zirconium Base Alloys,” *J. ASTM Int.*, vol. 2, no. 4, pp. 25–50, 2005, doi: 10.1520/JAI12945.

[80] C. J. Simpson and C. E. Ells, “Delayed hydrogen embrittlement in Zr-2.5 wt % Nb,” *J. Nucl. Mater.*, vol. 52, no. 2, pp. 289–295, Oct. 1974, doi: 10.1016/0022-3115(74)90174-3.

[81] IAEA - International Atomic Energy Agency, “Delayed hydride cracking in zirconium alloys in pressure tube nuclear reactors IAEA-TECDOC-1410,” *October*, no. October, p. 43, 2004.

[82] Y. Y. Bum, Y. K. Suk, K. I. Soo, and C. Y. Moo, “Effect of Hydride Reorientation on Delayed Hydride Cracking In Zr-2.5Nb Tubes,” *J. Korean Nucl. Soc.*, vol. 35, no. 6, pp. 529–536, 2003, [Online]. Available: https://koreascience.kr/article/JAKO200325720301220.pdf

[83] G. J. C. Carpenter, “The dilatational misfit of zirconium hydrides precipitated in zirconium,” *J. Nucl. Mater.*, vol. 48, no. 3, pp. 264–266, 1973, doi: 10.1016/0022-3115(73)90022-6.

[84] A. T. W. Barrow, A. Korinek, and M. R. Daymond, “Evaluating zirconium-zirconium hydride interfacial strains by nano-beam electron diffraction,” *J. Nucl. Mater.*, vol. 432, no. 1–3, pp. 366–370, 2013, doi: 10.1016/j.jnucmat.2012.08.003.

[85] M. Kerr, M. R. Daymond, R. A. Holt, and J. D. Almer, “Strain evolution of zirconium hydride embedded in a Zircaloy-2 matrix,” *J. Nucl. Mater.*, vol. 380, no. 1–3, pp. 70–75, 2008, doi: 10.1016/j.jnucmat.2008.07.004.

[86] G. B. Allen, M. Kerr, and M. R. Daymond, “Measurement and modeling of strain fields in zirconium hydrides precipitated at a stress concentration,” *J. Nucl. Mater.*, vol. 430, no. 1–3, pp. 27–36, 2012, doi: 10.1016/j.jnucmat.2012.06.037.

[87] L. Reali, D. S. Balint, and M. R. Wenman, "Dislocation modelling of the plastic relaxation and thermal ratchetting induced by zirconium hydride precipitation," *J. Mech. Phys. Solids*, vol. 167, no. June, p. 104988, 2022, doi: 10.1016/j.jmps.2022.104988.

[88] D. Rugg, M. Dixon, and F. P. E. Dunne, "Effective structural unit size in titanium alloys," *J. Strain Anal. Eng. Des.*, vol. 42, no. 4, pp. 269–279, 2007, doi: 10.1243/03093247JSA273.

[89] J. Cappola *et al.*, "On the Localization of Plastic Strain in Microtextured Regions of Ti-6Al-4V," *Acta Mater.*, vol. 204, pp. 1–15, 2021, doi: 10.1016/j.actamat.2020.116492.

[90] L. Germain, N. Gey, M. Humbert, P. Vo, M. Jahazi, and P. Bocher, "Texture heterogeneities induced by subtransus processing of near α titanium alloys," *Acta Mater.*, vol. 56, no. 16, pp. 4298–4308, 2008, doi: 10.1016/j.actamat.2008.04.065.

[91] A. J. Wilkinson and T. Ben Britton, "Strains, planes, and EBSD in materials science," *Mater. Today*, vol. 15, no. 9, pp. 366–376, 2012, doi: 10.1016/S1369-7021(12)70163-3.

[92] M. Humbert, H. Moustahfid, F. Wagner, and M. J. Philippe, "Evaluation of the high temperature texture of the β phase of a TA6V sample from the individual orientations of grains of the low temperature α phase," *Scr. Metall. Mater.*, vol. 30, no. 3, pp. 377–382, 1994, doi: 10.1016/0956-716X(94)90392-1.

[93] M. Humbert, F. Wagner, H. Moustahfid, and C. Esling, "Determination of the Orientation of a Parent β Grain from the Orientations of the Inherited α Plates in the Phase Transformation from Body-Centred Cubic to Hexagonal Close Packed," *J. Appl. Crystallogr.*, vol. 28, no. 5, pp. 571–576, 1995, doi: 10.1107/s0021889895004067.

[94] M. Humbert and N. Gey, "The calculation of a parent grain orientation from inherited variants for approximate (b.c.c.-h.c.p.) orientation relations," *J. Appl. Crystallogr.*, vol. 35, no. 4, pp. 401–405, 2002, doi: 10.1107/S0021889802005824.

[95] V. Tari, A. D. Rollett, and H. Beladi, "Back calculation of parent austenite orientation using a clustering approach," *J. Appl. Crystallogr.*, vol. 46, no. 1, pp. 210–215, 2013, doi: 10.1107/S002188981204914X.

[96] N. Gey and M. Humbert, "Specific analysis of EBSD data to study the texture inheritance due to the β → α phase transformation," *J. Mater. Sci.*, vol. 38, no. 6, pp. 1289–1294, 2003, doi: 10.1023/A:1022842712172.

[97] L. Germain, N. Gey, R. Mercier, P. Blaineau, and M. Humbert, "An advanced approach to reconstructing parent orientation maps in the case of approximate orientation relations: Application to steels," *Acta Mater.*, vol. 60, no. 11, pp. 4551–4562, 2012, doi: 10.1016/j.actamat.2012.04.034.

[98] C. Cayron, "ARPGE: A computer program to automatically reconstruct the parent grains from

electron backscatter diffraction data," *J. Appl. Crystallogr.*, vol. 40, no. 6, pp. 1183–1188, 2007, doi: 10.1107/S0021889807048777.

[99] L. Germain, N. Gey, and M. Humbert, "Reconstruction of deformed parent grains from microstructure inherited by phase transformations," *Scr. Mater.*, vol. 158, pp. 91–94, 2019, doi: 10.1016/j.scriptamat.2018.08.042.

[100] M. G. Glavicic, P. A. Kobryn, T. R. Bieler, and S. L. Semiatin, "An automated method to determine the orientation of the high-temperature beta phase from measured EBSD data for the low-temperature alpha-phase in Ti-6Al-4V," *Mater. Sci. Eng. A*, vol. 351, no. 1–2, pp. 258–264, 2003, doi: 10.1016/S0921-5093(02)00844-4.

[101] S. Hadke, M. S. Parihar, S. Shekhawat, and R. K. Khatirkar, "A new method for automated reconstruction of pre-transformation microstructures," *Philos. Mag. Lett.*, vol. 96, no. 5, pp. 175–182, 2016, doi: 10.1080/09500839.2016.1180436.

[102] P. S. Davies, "PhD Thesis," The University of Sheffield, 2009. doi: 10.1515/9783112335802.

[103] T. Nyyssönen, P. Peura, and V. T. Kuokkala, "Crystallography, Morphology, and Martensite Transformation of Prior Austenite in Intercritically Annealed High-Aluminum Steel," *Metall. Mater. Trans. A Phys. Metall. Mater. Sci.*, vol. 49, no. 12, pp. 6426–6441, 2018, doi: 10.1007/s11661-018-4904-9.

[104] S. van Dongen, "PhD Thesis," University of Utrecht, 2000. [Online]. Available: https://micans.org/mcl/index.html?sec_thesisetc

[105] M. Humbert, L. Germain, N. Gey, and E. Boucard, "Evaluation of the orientation relations from misorientation between inherited variants: Application to ausformed martensite," *Acta Mater.*, vol. 82, pp. 137–144, 2015, doi: 10.1016/j.actamat.2014.09.007.

[106] L. Germain, S. R. Dey, M. Humbert, and N. Gey, "Determination of parent orientation maps in advanced titanium-based alloys," *J. Microsc.*, vol. 227, no. 3, pp. 284–291, 2007, doi: 10.1111/j.1365-2818.2007.01812.x.

[107] C. Cayron, B. Artaud, and L. Briottet, "Reconstruction of parent grains from EBSD data," *Mater. Charact.*, vol. 57, pp. 386–401, 2006, doi: 10.1016/j.matchar.2006.03.008.

[108] T. Nyyssönen, "Manual for the Parent Austenite Reconstruction Graphical User."

[109] T. Nyyssönen, M. Isakov, P. Peura, and V. T. Kuokkala, "Iterative Determination of the Orientation Relationship Between Austenite and Martensite from a Large Amount of Grain Pair Misorientations," *Metall. Mater. Trans. A Phys. Metall. Mater. Sci.*, vol. 47, no. 6, pp. 2587–2590, 2016, doi: 10.1007/s11661-016-3462-2.

[110] K. V. M. Krishna *et al.*, “Automated reconstruction of pre-transformation microstructures in zirconium,” *Scr. Mater.*, vol. 62, no. 6, pp. 391–394, 2010, doi: 10.1016/j.scriptamat.2009.11.031.

[111] C. Cayron, “Groupoid of orientational variants,” *Acta Crystallogr. Sect. A Found. Crystallogr.*, vol. 62, no. 1, pp. 21–40, 2006, doi: 10.1107/S010876730503686X.

[112] E. Gomes and L. A. I. Kestens, “Fully automated orientation relationship calculation and prior austenite reconstruction by random walk clustering,” *IOP Conf. Ser. Mater. Sci. Eng.*, vol. 82, pp. 1–4, 2015, doi: 10.1088/1757-899X/82/1/012059.

[113] M. G. Glavicic, P. A. Kobryn, T. R. Bieler, and S. L. Semiatin, “A method to determine the orientation of the high-temperature beta phase from measured EBSD data for the low-temperature alpha phase in Ti-6Al-4V,” *Mater. Sci. Eng. A*, vol. 346, pp. 50–59, 2003, doi: 10.1016/S0921-5093(02)00844-4.

[114] N. Bernier, L. Bracke, L. Malet, and S. Godet, “An alternative to the crystallographic reconstruction of austenite in steels,” *Mater. Charact.*, vol. 89, pp. 23–32, 2014, doi: 10.1016/j.matchar.2013.12.014.

[115] G. Miyamoto, N. Takayama, and T. Furuhara, “Accurate measurement of the orientation relationship of lath martensite and bainite by electron backscatter diffraction analysis,” *Scr. Mater.*, vol. 60, no. 12, pp. 1113–1116, 2009, doi: 10.1016/j.scriptamat.2009.02.053.

[116] M. Humbert, P. Blaineau, L. Germain, and N. Gey, “Refinement of orientation relations occurring in phase transformation based on considering only the orientations of the variants,” *Scr. Mater.*, vol. 64, no. 2, pp. 114–117, 2011, doi: 10.1016/j.scriptamat.2010.09.016.

[117] G. Miyamoto, N. Iwata, N. Takayama, and T. Furuhara, “Mapping the parent austenite orientation reconstructed from the orientation of martensite by EBSD and its application to ausformed martensite,” *Acta Mater.*, vol. 58, no. 19, pp. 6393–6403, 2010, doi: 10.1016/j.actamat.2010.08.001.

[118] EDAX, “OIM Analysis v8,” *AMETEK*. https://www.edax.com/products/ebsd/oim-analysis/oim-analysis-v8 (accessed Jul. 02, 2022).

[119] C. Ranger, V. Tari, S. Farjami, M. J. Merwin, L. Germain, and A. Rollett, “Austenite Reconstruction Elucidates Prior Grain Size Dependence of Toughness in a Low Alloy Steel,” *Metall. Mater. Trans. A Phys. Metall. Mater. Sci.*, vol. 49, no. 10, pp. 4521–4535, 2018, doi: 10.1007/s11661-018-4825-7.

[120] EDAX, “Parent Phase Reconstruction,” *AMETEK*. https://www.edax.com/resources/application-notes/parent-phase-reconstruction (accessed Jul. 02, 2022).

[121] Oxford Instruments, “AZtecCrystal.” https://nano.oxinst.com/azteccrystal (accessed Aug. 02, 2022).

[122] Oxford Instruments, “Parent Grain Reconstruction.” https://www.ebsd.com/ois-ebsd-system/parent-grain-reconstruction (accessed Aug. 02, 2022).

[123] C.-Y. Huang, H.-C. Ni, and H.-W. Yen, “New protocol for orientation reconstruction from martensite

to austenite in steels," *Materialia*, vol. 9, p. 100554, Mar. 2020, doi: 10.1016/j.mtla.2019.100554.

[124] J. A. Nelder and R. Mead, "A simplex method for function minimization," *Comput. J.*, vol. 7, no. 4, pp. 308–313, 1965.

[125] K. G. Lusby, "Investigation into Blocky Alpha Microstructures in Zircaloy-4 Welds," 2017.

[126] D. J. Barber, "Thin foils of non-metals made for electron microscopy by sputter-etching," *J. Mater. Sci.*, vol. 5, no. 1, pp. 1–8, 1970, doi: 10.1007/bf00553437.

[127] R. Alani and P. R. Swann, "Precision Ion Polishing System -A New Instrument for TEM Specimen Preparation of Materials," *MRS Proc.*, vol. 254, no. 43, 1991, doi: 10.1557/PROC-254-43.

[128] Gatan and Ametec, "PIPS II System." https://www.gatan.com/products/tem-specimen-preparation/pips-ii-system (accessed Aug. 02, 2022).

[129] X. Zhong *et al.*, "Comparing Xe+pFIB and Ga+FIB for TEM sample preparation of Al alloys: Minimising FIB-induced artefacts," *J. Microsc.*, vol. 282, no. 2, pp. 101–112, 2021, doi: 10.1111/jmi.12983.

[130] K. W. Jin and M. De Graef, "c-Axis orientation determination of α-titanium using Computational Polarized Light Microscopy," *Mater. Charact.*, vol. 167, no. July, p. 110503, 2020, doi: 10.1016/j.matchar.2020.110503.

[131] L. Böhme, L. Morales-Rivas, S. Diederichs, and E. Kerscher, "Crystal c-axis mapping of hcp metals by conventional reflected polarized light microscopy: Application to untextured and textured cp-Titanium," *Mater. Charact.*, vol. 145, no. September, pp. 573–581, 2018, doi: 10.1016/j.matchar.2018.09.024.

[132] "Polarized Reflected Light Microscopy," *Carl Zeiss*. https://zeiss-campus.magnet.fsu.edu/articles/basics/reflectedcontrast.html (accessed Jun. 22, 2022).

[133] L. Reimer, "Emission of Backscattered and Secondary Electrons," in *Scanning Electron Microscopy Physics of Image Formation and Microanalysis*, 2nd ed., P. W. Hawkes, Ed. Springer, 1998, pp. 135–169.

[134] "ARGUS FSE/BSE Imaging System," *Bruker*. https://www.bruker.com/en/products-and-solutions/elemental-analyzers/eds-wds-ebsd-SEM-Micro-XRF/quantax-ebsd/argus-fse-bse-imaging-system.html (accessed May 17, 2022).

[135] T. Ben Britton, D. Goran, and V. S. Tong, "Space rocks and optimising scanning electron channelling contrast," *Mater. Charact.*, vol. 142, no. June, pp. 422–431, 2018, doi: 10.1016/j.matchar.2018.06.001.

[136] T. Ben Britton, "Introduction to Crystallography and Diffraction (Presentation)." pp. 1–146, 2021.

[137] D. O. Northwood, "The development and applications of zirconium alloys," *Mater. Des.*, vol. 6, no. 2,

pp. 58–70, 1985, doi: 10.1016/0261-3069(85)90165-7.

[138] V. S. Tong, “EBSD characterisation of heterogeneous microstructures in zirconium alloys [PhD thesis],” Imperial College London, 2016.

[139] F. Mc Namara, “Hydrides in Zironium Alloys,” 2011.

[140] P. Vizcaíno, A. . Banchik, and J. . Abriata, “Solubility of hydrogen in Zircaloy-4: irradiation induced increase and thermal recovery,” *J. Nucl. Mater.*, vol. 304, no. 2–3, pp. 96–106, Aug. 2002, doi: 10.1016/S0022-3115(02)00883-8.

[141] LECO, “Hydrogen Determinators and Analyzers.” https://www.leco.com/hydrogen (accessed Jun. 27, 2022).

[142] J. J. Kearns, “Diffusion coefficient of hydrogen in alpha zirconium, Zircaloy-2 and Zircaloy-4,” *J. Nucl. Mater.*, vol. 43, no. 3, pp. 330–338, 1972, doi: 10.1016/0022-3115(72)90065-7.

[143] B. Nath, G. W. Lorimer, and N. Ridley, “Effect of hydrogen concentration and cooling rate on hydride precipitation in alpha-zirconium,” *J. Nucl. Mater.*, vol. 58, no. 2, pp. 153–162, 1975, doi: 10.1016/0022-3115(75)90101-4.

[144] Gatan Inc., *Precision Etching and Coating System - Owner’s Manual and User’s Guide*, no. Rev 2.0. 2014.

[145] N. Fang, R. Birch, and T. Ben Britton, “Optimizing broad ion beam polishing of zircaloy-4 for electron backscatter diffraction analysis,” pp. 1–34, 2022, doi: https://doi.org/10.48550/arXiv.2201.02501.

[146] Y. Chang *et al.*, “Ti and its alloys as examples of cryogenic focused ion beam milling of environmentally-sensitive materials,” *Nat. Commun.*, vol. 10, no. 1, pp. 1–10, 2019, doi: 10.1038/s41467-019-08752-7.

[147] S. M. Hanlon, S. Y. Persaud, F. Long, A. Korinek, and M. R. Daymond, “A solution to FIB induced artefact hydrides in Zr alloys,” *J. Nucl. Mater.*, vol. 515, pp. 122–134, 2019, doi: 10.1016/j.jnucmat.2018.12.020.

[148] CAMECA and AMETEK, “Atom Probe Tomography Consumables, Accessories, and Options.” https://www.atomprobe.com/keyaptlinks/options-accessories-consumables (accessed Jul. 30, 2022).

[149] *Murano 525 heating stage with USB Temperature Controller - Operator’s Handbook*, vol. 44, no. 04. Gatan UK, 2015.

[150] G. Nichols, “Light Microscopy,” *Polymorph. Pharm. Ind.*, pp. 167–209, 2006, doi: 10.1002/3527607889.ch7.

[151] D. T. Grubb, *Optical Microscopy*, vol. 2. Elsevier B.V., 2012. doi: 10.1016/B978-0-444-53349-4.00035-

2.

[152] A. P. Day and T. E. Quested, “A comparison of grain imaging and measurement using horizontal orientation and colour orientation contrast imaging, electron backscatter pattern and optical methods,” *J. Microsc.*, vol. 195, no. 3, pp. 186–196, 1999, doi: 10.1046/j.1365-2818.1999.00571.x.

[153] Bruker, “Software: ESPRIT Family.” https://www.bruker.com/en/products-and-solutions/elemental-analyzers/eds-wds-ebsd-SEM-Micro-XRF/software-esprit-family.html (accessed Jun. 11, 2022).

[154] F. Bachmann, R. Hielscher, and H. Schaeben, “Texture analysis with MTEX- Free and open source software toolbox,” *Solid State Phenom.*, vol. 160, pp. 63–68, 2010, doi: 10.4028/www.scientific.net/SSP.160.63.

[155] T. B. Britton *et al.*, “Tutorial: Crystal orientations and EBSD - Or which way is up?,” *Mater. Charact.*, vol. 117, pp. 113–126, 2016, doi: 10.1016/j.matchar.2016.04.008.

[156] T. B. Britton and A. J. Wilkinson, “High resolution electron backscatter diffraction measurements of elastic strain variations in the presence of larger lattice rotations,” *Ultramicroscopy*, vol. 114, pp. 82–95, 2012, doi: 10.1016/j.ultramic.2012.01.004.

[157] A. J. Wilkinson and D. Randman, “Determination of elastic strain fields and geometrically necessary dislocation distributions near nanoindents using electron back scatter diffraction,” *Philos. Mag.*, vol. 90, no. 9, pp. 1159–1177, 2010, doi: 10.1080/14786430903304145.

[158] T. B. Britton, H. Liang, F. P. E. Dunne, and A. J. Wilkinson, “The effect of crystal orientation on the indentation response of commercially pure titanium: Experiments and simulations,” *Proc. R. Soc. A Math. Phys. Eng. Sci.*, vol. 466, no. 2115, pp. 695–719, 2010, doi: 10.1098/rspa.2009.0455.

[159] R. Birch and T. B. Britton, “Effective structural unit analysis in hexagonal close-packed alloys – reconstruction of parent β microstructures and crystal orientation post-processing analysis,” *Arxiv*, vol. v2, pp. 1–23, Feb. 2021, doi: 10.48550/arXiv.2104.10648.

[160] T. Karthikeyan, S. Saroja, and M. Vijayalakshmi, “Evaluation of misorientation angle-axis set between variants during transformation of bcc to hcp phase obeying Burgers orientation relation,” *Scr. Mater.*, vol. 55, pp. 771–774, 2006, doi: 10.1016/j.scriptamat.2006.07.022.

[161] S. Morito, H. Tanaka, R. Konishi, T. Furuhara, and T. Maki, “The morphology and crystallography of lath martensite in Fe-C alloys,” *Acta Mater.*, vol. 51, no. 6, pp. 1789–1799, 2003, doi: 10.1016/S1359-6454(02)00577-3.

[162] J. L. W. Warwick, N. G. Jones, I. Bantounas, M. Preuss, and D. Dye, “In situ observation of texture and microstructure evolution during rolling and globularization of Ti-6Al-4V,” *Acta Mater.*, vol. 61, no. 5, pp. 1603–1615, 2013, doi: 10.1016/j.actamat.2012.11.037.

[163] E. Uta, N. Gey, P. Bocher, M. Humbert, and J. Gilgert, "Texture heterogeneities in αp/αs titanium forging analysed by EBSD-Relation to fatigue crack propagation," *J. Microsc.*, vol. 233, no. 3, pp. 451–459, 2009, doi: 10.1111/j.1365-2818.2009.03141.x.

[164] R. Shi, V. Dixit, G. B. Viswanathan, H. L. Fraser, and Y. Wang, "Experimental assessment of variant selection rules for grain boundary α in titanium alloys," *Acta Mater.*, vol. 102, pp. 197–211, 2016, doi: 10.1016/j.actamat.2015.09.021.

[165] W. C. Lenthe, L. Germain, M. R. Chini, N. Gey, and M. De Graef, "Spherical indexing of overlap EBSD patterns for orientation-related phases – Application to titanium," *Acta Mater.*, vol. 188, pp. 579–590, 2020, doi: 10.1016/j.actamat.2020.02.025.

[166] C. Toffolon-Masclet, T. Guilbert, and J. C. Brachet, "Study of secondary intermetallic phase precipitation/dissolution in Zr alloys by high temperature-high sensitivity calorimetry," *J. Nucl. Mater.*, vol. 372, no. 2–3, pp. 367–378, 2008, doi: 10.1016/j.jnucmat.2007.04.042.

[167] TedPella, "PELCO ® High Temperature Carbon Paste , 50g," no. 16057, pp. 1–2, 2017, [Online]. Available: https://www.tedpella.com/technote_html/16057 TN.pdf

[168] Bruker, "Personal Communication." 2021.

[169] S. D. Stolbov *et al.*, "Effect of the Stressed State on the Phase Transformations in Zirconium-Based Alloys," *Russ. Metall.*, vol. 2022, no. 3, pp. 250–260, 2022, doi: 10.1134/S0036029522030119.

[170] T. B. Britton, V. S. Tong, J. Hickey, A. Foden, and A. J. Wilkinson, "AstroEBSD: Exploring new space in pattern indexing with methods launched from an astronomical approach," *J. Appl. Crystallogr.*, vol. 51, no. 6, pp. 1525–1534, 2018, doi: 10.1107/S1600576718010373.

[171] J. Pegoud and J. Guillaumin, "Orientations dans cristallographiques le zircaloy-2 polycristallin," *JoNM*, vol. 45, pp. 69–72, 1972.

[172] J. S. Bradbrook, G. W. Lorimer, and N. Ridley, "The precipitation of zirconium hydride in zirconium and zircaloy-2," *J. Nucl. Mater.*, vol. 42, pp. 142–160, 1972, doi: 10.1016/0001-6160(78)90006-8.

[173] K. Une, K. Nogita, S. Ishimoto, and K. Ogata, "Crystallography of Zirconium Hydrides in Recrystallized Zircaloy-2 Fuel Cladding by Electron Backscatter Diffraction," *J. Nucl. Sci. Technol. J. J. Nucl. Sci. Technol.*, vol. 417, pp. 22–3131, 2004, doi: 10.1080/18811248.2004.9715540.

[174] W. Lu *et al.*, "Nanoscale characterisation of hydrides and secondary phase particles in Zircaloy-4," *Arxiv*, vol. [Preprint], no. v1, Sep. 2021, [Online]. Available: http://arxiv.org/abs/2109.10955

[175] W. Guo *et al.*, "Texture development and mechanical behavior of Zircaloy-4 alloy plates fabricated by cold rolling and annealing," *Mater. Sci. Eng. A*, vol. 807, no. February, p. 140846, 2021, doi: 10.1016/j.msea.2021.140846.

[176] T. Benjamin Britton and A. J. Wilkinson, “Stress fields and geometrically necessary dislocation density distributions near the head of a blocked slip band,” *Acta Mater.*, vol. 60, no. 16, pp. 5773–5782, 2012, doi: 10.1016/j.actamat.2012.07.004.

[177] R. Hielscher, T. Nyyssönen, F. Niessen, and A. A. Gazder, “The variant graph approach to improved parent grain reconstruction,” *Materialia*, vol. 22, no. March, p. 101399, 2022, doi: 10.1016/j.mtla.2022.101399.

Appendix A: Plotting Details

EBSD maps

Table 27 contains settings used for EBSD mapping for the output plots used in the figures in this thesis.

Table 27 - EBSD settings

Map	Figure(s)	EBSD settings			
		Working distance	EBSP resolution	Exposure time (ms)	Step size (µm)
WQ10min	Figure 63 Figure 64 Figure 65 Figure 66 Figure 67 Figure 68	15.0	320 x 240	38	0.14
Ex situ – map 1 (pre-HT)	Figure 94 Figure 95 Figure 96 Figure 99 Figure 100	14.7	160 x 120	7	1
Ex situ – map 1 (post-HT)	Figure 94 Figure 95 Figure 96 Figure 99 Figure 100	14.6	160 x 120	7	1
Ex situ – map 2 (pre-HT)	Figure 94 Figure 95 Figure 96 Figure 98	14.8	160 x 120	7	1
Ex situ – map 2 (post-HT)	Figure 94 Figure 95 Figure 96 Figure 98	14.8	160 x 120	7	1
Ex situ – map 3 (pre-HT)	Figure 94 Figure 95 Figure 96 Figure 97	14.7	160 x 120	7	1
Ex situ – map 3 (post-HT)	Figure 94 Figure 95 Figure 96 Figure 97	14.7	160 x 120	7	1
Ex situ – map 4 (pre-HT)	Figure 94 Figure 95 Figure 96	14.6	160 x 120	7	1
Ex situ – map 4 (post-HT)	Figure 94 Figure 95 Figure 96	14.6	160 x 120	7	1
In situ – expt 1 (Initial)	Figure 101 Figure 104 Figure 106 Figure 107	20.0	320 x 240	40	1

Map	Figure(s)	EBSD settings			
		Working distance	**EBSP resolution**	**Exposure time (ms)**	**Step size (µm)**
	Figure 108 Figure 113				
In situ – expt 1 (HT1)	Figure 101 Figure 104 Figure 106 Figure 107 Figure 108 Figure 113	20.0	160 x 120	10	1
In situ – expt 2 (Initial)	Figure 107 Figure 108	20.0	160 x 120	7	0.8
In situ – expt 2 (HT1)	Figure 107 Figure 108	19.9	160 x 120	7	1
In situ – expt 3 (Initial)	Figure 107 Figure 109 Figure 110 Figure 111 Figure 112 Figure 131 Figure 132	20.3	160 x 120	7	1
In situ – expt 3 (HT1)	Figure 107 Figure 109 Figure 110 Figure 111 Figure 112 Figure 131 Figure 132	20.0	160 x 120	7	1
In situ – expt 3 (HT2)	Figure 112 Figure 131 Figure 132	20.0	160 x 120	7	1
Grain boundary hydride	Figure 115 Figure 116	16.4	800 x 600	150	0.1
Triple junction hydride	Figure 118 Figure 119 Figure 120	16.4	800 x 600	150	0.08
Pinch off hydride	Figure 122 Figure 123	16.5	800 x 600	150	0.1
Spiky hydride	Figure 127 Figure 128	16.5	800 x 600	150	0.1

Note: Unless otherwise stated, maps were processed in MTEX using a grain boundary threshold of 4 °, small grains of 5 pixels and a smoothing value of 2 or 3 (smoothing not used for reconstruction maps).

Reconstruction details

Table 28 contains the ParentBOR code settings used for processing for the figures in this thesis, along with reconstruction output values such as the average angular deviation (of the α grains orientations) to the calculated α variants (using BOR and the assigned parent β orientation for the experimental α grain).

Table 28 - ParentBOR code settings and outputs

Chapter	Sample	Figure(s)	Grain processing settings			Reconstruction settings		Reconstruction outputs					
			gB threshold (°)	Small grains (pixels)	Smoothing[17]	Cut-off (°)	Inflation power	No of α grains	BOR matched gB (%)	Non-BOR gB (%)	No of discrete clusters (MCL)	Avg. deviation from BOR (°)	No of β grains
4	Example dataset	Figure 62	4	1	0	4	1.6	40	71.6	28.4	7	0.03	6
4	BCWQ10min2	Figure 63 Figure 64 Figure 66 Figure 67 Figure 68	4	5	2	5	1.6	Run prior to settings capture script being added to ParentBOR code					
4	BCWQ10min2 Split grain pair only	Figure 65	4	5	2	4	1.2	640	84.6	15.4	21	3.00	19
6	*Ex situ* Map1 (pre-HT)	Figure 94 Figure 95 Figure 96 Figure 99 Figure 100	4	15	3	4	1.4	21889	93.9	6.1	600	1.17	356
6	*Ex situ* Map1 (post-HT)	Figure 94 Figure 95 Figure 96 Figure 99 Figure 100	4	15	3	4	1.4	9268	86.3	13.8	640	1.29	505

[17] Note: smoothing usually not used for grain boundaries in reconstruction output plots.

Chapter	Sample	Figure(s)	Grain processing settings			Reconstruction settings		Reconstruction outputs					
			gB threshold (°)	Small grains (pixels)	Smoothing[17]	Cut-off (°)	Inflation power	No of α grains	BOR matched gB (%)	Non-BOR gB (%)	No of discrete clusters (MCL)	Avg. deviation from BOR (°)	No of β grains
6	*Ex situ* Map2 (pre-HT)	Figure 94 Figure 95 Figure 96 Figure 98	4	15	3	4	1.4	22879	91.6	8.4	481	1.28	272
6	*Ex situ* Map2 (post-HT)	Figure 94 Figure 95 Figure 96 Figure 98	4	15	3	4	1.4	1720	46.8	53.2	599	1.19	548
6 6	*Ex situ* Map3 (pre-HT)	Figure 94 Figure 95 Figure 96	4	15	3	4	1.4	18021	93.2	6.8	400	1.21	209
6	*Ex situ* Map3 (post-HT)	Figure 94 Figure 95 Figure 96 Figure 97	4	15	3	4	1.5	635	41.9	58.1	283	0.98	252
6	*Ex situ* Map4 (pre-HT)	Figure 94 Figure 95 Figure 96	4	15	3	4	1.4	12458	94.6	5.4	485	1.54	282
6	*Ex situ* Map4 (post-HT)	Figure 94 Figure 95 Figure 96	4	15	3	4	1.4	3253	88.9	11.1	216	1.31	171
7	*In situ* Expt 3 (initial)	Figure 109 Figure 110 Figure 111 Figure 112 Figure 131 Figure 132	4	15	3	4	1.4	24304	91.6	8.4	574	0.76	310

Chapter	Sample	Figure(s)	Grain processing settings			Reconstruction settings		Reconstruction outputs					
			gB threshold (°)	Small grains (pixels)	Smoothing[17]	Cut-off (°)	Inflation power	No of α grains	BOR matched gB (%)	Non-BOR gB (%)	No of discrete clusters (MCL)	Avg. deviation from BOR (°)	No of β grains
7	*In situ* Expt 3 (HT1)	Figure 107 Figure 109 Figure 110 Figure 111 Figure 112 Figure 131 Figure 132	4	15	3	4	1.4	11177	90	8.0	221	0.74	103
7	*In situ* Expt 3 (HT2)	Figure 112	4	15	3	4	1.4	13069	93.0	7.0	244	0.74	111
7	*In situ* Expt 1 (initial)	Figure 101 Figure 104 Figure 106	Run prior to settings capture script being added to ParentBOR										
7	*In situ* Expt 1 (HT1)	Figure 101 Figure 104 Figure 106 Figure 107											
7	*In situ* Expt 2 (initial + HT1)	Figure 107											

HR-EBSD settings

All maps run through the HR-EBSD code used:

Grain processing:

- GrainID_Setup.mis_tol = 4; % in degrees
- GrainID_Setup.GrainID_minsize = 10; % in pixels (min grainsize for GrainID)

General settings:

- iSet.Mis_Thresh = 10; % total misorientation angle, in degrees
- iSet.PH_Thresh = 0.2; % min peak height
- iSet.MAE_Thresh = [0.4; 3E-3]; % Mean angular error limits

Plotting limits chosen for each map are detailed in Table 29.

Table 29 - HR-EBSD plot settings

Figure	Map	Mask settings		Colour ranges				
		PH	MAE	PH	MAE	Rotation (rad)	Stress (GPa)	GND
Figure 117	Grain boundary	0.3	$1x10^{-3}$	0 - 1	0 - $1x10^{-2}$	± $1x10^{-3}$	± 0.75	11 - 13.5
Figure 121	Triple junction	0.3	$5x10^{-4}$	0 - 1	0 - $1x10^{-3}$	± $1x10^{-3}$	± 0.75	11 - 13.5
Figure 124	Pinch off	0.3	$5x10^{-4}$	0 - 1	0 - $1x10^{-2}$	± $5x10^{-3}$	± 0.40	11 - 13.5
Figure 125 Figure 126	Pinch off - tips	0.3	$5x10^{-4}$	0 - 1	0 - $1x10^{-2}$	± $5x10^{-3}$	± 0.40	11 - 13.5
Figure 129	Spiky	0.3	$5x10^{-4}$	0 - 1	0 - $1x10^{-2}$	± $5x10^{-3}$	± 0.40	11 - 13.5
Figure 130	Spiky - tips	0.3	$5x10^{-4}$	0 - 1	0 - $1x10^{-2}$	± $5x10^{-3}$	± 0.40	11 - 13.5

Appendix B: Figure permissions

Figures directly reproduced from other work and copyright permissions are captured in the table below.

Figure No.	Source of work		Section reproduced	Copyright © holder	Requested on	Permission yes /no	Permission note
Figure 1	Jeong, 1993	[14]	Fig 1	Taylor & Francis	N/A	Yes	"Taylor & Francis is pleased to offer reuses of its content for a thesis or dissertation free of charge contingent on resubmission of permission request if work is published."
Figure 2	Zuzek, 1990	[28]	2nd diagram in Fig 1	Springer Nature: Bulletin of alloy phase diagrams	11/12/22	Yes	License No: 5385910857636 See attachment.
Figure 4 Figure 5 Figure 9	Holt, 1970	[31]	Fig 1, Fig 2, Table 1, Fig 6	Elsevier: Journal of Nuclear Materials	12/11/22	Yes	License No: 5386350816701 See attachment.
Figure 6	Ökvist, 1970	[34]	Fig 3, Fig 4	Elsevier: Journal of Nuclear Materials	12/11/22	Yes	License No: 5386351028875 See attachment.
Figure 7	Woo, 1979	[33]	Fig 11	Elsevier: Journal of Nuclear Materials	12/11/22	Yes	License No: 5386371062420 See attachment.
Figure 8	Massih, 2004	[36]	Fig 5	Elsevier: Journal of Physics and Chemistry of Solids	12/11/22	Yes	License No: 5386371236415 See attachment.
Figure 9	Jung, 1989	[38]	Fig 4	Taylor & Francis	N/A	Yes	"Taylor & Francis is pleased to offer reuses of its content for a thesis or dissertation free of charge contingent on resubmission of permission request if work is published."
Figure 11	Parga, 2017	[43]	Fig 16, Fig 17, Fig 18	Elsevier: Journal of Materials Processing Technology	11/12/22	Yes	License No: 5386050631442 See attachment.
Figure 12 Figure 16	Tong, 2017	[48]	Fig 1, graphical abstract, Fig 8	-	N/A	Yes	Licensed with a Creative Commons Attribution 4.0 International (CC BY 4.0)

Figure No.	Source of work		Section reproduced	Copyright © holder	Requested on	Permission yes /no	Permission note
Figure 13 Figure 30 Figure *31*	Taylor, 2019	[44]	Fig 1, Fig 2, Fig 3, Fig 4	Springer Nature: JOM Journal of the Minerals, Metals and Materials Society	12/11/22	Yes	License No: 5386741318717 See attachment.
Figure 14 Figure 17	Echols, 2021	[52]	Fig 5, Fig 9	Elsevier: Journal of Nuclear Materials	12/11/22	Yes	License No: 5386370932505 See attachment.
Figure 15	Loucif, 1994	[53]	Fig 12	Elsevier: Journal of Nuclear Materials	12/11/22	Yes	License No: 5386380102696 See attachment.
Figure 18	Grosse, 2008	[64]	Fig 8	Springer Nature: Oxidation of Metals	12/11/22	Yes	License No: 5386380249229 See attachment.
Figure 19	Tikare, 2013	[71]	Fig 10	www.energy.gov	-	-	Covered by fair usage policy: https://www.energy.gov/about-us/web-policies
Figure 20	Suman, 2015	[63]	Fig 9	Elsevier: International Journal of Hydrogen Energy	12/11/22	Yes	License No: 5386390352792 See attachment.
Figure 21 Figure 43	Birch, 2019	[54]	Fig 2, Fig 3	Elsevier: Journal of Nuclear Materials	N/A	Yes	Author of article: ok to use in thesis with reference to journal
Figure 22	Weekes, 2016	[20]	Fig 1	Elsevier: Journal of Nuclear Materials	12/11/22	Yes	License No: 5386390467069 See attachment.
Figure 25	Bailey, 1963	[76]	Fig 4(b), Fig 10	Elsevier: Acta Metallurgica	12/11/22	Yes	License No: 5386391492814 See attachment.
Figure 26	Barrow, 2013	[84]	Fig 2	Elsevier: Journal of Nuclear Materials	12/11/22	Yes	License No: 5386400125045 See attachment.
Figure 27	Allen, 2012	[86]	Fig 3, Fig 6	Elsevier: Journal of Nuclear Materials	12/11/22	Yes	License No: 5386400233393 See attachment.
Figure 28	Reali, 2022	[87]	Fig 7	-	N/A	Yes	Licensed with a Creative Commons Attribution 4.0 International (CC BY 4.0)
Figure 35 Figure 36 Figure 37 Figure 38	Britton, 2021	[136]	From ppt slides	-	-	Yes	Reproduced with permission

Figure No.	Source of work		Section reproduced	Copyright © holder	Requested on	Permission yes /no	Permission note
Figure 58 Figure 59 Figure 60 Figure 61 Figure 62 Figure 63 Figure 64 Figure 65 Figure 66 Figure 67 Figure 68	Birch, 2022	[1]	All figures in paper	-	-	Yes	Author's work. Licensed with a Creative Commons Attribution 4.0 International (CC BY 4.0)

RightsLink

Home | Help | Email Support | Ruth Birch

Effect of Beta Heat Treatment on Microstructure and Nodular Corrosion of Zircaloy-4

Author: Yong Hwan JEONG, , Karp Soon RHEEM, et al
Publication: Journal of Nuclear Science and Technology
Publisher: Taylor & Francis
Date: Feb 1, 1993

Rights managed by Taylor & Francis

Thesis/Dissertation Reuse Request

Taylor & Francis is pleased to offer reuses of its content for a thesis or dissertation free of charge contingent on resubmission of permission request if work is published.

BACK CLOSE

© 2022 Copyright - All Rights Reserved | Copyright Clearance Center, Inc. | Privacy statement | Data Security and Privacy | For California Residents | Terms and ConditionsComments? We would like to hear from you. E-mail us at customercare@copyright.com

SPRINGER NATURE LICENSE TERMS AND CONDITIONS

Sep 12, 2022

This Agreement between Ruth Birch ("You") and Springer Nature ("Springer Nature") consists of your license details and the terms and conditions provided by Springer Nature and Copyright Clearance Center.

License Number	5385910857636
License date	Sep 11, 2022
Licensed Content Publisher	Springer Nature
Licensed Content Publication	Bulletin of alloy phase diagrams
Licensed Content Title	The H-Zr (hydrogen-zirconium) system
Licensed Content Author	E. Zuzek et al
Licensed Content Date	Jan 1, 1990
Type of Use	Thesis/Dissertation
Requestor type	academic/university or research institute
Format	print and electronic
Portion	figures/tables/illustrations
Number of figures/tables /illustrations	1
Will you be translating?	no
Circulation/distribution	1 - 29
Author of this Springer Nature content	no
Title	PhD Thesis
Institution name	Imperial College London
Expected presentation date	Sep 2022
Portions	Figure 1
Requestor Location	Ruth Birch 9 Hance Lane Braintree, CM77 6TH United Kingdom Attn: Ruth Birch
Total	**0.00 GBP**
Terms and Conditions	

Springer Nature Customer Service Centre GmbH
Terms and Conditions

This agreement sets out the terms and conditions of the licence (the **Licence**) between you and **Springer Nature Customer Service Centre GmbH** (the **Licensor**). By clicking 'accept' and completing the transaction for the material (**Licensed Material**), you also confirm your acceptance of these terms and conditions.

1. Grant of License

1. 1. The Licensor grants you a personal, non-exclusive, non-transferable, world-wide licence to reproduce the Licensed Material for the purpose specified in your order only. Licences are granted for the specific use requested in the order and for no other use, subject to the conditions below.

1. 2. The Licensor warrants that it has, to the best of its knowledge, the rights to license reuse of the Licensed Material. However, you should ensure that the material you are requesting is original to the Licensor and does not

carry the copyright of another entity (as credited in the published version).

1. 3. If the credit line on any part of the material you have requested indicates that it was reprinted or adapted with permission from another source, then you should also seek permission from that source to reuse the material.

2. Scope of Licence

2. 1. You may only use the Licensed Content in the manner and to the extent permitted by these Ts&Cs and any applicable laws.

2. 2. A separate licence may be required for any additional use of the Licensed Material, e.g. where a licence has been purchased for print only use, separate permission must be obtained for electronic re-use. Similarly, a licence is only valid in the language selected and does not apply for editions in other languages unless additional translation rights have been granted separately in the licence. Any content owned by third parties are expressly excluded from the licence.

2. 3. Similarly, rights for additional components such as custom editions and derivatives require additional permission and may be subject to an additional fee. Please apply to Journalpermissions@springernature.com/bookpermissions@springernature.com for these rights.

2. 4. Where permission has been granted **free of charge** for material in print, permission may also be granted for any electronic version of that work, provided that the material is incidental to your work as a whole and that the electronic version is essentially equivalent to, or substitutes for, the print version.

2. 5. An alternative scope of licence may apply to signatories of the STM Permissions Guidelines, as amended from time to time.

3. Duration of Licence

3. 1. A licence for is valid from the date of purchase ('Licence Date') at the end of the relevant period in the below table:

Scope of Licence	Duration of Licence
Post on a website	12 months
Presentations	12 months
Books and journals	Lifetime of the edition in the language purchased

4. Acknowledgement

4. 1. The Licensor's permission must be acknowledged next to the Licenced Material in print. In electronic form, this acknowledgement must be visible at the same time as the figures/tables/illustrations or abstract, and must be hyperlinked to the journal/book's homepage. Our required acknowledgement format is in the Appendix below.

5. Restrictions on use

5. 1. Use of the Licensed Material may be permitted for incidental promotional use and minor editing privileges e.g. minor adaptations of single figures, changes of format, colour and/or style where the adaptation is credited as set out in Appendix 1 below. Any other changes including but not limited to, cropping, adapting, omitting material that affect the meaning, intention or moral rights of the author are strictly prohibited.

5. 2. You must not use any Licensed Material as part of any design or trademark.

5. 3. Licensed Material may be used in Open Access Publications (OAP) before publication by Springer Nature, but any Licensed Material must be removed from OAP sites prior to final publication.

6. Ownership of Rights

6. 1. Licensed Material remains the property of either Licensor or the relevant third party and any rights not explicitly

granted herein are expressly reserved.

7. Warranty

IN NO EVENT SHALL LICENSOR BE LIABLE TO YOU OR ANY OTHER PARTY OR ANY OTHER PERSON OR FOR ANY SPECIAL, CONSEQUENTIAL, INCIDENTAL OR INDIRECT DAMAGES, HOWEVER CAUSED, ARISING OUT OF OR IN CONNECTION WITH THE DOWNLOADING, VIEWING OR USE OF THE MATERIALS REGARDLESS OF THE FORM OF ACTION, WHETHER FOR BREACH OF CONTRACT, BREACH OF WARRANTY, TORT, NEGLIGENCE, INFRINGEMENT OR OTHERWISE (INCLUDING, WITHOUT LIMITATION, DAMAGES BASED ON LOSS OF PROFITS, DATA, FILES, USE, BUSINESS OPPORTUNITY OR CLAIMS OF THIRD PARTIES), AND
WHETHER OR NOT THE PARTY HAS BEEN ADVISED OF THE POSSIBILITY OF SUCH DAMAGES. THIS LIMITATION SHALL APPLY NOTWITHSTANDING ANY FAILURE OF ESSENTIAL PURPOSE OF ANY LIMITED REMEDY PROVIDED HEREIN.

8. Limitations

8. 1. ***BOOKS ONLY:***Where **'reuse in a dissertation/thesis'** has been selected the following terms apply: Print rights of the final author's accepted manuscript (for clarity, NOT the published version) for up to 100 copies, electronic rights for use only on a personal website or institutional repository as defined by the Sherpa guideline (www.sherpa.ac.uk/romeo/).

8. 2. For content reuse requests that qualify for permission under the STM Permissions Guidelines, which may be updated from time to time, the STM Permissions Guidelines supersede the terms and conditions contained in this licence.

9. Termination and Cancellation

9. 1. Licences will expire after the period shown in Clause 3 (above).

9. 2. Licensee reserves the right to terminate the Licence in the event that payment is not received in full or if there has been a breach of this agreement by you.

Appendix 1 — Acknowledgements:

For Journal Content:
Reprinted by permission from [**the Licensor**]: [**Journal Publisher** (e.g. Nature/Springer/Palgrave)] [**JOURNAL NAME**] [**REFERENCE CITATION** (Article name, Author(s) Name), [**COPYRIGHT**] (year of publication)

For **Advance Online Publication papers:**
Reprinted by permission from [**the Licensor**]: [**Journal Publisher** (e.g. Nature/Springer/Palgrave)] [**JOURNAL NAME**] [**REFERENCE CITATION** (Article name, Author(s) Name), [**COPYRIGHT**] (year of publication), advance online publication, day month year (doi: 10.1038/sj.[JOURNAL ACRONYM].)

For Adaptations/Translations:
Adapted/Translated by permission from [**the Licensor**]: [**Journal Publisher** (e.g. Nature/Springer/Palgrave)] [**JOURNAL NAME**] [**REFERENCE CITATION** (Article name, Author(s) Name), [**COPYRIGHT**] (year of publication)

Note: For any republication from the British Journal of Cancer, the following credit line style applies:

Reprinted/adapted/translated by permission from [**the Licensor**]: on behalf of Cancer Research UK: : [**Journal Publisher** (e.g. Nature/Springer/Palgrave)] [**JOURNAL NAME**] [**REFERENCE CITATION** (Article name, Author(s) Name), [**COPYRIGHT]** (year of publication)

For **Advance Online Publication** papers:
Reprinted by permission from The [**the Licensor**]: on behalf of Cancer Research UK: [**Journal Publisher** (e.g. Nature/Springer/Palgrave)] [**JOURNAL NAME**] [**REFERENCE CITATION** (Article name, Author(s) Name), [**COPYRIGHT**] (year of publication), advance online publication, day month year (doi: 10.1038/sj.[JOURNAL ACRONYM])

For Book content:
Reprinted/adapted by permission from [**the Licensor**]: [**Book Publisher** (e.g. Palgrave Macmillan, Springer etc)

[**Book Title**] by [**Book author**(s)] [**COPYRIGHT**] (year of publication)

Other Conditions:

Version 1.3

Questions? customercare@copyright.com or +1-855-239-3415 (toll free in the US) or +1-978-646-2777.

ELSEVIER LICENSE TERMS AND CONDITIONS

Sep 12, 2022

This Agreement between Ruth Birch ("You") and Elsevier ("Elsevier") consists of your license details and the terms and conditions provided by Elsevier and Copyright Clearance Center.

License Number	5386350816701
License date	Sep 12, 2022
Licensed Content Publisher	Elsevier
Licensed Content Publication	Journal of Nuclear Materials
Licensed Content Title	The beta to alpha phase transformation in zircaloy-4
Licensed Content Author	R.A Holt
Licensed Content Date	Jun 1, 1970
Licensed Content Volume	35
Licensed Content Issue	3
Licensed Content Pages	13
Start Page	322
End Page	334
Type of Use	reuse in a thesis/dissertation
Portion	figures/tables/illustrations
Number of figures/tables /illustrations	4
Format	both print and electronic
Are you the author of this Elsevier article?	No
Will you be translating?	No
Title	PhD Thesis
Institution name	Imperial College London
Expected presentation date	Sep 2022
Portions	Figures 1, 2, 6 Table 1
Requestor Location	Ruth Birch Department of materials Imperial college london London, SW7 2AZ United Kingdom Attn: Ruth Birch
Publisher Tax ID	GB 494 6272 12
Total	**0.00 GBP**
Terms and Conditions	

INTRODUCTION

1. The publisher for this copyrighted material is Elsevier. By clicking "accept" in connection with completing this licensing transaction, you agree that the following terms and conditions apply to this transaction (along with the Billing and Payment terms and conditions established by Copyright Clearance Center, Inc. ("CCC"), at the time that you opened your Rightslink account and that are available at any time at http://myaccount.copyright.com).

GENERAL TERMS

2. Elsevier hereby grants you permission to reproduce the aforementioned material subject to the terms and conditions indicated.

3. Acknowledgement: If any part of the material to be used (for example, figures) has appeared in our publication with credit or acknowledgement to another source, permission must also be sought from that source. If such permission is not obtained then that material may not be included in your publication/copies. Suitable acknowledgement to the source must be made, either as a footnote or in a reference list at the end of your publication, as follows:
"Reprinted from Publication title, Vol /edition number, Author(s), Title of article / title of chapter, Pages No., Copyright (Year), with permission from Elsevier [OR APPLICABLE SOCIETY COPYRIGHT OWNER]." Also Lancet special credit - "Reprinted from The Lancet, Vol. number, Author(s), Title of article, Pages No., Copyright (Year), with permission from Elsevier."
4. Reproduction of this material is confined to the purpose and/or media for which permission is hereby given.
5. Altering/Modifying Material: Not Permitted. However figures and illustrations may be altered/adapted minimally to serve your work. Any other abbreviations, additions, deletions and/or any other alterations shall be made only with prior written authorization of Elsevier Ltd. (Please contact Elsevier's permissions helpdesk here). No modifications can be made to any Lancet figures/tables and they must be reproduced in full.
6. If the permission fee for the requested use of our material is waived in this instance, please be advised that your future requests for Elsevier materials may attract a fee.
7. Reservation of Rights: Publisher reserves all rights not specifically granted in the combination of (i) the license details provided by you and accepted in the course of this licensing transaction, (ii) these terms and conditions and (iii) CCC's Billing and Payment terms and conditions.
8. License Contingent Upon Payment: While you may exercise the rights licensed immediately upon issuance of the license at the end of the licensing process for the transaction, provided that you have disclosed complete and accurate details of your proposed use, no license is finally effective unless and until full payment is received from you (either by publisher or by CCC) as provided in CCC's Billing and Payment terms and conditions. If full payment is not received on a timely basis, then any license preliminarily granted shall be deemed automatically revoked and shall be void as if never granted. Further, in the event that you breach any of these terms and conditions or any of CCC's Billing and Payment terms and conditions, the license is automatically revoked and shall be void as if never granted. Use of materials as described in a revoked license, as well as any use of the materials beyond the scope of an unrevoked license, may constitute copyright infringement and publisher reserves the right to take any and all action to protect its copyright in the materials.
9. Warranties: Publisher makes no representations or warranties with respect to the licensed material.
10. Indemnity: You hereby indemnify and agree to hold harmless publisher and CCC, and their respective officers, directors, employees and agents, from and against any and all claims arising out of your use of the licensed material other than as specifically authorized pursuant to this license.
11. No Transfer of License: This license is personal to you and may not be sublicensed, assigned, or transferred by you to any other person without publisher's written permission.
12. No Amendment Except in Writing: This license may not be amended except in a writing signed by both parties (or, in the case of publisher, by CCC on publisher's behalf).
13. Objection to Contrary Terms: Publisher hereby objects to any terms contained in any purchase order, acknowledgment, check endorsement or other writing prepared by you, which terms are inconsistent with these terms and conditions or CCC's Billing and Payment terms and conditions. These terms and conditions, together with CCC's Billing and Payment terms and conditions (which are incorporated herein), comprise the entire agreement between you and publisher (and CCC) concerning this licensing transaction. In the event of any conflict between your obligations established by these terms and conditions and those established by CCC's Billing and Payment terms and conditions, these terms and conditions shall control.
14. Revocation: Elsevier or Copyright Clearance Center may deny the permissions described in this License at their sole discretion, for any reason or no reason, with a full refund payable to you. Notice of such denial will be made using the contact information provided by you. Failure to receive such notice will not alter or invalidate the denial. In no event will Elsevier or Copyright Clearance Center be responsible or liable for any costs, expenses or damage incurred by you as a result of a denial of your permission request, other than a refund of the amount(s) paid by you to Elsevier and/or Copyright Clearance Center for denied permissions.

LIMITED LICENSE

The following terms and conditions apply only to specific license types:
15. **Translation**: This permission is granted for non-exclusive world **English** rights only unless your license was granted for translation rights. If you licensed translation rights you may only translate this content into the languages you requested. A professional translator must perform all translations and reproduce the content word for word preserving the integrity of the article.
16. **Posting licensed content on any Website**: The following terms and conditions apply as follows: Licensing material from an Elsevier journal: All content posted to the web site must maintain the copyright information line on the bottom of each image; A hyper-text must be included to the Homepage of the journal from which you are licensing at http://www.sciencedirect.com/science/journal/xxxxx or the Elsevier homepage for books at http://www.elsevier.com; Central Storage: This license does not include permission for a scanned version of the material to be stored in a central repository such as that provided by Heron/XanEdu.
Licensing material from an Elsevier book: A hyper-text link must be included to the Elsevier homepage at http://www.elsevier.com . All content posted to the web site must maintain the copyright information line on the bottom of each image.

Posting licensed content on Electronic reserve: In addition to the above the following clauses are applicable: The web site must be password-protected and made available only to bona fide students registered on a relevant course. This permission

is granted for 1 year only. You may obtain a new license for future website posting.
17. **For journal authors:** the following clauses are applicable in addition to the above:
Preprints:
A preprint is an author's own write-up of research results and analysis, it has not been peer-reviewed, nor has it had any other value added to it by a publisher (such as formatting, copyright, technical enhancement etc.).
Authors can share their preprints anywhere at any time. Preprints should not be added to or enhanced in any way in order to appear more like, or to substitute for, the final versions of articles however authors can update their preprints on arXiv or RePEc with their Accepted Author Manuscript (see below).
If accepted for publication, we encourage authors to link from the preprint to their formal publication via its DOI. Millions of researchers have access to the formal publications on ScienceDirect, and so links will help users to find, access, cite and use the best available version. Please note that Cell Press, The Lancet and some society-owned have different preprint policies. Information on these policies is available on the journal homepage.
Accepted Author Manuscripts: An accepted author manuscript is the manuscript of an article that has been accepted for publication and which typically includes author-incorporated changes suggested during submission, peer review and editor-author communications.
Authors can share their accepted author manuscript:

- immediately
    - via their non-commercial person homepage or blog
    - by updating a preprint in arXiv or RePEc with the accepted manuscript
    - via their research institute or institutional repository for internal institutional uses or as part of an invitation-only research collaboration work-group
    - directly by providing copies to their students or to research collaborators for their personal use
    - for private scholarly sharing as part of an invitation-only work group on commercial sites with which Elsevier has an agreement
- After the embargo period
    - via non-commercial hosting platforms such as their institutional repository
    - via commercial sites with which Elsevier has an agreement

In all cases accepted manuscripts should:

- link to the formal publication via its DOI
- bear a CC-BY-NC-ND license - this is easy to do
- if aggregated with other manuscripts, for example in a repository or other site, be shared in alignment with our hosting policy not be added to or enhanced in any way to appear more like, or to substitute for, the published journal article.

Published journal article (JPA): A published journal article (PJA) is the definitive final record of published research that appears or will appear in the journal and embodies all value-adding publishing activities including peer review co-ordination, copy-editing, formatting, (if relevant) pagination and online enrichment.
Policies for sharing publishing journal articles differ for subscription and gold open access articles:
Subscription Articles: If you are an author, please share a link to your article rather than the full-text. Millions of researchers have access to the formal publications on ScienceDirect, and so links will help your users to find, access, cite, and use the best available version.
Theses and dissertations which contain embedded PJAs as part of the formal submission can be posted publicly by the awarding institution with DOI links back to the formal publications on ScienceDirect.
If you are affiliated with a library that subscribes to ScienceDirect you have additional private sharing rights for others' research accessed under that agreement. This includes use for classroom teaching and internal training at the institution (including use in course packs and courseware programs), and inclusion of the article for grant funding purposes.
Gold Open Access Articles: May be shared according to the author-selected end-user license and should contain a CrossMark logo, the end user license, and a DOI link to the formal publication on ScienceDirect.
Please refer to Elsevier's posting policy for further information.
18. **For book authors** the following clauses are applicable in addition to the above: Authors are permitted to place a brief summary of their work online only. You are not allowed to download and post the published electronic version of your chapter, nor may you scan the printed edition to create an electronic version. **Posting to a repository:** Authors are permitted to post a summary of their chapter only in their institution's repository.
19. **Thesis/Dissertation**: If your license is for use in a thesis/dissertation your thesis may be submitted to your institution in either print or electronic form. Should your thesis be published commercially, please reapply for permission. These requirements include permission for the Library and Archives of Canada to supply single copies, on demand, of the complete thesis and include permission for Proquest/UMI to supply single copies, on demand, of the complete thesis. Should your thesis be published commercially, please reapply for permission. Theses and dissertations which contain embedded PJAs as part of the formal submission can be posted publicly by the awarding institution with DOI links back to the formal publications on ScienceDirect.

Elsevier Open Access Terms and Conditions

You can publish open access with Elsevier in hundreds of open access journals or in nearly 2000 established subscription journals that support open access publishing. Permitted third party re-use of these open access articles is defined by the author's choice of Creative Commons user license. See our open access license policy for more information.

Terms & Conditions applicable to all Open Access articles published with Elsevier:

Any reuse of the article must not represent the author as endorsing the adaptation of the article nor should the article be modified in such a way as to damage the author's honour or reputation. If any changes have been made, such changes must be clearly indicated.

The author(s) must be appropriately credited and we ask that you include the end user license and a DOI link to the formal publication on ScienceDirect.

If any part of the material to be used (for example, figures) has appeared in our publication with credit or acknowledgement to another source it is the responsibility of the user to ensure their reuse complies with the terms and conditions determined by the rights holder.

Additional Terms & Conditions applicable to each Creative Commons user license:

CC BY: The CC-BY license allows users to copy, to create extracts, abstracts and new works from the Article, to alter and revise the Article and to make commercial use of the Article (including reuse and/or resale of the Article by commercial entities), provided the user gives appropriate credit (with a link to the formal publication through the relevant DOI), provides a link to the license, indicates if changes were made and the licensor is not represented as endorsing the use made of the work. The full details of the license are available at http://creativecommons.org/licenses/by/4.0.

CC BY NC SA: The CC BY-NC-SA license allows users to copy, to create extracts, abstracts and new works from the Article, to alter and revise the Article, provided this is not done for commercial purposes, and that the user gives appropriate credit (with a link to the formal publication through the relevant DOI), provides a link to the license, indicates if changes were made and the licensor is not represented as endorsing the use made of the work. Further, any new works must be made available on the same conditions. The full details of the license are available at http://creativecommons.org/licenses/by-nc-sa/4.0.

CC BY NC ND: The CC BY-NC-ND license allows users to copy and distribute the Article, provided this is not done for commercial purposes and further does not permit distribution of the Article if it is changed or edited in any way, and provided the user gives appropriate credit (with a link to the formal publication through the relevant DOI), provides a link to the license, and that the licensor is not represented as endorsing the use made of the work. The full details of the license are available at http://creativecommons.org/licenses/by-nc-nd/4.0. Any commercial reuse of Open Access articles published with a CC BY NC SA or CC BY NC ND license requires permission from Elsevier and will be subject to a fee.

Commercial reuse includes:

- Associating advertising with the full text of the Article
- Charging fees for document delivery or access
- Article aggregation
- Systematic distribution via e-mail lists or share buttons

Posting or linking by commercial companies for use by customers of those companies.

20. **Other Conditions**:

v1.10

Questions? customercare@copyright.com or +1-855-239-3415 (toll free in the US) or +1-978-646-2777.

ELSEVIER LICENSE TERMS AND CONDITIONS

Sep 12, 2022

This Agreement between Ruth Birch ("You") and Elsevier ("Elsevier") consists of your license details and the terms and conditions provided by Elsevier and Copyright Clearance Center.

License Number	5386351028875
License date	Sep 12, 2022
Licensed Content Publisher	Elsevier
Licensed Content Publication	Journal of Nuclear Materials
Licensed Content Title	The effect of zirconium carbide on the β → α transformation structur in zircaloy
Licensed Content Author	G. Ökvist,K. Källström
Licensed Content Date	Jun 1, 1970
Licensed Content Volume	35
Licensed Content Issue	3
Licensed Content Pages	6
Start Page	316
End Page	321
Type of Use	reuse in a thesis/dissertation
Portion	figures/tables/illustrations
Number of figures/tables /illustrations	2
Format	both print and electronic
Are you the author of this Elsevier article?	No
Will you be translating?	No
Title	PhD Thesis
Institution name	Imperial College London
Expected presentation date	Sep 2022
Portions	Figures 3 & 4
Requestor Location	Ruth Birch Department of materials Imperial college london London, SW7 2AZ United Kingdom Attn: Ruth Birch
Publisher Tax ID	GB 494 6272 12
Total	**0.00 GBP**
Terms and Conditions	

INTRODUCTION

1. The publisher for this copyrighted material is Elsevier. By clicking "accept" in connection with completing this licensing transaction, you agree that the following terms and conditions apply to this transaction (along with the Billing and Payment terms and conditions established by Copyright Clearance Center, Inc. ("CCC"), at the time that you opened your Rightslink account and that are available at any time at http://myaccount.copyright.com).

GENERAL TERMS

2. Elsevier hereby grants you permission to reproduce the aforementioned material subject to the terms and conditions indicated.

3. Acknowledgement: If any part of the material to be used (for example, figures) has appeared in our publication with credit or acknowledgement to another source, permission must also be sought from that source. If such permission is not obtained then that material may not be included in your publication/copies. Suitable acknowledgement to the source must be made, either as a footnote or in a reference list at the end of your publication, as follows:
"Reprinted from Publication title, Vol /edition number, Author(s), Title of article / title of chapter, Pages No., Copyright (Year), with permission from Elsevier [OR APPLICABLE SOCIETY COPYRIGHT OWNER]." Also Lancet special credit - "Reprinted from The Lancet, Vol. number, Author(s), Title of article, Pages No., Copyright (Year), with permission from Elsevier."
4. Reproduction of this material is confined to the purpose and/or media for which permission is hereby given.
5. Altering/Modifying Material: Not Permitted. However figures and illustrations may be altered/adapted minimally to serve your work. Any other abbreviations, additions, deletions and/or any other alterations shall be made only with prior written authorization of Elsevier Ltd. (Please contact Elsevier's permissions helpdesk here). No modifications can be made to any Lancet figures/tables and they must be reproduced in full.
6. If the permission fee for the requested use of our material is waived in this instance, please be advised that your future requests for Elsevier materials may attract a fee.
7. Reservation of Rights: Publisher reserves all rights not specifically granted in the combination of (i) the license details provided by you and accepted in the course of this licensing transaction, (ii) these terms and conditions and (iii) CCC's Billing and Payment terms and conditions.
8. License Contingent Upon Payment: While you may exercise the rights licensed immediately upon issuance of the license at the end of the licensing process for the transaction, provided that you have disclosed complete and accurate details of your proposed use, no license is finally effective unless and until full payment is received from you (either by publisher or by CCC) as provided in CCC's Billing and Payment terms and conditions. If full payment is not received on a timely basis, then any license preliminarily granted shall be deemed automatically revoked and shall be void as if never granted. Further, in the event that you breach any of these terms and conditions or any of CCC's Billing and Payment terms and conditions, the license is automatically revoked and shall be void as if never granted. Use of materials as described in a revoked license, as well as any use of the materials beyond the scope of an unrevoked license, may constitute copyright infringement and publisher reserves the right to take any and all action to protect its copyright in the materials.
9. Warranties: Publisher makes no representations or warranties with respect to the licensed material.
10. Indemnity: You hereby indemnify and agree to hold harmless publisher and CCC, and their respective officers, directors, employees and agents, from and against any and all claims arising out of your use of the licensed material other than as specifically authorized pursuant to this license.
11. No Transfer of License: This license is personal to you and may not be sublicensed, assigned, or transferred by you to any other person without publisher's written permission.
12. No Amendment Except in Writing: This license may not be amended except in a writing signed by both parties (or, in the case of publisher, by CCC on publisher's behalf).
13. Objection to Contrary Terms: Publisher hereby objects to any terms contained in any purchase order, acknowledgment, check endorsement or other writing prepared by you, which terms are inconsistent with these terms and conditions or CCC's Billing and Payment terms and conditions. These terms and conditions, together with CCC's Billing and Payment terms and conditions (which are incorporated herein), comprise the entire agreement between you and publisher (and CCC) concerning this licensing transaction. In the event of any conflict between your obligations established by these terms and conditions and those established by CCC's Billing and Payment terms and conditions, these terms and conditions shall control.
14. Revocation: Elsevier or Copyright Clearance Center may deny the permissions described in this License at their sole discretion, for any reason or no reason, with a full refund payable to you. Notice of such denial will be made using the contact information provided by you. Failure to receive such notice will not alter or invalidate the denial. In no event will Elsevier or Copyright Clearance Center be responsible or liable for any costs, expenses or damage incurred by you as a result of a denial of your permission request, other than a refund of the amount(s) paid by you to Elsevier and/or Copyright Clearance Center for denied permissions.

LIMITED LICENSE

The following terms and conditions apply only to specific license types:
15. **Translation**: This permission is granted for non-exclusive world **English** rights only unless your license was granted for translation rights. If you licensed translation rights you may only translate this content into the languages you requested. A professional translator must perform all translations and reproduce the content word for word preserving the integrity of the article.
16. **Posting licensed content on any Website**: The following terms and conditions apply as follows: Licensing material from an Elsevier journal: All content posted to the web site must maintain the copyright information line on the bottom of each image; A hyper-text must be included to the Homepage of the journal from which you are licensing at http://www.sciencedirect.com/science/journal/xxxxx or the Elsevier homepage for books at http://www.elsevier.com; Central Storage: This license does not include permission for a scanned version of the material to be stored in a central repository such as that provided by Heron/XanEdu.
Licensing material from an Elsevier book: A hyper-text link must be included to the Elsevier homepage at http://www.elsevier.com . All content posted to the web site must maintain the copyright information line on the bottom of each image.

Posting licensed content on Electronic reserve: In addition to the above the following clauses are applicable: The web site must be password-protected and made available only to bona fide students registered on a relevant course. This permission

is granted for 1 year only. You may obtain a new license for future website posting.
17. **For journal authors:** the following clauses are applicable in addition to the above:
Preprints:
A preprint is an author's own write-up of research results and analysis, it has not been peer-reviewed, nor has it had any other value added to it by a publisher (such as formatting, copyright, technical enhancement etc.).
Authors can share their preprints anywhere at any time. Preprints should not be added to or enhanced in any way in order to appear more like, or to substitute for, the final versions of articles however authors can update their preprints on arXiv or RePEc with their Accepted Author Manuscript (see below).
If accepted for publication, we encourage authors to link from the preprint to their formal publication via its DOI. Millions of researchers have access to the formal publications on ScienceDirect, and so links will help users to find, access, cite and use the best available version. Please note that Cell Press, The Lancet and some society-owned have different preprint policies. Information on these policies is available on the journal homepage.
Accepted Author Manuscripts: An accepted author manuscript is the manuscript of an article that has been accepted for publication and which typically includes author-incorporated changes suggested during submission, peer review and editor-author communications.
Authors can share their accepted author manuscript:

- immediately
    - via their non-commercial person homepage or blog
    - by updating a preprint in arXiv or RePEc with the accepted manuscript
    - via their research institute or institutional repository for internal institutional uses or as part of an invitation-only research collaboration work-group
    - directly by providing copies to their students or to research collaborators for their personal use
    - for private scholarly sharing as part of an invitation-only work group on commercial sites with which Elsevier has an agreement
- After the embargo period
    - via non-commercial hosting platforms such as their institutional repository
    - via commercial sites with which Elsevier has an agreement

In all cases accepted manuscripts should:

- link to the formal publication via its DOI
- bear a CC-BY-NC-ND license - this is easy to do
- if aggregated with other manuscripts, for example in a repository or other site, be shared in alignment with our hosting policy not be added to or enhanced in any way to appear more like, or to substitute for, the published journal article.

Published journal article (JPA): A published journal article (PJA) is the definitive final record of published research that appears or will appear in the journal and embodies all value-adding publishing activities including peer review co-ordination, copy-editing, formatting, (if relevant) pagination and online enrichment.
Policies for sharing publishing journal articles differ for subscription and gold open access articles:
Subscription Articles: If you are an author, please share a link to your article rather than the full-text. Millions of researchers have access to the formal publications on ScienceDirect, and so links will help your users to find, access, cite, and use the best available version.
Theses and dissertations which contain embedded PJAs as part of the formal submission can be posted publicly by the awarding institution with DOI links back to the formal publications on ScienceDirect.
If you are affiliated with a library that subscribes to ScienceDirect you have additional private sharing rights for others' research accessed under that agreement. This includes use for classroom teaching and internal training at the institution (including use in course packs and courseware programs), and inclusion of the article for grant funding purposes.
Gold Open Access Articles: May be shared according to the author-selected end-user license and should contain a CrossMark logo, the end user license, and a DOI link to the formal publication on ScienceDirect.
Please refer to Elsevier's posting policy for further information.
18. **For book authors** the following clauses are applicable in addition to the above: Authors are permitted to place a brief summary of their work online only. You are not allowed to download and post the published electronic version of your chapter, nor may you scan the printed edition to create an electronic version. **Posting to a repository:** Authors are permitted to post a summary of their chapter only in their institution's repository.
19. **Thesis/Dissertation**: If your license is for use in a thesis/dissertation your thesis may be submitted to your institution in either print or electronic form. Should your thesis be published commercially, please reapply for permission. These requirements include permission for the Library and Archives of Canada to supply single copies, on demand, of the complete thesis and include permission for Proquest/UMI to supply single copies, on demand, of the complete thesis. Should your thesis be published commercially, please reapply for permission. Theses and dissertations which contain embedded PJAs as part of the formal submission can be posted publicly by the awarding institution with DOI links back to the formal publications on ScienceDirect.

Elsevier Open Access Terms and Conditions

You can publish open access with Elsevier in hundreds of open access journals or in nearly 2000 established subscription journals that support open access publishing. Permitted third party re-use of these open access articles is defined by the author's choice of Creative Commons user license. See our open access license policy for more information.

Terms & Conditions applicable to all Open Access articles published with Elsevier:

Any reuse of the article must not represent the author as endorsing the adaptation of the article nor should the article be modified in such a way as to damage the author's honour or reputation. If any changes have been made, such changes must be clearly indicated.

The author(s) must be appropriately credited and we ask that you include the end user license and a DOI link to the formal publication on ScienceDirect.

If any part of the material to be used (for example, figures) has appeared in our publication with credit or acknowledgement to another source it is the responsibility of the user to ensure their reuse complies with the terms and conditions determined by the rights holder.

Additional Terms & Conditions applicable to each Creative Commons user license:

CC BY: The CC-BY license allows users to copy, to create extracts, abstracts and new works from the Article, to alter and revise the Article and to make commercial use of the Article (including reuse and/or resale of the Article by commercial entities), provided the user gives appropriate credit (with a link to the formal publication through the relevant DOI), provides a link to the license, indicates if changes were made and the licensor is not represented as endorsing the use made of the work. The full details of the license are available at http://creativecommons.org/licenses/by/4.0.

CC BY NC SA: The CC BY-NC-SA license allows users to copy, to create extracts, abstracts and new works from the Article, to alter and revise the Article, provided this is not done for commercial purposes, and that the user gives appropriate credit (with a link to the formal publication through the relevant DOI), provides a link to the license, indicates if changes were made and the licensor is not represented as endorsing the use made of the work. Further, any new works must be made available on the same conditions. The full details of the license are available at http://creativecommons.org/licenses/by-nc-sa/4.0.

CC BY NC ND: The CC BY-NC-ND license allows users to copy and distribute the Article, provided this is not done for commercial purposes and further does not permit distribution of the Article if it is changed or edited in any way, and provided the user gives appropriate credit (with a link to the formal publication through the relevant DOI), provides a link to the license, and that the licensor is not represented as endorsing the use made of the work. The full details of the license are available at http://creativecommons.org/licenses/by-nc-nd/4.0. Any commercial reuse of Open Access articles published with a CC BY NC SA or CC BY NC ND license requires permission from Elsevier and will be subject to a fee.

Commercial reuse includes:

- Associating advertising with the full text of the Article
- Charging fees for document delivery or access
- Article aggregation
- Systematic distribution via e-mail lists or share buttons

Posting or linking by commercial companies for use by customers of those companies.

20. **Other Conditions**:

v1.10

Questions? customercare@copyright.com or +1-855-239-3415 (toll free in the US) or +1-978-646-2777.

ELSEVIER LICENSE TERMS AND CONDITIONS

Sep 12, 2022

This Agreement between Ruth Birch ("You") and Elsevier ("Elsevier") consists of your license details and the terms and conditions provided by Elsevier and Copyright Clearance Center.

License Number	5386371062420
License date	Sep 12, 2022
Licensed Content Publisher	Elsevier
Licensed Content Publication	Journal of Nuclear Materials
Licensed Content Title	Transformation characteristics of rapidly heated and quenched zircaloy-4-oxygen alloys
Licensed Content Author	O.T. Woo,K. Tangri
Licensed Content Date	Jan 1, 1979
Licensed Content Volume	79
Licensed Content Issue	1
Licensed Content Pages	12
Start Page	83
End Page	94
Type of Use	reuse in a thesis/dissertation
Portion	figures/tables/illustrations
Number of figures/tables /illustrations	1
Format	both print and electronic
Are you the author of this Elsevier article?	No
Will you be translating?	No
Title	PhD Thesis
Institution name	Imperial College London
Expected presentation date	Sep 2022
Portions	Figure 11
Requestor Location	Ruth Birch Department of materials Imperial college london London, SW7 2AZ United Kingdom Attn: Ruth Birch
Publisher Tax ID	GB 494 6272 12
Total	**0.00 GBP**
Terms and Conditions	

INTRODUCTION

1. The publisher for this copyrighted material is Elsevier. By clicking "accept" in connection with completing this licensing transaction, you agree that the following terms and conditions apply to this transaction (along with the Billing and Payment terms and conditions established by Copyright Clearance Center, Inc. ("CCC"), at the time that you opened your Rightslink account and that are available at any time at http://myaccount.copyright.com).

GENERAL TERMS

2. Elsevier hereby grants you permission to reproduce the aforementioned material subject to the terms and conditions indicated.

3. Acknowledgement: If any part of the material to be used (for example, figures) has appeared in our publication with credit or acknowledgement to another source, permission must also be sought from that source. If such permission is not obtained then that material may not be included in your publication/copies. Suitable acknowledgement to the source must be made, either as a footnote or in a reference list at the end of your publication, as follows:
"Reprinted from Publication title, Vol /edition number, Author(s), Title of article / title of chapter, Pages No., Copyright (Year), with permission from Elsevier [OR APPLICABLE SOCIETY COPYRIGHT OWNER]." Also Lancet special credit - "Reprinted from The Lancet, Vol. number, Author(s), Title of article, Pages No., Copyright (Year), with permission from Elsevier."
4. Reproduction of this material is confined to the purpose and/or media for which permission is hereby given.
5. Altering/Modifying Material: Not Permitted. However figures and illustrations may be altered/adapted minimally to serve your work. Any other abbreviations, additions, deletions and/or any other alterations shall be made only with prior written authorization of Elsevier Ltd. (Please contact Elsevier's permissions helpdesk here). No modifications can be made to any Lancet figures/tables and they must be reproduced in full.
6. If the permission fee for the requested use of our material is waived in this instance, please be advised that your future requests for Elsevier materials may attract a fee.
7. Reservation of Rights: Publisher reserves all rights not specifically granted in the combination of (i) the license details provided by you and accepted in the course of this licensing transaction, (ii) these terms and conditions and (iii) CCC's Billing and Payment terms and conditions.
8. License Contingent Upon Payment: While you may exercise the rights licensed immediately upon issuance of the license at the end of the licensing process for the transaction, provided that you have disclosed complete and accurate details of your proposed use, no license is finally effective unless and until full payment is received from you (either by publisher or by CCC) as provided in CCC's Billing and Payment terms and conditions. If full payment is not received on a timely basis, then any license preliminarily granted shall be deemed automatically revoked and shall be void as if never granted. Further, in the event that you breach any of these terms and conditions or any of CCC's Billing and Payment terms and conditions, the license is automatically revoked and shall be void as if never granted. Use of materials as described in a revoked license, as well as any use of the materials beyond the scope of an unrevoked license, may constitute copyright infringement and publisher reserves the right to take any and all action to protect its copyright in the materials.
9. Warranties: Publisher makes no representations or warranties with respect to the licensed material.
10. Indemnity: You hereby indemnify and agree to hold harmless publisher and CCC, and their respective officers, directors, employees and agents, from and against any and all claims arising out of your use of the licensed material other than as specifically authorized pursuant to this license.
11. No Transfer of License: This license is personal to you and may not be sublicensed, assigned, or transferred by you to any other person without publisher's written permission.
12. No Amendment Except in Writing: This license may not be amended except in a writing signed by both parties (or, in the case of publisher, by CCC on publisher's behalf).
13. Objection to Contrary Terms: Publisher hereby objects to any terms contained in any purchase order, acknowledgment, check endorsement or other writing prepared by you, which terms are inconsistent with these terms and conditions or CCC's Billing and Payment terms and conditions. These terms and conditions, together with CCC's Billing and Payment terms and conditions (which are incorporated herein), comprise the entire agreement between you and publisher (and CCC) concerning this licensing transaction. In the event of any conflict between your obligations established by these terms and conditions and those established by CCC's Billing and Payment terms and conditions, these terms and conditions shall control.
14. Revocation: Elsevier or Copyright Clearance Center may deny the permissions described in this License at their sole discretion, for any reason or no reason, with a full refund payable to you. Notice of such denial will be made using the contact information provided by you. Failure to receive such notice will not alter or invalidate the denial. In no event will Elsevier or Copyright Clearance Center be responsible or liable for any costs, expenses or damage incurred by you as a result of a denial of your permission request, other than a refund of the amount(s) paid by you to Elsevier and/or Copyright Clearance Center for denied permissions.

LIMITED LICENSE

The following terms and conditions apply only to specific license types:
15. **Translation**: This permission is granted for non-exclusive world **English** rights only unless your license was granted for translation rights. If you licensed translation rights you may only translate this content into the languages you requested. A professional translator must perform all translations and reproduce the content word for word preserving the integrity of the article.
16. **Posting licensed content on any Website**: The following terms and conditions apply as follows: Licensing material from an Elsevier journal: All content posted to the web site must maintain the copyright information line on the bottom of each image; A hyper-text must be included to the Homepage of the journal from which you are licensing at http://www.sciencedirect.com/science/journal/xxxxx or the Elsevier homepage for books at http://www.elsevier.com; Central Storage: This license does not include permission for a scanned version of the material to be stored in a central repository such as that provided by Heron/XanEdu.
Licensing material from an Elsevier book: A hyper-text link must be included to the Elsevier homepage at http://www.elsevier.com . All content posted to the web site must maintain the copyright information line on the bottom of each image.

Posting licensed content on Electronic reserve: In addition to the above the following clauses are applicable: The web site must be password-protected and made available only to bona fide students registered on a relevant course. This permission

is granted for 1 year only. You may obtain a new license for future website posting.
17. **For journal authors:** the following clauses are applicable in addition to the above:
Preprints:
A preprint is an author's own write-up of research results and analysis, it has not been peer-reviewed, nor has it had any other value added to it by a publisher (such as formatting, copyright, technical enhancement etc.).
Authors can share their preprints anywhere at any time. Preprints should not be added to or enhanced in any way in order to appear more like, or to substitute for, the final versions of articles however authors can update their preprints on arXiv or RePEc with their Accepted Author Manuscript (see below).
If accepted for publication, we encourage authors to link from the preprint to their formal publication via its DOI. Millions of researchers have access to the formal publications on ScienceDirect, and so links will help users to find, access, cite and use the best available version. Please note that Cell Press, The Lancet and some society-owned have different preprint policies. Information on these policies is available on the journal homepage.
Accepted Author Manuscripts: An accepted author manuscript is the manuscript of an article that has been accepted for publication and which typically includes author-incorporated changes suggested during submission, peer review and editor-author communications.
Authors can share their accepted author manuscript:

- immediately
    - via their non-commercial person homepage or blog
    - by updating a preprint in arXiv or RePEc with the accepted manuscript
    - via their research institute or institutional repository for internal institutional uses or as part of an invitation-only research collaboration work-group
    - directly by providing copies to their students or to research collaborators for their personal use
    - for private scholarly sharing as part of an invitation-only work group on commercial sites with which Elsevier has an agreement
- After the embargo period
    - via non-commercial hosting platforms such as their institutional repository
    - via commercial sites with which Elsevier has an agreement

In all cases accepted manuscripts should:

- link to the formal publication via its DOI
- bear a CC-BY-NC-ND license - this is easy to do
- if aggregated with other manuscripts, for example in a repository or other site, be shared in alignment with our hosting policy not be added to or enhanced in any way to appear more like, or to substitute for, the published journal article.

Published journal article (JPA): A published journal article (PJA) is the definitive final record of published research that appears or will appear in the journal and embodies all value-adding publishing activities including peer review co-ordination, copy-editing, formatting, (if relevant) pagination and online enrichment.
Policies for sharing publishing journal articles differ for subscription and gold open access articles:
Subscription Articles: If you are an author, please share a link to your article rather than the full-text. Millions of researchers have access to the formal publications on ScienceDirect, and so links will help your users to find, access, cite, and use the best available version.
Theses and dissertations which contain embedded PJAs as part of the formal submission can be posted publicly by the awarding institution with DOI links back to the formal publications on ScienceDirect.
If you are affiliated with a library that subscribes to ScienceDirect you have additional private sharing rights for others' research accessed under that agreement. This includes use for classroom teaching and internal training at the institution (including use in course packs and courseware programs), and inclusion of the article for grant funding purposes.
Gold Open Access Articles: May be shared according to the author-selected end-user license and should contain a CrossMark logo, the end user license, and a DOI link to the formal publication on ScienceDirect.
Please refer to Elsevier's posting policy for further information.
18. **For book authors** the following clauses are applicable in addition to the above: Authors are permitted to place a brief summary of their work online only. You are not allowed to download and post the published electronic version of your chapter, nor may you scan the printed edition to create an electronic version. **Posting to a repository:** Authors are permitted to post a summary of their chapter only in their institution's repository.
19. **Thesis/Dissertation**: If your license is for use in a thesis/dissertation your thesis may be submitted to your institution in either print or electronic form. Should your thesis be published commercially, please reapply for permission. These requirements include permission for the Library and Archives of Canada to supply single copies, on demand, of the complete thesis and include permission for Proquest/UMI to supply single copies, on demand, of the complete thesis. Should your thesis be published commercially, please reapply for permission. Theses and dissertations which contain embedded PJAs as part of the formal submission can be posted publicly by the awarding institution with DOI links back to the formal publications on ScienceDirect.

Elsevier Open Access Terms and Conditions

You can publish open access with Elsevier in hundreds of open access journals or in nearly 2000 established subscription journals that support open access publishing. Permitted third party re-use of these open access articles is defined by the author's choice of Creative Commons user license. See our open access license policy for more information.

Terms & Conditions applicable to all Open Access articles published with Elsevier:

Any reuse of the article must not represent the author as endorsing the adaptation of the article nor should the article be modified in such a way as to damage the author's honour or reputation. If any changes have been made, such changes must be clearly indicated.

The author(s) must be appropriately credited and we ask that you include the end user license and a DOI link to the formal publication on ScienceDirect.

If any part of the material to be used (for example, figures) has appeared in our publication with credit or acknowledgement to another source it is the responsibility of the user to ensure their reuse complies with the terms and conditions determined by the rights holder.

Additional Terms & Conditions applicable to each Creative Commons user license:

CC BY: The CC-BY license allows users to copy, to create extracts, abstracts and new works from the Article, to alter and revise the Article and to make commercial use of the Article (including reuse and/or resale of the Article by commercial entities), provided the user gives appropriate credit (with a link to the formal publication through the relevant DOI), provides a link to the license, indicates if changes were made and the licensor is not represented as endorsing the use made of the work. The full details of the license are available at http://creativecommons.org/licenses/by/4.0.

CC BY NC SA: The CC BY-NC-SA license allows users to copy, to create extracts, abstracts and new works from the Article, to alter and revise the Article, provided this is not done for commercial purposes, and that the user gives appropriate credit (with a link to the formal publication through the relevant DOI), provides a link to the license, indicates if changes were made and the licensor is not represented as endorsing the use made of the work. Further, any new works must be made available on the same conditions. The full details of the license are available at http://creativecommons.org/licenses/by-nc-sa/4.0.

CC BY NC ND: The CC BY-NC-ND license allows users to copy and distribute the Article, provided this is not done for commercial purposes and further does not permit distribution of the Article if it is changed or edited in any way, and provided the user gives appropriate credit (with a link to the formal publication through the relevant DOI), provides a link to the license, and that the licensor is not represented as endorsing the use made of the work. The full details of the license are available at http://creativecommons.org/licenses/by-nc-nd/4.0. Any commercial reuse of Open Access articles published with a CC BY NC SA or CC BY NC ND license requires permission from Elsevier and will be subject to a fee.

Commercial reuse includes:

- Associating advertising with the full text of the Article
- Charging fees for document delivery or access
- Article aggregation
- Systematic distribution via e-mail lists or share buttons

Posting or linking by commercial companies for use by customers of those companies.

20. **Other Conditions**:

v1.10

Questions? customercare@copyright.com or +1-855-239-3415 (toll free in the US) or +1-978-646-2777.

ELSEVIER LICENSE TERMS AND CONDITIONS

Sep 12, 2022

This Agreement between Ruth Birch ("You") and Elsevier ("Elsevier") consists of your license details and the terms and conditions provided by Elsevier and Copyright Clearance Center.

License Number	5386371236415
License date	Sep 12, 2022
Licensed Content Publisher	Elsevier
Licensed Content Publication	Journal of Physics and Chemistry of Solids
Licensed Content Title	Phase ordering under quenching: a case of Zr-alloy
Licensed Content Author	A.R. Massih,L.O. Jernkvist
Licensed Content Date	Jun 1, 2004
Licensed Content Volume	65
Licensed Content Issue	6
Licensed Content Pages	6
Start Page	1193
End Page	1198
Type of Use	reuse in a thesis/dissertation
Portion	figures/tables/illustrations
Number of figures/tables /illustrations	1
Format	both print and electronic
Are you the author of this Elsevier article?	No
Will you be translating?	No
Title	PhD Thesis
Institution name	Imperial College London
Expected presentation date	Sep 2022
Portions	Figure 5
Requestor Location	Ruth Birch Department of materials Imperial college london London, SW7 2AZ United Kingdom Attn: Ruth Birch
Publisher Tax ID	GB 494 6272 12
Total	**0.00 GBP**
Terms and Conditions	

INTRODUCTION

1. The publisher for this copyrighted material is Elsevier. By clicking "accept" in connection with completing this licensing transaction, you agree that the following terms and conditions apply to this transaction (along with the Billing and Payment terms and conditions established by Copyright Clearance Center, Inc. ("CCC"), at the time that you opened your Rightslink account and that are available at any time at http://myaccount.copyright.com).

GENERAL TERMS

2. Elsevier hereby grants you permission to reproduce the aforementioned material subject to the terms and conditions indicated.

3. Acknowledgement: If any part of the material to be used (for example, figures) has appeared in our publication with credit or acknowledgement to another source, permission must also be sought from that source. If such permission is not obtained then that material may not be included in your publication/copies. Suitable acknowledgement to the source must be made, either as a footnote or in a reference list at the end of your publication, as follows:
"Reprinted from Publication title, Vol /edition number, Author(s), Title of article / title of chapter, Pages No., Copyright (Year), with permission from Elsevier [OR APPLICABLE SOCIETY COPYRIGHT OWNER]." Also Lancet special credit - "Reprinted from The Lancet, Vol. number, Author(s), Title of article, Pages No., Copyright (Year), with permission from Elsevier."
4. Reproduction of this material is confined to the purpose and/or media for which permission is hereby given.
5. Altering/Modifying Material: Not Permitted. However figures and illustrations may be altered/adapted minimally to serve your work. Any other abbreviations, additions, deletions and/or any other alterations shall be made only with prior written authorization of Elsevier Ltd. (Please contact Elsevier's permissions helpdesk here). No modifications can be made to any Lancet figures/tables and they must be reproduced in full.
6. If the permission fee for the requested use of our material is waived in this instance, please be advised that your future requests for Elsevier materials may attract a fee.
7. Reservation of Rights: Publisher reserves all rights not specifically granted in the combination of (i) the license details provided by you and accepted in the course of this licensing transaction, (ii) these terms and conditions and (iii) CCC's Billing and Payment terms and conditions.
8. License Contingent Upon Payment: While you may exercise the rights licensed immediately upon issuance of the license at the end of the licensing process for the transaction, provided that you have disclosed complete and accurate details of your proposed use, no license is finally effective unless and until full payment is received from you (either by publisher or by CCC) as provided in CCC's Billing and Payment terms and conditions. If full payment is not received on a timely basis, then any license preliminarily granted shall be deemed automatically revoked and shall be void as if never granted. Further, in the event that you breach any of these terms and conditions or any of CCC's Billing and Payment terms and conditions, the license is automatically revoked and shall be void as if never granted. Use of materials as described in a revoked license, as well as any use of the materials beyond the scope of an unrevoked license, may constitute copyright infringement and publisher reserves the right to take any and all action to protect its copyright in the materials.
9. Warranties: Publisher makes no representations or warranties with respect to the licensed material.
10. Indemnity: You hereby indemnify and agree to hold harmless publisher and CCC, and their respective officers, directors, employees and agents, from and against any and all claims arising out of your use of the licensed material other than as specifically authorized pursuant to this license.
11. No Transfer of License: This license is personal to you and may not be sublicensed, assigned, or transferred by you to any other person without publisher's written permission.
12. No Amendment Except in Writing: This license may not be amended except in a writing signed by both parties (or, in the case of publisher, by CCC on publisher's behalf).
13. Objection to Contrary Terms: Publisher hereby objects to any terms contained in any purchase order, acknowledgment, check endorsement or other writing prepared by you, which terms are inconsistent with these terms and conditions or CCC's Billing and Payment terms and conditions. These terms and conditions, together with CCC's Billing and Payment terms and conditions (which are incorporated herein), comprise the entire agreement between you and publisher (and CCC) concerning this licensing transaction. In the event of any conflict between your obligations established by these terms and conditions and those established by CCC's Billing and Payment terms and conditions, these terms and conditions shall control.
14. Revocation: Elsevier or Copyright Clearance Center may deny the permissions described in this License at their sole discretion, for any reason or no reason, with a full refund payable to you. Notice of such denial will be made using the contact information provided by you. Failure to receive such notice will not alter or invalidate the denial. In no event will Elsevier or Copyright Clearance Center be responsible or liable for any costs, expenses or damage incurred by you as a result of a denial of your permission request, other than a refund of the amount(s) paid by you to Elsevier and/or Copyright Clearance Center for denied permissions.

LIMITED LICENSE

The following terms and conditions apply only to specific license types:
15. **Translation**: This permission is granted for non-exclusive world **English** rights only unless your license was granted for translation rights. If you licensed translation rights you may only translate this content into the languages you requested. A professional translator must perform all translations and reproduce the content word for word preserving the integrity of the article.
16. **Posting licensed content on any Website**: The following terms and conditions apply as follows: Licensing material from an Elsevier journal: All content posted to the web site must maintain the copyright information line on the bottom of each image; A hyper-text must be included to the Homepage of the journal from which you are licensing at http://www.sciencedirect.com/science/journal/xxxxx or the Elsevier homepage for books at http://www.elsevier.com; Central Storage: This license does not include permission for a scanned version of the material to be stored in a central repository such as that provided by Heron/XanEdu.
Licensing material from an Elsevier book: A hyper-text link must be included to the Elsevier homepage at http://www.elsevier.com . All content posted to the web site must maintain the copyright information line on the bottom of each image.

Posting licensed content on Electronic reserve: In addition to the above the following clauses are applicable: The web site must be password-protected and made available only to bona fide students registered on a relevant course. This permission

is granted for 1 year only. You may obtain a new license for future website posting.
17. **For journal authors:** the following clauses are applicable in addition to the above:
Preprints:
A preprint is an author's own write-up of research results and analysis, it has not been peer-reviewed, nor has it had any other value added to it by a publisher (such as formatting, copyright, technical enhancement etc.).
Authors can share their preprints anywhere at any time. Preprints should not be added to or enhanced in any way in order to appear more like, or to substitute for, the final versions of articles however authors can update their preprints on arXiv or RePEc with their Accepted Author Manuscript (see below).
If accepted for publication, we encourage authors to link from the preprint to their formal publication via its DOI. Millions of researchers have access to the formal publications on ScienceDirect, and so links will help users to find, access, cite and use the best available version. Please note that Cell Press, The Lancet and some society-owned have different preprint policies. Information on these policies is available on the journal homepage.
Accepted Author Manuscripts: An accepted author manuscript is the manuscript of an article that has been accepted for publication and which typically includes author-incorporated changes suggested during submission, peer review and editor-author communications.
Authors can share their accepted author manuscript:

- immediately
    - via their non-commercial person homepage or blog
    - by updating a preprint in arXiv or RePEc with the accepted manuscript
    - via their research institute or institutional repository for internal institutional uses or as part of an invitation-only research collaboration work-group
    - directly by providing copies to their students or to research collaborators for their personal use
    - for private scholarly sharing as part of an invitation-only work group on commercial sites with which Elsevier has an agreement
- After the embargo period
    - via non-commercial hosting platforms such as their institutional repository
    - via commercial sites with which Elsevier has an agreement

In all cases accepted manuscripts should:

- link to the formal publication via its DOI
- bear a CC-BY-NC-ND license - this is easy to do
- if aggregated with other manuscripts, for example in a repository or other site, be shared in alignment with our hosting policy not be added to or enhanced in any way to appear more like, or to substitute for, the published journal article.

Published journal article (JPA): A published journal article (PJA) is the definitive final record of published research that appears or will appear in the journal and embodies all value-adding publishing activities including peer review co-ordination, copy-editing, formatting, (if relevant) pagination and online enrichment.
Policies for sharing publishing journal articles differ for subscription and gold open access articles:
Subscription Articles: If you are an author, please share a link to your article rather than the full-text. Millions of researchers have access to the formal publications on ScienceDirect, and so links will help your users to find, access, cite, and use the best available version.
Theses and dissertations which contain embedded PJAs as part of the formal submission can be posted publicly by the awarding institution with DOI links back to the formal publications on ScienceDirect.
If you are affiliated with a library that subscribes to ScienceDirect you have additional private sharing rights for others' research accessed under that agreement. This includes use for classroom teaching and internal training at the institution (including use in course packs and courseware programs), and inclusion of the article for grant funding purposes.
Gold Open Access Articles: May be shared according to the author-selected end-user license and should contain a CrossMark logo, the end user license, and a DOI link to the formal publication on ScienceDirect.
Please refer to Elsevier's posting policy for further information.
18. **For book authors** the following clauses are applicable in addition to the above: Authors are permitted to place a brief summary of their work online only. You are not allowed to download and post the published electronic version of your chapter, nor may you scan the printed edition to create an electronic version. **Posting to a repository:** Authors are permitted to post a summary of their chapter only in their institution's repository.
19. **Thesis/Dissertation**: If your license is for use in a thesis/dissertation your thesis may be submitted to your institution in either print or electronic form. Should your thesis be published commercially, please reapply for permission. These requirements include permission for the Library and Archives of Canada to supply single copies, on demand, of the complete thesis and include permission for Proquest/UMI to supply single copies, on demand, of the complete thesis. Should your thesis be published commercially, please reapply for permission. Theses and dissertations which contain embedded PJAs as part of the formal submission can be posted publicly by the awarding institution with DOI links back to the formal publications on ScienceDirect.

Elsevier Open Access Terms and Conditions

You can publish open access with Elsevier in hundreds of open access journals or in nearly 2000 established subscription journals that support open access publishing. Permitted third party re-use of these open access articles is defined by the author's choice of Creative Commons user license. See our open access license policy for more information.

Terms & Conditions applicable to all Open Access articles published with Elsevier:

Any reuse of the article must not represent the author as endorsing the adaptation of the article nor should the article be modified in such a way as to damage the author's honour or reputation. If any changes have been made, such changes must be clearly indicated.

The author(s) must be appropriately credited and we ask that you include the end user license and a DOI link to the formal publication on ScienceDirect.

If any part of the material to be used (for example, figures) has appeared in our publication with credit or acknowledgement to another source it is the responsibility of the user to ensure their reuse complies with the terms and conditions determined by the rights holder.

Additional Terms & Conditions applicable to each Creative Commons user license:

CC BY: The CC-BY license allows users to copy, to create extracts, abstracts and new works from the Article, to alter and revise the Article and to make commercial use of the Article (including reuse and/or resale of the Article by commercial entities), provided the user gives appropriate credit (with a link to the formal publication through the relevant DOI), provides a link to the license, indicates if changes were made and the licensor is not represented as endorsing the use made of the work. The full details of the license are available at http://creativecommons.org/licenses/by/4.0.

CC BY NC SA: The CC BY-NC-SA license allows users to copy, to create extracts, abstracts and new works from the Article, to alter and revise the Article, provided this is not done for commercial purposes, and that the user gives appropriate credit (with a link to the formal publication through the relevant DOI), provides a link to the license, indicates if changes were made and the licensor is not represented as endorsing the use made of the work. Further, any new works must be made available on the same conditions. The full details of the license are available at http://creativecommons.org/licenses/by-nc-sa/4.0.

CC BY NC ND: The CC BY-NC-ND license allows users to copy and distribute the Article, provided this is not done for commercial purposes and further does not permit distribution of the Article if it is changed or edited in any way, and provided the user gives appropriate credit (with a link to the formal publication through the relevant DOI), provides a link to the license, and that the licensor is not represented as endorsing the use made of the work. The full details of the license are available at http://creativecommons.org/licenses/by-nc-nd/4.0. Any commercial reuse of Open Access articles published with a CC BY NC SA or CC BY NC ND license requires permission from Elsevier and will be subject to a fee.

Commercial reuse includes:

- Associating advertising with the full text of the Article
- Charging fees for document delivery or access
- Article aggregation
- Systematic distribution via e-mail lists or share buttons

Posting or linking by commercial companies for use by customers of those companies.

20. **Other Conditions**:

v1.10

Questions? customercare@copyright.com or +1-855-239-3415 (toll free in the US) or +1-978-646-2777.

RightsLink

Home Help Email Support Ruth Birch

Effect of β-Heat Treatment on Microstructure and Mechanical Anisotropy of Zircaloy-4 Fuel Cladding

Author: Sung-Hoon JUNG, , In-Sup KIM
Publication: Journal of Nuclear Science and Technology
Publisher: Taylor & Francis
Date: May 1, 1989

Rights managed by Taylor & Francis

Thesis/Dissertation Reuse Request

Taylor & Francis is pleased to offer reuses of its content for a thesis or dissertation free of charge contingent on resubmission of permission request if work is published.

BACK CLOSE

© 2022 Copyright - All Rights Reserved | Copyright Clearance Center, Inc. | Privacy statement | Data Security and Privacy | For California Residents | Terms and ConditionsComments? We would like to hear from you. E-mail us at customercare@copyright.com

ELSEVIER LICENSE TERMS AND CONDITIONS

Sep 12, 2022

This Agreement between Ruth Birch ("You") and Elsevier ("Elsevier") consists of your license details and the terms and conditions provided by Elsevier and Copyright Clearance Center.

License Number	5386050631442
License date	Sep 11, 2022
Licensed Content Publisher	Elsevier
Licensed Content Publication	Journal of Materials Processing Technology
Licensed Content Title	Room temperature mechanical properties of electron beam welded zircaloy-4 sheet
Licensed Content Author	C.J. Parga,I.J. van Rooyen,B.D. Coryell,W.R. Lloyd,L.N. Valenti,H. Usman
Licensed Content Date	Mar 1, 2017
Licensed Content Volume	241
Licensed Content Issue	n/a
Licensed Content Pages	13
Start Page	73
End Page	85
Type of Use	reuse in a thesis/dissertation
Portion	figures/tables/illustrations
Number of figures/tables /illustrations	3
Format	both print and electronic
Are you the author of this Elsevier article?	No
Will you be translating?	No
Title	PhD Thesis
Institution name	Imperial College London
Expected presentation date	Sep 2022
Portions	Figures 16, 17 & 18
Requestor Location	Ruth Birch 9 Hance Lane Braintree, CM77 6TH United Kingdom Attn: Ruth Birch
Publisher Tax ID	GB 494 6272 12
Total	**0.00 GBP**
Terms and Conditions	

INTRODUCTION

1. The publisher for this copyrighted material is Elsevier. By clicking "accept" in connection with completing this licensing transaction, you agree that the following terms and conditions apply to this transaction (along with the Billing and Payment terms and conditions established by Copyright Clearance Center, Inc. ("CCC"), at the time that you opened your Rightslink account and that are available at any time at http://myaccount.copyright.com).

GENERAL TERMS

2. Elsevier hereby grants you permission to reproduce the aforementioned material subject to the terms and conditions indicated.

3. Acknowledgement: If any part of the material to be used (for example, figures) has appeared in our publication with credit or acknowledgement to another source, permission must also be sought from that source. If such permission is not obtained then that material may not be included in your publication/copies. Suitable acknowledgement to the source must be made, either as a footnote or in a reference list at the end of your publication, as follows:
"Reprinted from Publication title, Vol /edition number, Author(s), Title of article / title of chapter, Pages No., Copyright (Year), with permission from Elsevier [OR APPLICABLE SOCIETY COPYRIGHT OWNER]." Also Lancet special credit - "Reprinted from The Lancet, Vol. number, Author(s), Title of article, Pages No., Copyright (Year), with permission from Elsevier."
4. Reproduction of this material is confined to the purpose and/or media for which permission is hereby given.
5. Altering/Modifying Material: Not Permitted. However figures and illustrations may be altered/adapted minimally to serve your work. Any other abbreviations, additions, deletions and/or any other alterations shall be made only with prior written authorization of Elsevier Ltd. (Please contact Elsevier's permissions helpdesk here). No modifications can be made to any Lancet figures/tables and they must be reproduced in full.
6. If the permission fee for the requested use of our material is waived in this instance, please be advised that your future requests for Elsevier materials may attract a fee.
7. Reservation of Rights: Publisher reserves all rights not specifically granted in the combination of (i) the license details provided by you and accepted in the course of this licensing transaction, (ii) these terms and conditions and (iii) CCC's Billing and Payment terms and conditions.
8. License Contingent Upon Payment: While you may exercise the rights licensed immediately upon issuance of the license at the end of the licensing process for the transaction, provided that you have disclosed complete and accurate details of your proposed use, no license is finally effective unless and until full payment is received from you (either by publisher or by CCC) as provided in CCC's Billing and Payment terms and conditions. If full payment is not received on a timely basis, then any license preliminarily granted shall be deemed automatically revoked and shall be void as if never granted. Further, in the event that you breach any of these terms and conditions or any of CCC's Billing and Payment terms and conditions, the license is automatically revoked and shall be void as if never granted. Use of materials as described in a revoked license, as well as any use of the materials beyond the scope of an unrevoked license, may constitute copyright infringement and publisher reserves the right to take any and all action to protect its copyright in the materials.
9. Warranties: Publisher makes no representations or warranties with respect to the licensed material.
10. Indemnity: You hereby indemnify and agree to hold harmless publisher and CCC, and their respective officers, directors, employees and agents, from and against any and all claims arising out of your use of the licensed material other than as specifically authorized pursuant to this license.
11. No Transfer of License: This license is personal to you and may not be sublicensed, assigned, or transferred by you to any other person without publisher's written permission.
12. No Amendment Except in Writing: This license may not be amended except in a writing signed by both parties (or, in the case of publisher, by CCC on publisher's behalf).
13. Objection to Contrary Terms: Publisher hereby objects to any terms contained in any purchase order, acknowledgment, check endorsement or other writing prepared by you, which terms are inconsistent with these terms and conditions or CCC's Billing and Payment terms and conditions. These terms and conditions, together with CCC's Billing and Payment terms and conditions (which are incorporated herein), comprise the entire agreement between you and publisher (and CCC) concerning this licensing transaction. In the event of any conflict between your obligations established by these terms and conditions and those established by CCC's Billing and Payment terms and conditions, these terms and conditions shall control.
14. Revocation: Elsevier or Copyright Clearance Center may deny the permissions described in this License at their sole discretion, for any reason or no reason, with a full refund payable to you. Notice of such denial will be made using the contact information provided by you. Failure to receive such notice will not alter or invalidate the denial. In no event will Elsevier or Copyright Clearance Center be responsible or liable for any costs, expenses or damage incurred by you as a result of a denial of your permission request, other than a refund of the amount(s) paid by you to Elsevier and/or Copyright Clearance Center for denied permissions.

LIMITED LICENSE

The following terms and conditions apply only to specific license types:
15. **Translation**: This permission is granted for non-exclusive world **English** rights only unless your license was granted for translation rights. If you licensed translation rights you may only translate this content into the languages you requested. A professional translator must perform all translations and reproduce the content word for word preserving the integrity of the article.
16. **Posting licensed content on any Website**: The following terms and conditions apply as follows: Licensing material from an Elsevier journal: All content posted to the web site must maintain the copyright information line on the bottom of each image; A hyper-text must be included to the Homepage of the journal from which you are licensing at http://www.sciencedirect.com/science/journal/xxxxx or the Elsevier homepage for books at http://www.elsevier.com; Central Storage: This license does not include permission for a scanned version of the material to be stored in a central repository such as that provided by Heron/XanEdu.
Licensing material from an Elsevier book: A hyper-text link must be included to the Elsevier homepage at http://www.elsevier.com . All content posted to the web site must maintain the copyright information line on the bottom of each image.

Posting licensed content on Electronic reserve: In addition to the above the following clauses are applicable: The web site must be password-protected and made available only to bona fide students registered on a relevant course. This permission

is granted for 1 year only. You may obtain a new license for future website posting.
17. **For journal authors:** the following clauses are applicable in addition to the above:
Preprints:
A preprint is an author's own write-up of research results and analysis, it has not been peer-reviewed, nor has it had any other value added to it by a publisher (such as formatting, copyright, technical enhancement etc.).
Authors can share their preprints anywhere at any time. Preprints should not be added to or enhanced in any way in order to appear more like, or to substitute for, the final versions of articles however authors can update their preprints on arXiv or RePEc with their Accepted Author Manuscript (see below).
If accepted for publication, we encourage authors to link from the preprint to their formal publication via its DOI. Millions of researchers have access to the formal publications on ScienceDirect, and so links will help users to find, access, cite and use the best available version. Please note that Cell Press, The Lancet and some society-owned have different preprint policies. Information on these policies is available on the journal homepage.
Accepted Author Manuscripts: An accepted author manuscript is the manuscript of an article that has been accepted for publication and which typically includes author-incorporated changes suggested during submission, peer review and editor-author communications.
Authors can share their accepted author manuscript:

- immediately
    - via their non-commercial person homepage or blog
    - by updating a preprint in arXiv or RePEc with the accepted manuscript
    - via their research institute or institutional repository for internal institutional uses or as part of an invitation-only research collaboration work-group
    - directly by providing copies to their students or to research collaborators for their personal use
    - for private scholarly sharing as part of an invitation-only work group on commercial sites with which Elsevier has an agreement
- After the embargo period
    - via non-commercial hosting platforms such as their institutional repository
    - via commercial sites with which Elsevier has an agreement

In all cases accepted manuscripts should:

- link to the formal publication via its DOI
- bear a CC-BY-NC-ND license - this is easy to do
- if aggregated with other manuscripts, for example in a repository or other site, be shared in alignment with our hosting policy not be added to or enhanced in any way to appear more like, or to substitute for, the published journal article.

Published journal article (JPA): A published journal article (PJA) is the definitive final record of published research that appears or will appear in the journal and embodies all value-adding publishing activities including peer review co-ordination, copy-editing, formatting, (if relevant) pagination and online enrichment.
Policies for sharing publishing journal articles differ for subscription and gold open access articles:
Subscription Articles: If you are an author, please share a link to your article rather than the full-text. Millions of researchers have access to the formal publications on ScienceDirect, and so links will help your users to find, access, cite, and use the best available version.
Theses and dissertations which contain embedded PJAs as part of the formal submission can be posted publicly by the awarding institution with DOI links back to the formal publications on ScienceDirect.
If you are affiliated with a library that subscribes to ScienceDirect you have additional private sharing rights for others' research accessed under that agreement. This includes use for classroom teaching and internal training at the institution (including use in course packs and courseware programs), and inclusion of the article for grant funding purposes.
Gold Open Access Articles: May be shared according to the author-selected end-user license and should contain a CrossMark logo, the end user license, and a DOI link to the formal publication on ScienceDirect.
Please refer to Elsevier's posting policy for further information.
18. **For book authors** the following clauses are applicable in addition to the above: Authors are permitted to place a brief summary of their work online only. You are not allowed to download and post the published electronic version of your chapter, nor may you scan the printed edition to create an electronic version. **Posting to a repository:** Authors are permitted to post a summary of their chapter only in their institution's repository.
19. **Thesis/Dissertation**: If your license is for use in a thesis/dissertation your thesis may be submitted to your institution in either print or electronic form. Should your thesis be published commercially, please reapply for permission. These requirements include permission for the Library and Archives of Canada to supply single copies, on demand, of the complete thesis and include permission for Proquest/UMI to supply single copies, on demand, of the complete thesis. Should your thesis be published commercially, please reapply for permission. Theses and dissertations which contain embedded PJAs as part of the formal submission can be posted publicly by the awarding institution with DOI links back to the formal publications on ScienceDirect.

Elsevier Open Access Terms and Conditions

You can publish open access with Elsevier in hundreds of open access journals or in nearly 2000 established subscription journals that support open access publishing. Permitted third party re-use of these open access articles is defined by the author's choice of Creative Commons user license. See our open access license policy for more information.

Terms & Conditions applicable to all Open Access articles published with Elsevier:

Any reuse of the article must not represent the author as endorsing the adaptation of the article nor should the article be modified in such a way as to damage the author's honour or reputation. If any changes have been made, such changes must be clearly indicated.

The author(s) must be appropriately credited and we ask that you include the end user license and a DOI link to the formal publication on ScienceDirect.

If any part of the material to be used (for example, figures) has appeared in our publication with credit or acknowledgement to another source it is the responsibility of the user to ensure their reuse complies with the terms and conditions determined by the rights holder.

Additional Terms & Conditions applicable to each Creative Commons user license:

CC BY: The CC-BY license allows users to copy, to create extracts, abstracts and new works from the Article, to alter and revise the Article and to make commercial use of the Article (including reuse and/or resale of the Article by commercial entities), provided the user gives appropriate credit (with a link to the formal publication through the relevant DOI), provides a link to the license, indicates if changes were made and the licensor is not represented as endorsing the use made of the work. The full details of the license are available at http://creativecommons.org/licenses/by/4.0.

CC BY NC SA: The CC BY-NC-SA license allows users to copy, to create extracts, abstracts and new works from the Article, to alter and revise the Article, provided this is not done for commercial purposes, and that the user gives appropriate credit (with a link to the formal publication through the relevant DOI), provides a link to the license, indicates if changes were made and the licensor is not represented as endorsing the use made of the work. Further, any new works must be made available on the same conditions. The full details of the license are available at http://creativecommons.org/licenses/by-nc-sa/4.0.

CC BY NC ND: The CC BY-NC-ND license allows users to copy and distribute the Article, provided this is not done for commercial purposes and further does not permit distribution of the Article if it is changed or edited in any way, and provided the user gives appropriate credit (with a link to the formal publication through the relevant DOI), provides a link to the license, and that the licensor is not represented as endorsing the use made of the work. The full details of the license are available at http://creativecommons.org/licenses/by-nc-nd/4.0. Any commercial reuse of Open Access articles published with a CC BY NC SA or CC BY NC ND license requires permission from Elsevier and will be subject to a fee.

Commercial reuse includes:

- Associating advertising with the full text of the Article
- Charging fees for document delivery or access
- Article aggregation
- Systematic distribution via e-mail lists or share buttons

Posting or linking by commercial companies for use by customers of those companies.

20. **Other Conditions**:

v1.10

Questions? customercare@copyright.com or +1-855-239-3415 (toll free in the US) or +1-978-646-2777.

SPRINGER NATURE LICENSE TERMS AND CONDITIONS

Sep 12, 2022

This Agreement between Ruth Birch ("You") and Springer Nature ("Springer Nature") consists of your license details and the terms and conditions provided by Springer Nature and Copyright Clearance Center.

License Number	5386741318717
License date	Sep 12, 2022
Licensed Content Publisher	Springer Nature
Licensed Content Publication	JOM Journal of the Minerals, Metals and Materials Society
Licensed Content Title	Blocky Alpha Transformation in Zircaloy-4 Weldments
Licensed Content Author	Helen Taylor et al
Licensed Content Date	Jun 19, 2019
Type of Use	Thesis/Dissertation
Requestor type	academic/university or research institute
Format	print and electronic
Portion	figures/tables/illustrations
Number of figures/tables /illustrations	4
Will you be translating?	no
Circulation/distribution	1 - 29
Author of this Springer Nature content	no
Title	PhD Thesis
Institution name	Imperial College London
Expected presentation date	Sep 2022
Portions	Figures 1-4
Requestor Location	Ruth Birch Department of materials Imperial college london London, SW7 2AZ United Kingdom Attn: Ruth Birch
Total	**0.00 GBP**
Terms and Conditions	

Springer Nature Customer Service Centre GmbH
Terms and Conditions

This agreement sets out the terms and conditions of the licence (the **Licence**) between you and **Springer Nature Customer Service Centre GmbH** (the **Licensor**). By clicking 'accept' and completing the transaction for the material (**Licensed Material**), you also confirm your acceptance of these terms and conditions.

1. Grant of License

1. 1. The Licensor grants you a personal, non-exclusive, non-transferable, world-wide licence to reproduce the Licensed Material for the purpose specified in your order only. Licences are granted for the specific use requested in the order and for no other use, subject to the conditions below.

1. 2. The Licensor warrants that it has, to the best of its knowledge, the rights to license reuse of the Licensed Material. However, you should ensure that the material you are requesting is original to the Licensor and does not

carry the copyright of another entity (as credited in the published version).

1. 3. If the credit line on any part of the material you have requested indicates that it was reprinted or adapted with permission from another source, then you should also seek permission from that source to reuse the material.

2. Scope of Licence

2. 1. You may only use the Licensed Content in the manner and to the extent permitted by these Ts&Cs and any applicable laws.

2. 2. A separate licence may be required for any additional use of the Licensed Material, e.g. where a licence has been purchased for print only use, separate permission must be obtained for electronic re-use. Similarly, a licence is only valid in the language selected and does not apply for editions in other languages unless additional translation rights have been granted separately in the licence. Any content owned by third parties are expressly excluded from the licence.

2. 3. Similarly, rights for additional components such as custom editions and derivatives require additional permission and may be subject to an additional fee. Please apply to Journalpermissions@springernature.com/bookpermissions@springernature.com for these rights.

2. 4. Where permission has been granted **free of charge** for material in print, permission may also be granted for any electronic version of that work, provided that the material is incidental to your work as a whole and that the electronic version is essentially equivalent to, or substitutes for, the print version.

2. 5. An alternative scope of licence may apply to signatories of the STM Permissions Guidelines, as amended from time to time.

3. Duration of Licence

3. 1. A licence for is valid from the date of purchase ('Licence Date') at the end of the relevant period in the below table:

Scope of Licence	Duration of Licence
Post on a website	12 months
Presentations	12 months
Books and journals	Lifetime of the edition in the language purchased

4. Acknowledgement

4. 1. The Licensor's permission must be acknowledged next to the Licenced Material in print. In electronic form, this acknowledgement must be visible at the same time as the figures/tables/illustrations or abstract, and must be hyperlinked to the journal/book's homepage. Our required acknowledgement format is in the Appendix below.

5. Restrictions on use

5. 1. Use of the Licensed Material may be permitted for incidental promotional use and minor editing privileges e.g. minor adaptations of single figures, changes of format, colour and/or style where the adaptation is credited as set out in Appendix 1 below. Any other changes including but not limited to, cropping, adapting, omitting material that affect the meaning, intention or moral rights of the author are strictly prohibited.

5. 2. You must not use any Licensed Material as part of any design or trademark.

5. 3. Licensed Material may be used in Open Access Publications (OAP) before publication by Springer Nature, but any Licensed Material must be removed from OAP sites prior to final publication.

6. Ownership of Rights

6. 1. Licensed Material remains the property of either Licensor or the relevant third party and any rights not explicitly

granted herein are expressly reserved.

7. Warranty

IN NO EVENT SHALL LICENSOR BE LIABLE TO YOU OR ANY OTHER PARTY OR ANY OTHER PERSON OR FOR ANY SPECIAL, CONSEQUENTIAL, INCIDENTAL OR INDIRECT DAMAGES, HOWEVER CAUSED, ARISING OUT OF OR IN CONNECTION WITH THE DOWNLOADING, VIEWING OR USE OF THE MATERIALS REGARDLESS OF THE FORM OF ACTION, WHETHER FOR BREACH OF CONTRACT, BREACH OF WARRANTY, TORT, NEGLIGENCE, INFRINGEMENT OR OTHERWISE (INCLUDING, WITHOUT LIMITATION, DAMAGES BASED ON LOSS OF PROFITS, DATA, FILES, USE, BUSINESS OPPORTUNITY OR CLAIMS OF THIRD PARTIES), AND
WHETHER OR NOT THE PARTY HAS BEEN ADVISED OF THE POSSIBILITY OF SUCH DAMAGES. THIS LIMITATION SHALL APPLY NOTWITHSTANDING ANY FAILURE OF ESSENTIAL PURPOSE OF ANY LIMITED REMEDY PROVIDED HEREIN.

8. Limitations

8. 1. ***BOOKS ONLY:***Where **'reuse in a dissertation/thesis'** has been selected the following terms apply: Print rights of the final author's accepted manuscript (for clarity, NOT the published version) for up to 100 copies, electronic rights for use only on a personal website or institutional repository as defined by the Sherpa guideline (www.sherpa.ac.uk/romeo/).

8. 2. For content reuse requests that qualify for permission under the STM Permissions Guidelines, which may be updated from time to time, the STM Permissions Guidelines supersede the terms and conditions contained in this licence.

9. Termination and Cancellation

9. 1. Licences will expire after the period shown in Clause 3 (above).

9. 2. Licensee reserves the right to terminate the Licence in the event that payment is not received in full or if there has been a breach of this agreement by you.

Appendix 1 — Acknowledgements:

For Journal Content:
Reprinted by permission from [**the Licensor**]: [**Journal Publisher** (e.g. Nature/Springer/Palgrave)] [**JOURNAL NAME**] [**REFERENCE CITATION** (Article name, Author(s) Name), [**COPYRIGHT**] (year of publication)

For **Advance Online Publication papers:**
Reprinted by permission from [**the Licensor**]: [**Journal Publisher** (e.g. Nature/Springer/Palgrave)] [**JOURNAL NAME**] [**REFERENCE CITATION** (Article name, Author(s) Name), [**COPYRIGHT**] (year of publication), advance online publication, day month year (doi: 10.1038/sj.[JOURNAL ACRONYM].)

For Adaptations/Translations:
Adapted/Translated by permission from [**the Licensor**]: [**Journal Publisher** (e.g. Nature/Springer/Palgrave)] [**JOURNAL NAME**] [**REFERENCE CITATION** (Article name, Author(s) Name), [**COPYRIGHT**] (year of publication)

Note: For any republication from the British Journal of Cancer, the following credit line style applies:

Reprinted/adapted/translated by permission from [**the Licensor**]: on behalf of Cancer Research UK: : [**Journal Publisher** (e.g. Nature/Springer/Palgrave)] [**JOURNAL NAME**] [**REFERENCE CITATION** (Article name, Author(s) Name), [**COPYRIGHT]** (year of publication)

For **Advance Online Publication** papers:
Reprinted by permission from The [**the Licensor**]: on behalf of Cancer Research UK: [**Journal Publisher** (e.g. Nature/Springer/Palgrave)] [**JOURNAL NAME**] [**REFERENCE CITATION** (Article name, Author(s) Name), [**COPYRIGHT**] (year of publication), advance online publication, day month year (doi: 10.1038/sj.[JOURNAL ACRONYM])

For Book content:
Reprinted/adapted by permission from [**the Licensor**]: [**Book Publisher** (e.g. Palgrave Macmillan, Springer etc)

[**Book Title**] by [**Book author**(s)] [**COPYRIGHT**] (year of publication)

Other Conditions:

Version 1.3

Questions? customercare@copyright.com or +1-855-239-3415 (toll free in the US) or +1-978-646-2777.

ELSEVIER LICENSE TERMS AND CONDITIONS

Sep 12, 2022

This Agreement between Ruth Birch ("You") and Elsevier ("Elsevier") consists of your license details and the terms and conditions provided by Elsevier and Copyright Clearance Center.

License Number	5386370932505
License date	Sep 12, 2022
Licensed Content Publisher	Elsevier
Licensed Content Publication	Journal of Nuclear Materials
Licensed Content Title	Temperature and time effects of post-weld heat treatments on tensile properties and microstructure of Zircaloy-4
Licensed Content Author	John Echols,Lauren Garrison,Chinthaka Silva,Elizabeth Lindquist
Licensed Content Date	Aug 1, 2021
Licensed Content Volume	551
Licensed Content Issue	n/a
Licensed Content Pages	1
Start Page	152952
End Page	0
Type of Use	reuse in a thesis/dissertation
Portion	figures/tables/illustrations
Number of figures/tables /illustrations	2
Format	both print and electronic
Are you the author of this Elsevier article?	No
Will you be translating?	No
Title	PhD Thesis
Institution name	Imperial College London
Expected presentation date	Sep 2022
Portions	Figures 5 & 9
Requestor Location	Ruth Birch Department of materials Imperial college london London, SW7 2AZ United Kingdom Attn: Ruth Birch
Publisher Tax ID	GB 494 6272 12
Total	**0.00 GBP**
Terms and Conditions	

INTRODUCTION

1. The publisher for this copyrighted material is Elsevier. By clicking "accept" in connection with completing this licensing transaction, you agree that the following terms and conditions apply to this transaction (along with the Billing and Payment terms and conditions established by Copyright Clearance Center, Inc. ("CCC"), at the time that you opened your Rightslink account and that are available at any time at http://myaccount.copyright.com).

GENERAL TERMS

2. Elsevier hereby grants you permission to reproduce the aforementioned material subject to the terms and conditions

indicated.
3. Acknowledgement: If any part of the material to be used (for example, figures) has appeared in our publication with credit or acknowledgement to another source, permission must also be sought from that source. If such permission is not obtained then that material may not be included in your publication/copies. Suitable acknowledgement to the source must be made, either as a footnote or in a reference list at the end of your publication, as follows:
"Reprinted from Publication title, Vol /edition number, Author(s), Title of article / title of chapter, Pages No., Copyright (Year), with permission from Elsevier [OR APPLICABLE SOCIETY COPYRIGHT OWNER]." Also Lancet special credit - "Reprinted from The Lancet, Vol. number, Author(s), Title of article, Pages No., Copyright (Year), with permission from Elsevier."
4. Reproduction of this material is confined to the purpose and/or media for which permission is hereby given.
5. Altering/Modifying Material: Not Permitted. However figures and illustrations may be altered/adapted minimally to serve your work. Any other abbreviations, additions, deletions and/or any other alterations shall be made only with prior written authorization of Elsevier Ltd. (Please contact Elsevier's permissions helpdesk here). No modifications can be made to any Lancet figures/tables and they must be reproduced in full.
6. If the permission fee for the requested use of our material is waived in this instance, please be advised that your future requests for Elsevier materials may attract a fee.
7. Reservation of Rights: Publisher reserves all rights not specifically granted in the combination of (i) the license details provided by you and accepted in the course of this licensing transaction, (ii) these terms and conditions and (iii) CCC's Billing and Payment terms and conditions.
8. License Contingent Upon Payment: While you may exercise the rights licensed immediately upon issuance of the license at the end of the licensing process for the transaction, provided that you have disclosed complete and accurate details of your proposed use, no license is finally effective unless and until full payment is received from you (either by publisher or by CCC) as provided in CCC's Billing and Payment terms and conditions. If full payment is not received on a timely basis, then any license preliminarily granted shall be deemed automatically revoked and shall be void as if never granted. Further, in the event that you breach any of these terms and conditions or any of CCC's Billing and Payment terms and conditions, the license is automatically revoked and shall be void as if never granted. Use of materials as described in a revoked license, as well as any use of the materials beyond the scope of an unrevoked license, may constitute copyright infringement and publisher reserves the right to take any and all action to protect its copyright in the materials.
9. Warranties: Publisher makes no representations or warranties with respect to the licensed material.
10. Indemnity: You hereby indemnify and agree to hold harmless publisher and CCC, and their respective officers, directors, employees and agents, from and against any and all claims arising out of your use of the licensed material other than as specifically authorized pursuant to this license.
11. No Transfer of License: This license is personal to you and may not be sublicensed, assigned, or transferred by you to any other person without publisher's written permission.
12. No Amendment Except in Writing: This license may not be amended except in a writing signed by both parties (or, in the case of publisher, by CCC on publisher's behalf).
13. Objection to Contrary Terms: Publisher hereby objects to any terms contained in any purchase order, acknowledgment, check endorsement or other writing prepared by you, which terms are inconsistent with these terms and conditions or CCC's Billing and Payment terms and conditions. These terms and conditions, together with CCC's Billing and Payment terms and conditions (which are incorporated herein), comprise the entire agreement between you and publisher (and CCC) concerning this licensing transaction. In the event of any conflict between your obligations established by these terms and conditions and those established by CCC's Billing and Payment terms and conditions, these terms and conditions shall control.
14. Revocation: Elsevier or Copyright Clearance Center may deny the permissions described in this License at their sole discretion, for any reason or no reason, with a full refund payable to you. Notice of such denial will be made using the contact information provided by you. Failure to receive such notice will not alter or invalidate the denial. In no event will Elsevier or Copyright Clearance Center be responsible or liable for any costs, expenses or damage incurred by you as a result of a denial of your permission request, other than a refund of the amount(s) paid by you to Elsevier and/or Copyright Clearance Center for denied permissions.

LIMITED LICENSE

The following terms and conditions apply only to specific license types:
15. **Translation**: This permission is granted for non-exclusive world **English** rights only unless your license was granted for translation rights. If you licensed translation rights you may only translate this content into the languages you requested. A professional translator must perform all translations and reproduce the content word for word preserving the integrity of the article.
16. **Posting licensed content on any Website**: The following terms and conditions apply as follows: Licensing material from an Elsevier journal: All content posted to the web site must maintain the copyright information line on the bottom of each image; A hyper-text must be included to the Homepage of the journal from which you are licensing at http://www.sciencedirect.com/science/journal/xxxxx or the Elsevier homepage for books at http://www.elsevier.com; Central Storage: This license does not include permission for a scanned version of the material to be stored in a central repository such as that provided by Heron/XanEdu.
Licensing material from an Elsevier book: A hyper-text link must be included to the Elsevier homepage at http://www.elsevier.com . All content posted to the web site must maintain the copyright information line on the bottom of each image.

Posting licensed content on Electronic reserve: In addition to the above the following clauses are applicable: The web site

must be password-protected and made available only to bona fide students registered on a relevant course. This permission is granted for 1 year only. You may obtain a new license for future website posting.
17. **For journal authors:** the following clauses are applicable in addition to the above:
Preprints:
A preprint is an author's own write-up of research results and analysis, it has not been peer-reviewed, nor has it had any other value added to it by a publisher (such as formatting, copyright, technical enhancement etc.).
Authors can share their preprints anywhere at any time. Preprints should not be added to or enhanced in any way in order to appear more like, or to substitute for, the final versions of articles however authors can update their preprints on arXiv or RePEc with their Accepted Author Manuscript (see below).
If accepted for publication, we encourage authors to link from the preprint to their formal publication via its DOI. Millions of researchers have access to the formal publications on ScienceDirect, and so links will help users to find, access, cite and use the best available version. Please note that Cell Press, The Lancet and some society-owned have different preprint policies. Information on these policies is available on the journal homepage.
Accepted Author Manuscripts: An accepted author manuscript is the manuscript of an article that has been accepted for publication and which typically includes author-incorporated changes suggested during submission, peer review and editor-author communications.
Authors can share their accepted author manuscript:

- immediately
    - via their non-commercial person homepage or blog
    - by updating a preprint in arXiv or RePEc with the accepted manuscript
    - via their research institute or institutional repository for internal institutional uses or as part of an invitation-only research collaboration work-group
    - directly by providing copies to their students or to research collaborators for their personal use
    - for private scholarly sharing as part of an invitation-only work group on commercial sites with which Elsevier has an agreement
- After the embargo period
    - via non-commercial hosting platforms such as their institutional repository
    - via commercial sites with which Elsevier has an agreement

In all cases accepted manuscripts should:

- link to the formal publication via its DOI
- bear a CC-BY-NC-ND license - this is easy to do
- if aggregated with other manuscripts, for example in a repository or other site, be shared in alignment with our hosting policy not be added to or enhanced in any way to appear more like, or to substitute for, the published journal article.

Published journal article (JPA): A published journal article (PJA) is the definitive final record of published research that appears or will appear in the journal and embodies all value-adding publishing activities including peer review co-ordination, copy-editing, formatting, (if relevant) pagination and online enrichment.
Policies for sharing publishing journal articles differ for subscription and gold open access articles:
Subscription Articles: If you are an author, please share a link to your article rather than the full-text. Millions of researchers have access to the formal publications on ScienceDirect, and so links will help your users to find, access, cite, and use the best available version.
Theses and dissertations which contain embedded PJAs as part of the formal submission can be posted publicly by the awarding institution with DOI links back to the formal publications on ScienceDirect.
If you are affiliated with a library that subscribes to ScienceDirect you have additional private sharing rights for others' research accessed under that agreement. This includes use for classroom teaching and internal training at the institution (including use in course packs and courseware programs), and inclusion of the article for grant funding purposes.
Gold Open Access Articles: May be shared according to the author-selected end-user license and should contain a CrossMark logo, the end user license, and a DOI link to the formal publication on ScienceDirect.
Please refer to Elsevier's posting policy for further information.
18. **For book authors** the following clauses are applicable in addition to the above: Authors are permitted to place a brief summary of their work online only. You are not allowed to download and post the published electronic version of your chapter, nor may you scan the printed edition to create an electronic version. **Posting to a repository:** Authors are permitted to post a summary of their chapter only in their institution's repository.
19. **Thesis/Dissertation**: If your license is for use in a thesis/dissertation your thesis may be submitted to your institution in either print or electronic form. Should your thesis be published commercially, please reapply for permission. These requirements include permission for the Library and Archives of Canada to supply single copies, on demand, of the complete thesis and include permission for Proquest/UMI to supply single copies, on demand, of the complete thesis. Should your thesis be published commercially, please reapply for permission. Theses and dissertations which contain embedded PJAs as part of the formal submission can be posted publicly by the awarding institution with DOI links back to the formal publications on ScienceDirect.

Elsevier Open Access Terms and Conditions

You can publish open access with Elsevier in hundreds of open access journals or in nearly 2000 established subscription journals that support open access publishing. Permitted third party re-use of these open access articles is defined by the author's choice of Creative Commons user license. See our open access license policy for more information.

Terms & Conditions applicable to all Open Access articles published with Elsevier:

Any reuse of the article must not represent the author as endorsing the adaptation of the article nor should the article be modified in such a way as to damage the author's honour or reputation. If any changes have been made, such changes must be clearly indicated.

The author(s) must be appropriately credited and we ask that you include the end user license and a DOI link to the formal publication on ScienceDirect.

If any part of the material to be used (for example, figures) has appeared in our publication with credit or acknowledgement to another source it is the responsibility of the user to ensure their reuse complies with the terms and conditions determined by the rights holder.

Additional Terms & Conditions applicable to each Creative Commons user license:

CC BY: The CC-BY license allows users to copy, to create extracts, abstracts and new works from the Article, to alter and revise the Article and to make commercial use of the Article (including reuse and/or resale of the Article by commercial entities), provided the user gives appropriate credit (with a link to the formal publication through the relevant DOI), provides a link to the license, indicates if changes were made and the licensor is not represented as endorsing the use made of the work. The full details of the license are available at http://creativecommons.org/licenses/by/4.0.

CC BY NC SA: The CC BY-NC-SA license allows users to copy, to create extracts, abstracts and new works from the Article, to alter and revise the Article, provided this is not done for commercial purposes, and that the user gives appropriate credit (with a link to the formal publication through the relevant DOI), provides a link to the license, indicates if changes were made and the licensor is not represented as endorsing the use made of the work. Further, any new works must be made available on the same conditions. The full details of the license are available at http://creativecommons.org/licenses/by-nc-sa/4.0.

CC BY NC ND: The CC BY-NC-ND license allows users to copy and distribute the Article, provided this is not done for commercial purposes and further does not permit distribution of the Article if it is changed or edited in any way, and provided the user gives appropriate credit (with a link to the formal publication through the relevant DOI), provides a link to the license, and that the licensor is not represented as endorsing the use made of the work. The full details of the license are available at http://creativecommons.org/licenses/by-nc-nd/4.0. Any commercial reuse of Open Access articles published with a CC BY NC SA or CC BY NC ND license requires permission from Elsevier and will be subject to a fee.

Commercial reuse includes:

- Associating advertising with the full text of the Article
- Charging fees for document delivery or access
- Article aggregation
- Systematic distribution via e-mail lists or share buttons

Posting or linking by commercial companies for use by customers of those companies.

20. **Other Conditions**:

v1.10

Questions? customercare@copyright.com or +1-855-239-3415 (toll free in the US) or +1-978-646-2777.

ELSEVIER LICENSE TERMS AND CONDITIONS

Sep 12, 2022

This Agreement between Ruth Birch ("You") and Elsevier ("Elsevier") consists of your license details and the terms and conditions provided by Elsevier and Copyright Clearance Center.

License Number	5386380102696
License date	Sep 12, 2022
Licensed Content Publisher	Elsevier
Licensed Content Publication	Journal of Nuclear Materials
Licensed Content Title	Microstructural evolution of β-quenched Zircaloy-4 during agings between 100 and 750°C
Licensed Content Author	K. Loucif,R. Borrelly,P. Merle
Licensed Content Date	Jun 1, 1994
Licensed Content Volume	210
Licensed Content Issue	1-2
Licensed Content Pages	13
Start Page	84
End Page	96
Type of Use	reuse in a thesis/dissertation
Portion	figures/tables/illustrations
Number of figures/tables /illustrations	1
Format	both print and electronic
Are you the author of this Elsevier article?	No
Will you be translating?	No
Title	PhD Thesis
Institution name	Imperial College London
Expected presentation date	Sep 2022
Portions	Figure 12
Requestor Location	Ruth Birch Department of materials Imperial college london London, SW7 2AZ United Kingdom Attn: Ruth Birch
Publisher Tax ID	GB 494 6272 12
Total	**0.00 GBP**
Terms and Conditions	

INTRODUCTION

1. The publisher for this copyrighted material is Elsevier. By clicking "accept" in connection with completing this licensing transaction, you agree that the following terms and conditions apply to this transaction (along with the Billing and Payment terms and conditions established by Copyright Clearance Center, Inc. ("CCC"), at the time that you opened your Rightslink account and that are available at any time at http://myaccount.copyright.com).

GENERAL TERMS

2. Elsevier hereby grants you permission to reproduce the aforementioned material subject to the terms and conditions indicated.

3. Acknowledgement: If any part of the material to be used (for example, figures) has appeared in our publication with credit or acknowledgement to another source, permission must also be sought from that source. If such permission is not obtained then that material may not be included in your publication/copies. Suitable acknowledgement to the source must be made, either as a footnote or in a reference list at the end of your publication, as follows:
"Reprinted from Publication title, Vol /edition number, Author(s), Title of article / title of chapter, Pages No., Copyright (Year), with permission from Elsevier [OR APPLICABLE SOCIETY COPYRIGHT OWNER]." Also Lancet special credit - "Reprinted from The Lancet, Vol. number, Author(s), Title of article, Pages No., Copyright (Year), with permission from Elsevier."
4. Reproduction of this material is confined to the purpose and/or media for which permission is hereby given.
5. Altering/Modifying Material: Not Permitted. However figures and illustrations may be altered/adapted minimally to serve your work. Any other abbreviations, additions, deletions and/or any other alterations shall be made only with prior written authorization of Elsevier Ltd. (Please contact Elsevier's permissions helpdesk here). No modifications can be made to any Lancet figures/tables and they must be reproduced in full.
6. If the permission fee for the requested use of our material is waived in this instance, please be advised that your future requests for Elsevier materials may attract a fee.
7. Reservation of Rights: Publisher reserves all rights not specifically granted in the combination of (i) the license details provided by you and accepted in the course of this licensing transaction, (ii) these terms and conditions and (iii) CCC's Billing and Payment terms and conditions.
8. License Contingent Upon Payment: While you may exercise the rights licensed immediately upon issuance of the license at the end of the licensing process for the transaction, provided that you have disclosed complete and accurate details of your proposed use, no license is finally effective unless and until full payment is received from you (either by publisher or by CCC) as provided in CCC's Billing and Payment terms and conditions. If full payment is not received on a timely basis, then any license preliminarily granted shall be deemed automatically revoked and shall be void as if never granted. Further, in the event that you breach any of these terms and conditions or any of CCC's Billing and Payment terms and conditions, the license is automatically revoked and shall be void as if never granted. Use of materials as described in a revoked license, as well as any use of the materials beyond the scope of an unrevoked license, may constitute copyright infringement and publisher reserves the right to take any and all action to protect its copyright in the materials.
9. Warranties: Publisher makes no representations or warranties with respect to the licensed material.
10. Indemnity: You hereby indemnify and agree to hold harmless publisher and CCC, and their respective officers, directors, employees and agents, from and against any and all claims arising out of your use of the licensed material other than as specifically authorized pursuant to this license.
11. No Transfer of License: This license is personal to you and may not be sublicensed, assigned, or transferred by you to any other person without publisher's written permission.
12. No Amendment Except in Writing: This license may not be amended except in a writing signed by both parties (or, in the case of publisher, by CCC on publisher's behalf).
13. Objection to Contrary Terms: Publisher hereby objects to any terms contained in any purchase order, acknowledgment, check endorsement or other writing prepared by you, which terms are inconsistent with these terms and conditions or CCC's Billing and Payment terms and conditions. These terms and conditions, together with CCC's Billing and Payment terms and conditions (which are incorporated herein), comprise the entire agreement between you and publisher (and CCC) concerning this licensing transaction. In the event of any conflict between your obligations established by these terms and conditions and those established by CCC's Billing and Payment terms and conditions, these terms and conditions shall control.
14. Revocation: Elsevier or Copyright Clearance Center may deny the permissions described in this License at their sole discretion, for any reason or no reason, with a full refund payable to you. Notice of such denial will be made using the contact information provided by you. Failure to receive such notice will not alter or invalidate the denial. In no event will Elsevier or Copyright Clearance Center be responsible or liable for any costs, expenses or damage incurred by you as a result of a denial of your permission request, other than a refund of the amount(s) paid by you to Elsevier and/or Copyright Clearance Center for denied permissions.

LIMITED LICENSE

The following terms and conditions apply only to specific license types:
15. **Translation**: This permission is granted for non-exclusive world **English** rights only unless your license was granted for translation rights. If you licensed translation rights you may only translate this content into the languages you requested. A professional translator must perform all translations and reproduce the content word for word preserving the integrity of the article.
16. **Posting licensed content on any Website**: The following terms and conditions apply as follows: Licensing material from an Elsevier journal: All content posted to the web site must maintain the copyright information line on the bottom of each image; A hyper-text must be included to the Homepage of the journal from which you are licensing at http://www.sciencedirect.com/science/journal/xxxxx or the Elsevier homepage for books at http://www.elsevier.com; Central Storage: This license does not include permission for a scanned version of the material to be stored in a central repository such as that provided by Heron/XanEdu.
Licensing material from an Elsevier book: A hyper-text link must be included to the Elsevier homepage at http://www.elsevier.com . All content posted to the web site must maintain the copyright information line on the bottom of each image.

Posting licensed content on Electronic reserve: In addition to the above the following clauses are applicable: The web site must be password-protected and made available only to bona fide students registered on a relevant course. This permission

is granted for 1 year only. You may obtain a new license for future website posting.
17. **For journal authors:** the following clauses are applicable in addition to the above:
Preprints:
A preprint is an author's own write-up of research results and analysis, it has not been peer-reviewed, nor has it had any other value added to it by a publisher (such as formatting, copyright, technical enhancement etc.).
Authors can share their preprints anywhere at any time. Preprints should not be added to or enhanced in any way in order to appear more like, or to substitute for, the final versions of articles however authors can update their preprints on arXiv or RePEc with their Accepted Author Manuscript (see below).
If accepted for publication, we encourage authors to link from the preprint to their formal publication via its DOI. Millions of researchers have access to the formal publications on ScienceDirect, and so links will help users to find, access, cite and use the best available version. Please note that Cell Press, The Lancet and some society-owned have different preprint policies. Information on these policies is available on the journal homepage.
Accepted Author Manuscripts: An accepted author manuscript is the manuscript of an article that has been accepted for publication and which typically includes author-incorporated changes suggested during submission, peer review and editor-author communications.
Authors can share their accepted author manuscript:

- immediately
    - via their non-commercial person homepage or blog
    - by updating a preprint in arXiv or RePEc with the accepted manuscript
    - via their research institute or institutional repository for internal institutional uses or as part of an invitation-only research collaboration work-group
    - directly by providing copies to their students or to research collaborators for their personal use
    - for private scholarly sharing as part of an invitation-only work group on commercial sites with which Elsevier has an agreement
- After the embargo period
    - via non-commercial hosting platforms such as their institutional repository
    - via commercial sites with which Elsevier has an agreement

In all cases accepted manuscripts should:

- link to the formal publication via its DOI
- bear a CC-BY-NC-ND license - this is easy to do
- if aggregated with other manuscripts, for example in a repository or other site, be shared in alignment with our hosting policy not be added to or enhanced in any way to appear more like, or to substitute for, the published journal article.

Published journal article (JPA): A published journal article (PJA) is the definitive final record of published research that appears or will appear in the journal and embodies all value-adding publishing activities including peer review co-ordination, copy-editing, formatting, (if relevant) pagination and online enrichment.
Policies for sharing publishing journal articles differ for subscription and gold open access articles:
Subscription Articles: If you are an author, please share a link to your article rather than the full-text. Millions of researchers have access to the formal publications on ScienceDirect, and so links will help your users to find, access, cite, and use the best available version.
Theses and dissertations which contain embedded PJAs as part of the formal submission can be posted publicly by the awarding institution with DOI links back to the formal publications on ScienceDirect.
If you are affiliated with a library that subscribes to ScienceDirect you have additional private sharing rights for others' research accessed under that agreement. This includes use for classroom teaching and internal training at the institution (including use in course packs and courseware programs), and inclusion of the article for grant funding purposes.
Gold Open Access Articles: May be shared according to the author-selected end-user license and should contain a CrossMark logo, the end user license, and a DOI link to the formal publication on ScienceDirect.
Please refer to Elsevier's posting policy for further information.
18. **For book authors** the following clauses are applicable in addition to the above: Authors are permitted to place a brief summary of their work online only. You are not allowed to download and post the published electronic version of your chapter, nor may you scan the printed edition to create an electronic version. **Posting to a repository:** Authors are permitted to post a summary of their chapter only in their institution's repository.
19. **Thesis/Dissertation**: If your license is for use in a thesis/dissertation your thesis may be submitted to your institution in either print or electronic form. Should your thesis be published commercially, please reapply for permission. These requirements include permission for the Library and Archives of Canada to supply single copies, on demand, of the complete thesis and include permission for Proquest/UMI to supply single copies, on demand, of the complete thesis. Should your thesis be published commercially, please reapply for permission. Theses and dissertations which contain embedded PJAs as part of the formal submission can be posted publicly by the awarding institution with DOI links back to the formal publications on ScienceDirect.

Elsevier Open Access Terms and Conditions

You can publish open access with Elsevier in hundreds of open access journals or in nearly 2000 established subscription journals that support open access publishing. Permitted third party re-use of these open access articles is defined by the author's choice of Creative Commons user license. See our open access license policy for more information.

Terms & Conditions applicable to all Open Access articles published with Elsevier:

Any reuse of the article must not represent the author as endorsing the adaptation of the article nor should the article be modified in such a way as to damage the author's honour or reputation. If any changes have been made, such changes must be clearly indicated.

The author(s) must be appropriately credited and we ask that you include the end user license and a DOI link to the formal publication on ScienceDirect.

If any part of the material to be used (for example, figures) has appeared in our publication with credit or acknowledgement to another source it is the responsibility of the user to ensure their reuse complies with the terms and conditions determined by the rights holder.

Additional Terms & Conditions applicable to each Creative Commons user license:

CC BY: The CC-BY license allows users to copy, to create extracts, abstracts and new works from the Article, to alter and revise the Article and to make commercial use of the Article (including reuse and/or resale of the Article by commercial entities), provided the user gives appropriate credit (with a link to the formal publication through the relevant DOI), provides a link to the license, indicates if changes were made and the licensor is not represented as endorsing the use made of the work. The full details of the license are available at http://creativecommons.org/licenses/by/4.0.

CC BY NC SA: The CC BY-NC-SA license allows users to copy, to create extracts, abstracts and new works from the Article, to alter and revise the Article, provided this is not done for commercial purposes, and that the user gives appropriate credit (with a link to the formal publication through the relevant DOI), provides a link to the license, indicates if changes were made and the licensor is not represented as endorsing the use made of the work. Further, any new works must be made available on the same conditions. The full details of the license are available at http://creativecommons.org/licenses/by-nc-sa/4.0.

CC BY NC ND: The CC BY-NC-ND license allows users to copy and distribute the Article, provided this is not done for commercial purposes and further does not permit distribution of the Article if it is changed or edited in any way, and provided the user gives appropriate credit (with a link to the formal publication through the relevant DOI), provides a link to the license, and that the licensor is not represented as endorsing the use made of the work. The full details of the license are available at http://creativecommons.org/licenses/by-nc-nd/4.0. Any commercial reuse of Open Access articles published with a CC BY NC SA or CC BY NC ND license requires permission from Elsevier and will be subject to a fee.

Commercial reuse includes:

- Associating advertising with the full text of the Article
- Charging fees for document delivery or access
- Article aggregation
- Systematic distribution via e-mail lists or share buttons

Posting or linking by commercial companies for use by customers of those companies.

20. **Other Conditions**:

v1.10

Questions? customercare@copyright.com or +1-855-239-3415 (toll free in the US) or +1-978-646-2777.

SPRINGER NATURE LICENSE TERMS AND CONDITIONS

Sep 12, 2022

This Agreement between Ruth Birch ("You") and Springer Nature ("Springer Nature") consists of your license details and the terms and conditions provided by Springer Nature and Copyright Clearance Center.

License Number	5386380249229
License date	Sep 12, 2022
Licensed Content Publisher	Springer Nature
Licensed Content Publication	Oxidation of Metals
Licensed Content Title	Kinetics of Hydrogen Absorption and Release in Zirconium Alloys During Steam Oxidation
Licensed Content Author	M. Grosse et al
Licensed Content Date	Jul 12, 2008
Type of Use	Thesis/Dissertation
Requestor type	academic/university or research institute
Format	print and electronic
Portion	figures/tables/illustrations
Number of figures/tables /illustrations	1
Will you be translating?	no
Circulation/distribution	1 - 29
Author of this Springer Nature content	no
Title	PhD Thesis
Institution name	Imperial College London
Expected presentation date	Sep 2022
Portions	Figure 8
Requestor Location	Ruth Birch Department of materials Imperial college london London, SW7 2AZ United Kingdom Attn: Ruth Birch
Total	**0.00 GBP**
Terms and Conditions	

Springer Nature Customer Service Centre GmbH
Terms and Conditions

This agreement sets out the terms and conditions of the licence (the **Licence**) between you and **Springer Nature Customer Service Centre GmbH** (the **Licensor**). By clicking 'accept' and completing the transaction for the material (**Licensed Material**), you also confirm your acceptance of these terms and conditions.

1. Grant of License

1. 1. The Licensor grants you a personal, non-exclusive, non-transferable, world-wide licence to reproduce the Licensed Material for the purpose specified in your order only. Licences are granted for the specific use requested in the order and for no other use, subject to the conditions below.

1. 2. The Licensor warrants that it has, to the best of its knowledge, the rights to license reuse of the Licensed Material. However, you should ensure that the material you are requesting is original to the Licensor and does not

carry the copyright of another entity (as credited in the published version).

1. 3. If the credit line on any part of the material you have requested indicates that it was reprinted or adapted with permission from another source, then you should also seek permission from that source to reuse the material.

2. Scope of Licence

2. 1. You may only use the Licensed Content in the manner and to the extent permitted by these Ts&Cs and any applicable laws.

2. 2. A separate licence may be required for any additional use of the Licensed Material, e.g. where a licence has been purchased for print only use, separate permission must be obtained for electronic re-use. Similarly, a licence is only valid in the language selected and does not apply for editions in other languages unless additional translation rights have been granted separately in the licence. Any content owned by third parties are expressly excluded from the licence.

2. 3. Similarly, rights for additional components such as custom editions and derivatives require additional permission and may be subject to an additional fee. Please apply to Journalpermissions@springernature.com/bookpermissions@springernature.com for these rights.

2. 4. Where permission has been granted **free of charge** for material in print, permission may also be granted for any electronic version of that work, provided that the material is incidental to your work as a whole and that the electronic version is essentially equivalent to, or substitutes for, the print version.

2. 5. An alternative scope of licence may apply to signatories of the STM Permissions Guidelines, as amended from time to time.

3. Duration of Licence

3. 1. A licence for is valid from the date of purchase ('Licence Date') at the end of the relevant period in the below table:

Scope of Licence	Duration of Licence
Post on a website	12 months
Presentations	12 months
Books and journals	Lifetime of the edition in the language purchased

4. Acknowledgement

4. 1. The Licensor's permission must be acknowledged next to the Licenced Material in print. In electronic form, this acknowledgement must be visible at the same time as the figures/tables/illustrations or abstract, and must be hyperlinked to the journal/book's homepage. Our required acknowledgement format is in the Appendix below.

5. Restrictions on use

5. 1. Use of the Licensed Material may be permitted for incidental promotional use and minor editing privileges e.g. minor adaptations of single figures, changes of format, colour and/or style where the adaptation is credited as set out in Appendix 1 below. Any other changes including but not limited to, cropping, adapting, omitting material that affect the meaning, intention or moral rights of the author are strictly prohibited.

5. 2. You must not use any Licensed Material as part of any design or trademark.

5. 3. Licensed Material may be used in Open Access Publications (OAP) before publication by Springer Nature, but any Licensed Material must be removed from OAP sites prior to final publication.

6. Ownership of Rights

6. 1. Licensed Material remains the property of either Licensor or the relevant third party and any rights not explicitly

granted herein are expressly reserved.

7. Warranty

IN NO EVENT SHALL LICENSOR BE LIABLE TO YOU OR ANY OTHER PARTY OR ANY OTHER PERSON OR FOR ANY SPECIAL, CONSEQUENTIAL, INCIDENTAL OR INDIRECT DAMAGES, HOWEVER CAUSED, ARISING OUT OF OR IN CONNECTION WITH THE DOWNLOADING, VIEWING OR USE OF THE MATERIALS REGARDLESS OF THE FORM OF ACTION, WHETHER FOR BREACH OF CONTRACT, BREACH OF WARRANTY, TORT, NEGLIGENCE, INFRINGEMENT OR OTHERWISE (INCLUDING, WITHOUT LIMITATION, DAMAGES BASED ON LOSS OF PROFITS, DATA, FILES, USE, BUSINESS OPPORTUNITY OR CLAIMS OF THIRD PARTIES), AND
WHETHER OR NOT THE PARTY HAS BEEN ADVISED OF THE POSSIBILITY OF SUCH DAMAGES. THIS LIMITATION SHALL APPLY NOTWITHSTANDING ANY FAILURE OF ESSENTIAL PURPOSE OF ANY LIMITED REMEDY PROVIDED HEREIN.

8. Limitations

8. 1. ***BOOKS ONLY:***Where **'reuse in a dissertation/thesis'** has been selected the following terms apply: Print rights of the final author's accepted manuscript (for clarity, NOT the published version) for up to 100 copies, electronic rights for use only on a personal website or institutional repository as defined by the Sherpa guideline (www.sherpa.ac.uk/romeo/).

8. 2. For content reuse requests that qualify for permission under the STM Permissions Guidelines, which may be updated from time to time, the STM Permissions Guidelines supersede the terms and conditions contained in this licence.

9. Termination and Cancellation

9. 1. Licences will expire after the period shown in Clause 3 (above).

9. 2. Licensee reserves the right to terminate the Licence in the event that payment is not received in full or if there has been a breach of this agreement by you.

Appendix 1 — Acknowledgements:

For Journal Content:
Reprinted by permission from [**the Licensor**]: [**Journal Publisher** (e.g. Nature/Springer/Palgrave)] [**JOURNAL NAME**] [**REFERENCE CITATION** (Article name, Author(s) Name), [**COPYRIGHT**] (year of publication)

For **Advance Online Publication papers:**
Reprinted by permission from [**the Licensor**]: [**Journal Publisher** (e.g. Nature/Springer/Palgrave)] [**JOURNAL NAME**] [**REFERENCE CITATION** (Article name, Author(s) Name), [**COPYRIGHT**] (year of publication), advance online publication, day month year (doi: 10.1038/sj.[JOURNAL ACRONYM].)

For Adaptations/Translations:
Adapted/Translated by permission from [**the Licensor**]: [**Journal Publisher** (e.g. Nature/Springer/Palgrave)] [**JOURNAL NAME**] [**REFERENCE CITATION** (Article name, Author(s) Name), [**COPYRIGHT**] (year of publication)

Note: For any republication from the British Journal of Cancer, the following credit line style applies:

Reprinted/adapted/translated by permission from [**the Licensor**]: on behalf of Cancer Research UK: : [**Journal Publisher** (e.g. Nature/Springer/Palgrave)] [**JOURNAL NAME**] [**REFERENCE CITATION** (Article name, Author(s) Name), [**COPYRIGHT]** (year of publication)

For **Advance Online Publication** papers:
Reprinted by permission from The [**the Licensor**]: on behalf of Cancer Research UK: [**Journal Publisher** (e.g. Nature/Springer/Palgrave)] [**JOURNAL NAME**] [**REFERENCE CITATION** (Article name, Author(s) Name), [**COPYRIGHT**] (year of publication), advance online publication, day month year (doi: 10.1038/sj.[JOURNAL ACRONYM])

For Book content:
Reprinted/adapted by permission from [**the Licensor**]: [**Book Publisher** (e.g. Palgrave Macmillan, Springer etc)

[**Book Title**] by [**Book author**(s)] [**COPYRIGHT**] (year of publication)

Other Conditions:

Version 1.3

Questions? customercare@copyright.com or +1-855-239-3415 (toll free in the US) or +1-978-646-2777.

ELSEVIER LICENSE TERMS AND CONDITIONS

Sep 12, 2022

This Agreement between Ruth Birch ("You") and Elsevier ("Elsevier") consists of your license details and the terms and conditions provided by Elsevier and Copyright Clearance Center.

License Number	5386390352792
License date	Sep 12, 2022
Licensed Content Publisher	Elsevier
Licensed Content Publication	International Journal of Hydrogen Energy
Licensed Content Title	Hydrogen in Zircaloy: Mechanism and its impacts
Licensed Content Author	Siddharth Suman,Mohd. Kaleem Khan,Manabendra Pathak,R.N. Singh,J.K. Chakravartty
Licensed Content Date	May 11, 2015
Licensed Content Volume	40
Licensed Content Issue	17
Licensed Content Pages	19
Start Page	5976
End Page	5994
Type of Use	reuse in a thesis/dissertation
Portion	figures/tables/illustrations
Number of figures/tables /illustrations	1
Format	both print and electronic
Are you the author of this Elsevier article?	No
Will you be translating?	No
Title	PhD Thesis
Institution name	Imperial College London
Expected presentation date	Sep 2022
Portions	Figure 9
Requestor Location	Ruth Birch Department of materials Imperial college london London, SW7 2AZ United Kingdom Attn: Ruth Birch
Publisher Tax ID	GB 494 6272 12
Total	**0.00 GBP**
Terms and Conditions	

INTRODUCTION

1. The publisher for this copyrighted material is Elsevier. By clicking "accept" in connection with completing this licensing transaction, you agree that the following terms and conditions apply to this transaction (along with the Billing and Payment terms and conditions established by Copyright Clearance Center, Inc. ("CCC"), at the time that you opened your Rightslink account and that are available at any time at http://myaccount.copyright.com).

GENERAL TERMS

2. Elsevier hereby grants you permission to reproduce the aforementioned material subject to the terms and conditions indicated.

3. Acknowledgement: If any part of the material to be used (for example, figures) has appeared in our publication with credit or acknowledgement to another source, permission must also be sought from that source. If such permission is not obtained then that material may not be included in your publication/copies. Suitable acknowledgement to the source must be made, either as a footnote or in a reference list at the end of your publication, as follows:
"Reprinted from Publication title, Vol /edition number, Author(s), Title of article / title of chapter, Pages No., Copyright (Year), with permission from Elsevier [OR APPLICABLE SOCIETY COPYRIGHT OWNER]." Also Lancet special credit - "Reprinted from The Lancet, Vol. number, Author(s), Title of article, Pages No., Copyright (Year), with permission from Elsevier."
4. Reproduction of this material is confined to the purpose and/or media for which permission is hereby given.
5. Altering/Modifying Material: Not Permitted. However figures and illustrations may be altered/adapted minimally to serve your work. Any other abbreviations, additions, deletions and/or any other alterations shall be made only with prior written authorization of Elsevier Ltd. (Please contact Elsevier's permissions helpdesk here). No modifications can be made to any Lancet figures/tables and they must be reproduced in full.
6. If the permission fee for the requested use of our material is waived in this instance, please be advised that your future requests for Elsevier materials may attract a fee.
7. Reservation of Rights: Publisher reserves all rights not specifically granted in the combination of (i) the license details provided by you and accepted in the course of this licensing transaction, (ii) these terms and conditions and (iii) CCC's Billing and Payment terms and conditions.
8. License Contingent Upon Payment: While you may exercise the rights licensed immediately upon issuance of the license at the end of the licensing process for the transaction, provided that you have disclosed complete and accurate details of your proposed use, no license is finally effective unless and until full payment is received from you (either by publisher or by CCC) as provided in CCC's Billing and Payment terms and conditions. If full payment is not received on a timely basis, then any license preliminarily granted shall be deemed automatically revoked and shall be void as if never granted. Further, in the event that you breach any of these terms and conditions or any of CCC's Billing and Payment terms and conditions, the license is automatically revoked and shall be void as if never granted. Use of materials as described in a revoked license, as well as any use of the materials beyond the scope of an unrevoked license, may constitute copyright infringement and publisher reserves the right to take any and all action to protect its copyright in the materials.
9. Warranties: Publisher makes no representations or warranties with respect to the licensed material.
10. Indemnity: You hereby indemnify and agree to hold harmless publisher and CCC, and their respective officers, directors, employees and agents, from and against any and all claims arising out of your use of the licensed material other than as specifically authorized pursuant to this license.
11. No Transfer of License: This license is personal to you and may not be sublicensed, assigned, or transferred by you to any other person without publisher's written permission.
12. No Amendment Except in Writing: This license may not be amended except in a writing signed by both parties (or, in the case of publisher, by CCC on publisher's behalf).
13. Objection to Contrary Terms: Publisher hereby objects to any terms contained in any purchase order, acknowledgment, check endorsement or other writing prepared by you, which terms are inconsistent with these terms and conditions or CCC's Billing and Payment terms and conditions. These terms and conditions, together with CCC's Billing and Payment terms and conditions (which are incorporated herein), comprise the entire agreement between you and publisher (and CCC) concerning this licensing transaction. In the event of any conflict between your obligations established by these terms and conditions and those established by CCC's Billing and Payment terms and conditions, these terms and conditions shall control.
14. Revocation: Elsevier or Copyright Clearance Center may deny the permissions described in this License at their sole discretion, for any reason or no reason, with a full refund payable to you. Notice of such denial will be made using the contact information provided by you. Failure to receive such notice will not alter or invalidate the denial. In no event will Elsevier or Copyright Clearance Center be responsible or liable for any costs, expenses or damage incurred by you as a result of a denial of your permission request, other than a refund of the amount(s) paid by you to Elsevier and/or Copyright Clearance Center for denied permissions.

LIMITED LICENSE

The following terms and conditions apply only to specific license types:
15. **Translation**: This permission is granted for non-exclusive world **English** rights only unless your license was granted for translation rights. If you licensed translation rights you may only translate this content into the languages you requested. A professional translator must perform all translations and reproduce the content word for word preserving the integrity of the article.
16. **Posting licensed content on any Website**: The following terms and conditions apply as follows: Licensing material from an Elsevier journal: All content posted to the web site must maintain the copyright information line on the bottom of each image; A hyper-text must be included to the Homepage of the journal from which you are licensing at http://www.sciencedirect.com/science/journal/xxxxx or the Elsevier homepage for books at http://www.elsevier.com; Central Storage: This license does not include permission for a scanned version of the material to be stored in a central repository such as that provided by Heron/XanEdu.
Licensing material from an Elsevier book: A hyper-text link must be included to the Elsevier homepage at http://www.elsevier.com . All content posted to the web site must maintain the copyright information line on the bottom of each image.

Posting licensed content on Electronic reserve: In addition to the above the following clauses are applicable: The web site must be password-protected and made available only to bona fide students registered on a relevant course. This permission

is granted for 1 year only. You may obtain a new license for future website posting.
17. **For journal authors:** the following clauses are applicable in addition to the above:
Preprints:
A preprint is an author's own write-up of research results and analysis, it has not been peer-reviewed, nor has it had any other value added to it by a publisher (such as formatting, copyright, technical enhancement etc.).
Authors can share their preprints anywhere at any time. Preprints should not be added to or enhanced in any way in order to appear more like, or to substitute for, the final versions of articles however authors can update their preprints on arXiv or RePEc with their Accepted Author Manuscript (see below).
If accepted for publication, we encourage authors to link from the preprint to their formal publication via its DOI. Millions of researchers have access to the formal publications on ScienceDirect, and so links will help users to find, access, cite and use the best available version. Please note that Cell Press, The Lancet and some society-owned have different preprint policies. Information on these policies is available on the journal homepage.
Accepted Author Manuscripts: An accepted author manuscript is the manuscript of an article that has been accepted for publication and which typically includes author-incorporated changes suggested during submission, peer review and editor-author communications.
Authors can share their accepted author manuscript:

- immediately
    - via their non-commercial person homepage or blog
    - by updating a preprint in arXiv or RePEc with the accepted manuscript
    - via their research institute or institutional repository for internal institutional uses or as part of an invitation-only research collaboration work-group
    - directly by providing copies to their students or to research collaborators for their personal use
    - for private scholarly sharing as part of an invitation-only work group on commercial sites with which Elsevier has an agreement
- After the embargo period
    - via non-commercial hosting platforms such as their institutional repository
    - via commercial sites with which Elsevier has an agreement

In all cases accepted manuscripts should:

- link to the formal publication via its DOI
- bear a CC-BY-NC-ND license - this is easy to do
- if aggregated with other manuscripts, for example in a repository or other site, be shared in alignment with our hosting policy not be added to or enhanced in any way to appear more like, or to substitute for, the published journal article.

Published journal article (JPA): A published journal article (PJA) is the definitive final record of published research that appears or will appear in the journal and embodies all value-adding publishing activities including peer review co-ordination, copy-editing, formatting, (if relevant) pagination and online enrichment.
Policies for sharing publishing journal articles differ for subscription and gold open access articles:
Subscription Articles: If you are an author, please share a link to your article rather than the full-text. Millions of researchers have access to the formal publications on ScienceDirect, and so links will help your users to find, access, cite, and use the best available version.
Theses and dissertations which contain embedded PJAs as part of the formal submission can be posted publicly by the awarding institution with DOI links back to the formal publications on ScienceDirect.
If you are affiliated with a library that subscribes to ScienceDirect you have additional private sharing rights for others' research accessed under that agreement. This includes use for classroom teaching and internal training at the institution (including use in course packs and courseware programs), and inclusion of the article for grant funding purposes.
Gold Open Access Articles: May be shared according to the author-selected end-user license and should contain a CrossMark logo, the end user license, and a DOI link to the formal publication on ScienceDirect.
Please refer to Elsevier's posting policy for further information.
18. **For book authors** the following clauses are applicable in addition to the above: Authors are permitted to place a brief summary of their work online only. You are not allowed to download and post the published electronic version of your chapter, nor may you scan the printed edition to create an electronic version. **Posting to a repository:** Authors are permitted to post a summary of their chapter only in their institution's repository.
19. **Thesis/Dissertation**: If your license is for use in a thesis/dissertation your thesis may be submitted to your institution in either print or electronic form. Should your thesis be published commercially, please reapply for permission. These requirements include permission for the Library and Archives of Canada to supply single copies, on demand, of the complete thesis and include permission for Proquest/UMI to supply single copies, on demand, of the complete thesis. Should your thesis be published commercially, please reapply for permission. Theses and dissertations which contain embedded PJAs as part of the formal submission can be posted publicly by the awarding institution with DOI links back to the formal publications on ScienceDirect.

Elsevier Open Access Terms and Conditions

You can publish open access with Elsevier in hundreds of open access journals or in nearly 2000 established subscription journals that support open access publishing. Permitted third party re-use of these open access articles is defined by the author's choice of Creative Commons user license. See our open access license policy for more information.

Terms & Conditions applicable to all Open Access articles published with Elsevier:

Any reuse of the article must not represent the author as endorsing the adaptation of the article nor should the article be modified in such a way as to damage the author's honour or reputation. If any changes have been made, such changes must be clearly indicated.

The author(s) must be appropriately credited and we ask that you include the end user license and a DOI link to the formal publication on ScienceDirect.

If any part of the material to be used (for example, figures) has appeared in our publication with credit or acknowledgement to another source it is the responsibility of the user to ensure their reuse complies with the terms and conditions determined by the rights holder.

Additional Terms & Conditions applicable to each Creative Commons user license:

CC BY: The CC-BY license allows users to copy, to create extracts, abstracts and new works from the Article, to alter and revise the Article and to make commercial use of the Article (including reuse and/or resale of the Article by commercial entities), provided the user gives appropriate credit (with a link to the formal publication through the relevant DOI), provides a link to the license, indicates if changes were made and the licensor is not represented as endorsing the use made of the work. The full details of the license are available at http://creativecommons.org/licenses/by/4.0.

CC BY NC SA: The CC BY-NC-SA license allows users to copy, to create extracts, abstracts and new works from the Article, to alter and revise the Article, provided this is not done for commercial purposes, and that the user gives appropriate credit (with a link to the formal publication through the relevant DOI), provides a link to the license, indicates if changes were made and the licensor is not represented as endorsing the use made of the work. Further, any new works must be made available on the same conditions. The full details of the license are available at http://creativecommons.org/licenses/by-nc-sa/4.0.

CC BY NC ND: The CC BY-NC-ND license allows users to copy and distribute the Article, provided this is not done for commercial purposes and further does not permit distribution of the Article if it is changed or edited in any way, and provided the user gives appropriate credit (with a link to the formal publication through the relevant DOI), provides a link to the license, and that the licensor is not represented as endorsing the use made of the work. The full details of the license are available at http://creativecommons.org/licenses/by-nc-nd/4.0. Any commercial reuse of Open Access articles published with a CC BY NC SA or CC BY NC ND license requires permission from Elsevier and will be subject to a fee.

Commercial reuse includes:

- Associating advertising with the full text of the Article
- Charging fees for document delivery or access
- Article aggregation
- Systematic distribution via e-mail lists or share buttons

Posting or linking by commercial companies for use by customers of those companies.

20. **Other Conditions**:

v1.10

Questions? customercare@copyright.com or +1-855-239-3415 (toll free in the US) or +1-978-646-2777.

ELSEVIER LICENSE TERMS AND CONDITIONS

Sep 12, 2022

This Agreement between Ruth Birch ("You") and Elsevier ("Elsevier") consists of your license details and the terms and conditions provided by Elsevier and Copyright Clearance Center.

License Number	5386390467069
License date	Sep 12, 2022
Licensed Content Publisher	Elsevier
Licensed Content Publication	Journal of Nuclear Materials
Licensed Content Title	Hydride reorientation in Zircaloy-4 examined by in situ synchrotron X-ray diffraction
Licensed Content Author	H.E. Weekes,N.G. Jones,T.C. Lindley,D. Dye
Licensed Content Date	Sep 1, 2016
Licensed Content Volume	478
Licensed Content Issue	n/a
Licensed Content Pages	10
Start Page	32
End Page	41
Type of Use	reuse in a thesis/dissertation
Portion	figures/tables/illustrations
Number of figures/tables /illustrations	1
Format	both print and electronic
Are you the author of this Elsevier article?	No
Will you be translating?	No
Title	PhD Thesis
Institution name	Imperial College London
Expected presentation date	Sep 2022
Portions	Figure 1
Requestor Location	Ruth Birch Department of materials Imperial college london London, SW7 2AZ United Kingdom Attn: Ruth Birch
Publisher Tax ID	GB 494 6272 12
Total	**0.00 GBP**
Terms and Conditions	

INTRODUCTION

1. The publisher for this copyrighted material is Elsevier. By clicking "accept" in connection with completing this licensing transaction, you agree that the following terms and conditions apply to this transaction (along with the Billing and Payment terms and conditions established by Copyright Clearance Center, Inc. ("CCC"), at the time that you opened your Rightslink account and that are available at any time at http://myaccount.copyright.com).

GENERAL TERMS

2. Elsevier hereby grants you permission to reproduce the aforementioned material subject to the terms and conditions indicated.

3. Acknowledgement: If any part of the material to be used (for example, figures) has appeared in our publication with credit or acknowledgement to another source, permission must also be sought from that source. If such permission is not obtained then that material may not be included in your publication/copies. Suitable acknowledgement to the source must be made, either as a footnote or in a reference list at the end of your publication, as follows:
"Reprinted from Publication title, Vol /edition number, Author(s), Title of article / title of chapter, Pages No., Copyright (Year), with permission from Elsevier [OR APPLICABLE SOCIETY COPYRIGHT OWNER]." Also Lancet special credit - "Reprinted from The Lancet, Vol. number, Author(s), Title of article, Pages No., Copyright (Year), with permission from Elsevier."
4. Reproduction of this material is confined to the purpose and/or media for which permission is hereby given.
5. Altering/Modifying Material: Not Permitted. However figures and illustrations may be altered/adapted minimally to serve your work. Any other abbreviations, additions, deletions and/or any other alterations shall be made only with prior written authorization of Elsevier Ltd. (Please contact Elsevier's permissions helpdesk here). No modifications can be made to any Lancet figures/tables and they must be reproduced in full.
6. If the permission fee for the requested use of our material is waived in this instance, please be advised that your future requests for Elsevier materials may attract a fee.
7. Reservation of Rights: Publisher reserves all rights not specifically granted in the combination of (i) the license details provided by you and accepted in the course of this licensing transaction, (ii) these terms and conditions and (iii) CCC's Billing and Payment terms and conditions.
8. License Contingent Upon Payment: While you may exercise the rights licensed immediately upon issuance of the license at the end of the licensing process for the transaction, provided that you have disclosed complete and accurate details of your proposed use, no license is finally effective unless and until full payment is received from you (either by publisher or by CCC) as provided in CCC's Billing and Payment terms and conditions. If full payment is not received on a timely basis, then any license preliminarily granted shall be deemed automatically revoked and shall be void as if never granted. Further, in the event that you breach any of these terms and conditions or any of CCC's Billing and Payment terms and conditions, the license is automatically revoked and shall be void as if never granted. Use of materials as described in a revoked license, as well as any use of the materials beyond the scope of an unrevoked license, may constitute copyright infringement and publisher reserves the right to take any and all action to protect its copyright in the materials.
9. Warranties: Publisher makes no representations or warranties with respect to the licensed material.
10. Indemnity: You hereby indemnify and agree to hold harmless publisher and CCC, and their respective officers, directors, employees and agents, from and against any and all claims arising out of your use of the licensed material other than as specifically authorized pursuant to this license.
11. No Transfer of License: This license is personal to you and may not be sublicensed, assigned, or transferred by you to any other person without publisher's written permission.
12. No Amendment Except in Writing: This license may not be amended except in a writing signed by both parties (or, in the case of publisher, by CCC on publisher's behalf).
13. Objection to Contrary Terms: Publisher hereby objects to any terms contained in any purchase order, acknowledgment, check endorsement or other writing prepared by you, which terms are inconsistent with these terms and conditions or CCC's Billing and Payment terms and conditions. These terms and conditions, together with CCC's Billing and Payment terms and conditions (which are incorporated herein), comprise the entire agreement between you and publisher (and CCC) concerning this licensing transaction. In the event of any conflict between your obligations established by these terms and conditions and those established by CCC's Billing and Payment terms and conditions, these terms and conditions shall control.
14. Revocation: Elsevier or Copyright Clearance Center may deny the permissions described in this License at their sole discretion, for any reason or no reason, with a full refund payable to you. Notice of such denial will be made using the contact information provided by you. Failure to receive such notice will not alter or invalidate the denial. In no event will Elsevier or Copyright Clearance Center be responsible or liable for any costs, expenses or damage incurred by you as a result of a denial of your permission request, other than a refund of the amount(s) paid by you to Elsevier and/or Copyright Clearance Center for denied permissions.

LIMITED LICENSE

The following terms and conditions apply only to specific license types:
15. **Translation**: This permission is granted for non-exclusive world **English** rights only unless your license was granted for translation rights. If you licensed translation rights you may only translate this content into the languages you requested. A professional translator must perform all translations and reproduce the content word for word preserving the integrity of the article.
16. **Posting licensed content on any Website**: The following terms and conditions apply as follows: Licensing material from an Elsevier journal: All content posted to the web site must maintain the copyright information line on the bottom of each image; A hyper-text must be included to the Homepage of the journal from which you are licensing at http://www.sciencedirect.com/science/journal/xxxxx or the Elsevier homepage for books at http://www.elsevier.com; Central Storage: This license does not include permission for a scanned version of the material to be stored in a central repository such as that provided by Heron/XanEdu.
Licensing material from an Elsevier book: A hyper-text link must be included to the Elsevier homepage at http://www.elsevier.com . All content posted to the web site must maintain the copyright information line on the bottom of each image.

Posting licensed content on Electronic reserve: In addition to the above the following clauses are applicable: The web site must be password-protected and made available only to bona fide students registered on a relevant course. This permission

is granted for 1 year only. You may obtain a new license for future website posting.
17. **For journal authors:** the following clauses are applicable in addition to the above:
Preprints:
A preprint is an author's own write-up of research results and analysis, it has not been peer-reviewed, nor has it had any other value added to it by a publisher (such as formatting, copyright, technical enhancement etc.).
Authors can share their preprints anywhere at any time. Preprints should not be added to or enhanced in any way in order to appear more like, or to substitute for, the final versions of articles however authors can update their preprints on arXiv or RePEc with their Accepted Author Manuscript (see below).
If accepted for publication, we encourage authors to link from the preprint to their formal publication via its DOI. Millions of researchers have access to the formal publications on ScienceDirect, and so links will help users to find, access, cite and use the best available version. Please note that Cell Press, The Lancet and some society-owned have different preprint policies. Information on these policies is available on the journal homepage.
Accepted Author Manuscripts: An accepted author manuscript is the manuscript of an article that has been accepted for publication and which typically includes author-incorporated changes suggested during submission, peer review and editor-author communications.
Authors can share their accepted author manuscript:

- immediately
    - via their non-commercial person homepage or blog
    - by updating a preprint in arXiv or RePEc with the accepted manuscript
    - via their research institute or institutional repository for internal institutional uses or as part of an invitation-only research collaboration work-group
    - directly by providing copies to their students or to research collaborators for their personal use
    - for private scholarly sharing as part of an invitation-only work group on commercial sites with which Elsevier has an agreement
- After the embargo period
    - via non-commercial hosting platforms such as their institutional repository
    - via commercial sites with which Elsevier has an agreement

In all cases accepted manuscripts should:

- link to the formal publication via its DOI
- bear a CC-BY-NC-ND license - this is easy to do
- if aggregated with other manuscripts, for example in a repository or other site, be shared in alignment with our hosting policy not be added to or enhanced in any way to appear more like, or to substitute for, the published journal article.

Published journal article (JPA): A published journal article (PJA) is the definitive final record of published research that appears or will appear in the journal and embodies all value-adding publishing activities including peer review co-ordination, copy-editing, formatting, (if relevant) pagination and online enrichment.
Policies for sharing publishing journal articles differ for subscription and gold open access articles:
Subscription Articles: If you are an author, please share a link to your article rather than the full-text. Millions of researchers have access to the formal publications on ScienceDirect, and so links will help your users to find, access, cite, and use the best available version.
Theses and dissertations which contain embedded PJAs as part of the formal submission can be posted publicly by the awarding institution with DOI links back to the formal publications on ScienceDirect.
If you are affiliated with a library that subscribes to ScienceDirect you have additional private sharing rights for others' research accessed under that agreement. This includes use for classroom teaching and internal training at the institution (including use in course packs and courseware programs), and inclusion of the article for grant funding purposes.
Gold Open Access Articles: May be shared according to the author-selected end-user license and should contain a CrossMark logo, the end user license, and a DOI link to the formal publication on ScienceDirect.
Please refer to Elsevier's posting policy for further information.
18. **For book authors** the following clauses are applicable in addition to the above: Authors are permitted to place a brief summary of their work online only. You are not allowed to download and post the published electronic version of your chapter, nor may you scan the printed edition to create an electronic version. **Posting to a repository:** Authors are permitted to post a summary of their chapter only in their institution's repository.
19. **Thesis/Dissertation**: If your license is for use in a thesis/dissertation your thesis may be submitted to your institution in either print or electronic form. Should your thesis be published commercially, please reapply for permission. These requirements include permission for the Library and Archives of Canada to supply single copies, on demand, of the complete thesis and include permission for Proquest/UMI to supply single copies, on demand, of the complete thesis. Should your thesis be published commercially, please reapply for permission. Theses and dissertations which contain embedded PJAs as part of the formal submission can be posted publicly by the awarding institution with DOI links back to the formal publications on ScienceDirect.

Elsevier Open Access Terms and Conditions

You can publish open access with Elsevier in hundreds of open access journals or in nearly 2000 established subscription journals that support open access publishing. Permitted third party re-use of these open access articles is defined by the author's choice of Creative Commons user license. See our open access license policy for more information.

Terms & Conditions applicable to all Open Access articles published with Elsevier:

Any reuse of the article must not represent the author as endorsing the adaptation of the article nor should the article be modified in such a way as to damage the author's honour or reputation. If any changes have been made, such changes must be clearly indicated.

The author(s) must be appropriately credited and we ask that you include the end user license and a DOI link to the formal publication on ScienceDirect.

If any part of the material to be used (for example, figures) has appeared in our publication with credit or acknowledgement to another source it is the responsibility of the user to ensure their reuse complies with the terms and conditions determined by the rights holder.

Additional Terms & Conditions applicable to each Creative Commons user license:

CC BY: The CC-BY license allows users to copy, to create extracts, abstracts and new works from the Article, to alter and revise the Article and to make commercial use of the Article (including reuse and/or resale of the Article by commercial entities), provided the user gives appropriate credit (with a link to the formal publication through the relevant DOI), provides a link to the license, indicates if changes were made and the licensor is not represented as endorsing the use made of the work. The full details of the license are available at http://creativecommons.org/licenses/by/4.0.

CC BY NC SA: The CC BY-NC-SA license allows users to copy, to create extracts, abstracts and new works from the Article, to alter and revise the Article, provided this is not done for commercial purposes, and that the user gives appropriate credit (with a link to the formal publication through the relevant DOI), provides a link to the license, indicates if changes were made and the licensor is not represented as endorsing the use made of the work. Further, any new works must be made available on the same conditions. The full details of the license are available at http://creativecommons.org/licenses/by-nc-sa/4.0.

CC BY NC ND: The CC BY-NC-ND license allows users to copy and distribute the Article, provided this is not done for commercial purposes and further does not permit distribution of the Article if it is changed or edited in any way, and provided the user gives appropriate credit (with a link to the formal publication through the relevant DOI), provides a link to the license, and that the licensor is not represented as endorsing the use made of the work. The full details of the license are available at http://creativecommons.org/licenses/by-nc-nd/4.0. Any commercial reuse of Open Access articles published with a CC BY NC SA or CC BY NC ND license requires permission from Elsevier and will be subject to a fee.

Commercial reuse includes:

- Associating advertising with the full text of the Article
- Charging fees for document delivery or access
- Article aggregation
- Systematic distribution via e-mail lists or share buttons

Posting or linking by commercial companies for use by customers of those companies.

20. **Other Conditions**:

v1.10

Questions? customercare@copyright.com or +1-855-239-3415 (toll free in the US) or +1-978-646-2777.

ELSEVIER LICENSE TERMS AND CONDITIONS

Sep 12, 2022

This Agreement between Ruth Birch ("You") and Elsevier ("Elsevier") consists of your license details and the terms and conditions provided by Elsevier and Copyright Clearance Center.

License Number	5386391492814
License date	Sep 12, 2022
Licensed Content Publisher	Elsevier
Licensed Content Publication	Acta Metallurgica
Licensed Content Title	Electron microscope observations on the precipitation of zirconium hydride in zirconium
Licensed Content Author	J.E Bailey
Licensed Content Date	Apr 1, 1963
Licensed Content Volume	11
Licensed Content Issue	4
Licensed Content Pages	14
Start Page	267
End Page	280
Type of Use	reuse in a thesis/dissertation
Portion	figures/tables/illustrations
Number of figures/tables /illustrations	2
Format	both print and electronic
Are you the author of this Elsevier article?	No
Will you be translating?	No
Title	PhD Thesis
Institution name	Imperial College London
Expected presentation date	Sep 2022
Portions	Figure 4(b) & Figure 10
Requestor Location	Ruth Birch Department of materials Imperial college london London, SW7 2AZ United Kingdom Attn: Ruth Birch
Publisher Tax ID	GB 494 6272 12
Total	**0.00 GBP**
Terms and Conditions	

INTRODUCTION

1. The publisher for this copyrighted material is Elsevier. By clicking "accept" in connection with completing this licensing transaction, you agree that the following terms and conditions apply to this transaction (along with the Billing and Payment terms and conditions established by Copyright Clearance Center, Inc. ("CCC"), at the time that you opened your Rightslink account and that are available at any time at http://myaccount.copyright.com).

GENERAL TERMS

2. Elsevier hereby grants you permission to reproduce the aforementioned material subject to the terms and conditions indicated.

3. Acknowledgement: If any part of the material to be used (for example, figures) has appeared in our publication with credit or acknowledgement to another source, permission must also be sought from that source. If such permission is not obtained then that material may not be included in your publication/copies. Suitable acknowledgement to the source must be made, either as a footnote or in a reference list at the end of your publication, as follows:
"Reprinted from Publication title, Vol /edition number, Author(s), Title of article / title of chapter, Pages No., Copyright (Year), with permission from Elsevier [OR APPLICABLE SOCIETY COPYRIGHT OWNER]." Also Lancet special credit - "Reprinted from The Lancet, Vol. number, Author(s), Title of article, Pages No., Copyright (Year), with permission from Elsevier."
4. Reproduction of this material is confined to the purpose and/or media for which permission is hereby given.
5. Altering/Modifying Material: Not Permitted. However figures and illustrations may be altered/adapted minimally to serve your work. Any other abbreviations, additions, deletions and/or any other alterations shall be made only with prior written authorization of Elsevier Ltd. (Please contact Elsevier's permissions helpdesk here). No modifications can be made to any Lancet figures/tables and they must be reproduced in full.
6. If the permission fee for the requested use of our material is waived in this instance, please be advised that your future requests for Elsevier materials may attract a fee.
7. Reservation of Rights: Publisher reserves all rights not specifically granted in the combination of (i) the license details provided by you and accepted in the course of this licensing transaction, (ii) these terms and conditions and (iii) CCC's Billing and Payment terms and conditions.
8. License Contingent Upon Payment: While you may exercise the rights licensed immediately upon issuance of the license at the end of the licensing process for the transaction, provided that you have disclosed complete and accurate details of your proposed use, no license is finally effective unless and until full payment is received from you (either by publisher or by CCC) as provided in CCC's Billing and Payment terms and conditions. If full payment is not received on a timely basis, then any license preliminarily granted shall be deemed automatically revoked and shall be void as if never granted. Further, in the event that you breach any of these terms and conditions or any of CCC's Billing and Payment terms and conditions, the license is automatically revoked and shall be void as if never granted. Use of materials as described in a revoked license, as well as any use of the materials beyond the scope of an unrevoked license, may constitute copyright infringement and publisher reserves the right to take any and all action to protect its copyright in the materials.
9. Warranties: Publisher makes no representations or warranties with respect to the licensed material.
10. Indemnity: You hereby indemnify and agree to hold harmless publisher and CCC, and their respective officers, directors, employees and agents, from and against any and all claims arising out of your use of the licensed material other than as specifically authorized pursuant to this license.
11. No Transfer of License: This license is personal to you and may not be sublicensed, assigned, or transferred by you to any other person without publisher's written permission.
12. No Amendment Except in Writing: This license may not be amended except in a writing signed by both parties (or, in the case of publisher, by CCC on publisher's behalf).
13. Objection to Contrary Terms: Publisher hereby objects to any terms contained in any purchase order, acknowledgment, check endorsement or other writing prepared by you, which terms are inconsistent with these terms and conditions or CCC's Billing and Payment terms and conditions. These terms and conditions, together with CCC's Billing and Payment terms and conditions (which are incorporated herein), comprise the entire agreement between you and publisher (and CCC) concerning this licensing transaction. In the event of any conflict between your obligations established by these terms and conditions and those established by CCC's Billing and Payment terms and conditions, these terms and conditions shall control.
14. Revocation: Elsevier or Copyright Clearance Center may deny the permissions described in this License at their sole discretion, for any reason or no reason, with a full refund payable to you. Notice of such denial will be made using the contact information provided by you. Failure to receive such notice will not alter or invalidate the denial. In no event will Elsevier or Copyright Clearance Center be responsible or liable for any costs, expenses or damage incurred by you as a result of a denial of your permission request, other than a refund of the amount(s) paid by you to Elsevier and/or Copyright Clearance Center for denied permissions.

LIMITED LICENSE

The following terms and conditions apply only to specific license types:
15. **Translation**: This permission is granted for non-exclusive world **English** rights only unless your license was granted for translation rights. If you licensed translation rights you may only translate this content into the languages you requested. A professional translator must perform all translations and reproduce the content word for word preserving the integrity of the article.
16. **Posting licensed content on any Website**: The following terms and conditions apply as follows: Licensing material from an Elsevier journal: All content posted to the web site must maintain the copyright information line on the bottom of each image; A hyper-text must be included to the Homepage of the journal from which you are licensing at http://www.sciencedirect.com/science/journal/xxxxx or the Elsevier homepage for books at http://www.elsevier.com; Central Storage: This license does not include permission for a scanned version of the material to be stored in a central repository such as that provided by Heron/XanEdu.
Licensing material from an Elsevier book: A hyper-text link must be included to the Elsevier homepage at http://www.elsevier.com . All content posted to the web site must maintain the copyright information line on the bottom of each image.

Posting licensed content on Electronic reserve: In addition to the above the following clauses are applicable: The web site must be password-protected and made available only to bona fide students registered on a relevant course. This permission

is granted for 1 year only. You may obtain a new license for future website posting.
17. **For journal authors:** the following clauses are applicable in addition to the above:
Preprints:
A preprint is an author's own write-up of research results and analysis, it has not been peer-reviewed, nor has it had any other value added to it by a publisher (such as formatting, copyright, technical enhancement etc.).
Authors can share their preprints anywhere at any time. Preprints should not be added to or enhanced in any way in order to appear more like, or to substitute for, the final versions of articles however authors can update their preprints on arXiv or RePEc with their Accepted Author Manuscript (see below).
If accepted for publication, we encourage authors to link from the preprint to their formal publication via its DOI. Millions of researchers have access to the formal publications on ScienceDirect, and so links will help users to find, access, cite and use the best available version. Please note that Cell Press, The Lancet and some society-owned have different preprint policies. Information on these policies is available on the journal homepage.
Accepted Author Manuscripts: An accepted author manuscript is the manuscript of an article that has been accepted for publication and which typically includes author-incorporated changes suggested during submission, peer review and editor-author communications.
Authors can share their accepted author manuscript:

- immediately
    - via their non-commercial person homepage or blog
    - by updating a preprint in arXiv or RePEc with the accepted manuscript
    - via their research institute or institutional repository for internal institutional uses or as part of an invitation-only research collaboration work-group
    - directly by providing copies to their students or to research collaborators for their personal use
    - for private scholarly sharing as part of an invitation-only work group on commercial sites with which Elsevier has an agreement
- After the embargo period
    - via non-commercial hosting platforms such as their institutional repository
    - via commercial sites with which Elsevier has an agreement

In all cases accepted manuscripts should:

- link to the formal publication via its DOI
- bear a CC-BY-NC-ND license - this is easy to do
- if aggregated with other manuscripts, for example in a repository or other site, be shared in alignment with our hosting policy not be added to or enhanced in any way to appear more like, or to substitute for, the published journal article.

Published journal article (JPA): A published journal article (PJA) is the definitive final record of published research that appears or will appear in the journal and embodies all value-adding publishing activities including peer review co-ordination, copy-editing, formatting, (if relevant) pagination and online enrichment.
Policies for sharing publishing journal articles differ for subscription and gold open access articles:
Subscription Articles: If you are an author, please share a link to your article rather than the full-text. Millions of researchers have access to the formal publications on ScienceDirect, and so links will help your users to find, access, cite, and use the best available version.
Theses and dissertations which contain embedded PJAs as part of the formal submission can be posted publicly by the awarding institution with DOI links back to the formal publications on ScienceDirect.
If you are affiliated with a library that subscribes to ScienceDirect you have additional private sharing rights for others' research accessed under that agreement. This includes use for classroom teaching and internal training at the institution (including use in course packs and courseware programs), and inclusion of the article for grant funding purposes.
Gold Open Access Articles: May be shared according to the author-selected end-user license and should contain a CrossMark logo, the end user license, and a DOI link to the formal publication on ScienceDirect.
Please refer to Elsevier's posting policy for further information.
18. **For book authors** the following clauses are applicable in addition to the above: Authors are permitted to place a brief summary of their work online only. You are not allowed to download and post the published electronic version of your chapter, nor may you scan the printed edition to create an electronic version. **Posting to a repository:** Authors are permitted to post a summary of their chapter only in their institution's repository.
19. **Thesis/Dissertation**: If your license is for use in a thesis/dissertation your thesis may be submitted to your institution in either print or electronic form. Should your thesis be published commercially, please reapply for permission. These requirements include permission for the Library and Archives of Canada to supply single copies, on demand, of the complete thesis and include permission for Proquest/UMI to supply single copies, on demand, of the complete thesis. Should your thesis be published commercially, please reapply for permission. Theses and dissertations which contain embedded PJAs as part of the formal submission can be posted publicly by the awarding institution with DOI links back to the formal publications on ScienceDirect.

Elsevier Open Access Terms and Conditions

You can publish open access with Elsevier in hundreds of open access journals or in nearly 2000 established subscription journals that support open access publishing. Permitted third party re-use of these open access articles is defined by the author's choice of Creative Commons user license. See our open access license policy for more information.

Terms & Conditions applicable to all Open Access articles published with Elsevier:

Any reuse of the article must not represent the author as endorsing the adaptation of the article nor should the article be modified in such a way as to damage the author's honour or reputation. If any changes have been made, such changes must be clearly indicated.

The author(s) must be appropriately credited and we ask that you include the end user license and a DOI link to the formal publication on ScienceDirect.

If any part of the material to be used (for example, figures) has appeared in our publication with credit or acknowledgement to another source it is the responsibility of the user to ensure their reuse complies with the terms and conditions determined by the rights holder.

Additional Terms & Conditions applicable to each Creative Commons user license:

CC BY: The CC-BY license allows users to copy, to create extracts, abstracts and new works from the Article, to alter and revise the Article and to make commercial use of the Article (including reuse and/or resale of the Article by commercial entities), provided the user gives appropriate credit (with a link to the formal publication through the relevant DOI), provides a link to the license, indicates if changes were made and the licensor is not represented as endorsing the use made of the work. The full details of the license are available at http://creativecommons.org/licenses/by/4.0.

CC BY NC SA: The CC BY-NC-SA license allows users to copy, to create extracts, abstracts and new works from the Article, to alter and revise the Article, provided this is not done for commercial purposes, and that the user gives appropriate credit (with a link to the formal publication through the relevant DOI), provides a link to the license, indicates if changes were made and the licensor is not represented as endorsing the use made of the work. Further, any new works must be made available on the same conditions. The full details of the license are available at http://creativecommons.org/licenses/by-nc-sa/4.0.

CC BY NC ND: The CC BY-NC-ND license allows users to copy and distribute the Article, provided this is not done for commercial purposes and further does not permit distribution of the Article if it is changed or edited in any way, and provided the user gives appropriate credit (with a link to the formal publication through the relevant DOI), provides a link to the license, and that the licensor is not represented as endorsing the use made of the work. The full details of the license are available at http://creativecommons.org/licenses/by-nc-nd/4.0. Any commercial reuse of Open Access articles published with a CC BY NC SA or CC BY NC ND license requires permission from Elsevier and will be subject to a fee.

Commercial reuse includes:

- Associating advertising with the full text of the Article
- Charging fees for document delivery or access
- Article aggregation
- Systematic distribution via e-mail lists or share buttons

Posting or linking by commercial companies for use by customers of those companies.

20. **Other Conditions**:

v1.10

Questions? customercare@copyright.com or +1-855-239-3415 (toll free in the US) or +1-978-646-2777.

ELSEVIER LICENSE TERMS AND CONDITIONS

Sep 12, 2022

This Agreement between Ruth Birch ("You") and Elsevier ("Elsevier") consists of your license details and the terms and conditions provided by Elsevier and Copyright Clearance Center.

License Number	5386400125045
License date	Sep 12, 2022
Licensed Content Publisher	Elsevier
Licensed Content Publication	Journal of Nuclear Materials
Licensed Content Title	Evaluating zirconium–zirconium hydride interfacial strains by nano-beam electron diffraction
Licensed Content Author	A.T.W. Barrow,A. Korinek,M.R. Daymond
Licensed Content Date	Jan 1, 2013
Licensed Content Volume	432
Licensed Content Issue	1-3
Licensed Content Pages	5
Start Page	366
End Page	370
Type of Use	reuse in a thesis/dissertation
Portion	figures/tables/illustrations
Number of figures/tables /illustrations	1
Format	both print and electronic
Are you the author of this Elsevier article?	No
Will you be translating?	No
Title	PhD Thesis
Institution name	Imperial College London
Expected presentation date	Sep 2022
Portions	Figure 2
Requestor Location	Ruth Birch Department of materials Imperial college london London, SW7 2AZ United Kingdom Attn: Ruth Birch
Publisher Tax ID	GB 494 6272 12
Total	**0.00 GBP**
Terms and Conditions	

INTRODUCTION

1. The publisher for this copyrighted material is Elsevier. By clicking "accept" in connection with completing this licensing transaction, you agree that the following terms and conditions apply to this transaction (along with the Billing and Payment terms and conditions established by Copyright Clearance Center, Inc. ("CCC"), at the time that you opened your Rightslink account and that are available at any time at http://myaccount.copyright.com).

GENERAL TERMS

2. Elsevier hereby grants you permission to reproduce the aforementioned material subject to the terms and conditions indicated.

3. Acknowledgement: If any part of the material to be used (for example, figures) has appeared in our publication with credit or acknowledgement to another source, permission must also be sought from that source. If such permission is not obtained then that material may not be included in your publication/copies. Suitable acknowledgement to the source must be made, either as a footnote or in a reference list at the end of your publication, as follows:
"Reprinted from Publication title, Vol /edition number, Author(s), Title of article / title of chapter, Pages No., Copyright (Year), with permission from Elsevier [OR APPLICABLE SOCIETY COPYRIGHT OWNER]." Also Lancet special credit - "Reprinted from The Lancet, Vol. number, Author(s), Title of article, Pages No., Copyright (Year), with permission from Elsevier."
4. Reproduction of this material is confined to the purpose and/or media for which permission is hereby given.
5. Altering/Modifying Material: Not Permitted. However figures and illustrations may be altered/adapted minimally to serve your work. Any other abbreviations, additions, deletions and/or any other alterations shall be made only with prior written authorization of Elsevier Ltd. (Please contact Elsevier's permissions helpdesk here). No modifications can be made to any Lancet figures/tables and they must be reproduced in full.
6. If the permission fee for the requested use of our material is waived in this instance, please be advised that your future requests for Elsevier materials may attract a fee.
7. Reservation of Rights: Publisher reserves all rights not specifically granted in the combination of (i) the license details provided by you and accepted in the course of this licensing transaction, (ii) these terms and conditions and (iii) CCC's Billing and Payment terms and conditions.
8. License Contingent Upon Payment: While you may exercise the rights licensed immediately upon issuance of the license at the end of the licensing process for the transaction, provided that you have disclosed complete and accurate details of your proposed use, no license is finally effective unless and until full payment is received from you (either by publisher or by CCC) as provided in CCC's Billing and Payment terms and conditions. If full payment is not received on a timely basis, then any license preliminarily granted shall be deemed automatically revoked and shall be void as if never granted. Further, in the event that you breach any of these terms and conditions or any of CCC's Billing and Payment terms and conditions, the license is automatically revoked and shall be void as if never granted. Use of materials as described in a revoked license, as well as any use of the materials beyond the scope of an unrevoked license, may constitute copyright infringement and publisher reserves the right to take any and all action to protect its copyright in the materials.
9. Warranties: Publisher makes no representations or warranties with respect to the licensed material.
10. Indemnity: You hereby indemnify and agree to hold harmless publisher and CCC, and their respective officers, directors, employees and agents, from and against any and all claims arising out of your use of the licensed material other than as specifically authorized pursuant to this license.
11. No Transfer of License: This license is personal to you and may not be sublicensed, assigned, or transferred by you to any other person without publisher's written permission.
12. No Amendment Except in Writing: This license may not be amended except in a writing signed by both parties (or, in the case of publisher, by CCC on publisher's behalf).
13. Objection to Contrary Terms: Publisher hereby objects to any terms contained in any purchase order, acknowledgment, check endorsement or other writing prepared by you, which terms are inconsistent with these terms and conditions or CCC's Billing and Payment terms and conditions. These terms and conditions, together with CCC's Billing and Payment terms and conditions (which are incorporated herein), comprise the entire agreement between you and publisher (and CCC) concerning this licensing transaction. In the event of any conflict between your obligations established by these terms and conditions and those established by CCC's Billing and Payment terms and conditions, these terms and conditions shall control.
14. Revocation: Elsevier or Copyright Clearance Center may deny the permissions described in this License at their sole discretion, for any reason or no reason, with a full refund payable to you. Notice of such denial will be made using the contact information provided by you. Failure to receive such notice will not alter or invalidate the denial. In no event will Elsevier or Copyright Clearance Center be responsible or liable for any costs, expenses or damage incurred by you as a result of a denial of your permission request, other than a refund of the amount(s) paid by you to Elsevier and/or Copyright Clearance Center for denied permissions.

LIMITED LICENSE

The following terms and conditions apply only to specific license types:
15. **Translation**: This permission is granted for non-exclusive world **English** rights only unless your license was granted for translation rights. If you licensed translation rights you may only translate this content into the languages you requested. A professional translator must perform all translations and reproduce the content word for word preserving the integrity of the article.
16. **Posting licensed content on any Website**: The following terms and conditions apply as follows: Licensing material from an Elsevier journal: All content posted to the web site must maintain the copyright information line on the bottom of each image; A hyper-text must be included to the Homepage of the journal from which you are licensing at http://www.sciencedirect.com/science/journal/xxxxx or the Elsevier homepage for books at http://www.elsevier.com; Central Storage: This license does not include permission for a scanned version of the material to be stored in a central repository such as that provided by Heron/XanEdu.
Licensing material from an Elsevier book: A hyper-text link must be included to the Elsevier homepage at http://www.elsevier.com . All content posted to the web site must maintain the copyright information line on the bottom of each image.

Posting licensed content on Electronic reserve: In addition to the above the following clauses are applicable: The web site must be password-protected and made available only to bona fide students registered on a relevant course. This permission

is granted for 1 year only. You may obtain a new license for future website posting.
17. **For journal authors:** the following clauses are applicable in addition to the above:
Preprints:
A preprint is an author's own write-up of research results and analysis, it has not been peer-reviewed, nor has it had any other value added to it by a publisher (such as formatting, copyright, technical enhancement etc.).
Authors can share their preprints anywhere at any time. Preprints should not be added to or enhanced in any way in order to appear more like, or to substitute for, the final versions of articles however authors can update their preprints on arXiv or RePEc with their Accepted Author Manuscript (see below).
If accepted for publication, we encourage authors to link from the preprint to their formal publication via its DOI. Millions of researchers have access to the formal publications on ScienceDirect, and so links will help users to find, access, cite and use the best available version. Please note that Cell Press, The Lancet and some society-owned have different preprint policies. Information on these policies is available on the journal homepage.
Accepted Author Manuscripts: An accepted author manuscript is the manuscript of an article that has been accepted for publication and which typically includes author-incorporated changes suggested during submission, peer review and editor-author communications.
Authors can share their accepted author manuscript:

- immediately
    - via their non-commercial person homepage or blog
    - by updating a preprint in arXiv or RePEc with the accepted manuscript
    - via their research institute or institutional repository for internal institutional uses or as part of an invitation-only research collaboration work-group
    - directly by providing copies to their students or to research collaborators for their personal use
    - for private scholarly sharing as part of an invitation-only work group on commercial sites with which Elsevier has an agreement
- After the embargo period
    - via non-commercial hosting platforms such as their institutional repository
    - via commercial sites with which Elsevier has an agreement

In all cases accepted manuscripts should:

- link to the formal publication via its DOI
- bear a CC-BY-NC-ND license - this is easy to do
- if aggregated with other manuscripts, for example in a repository or other site, be shared in alignment with our hosting policy not be added to or enhanced in any way to appear more like, or to substitute for, the published journal article.

Published journal article (JPA): A published journal article (PJA) is the definitive final record of published research that appears or will appear in the journal and embodies all value-adding publishing activities including peer review co-ordination, copy-editing, formatting, (if relevant) pagination and online enrichment.
Policies for sharing publishing journal articles differ for subscription and gold open access articles:
Subscription Articles: If you are an author, please share a link to your article rather than the full-text. Millions of researchers have access to the formal publications on ScienceDirect, and so links will help your users to find, access, cite, and use the best available version.
Theses and dissertations which contain embedded PJAs as part of the formal submission can be posted publicly by the awarding institution with DOI links back to the formal publications on ScienceDirect.
If you are affiliated with a library that subscribes to ScienceDirect you have additional private sharing rights for others' research accessed under that agreement. This includes use for classroom teaching and internal training at the institution (including use in course packs and courseware programs), and inclusion of the article for grant funding purposes.
Gold Open Access Articles: May be shared according to the author-selected end-user license and should contain a CrossMark logo, the end user license, and a DOI link to the formal publication on ScienceDirect.
Please refer to Elsevier's posting policy for further information.
18. **For book authors** the following clauses are applicable in addition to the above: Authors are permitted to place a brief summary of their work online only. You are not allowed to download and post the published electronic version of your chapter, nor may you scan the printed edition to create an electronic version. **Posting to a repository:** Authors are permitted to post a summary of their chapter only in their institution's repository.
19. **Thesis/Dissertation**: If your license is for use in a thesis/dissertation your thesis may be submitted to your institution in either print or electronic form. Should your thesis be published commercially, please reapply for permission. These requirements include permission for the Library and Archives of Canada to supply single copies, on demand, of the complete thesis and include permission for Proquest/UMI to supply single copies, on demand, of the complete thesis. Should your thesis be published commercially, please reapply for permission. Theses and dissertations which contain embedded PJAs as part of the formal submission can be posted publicly by the awarding institution with DOI links back to the formal publications on ScienceDirect.

Elsevier Open Access Terms and Conditions

You can publish open access with Elsevier in hundreds of open access journals or in nearly 2000 established subscription journals that support open access publishing. Permitted third party re-use of these open access articles is defined by the author's choice of Creative Commons user license. See our open access license policy for more information.

Terms & Conditions applicable to all Open Access articles published with Elsevier:

Any reuse of the article must not represent the author as endorsing the adaptation of the article nor should the article be modified in such a way as to damage the author's honour or reputation. If any changes have been made, such changes must be clearly indicated.

The author(s) must be appropriately credited and we ask that you include the end user license and a DOI link to the formal publication on ScienceDirect.

If any part of the material to be used (for example, figures) has appeared in our publication with credit or acknowledgement to another source it is the responsibility of the user to ensure their reuse complies with the terms and conditions determined by the rights holder.

Additional Terms & Conditions applicable to each Creative Commons user license:

CC BY: The CC-BY license allows users to copy, to create extracts, abstracts and new works from the Article, to alter and revise the Article and to make commercial use of the Article (including reuse and/or resale of the Article by commercial entities), provided the user gives appropriate credit (with a link to the formal publication through the relevant DOI), provides a link to the license, indicates if changes were made and the licensor is not represented as endorsing the use made of the work. The full details of the license are available at http://creativecommons.org/licenses/by/4.0.

CC BY NC SA: The CC BY-NC-SA license allows users to copy, to create extracts, abstracts and new works from the Article, to alter and revise the Article, provided this is not done for commercial purposes, and that the user gives appropriate credit (with a link to the formal publication through the relevant DOI), provides a link to the license, indicates if changes were made and the licensor is not represented as endorsing the use made of the work. Further, any new works must be made available on the same conditions. The full details of the license are available at http://creativecommons.org/licenses/by-nc-sa/4.0.

CC BY NC ND: The CC BY-NC-ND license allows users to copy and distribute the Article, provided this is not done for commercial purposes and further does not permit distribution of the Article if it is changed or edited in any way, and provided the user gives appropriate credit (with a link to the formal publication through the relevant DOI), provides a link to the license, and that the licensor is not represented as endorsing the use made of the work. The full details of the license are available at http://creativecommons.org/licenses/by-nc-nd/4.0. Any commercial reuse of Open Access articles published with a CC BY NC SA or CC BY NC ND license requires permission from Elsevier and will be subject to a fee.

Commercial reuse includes:

- Associating advertising with the full text of the Article
- Charging fees for document delivery or access
- Article aggregation
- Systematic distribution via e-mail lists or share buttons

Posting or linking by commercial companies for use by customers of those companies.

20. **Other Conditions**:

v1.10

Questions? customercare@copyright.com or +1-855-239-3415 (toll free in the US) or +1-978-646-2777.

ELSEVIER LICENSE TERMS AND CONDITIONS

Sep 12, 2022

This Agreement between Ruth Birch ("You") and Elsevier ("Elsevier") consists of your license details and the terms and conditions provided by Elsevier and Copyright Clearance Center.

License Number	5386400233393
License date	Sep 12, 2022
Licensed Content Publisher	Elsevier
Licensed Content Publication	Journal of Nuclear Materials
Licensed Content Title	Measurement and modeling of strain fields in zirconium hydrides precipitated at a stress concentration
Licensed Content Author	Gregory B. Allen,Matthew Kerr,Mark R. Daymond
Licensed Content Date	Nov 1, 2012
Licensed Content Volume	430
Licensed Content Issue	1-3
Licensed Content Pages	10
Start Page	27
End Page	36
Type of Use	reuse in a thesis/dissertation
Portion	figures/tables/illustrations
Number of figures/tables /illustrations	2
Format	both print and electronic
Are you the author of this Elsevier article?	No
Will you be translating?	No
Title	PhD Thesis
Institution name	Imperial College London
Expected presentation date	Sep 2022
Portions	Figures 3 & 6
Requestor Location	Ruth Birch Department of materials Imperial college london London, SW7 2AZ United Kingdom Attn: Ruth Birch
Publisher Tax ID	GB 494 6272 12
Total	**0.00 GBP**
Terms and Conditions	

INTRODUCTION

1. The publisher for this copyrighted material is Elsevier. By clicking "accept" in connection with completing this licensing transaction, you agree that the following terms and conditions apply to this transaction (along with the Billing and Payment terms and conditions established by Copyright Clearance Center, Inc. ("CCC"), at the time that you opened your Rightslink account and that are available at any time at http://myaccount.copyright.com).

GENERAL TERMS

2. Elsevier hereby grants you permission to reproduce the aforementioned material subject to the terms and conditions

indicated.
3. Acknowledgement: If any part of the material to be used (for example, figures) has appeared in our publication with credit or acknowledgement to another source, permission must also be sought from that source. If such permission is not obtained then that material may not be included in your publication/copies. Suitable acknowledgement to the source must be made, either as a footnote or in a reference list at the end of your publication, as follows:
"Reprinted from Publication title, Vol /edition number, Author(s), Title of article / title of chapter, Pages No., Copyright (Year), with permission from Elsevier [OR APPLICABLE SOCIETY COPYRIGHT OWNER]." Also Lancet special credit - "Reprinted from The Lancet, Vol. number, Author(s), Title of article, Pages No., Copyright (Year), with permission from Elsevier."
4. Reproduction of this material is confined to the purpose and/or media for which permission is hereby given.
5. Altering/Modifying Material: Not Permitted. However figures and illustrations may be altered/adapted minimally to serve your work. Any other abbreviations, additions, deletions and/or any other alterations shall be made only with prior written authorization of Elsevier Ltd. (Please contact Elsevier's permissions helpdesk here). No modifications can be made to any Lancet figures/tables and they must be reproduced in full.
6. If the permission fee for the requested use of our material is waived in this instance, please be advised that your future requests for Elsevier materials may attract a fee.
7. Reservation of Rights: Publisher reserves all rights not specifically granted in the combination of (i) the license details provided by you and accepted in the course of this licensing transaction, (ii) these terms and conditions and (iii) CCC's Billing and Payment terms and conditions.
8. License Contingent Upon Payment: While you may exercise the rights licensed immediately upon issuance of the license at the end of the licensing process for the transaction, provided that you have disclosed complete and accurate details of your proposed use, no license is finally effective unless and until full payment is received from you (either by publisher or by CCC) as provided in CCC's Billing and Payment terms and conditions. If full payment is not received on a timely basis, then any license preliminarily granted shall be deemed automatically revoked and shall be void as if never granted. Further, in the event that you breach any of these terms and conditions or any of CCC's Billing and Payment terms and conditions, the license is automatically revoked and shall be void as if never granted. Use of materials as described in a revoked license, as well as any use of the materials beyond the scope of an unrevoked license, may constitute copyright infringement and publisher reserves the right to take any and all action to protect its copyright in the materials.
9. Warranties: Publisher makes no representations or warranties with respect to the licensed material.
10. Indemnity: You hereby indemnify and agree to hold harmless publisher and CCC, and their respective officers, directors, employees and agents, from and against any and all claims arising out of your use of the licensed material other than as specifically authorized pursuant to this license.
11. No Transfer of License: This license is personal to you and may not be sublicensed, assigned, or transferred by you to any other person without publisher's written permission.
12. No Amendment Except in Writing: This license may not be amended except in a writing signed by both parties (or, in the case of publisher, by CCC on publisher's behalf).
13. Objection to Contrary Terms: Publisher hereby objects to any terms contained in any purchase order, acknowledgment, check endorsement or other writing prepared by you, which terms are inconsistent with these terms and conditions or CCC's Billing and Payment terms and conditions. These terms and conditions, together with CCC's Billing and Payment terms and conditions (which are incorporated herein), comprise the entire agreement between you and publisher (and CCC) concerning this licensing transaction. In the event of any conflict between your obligations established by these terms and conditions and those established by CCC's Billing and Payment terms and conditions, these terms and conditions shall control.
14. Revocation: Elsevier or Copyright Clearance Center may deny the permissions described in this License at their sole discretion, for any reason or no reason, with a full refund payable to you. Notice of such denial will be made using the contact information provided by you. Failure to receive such notice will not alter or invalidate the denial. In no event will Elsevier or Copyright Clearance Center be responsible or liable for any costs, expenses or damage incurred by you as a result of a denial of your permission request, other than a refund of the amount(s) paid by you to Elsevier and/or Copyright Clearance Center for denied permissions.

LIMITED LICENSE

The following terms and conditions apply only to specific license types:
15. **Translation**: This permission is granted for non-exclusive world **English** rights only unless your license was granted for translation rights. If you licensed translation rights you may only translate this content into the languages you requested. A professional translator must perform all translations and reproduce the content word for word preserving the integrity of the article.
16. **Posting licensed content on any Website**: The following terms and conditions apply as follows: Licensing material from an Elsevier journal: All content posted to the web site must maintain the copyright information line on the bottom of each image; A hyper-text must be included to the Homepage of the journal from which you are licensing at http://www.sciencedirect.com/science/journal/xxxxx or the Elsevier homepage for books at http://www.elsevier.com; Central Storage: This license does not include permission for a scanned version of the material to be stored in a central repository such as that provided by Heron/XanEdu.
Licensing material from an Elsevier book: A hyper-text link must be included to the Elsevier homepage at http://www.elsevier.com . All content posted to the web site must maintain the copyright information line on the bottom of each image.

Posting licensed content on Electronic reserve: In addition to the above the following clauses are applicable: The web site

must be password-protected and made available only to bona fide students registered on a relevant course. This permission is granted for 1 year only. You may obtain a new license for future website posting.
17. **For journal authors:** the following clauses are applicable in addition to the above:
Preprints:
A preprint is an author's own write-up of research results and analysis, it has not been peer-reviewed, nor has it had any other value added to it by a publisher (such as formatting, copyright, technical enhancement etc.).
Authors can share their preprints anywhere at any time. Preprints should not be added to or enhanced in any way in order to appear more like, or to substitute for, the final versions of articles however authors can update their preprints on arXiv or RePEc with their Accepted Author Manuscript (see below).
If accepted for publication, we encourage authors to link from the preprint to their formal publication via its DOI. Millions of researchers have access to the formal publications on ScienceDirect, and so links will help users to find, access, cite and use the best available version. Please note that Cell Press, The Lancet and some society-owned have different preprint policies. Information on these policies is available on the journal homepage.
Accepted Author Manuscripts: An accepted author manuscript is the manuscript of an article that has been accepted for publication and which typically includes author-incorporated changes suggested during submission, peer review and editor-author communications.
Authors can share their accepted author manuscript:

- immediately
    - via their non-commercial person homepage or blog
    - by updating a preprint in arXiv or RePEc with the accepted manuscript
    - via their research institute or institutional repository for internal institutional uses or as part of an invitation-only research collaboration work-group
    - directly by providing copies to their students or to research collaborators for their personal use
    - for private scholarly sharing as part of an invitation-only work group on commercial sites with which Elsevier has an agreement
- After the embargo period
    - via non-commercial hosting platforms such as their institutional repository
    - via commercial sites with which Elsevier has an agreement

In all cases accepted manuscripts should:

- link to the formal publication via its DOI
- bear a CC-BY-NC-ND license - this is easy to do
- if aggregated with other manuscripts, for example in a repository or other site, be shared in alignment with our hosting policy not be added to or enhanced in any way to appear more like, or to substitute for, the published journal article.

Published journal article (JPA): A published journal article (PJA) is the definitive final record of published research that appears or will appear in the journal and embodies all value-adding publishing activities including peer review co-ordination, copy-editing, formatting, (if relevant) pagination and online enrichment.
Policies for sharing publishing journal articles differ for subscription and gold open access articles:
Subscription Articles: If you are an author, please share a link to your article rather than the full-text. Millions of researchers have access to the formal publications on ScienceDirect, and so links will help your users to find, access, cite, and use the best available version.
Theses and dissertations which contain embedded PJAs as part of the formal submission can be posted publicly by the awarding institution with DOI links back to the formal publications on ScienceDirect.
If you are affiliated with a library that subscribes to ScienceDirect you have additional private sharing rights for others' research accessed under that agreement. This includes use for classroom teaching and internal training at the institution (including use in course packs and courseware programs), and inclusion of the article for grant funding purposes.
Gold Open Access Articles: May be shared according to the author-selected end-user license and should contain a CrossMark logo, the end user license, and a DOI link to the formal publication on ScienceDirect.
Please refer to Elsevier's posting policy for further information.
18. **For book authors** the following clauses are applicable in addition to the above: Authors are permitted to place a brief summary of their work online only. You are not allowed to download and post the published electronic version of your chapter, nor may you scan the printed edition to create an electronic version. **Posting to a repository:** Authors are permitted to post a summary of their chapter only in their institution's repository.
19. **Thesis/Dissertation**: If your license is for use in a thesis/dissertation your thesis may be submitted to your institution in either print or electronic form. Should your thesis be published commercially, please reapply for permission. These requirements include permission for the Library and Archives of Canada to supply single copies, on demand, of the complete thesis and include permission for Proquest/UMI to supply single copies, on demand, of the complete thesis. Should your thesis be published commercially, please reapply for permission. Theses and dissertations which contain embedded PJAs as part of the formal submission can be posted publicly by the awarding institution with DOI links back to the formal publications on ScienceDirect.

Elsevier Open Access Terms and Conditions

You can publish open access with Elsevier in hundreds of open access journals or in nearly 2000 established subscription journals that support open access publishing. Permitted third party re-use of these open access articles is defined by the author's choice of Creative Commons user license. See our open access license policy for more information.

Terms & Conditions applicable to all Open Access articles published with Elsevier:

Any reuse of the article must not represent the author as endorsing the adaptation of the article nor should the article be modified in such a way as to damage the author's honour or reputation. If any changes have been made, such changes must be clearly indicated.

The author(s) must be appropriately credited and we ask that you include the end user license and a DOI link to the formal publication on ScienceDirect.

If any part of the material to be used (for example, figures) has appeared in our publication with credit or acknowledgement to another source it is the responsibility of the user to ensure their reuse complies with the terms and conditions determined by the rights holder.

Additional Terms & Conditions applicable to each Creative Commons user license:

CC BY: The CC-BY license allows users to copy, to create extracts, abstracts and new works from the Article, to alter and revise the Article and to make commercial use of the Article (including reuse and/or resale of the Article by commercial entities), provided the user gives appropriate credit (with a link to the formal publication through the relevant DOI), provides a link to the license, indicates if changes were made and the licensor is not represented as endorsing the use made of the work. The full details of the license are available at http://creativecommons.org/licenses/by/4.0.

CC BY NC SA: The CC BY-NC-SA license allows users to copy, to create extracts, abstracts and new works from the Article, to alter and revise the Article, provided this is not done for commercial purposes, and that the user gives appropriate credit (with a link to the formal publication through the relevant DOI), provides a link to the license, indicates if changes were made and the licensor is not represented as endorsing the use made of the work. Further, any new works must be made available on the same conditions. The full details of the license are available at http://creativecommons.org/licenses/by-nc-sa/4.0.

CC BY NC ND: The CC BY-NC-ND license allows users to copy and distribute the Article, provided this is not done for commercial purposes and further does not permit distribution of the Article if it is changed or edited in any way, and provided the user gives appropriate credit (with a link to the formal publication through the relevant DOI), provides a link to the license, and that the licensor is not represented as endorsing the use made of the work. The full details of the license are available at http://creativecommons.org/licenses/by-nc-nd/4.0. Any commercial reuse of Open Access articles published with a CC BY NC SA or CC BY NC ND license requires permission from Elsevier and will be subject to a fee.

Commercial reuse includes:

- Associating advertising with the full text of the Article
- Charging fees for document delivery or access
- Article aggregation
- Systematic distribution via e-mail lists or share buttons

Posting or linking by commercial companies for use by customers of those companies.

20. **Other Conditions**:

v1.10

Questions? customercare@copyright.com or +1-855-239-3415 (toll free in the US) or +1-978-646-2777.